Temporal and spatial dynamics of marine microorganisms in ice-covered seas

DISSERTATION
ZUR ERLANGUNG DES DOKTORGRADES DER NATURWISSENSCHAFTEN
- DR. RER. NAT. -
DEM FACHBEREICH GEOWISSENSCHAFTEN
DER UNIVERSITÄT BREMEN VORGELEGT VON

Magda Guadalupe Cardozo Miño

11th November 2022

Die vorliegende Doktorarbeit wurde im Rahmen des Programms International Max Planck Research School of Marine Microbiology (MarMic) mit finanzieller Unterstützung der Hector Fellow Academy in der Zeit von November 2018 bis September 2022 in der HGF MPG Brückengruppe für Tiefsee-Ökologie und Technologie am Alfred-Wegener-Institut Helmholtz-Zentrum für Polar- und Meeresforschung und dem Max-Planck-Institut für Marine Mikrobiologie angefertigt.

Gutachter: Prof. Dr. Antje Boetius

Gutachter: Prof. Dr. Thorsten Brinkhoff

This work is dedicated with love to
Fernando, Dora, Manuel and Nils

"…but the limits of the unknown had to recede step by step before the ever-increasing yearning after light and knowledge of the human mind, till they made a stand in the north at the threshold of Nature's great Ice Temple of the polar regions with their endless silence."

Fridtjof Nansen, Farthest North; Being a Record of a Voyage of Exploration of the Ship "Fram" 1893-96, 1897

Table of Contents

Summary

The anthropogenic emissions of CO_2 and other climate-active gases lead to a steep increase of global temperatures. Global climate change is particularly amplified in the Arctic (e.g., Serreze et al., 2009; Serreze and Barry, 2011). Increasing temperatures and the rapid sea ice decline have shown profound effects on life in the Arctic ecosystem (Wassmann et al., 2011). Climate model predictions suggest a seasonally sea ice-free Arctic well before the first half of this century (Overland and Wang, 2013; Docquier and Koenigk, 2021). The composition, structure and function of the Arctic microbiome will be altered with distinct effects on the marine system, on primary productivity, carbon fluxes and food web structures. Changes in the composition and structure of primary producers were already observed in Fram Strait (Nöthig et al., 2015), the boundary and highly dynamic zone between the Atlantic and the Arctic Ocean. These changes were reflected in the export flux of particulate organic matter (Lalande et al., 2013), also observable in the benthic communities (Jacob, 2014). Thus, understanding how the microbial communities changed over time under different environmental conditions is a scientific task needed to assess future changes in the Arctic ecosystem.

This thesis aimed to understand the composition, distribution and function of bacteria, archaea and eukaryotic communities in Fram Strait across different spatial and temporal scales and their relationship with environmental variables. The overall objective was to identify signature groups and key factors of change, to provide a baseline to the effects of climate change and sea ice retreat. It provides a comprehensive overview of the Arctic microbiome by the incorporation of seawater, sinking particles and sea ice samples to identify key microbial indicators of change and environmental drivers in these communities. Samples were obtained in the frame work of the Long-Term Ecological Research (LTER) site HAUSGARTEN and the FRontiers in Marine Monitoring (FRAM) program.

The results of Chapter I and Chapter II highlight the usage of methods free of compositional-bias and meta'omics approaches necessary to understand the role of microbial communities. The observations in Chapter I revealed that different water masses characterized by different physicochemical conditions harboured different active microbial communities. A late

phytoplankton bloom dominated by diatoms in the surface waters of the eastern Fram Strait was identified, where members of the *Bacteroidetes*, *Alteromonadales*, *Oceanospirillales* and *Rhodobacterales* were significantly active. Abundant transcripts of transporters and fundamental cellular functions supported the degradation of organic matter. The deeper waters of Atlantic origin were marked by strong chemolithotrophic activities by members of *Thaumarchaeota*.

In Chapter II I analysed bacterial and archaeal groups in deep-sea waters that benefitted from a phytoplankton bloom at the surface. Chapter III studied the development of microbial composition of sinking particles using a 12-year time-series study. The presence of sea ice and the passing warm anomaly were the drivers of change in these communities. In Chapter IV, microcosm experiments revealed bacterial taxa that responded to eukaryotes and substrates sourced from the sea ice during sea ice melt in seawater. Altogether, the results of this thesis provide baseline knowledge to better assess the effects of climate change on the Arctic microbiome and the consequences for ecosystem functioning and carbon cycling.

Zusammenfassung

Die anthropogenen Emissionen von CO_2 und anderen klimawirksamen Gasen führen zu einem steilen Anstieg der globalen Temperatur. Der globale Klimawandel ist in der Arktis besonders stark ausgeprägt (Serreze et al., 2009; Serreze and Barry, 2011). Die rasch ansteigenden Temperaturen und der schnelle Rückgang des Meereises haben tiefgreifende Auswirkungen auf das Leben im arktischen Ökosystem (Wassmann and Reigstad, 2011). Die meisten Klimamodelle sagen voraus, dass die der arktische Ozean schon vor dem Jahr 2050 im Sommer frei von Meereis sein wird (Overland and Wang, 2013; Docquier and Koenigk, 2021). Dies wird Auswirkungen auf die Zusammensetzung, Struktur und Funktion des arktischen Mikrobioms haben, und das gesamte marine System, einschließlich der Primärproduktivität, der Kohlenstoffflüsse und der Strukturen des Nahrungsnetzes verändern. Es wird erwartet, dass die Verringerung des Meereises den Kohlenstoffexport und die mikrobielle Konnektivität zwischen den oberen und tieferen Wasserschichten verringert (Fadeev et al., 2021a; von Appen et al., 2021). In der Framstraße (Nöthig et al., 2015) einer hochdynamischen Grenzzone zwischen dem Atlantik und dem Arktischen Ozean, wurden bereits signifikante Veränderungen in der Zusammensetzung und Struktur der Primärproduzenten beobachtet. Diese Veränderungen spiegeln sich im Export von partikulärem organischem Material wider (Lalande et al., 2013), welche auch die benthischen Gemeinschaften stark verändert (Jacob, 2014). Es sollte daher erforscht werden, wie sich die mikrobiellen Gemeinschaften im Laufe der Zeit unter verschiedenen Umweltbedingungen verändern haben, um so zukünftige Veränderungen im arktischen Ökosystem zu bewerten.

In dieser Arbeit untersuchte ich die Zusammensetzung, Verteilung und Funktion von Bakterien, Archaeen und eukaryotischen Gemeinschaften in der Framstraße auf verschiedenen räumlichen und zeitlichen Ebenen. Das übergeordnete Ziel bestand darin, charakteristische Gruppen von Mikroorganismen und Schlüsselfaktoren zu identifizieren, die eine Grundlage für die Bewertung der Auswirkungen des Klimawandels und des Rückgangs des Meereises auf das Ökosystem Arktischer Ozean bilden. Durch die Einbeziehung von Faktoren wie der Meerwasserzusammensetzung, Partikelfrachten und Meereisbedeckung wurde ein umfassender Überblick über das arktische Mikrobiom gewonnen. Die Proben

wurden im Rahmen der Langzeit-Ökologie-Forschungsstation (LTER) HAUSGARTEN und des FRontiers in Marine Monitoring (FRAM) Programms gewonnen.

In Kapitel I und Kapitel II werden Methoden werden Methoden aus dem Bereich Meta'-omics genutzt, um die Rolle der mikrobiellen Gemeinschaften zu verstehen. Kapitel I zeigt auf, dass die unterschiedlichen Wassermassen mit ihren charakteristischen physikalisch-chemischen Eigenschaften, unterschiedliche aktive mikrobielle Gemeinschaften beherbergen. Im Oberflächenwasser der östlichen Framstraße kam es zu einer späten, von Kieselalgen dominierten Phytoplanktonblüte. Als Folge dessen waren Bakterien aus den *Bacteroidetes*, *Alteromonadales*, *Oceanospirillales* und *Rhodobacterales* besonders aktiv. Die hohe Transkription von Genen für Transportprozesse und grundlegenden zellulären Funktionen waren ein Beleg für den verstärkten Abbau organischer Verbindungen. Dagegen konnte tieferen Wasserschichten atlantischen Ursprungs eine hohe chemolithotrophe Aktivität von *Thaumarchaeen* festgestellt werden.

In Kapitel II analysierte ich Bakterien- und Archaeengruppen in Tiefseegewässern, die besonders von der Phytoplanktonblüte an der Oberfläche profitierten. In Kapitel III wurden anhand einer 12-jährigen Zeitreihenstudie die Veränderungen in der mikrobiellen Zusammensetzung sinkender Partikel untersucht. Das Vorhandensein von Meereis und die vorübergehende Wärmeanomalie waren die treibenden Kräfte für die Veränderungen in diesen Gemeinschaften. In Kapitel IV wurden anhand der Ergebnisse der Mikrokosmenexperimente bestimmte Bakterientaxa identifiziert, die auf Eukaryoten und das aus dem Meereis stammende Substrat reagierten, und es wurden Erkenntnisse darüber gewonnen, wie die mikrobiellen Gemeinschaften der Arktis auf die Meereisschmelze reagieren. Insgesamt liefern die Ergebnisse dieser Arbeit ein Basiswissen zu den Auswirkungen des Klimawandels, der wärmeren Meerwassertemperaturen und des fortschreitenden Meereisrückgangs sowie zu den Auswirkungen auf die mikrobielle Vielfalt mit Folgen für das Funktionieren von Ökosystemen und den Kohlenstoffkreislauf.

List of Abbreviations

AO	Arctic Ocean
AW	Atlantic Water
PW	Polar Water
EGC	East Greenland Current
WSC	West Spitsbergen Current
PSWw	Warm Polar Surface Water
AW/RAW	Atlantic Water/Recirculating Atlantic Water
AAW/ RAAW	Arctic Atlantic Water/Return Atlantic Water
AIW	Arctic Intermediate Water
CBDW	Canadian Basin Deep Water
EBDW/GSDW	Eurasian Basin Deep Water/Greenland Sea Deep Water
RAW	Recirculating Atlantic Water
NDW	Nordic Seas Deep Water
LTER	Long-term ecological research
MIZ	Marginal ice zone
PP	Primary production
BCP	Biological carbon pump
POM	Particulate organic matter
POC	Particulate organic carbon
DOC	Dissolve organic carbon
FYI	First-year-ice
MYI	Multi-year-ice
AOA	Ammonia-oxidizing archaea
AD	Arctic dipole
SST	Sea surface temperature
NPP	Net primary production
MI	Microbial indicator
WWA	Warm water anomaly

1. Introduction

1.1 The Arctic Ocean

The Arctic Ocean (AO) is the smallest ocean on Earth comprising of ~4.3% of the total area of the world's oceans and ~1.4% of the volume (Jakobsson, 2002). It consists of a deep polar-centric central basin surrounded by the shelf seas Barents, Kara, Laptev, East Siberian, Chukchi, Beaufort, and Lincoln. The Lomonosov Ridge divides the central basin into the Eurasian and Amerasian Basins. The Amerasian Basin connects the AO to the Pacific Ocean through the Bering Strait, and the Eurasian Basin connects to the Atlantic Ocean through Fram Strait and the Barents Sea opening via the Greenland and Norwegian Seas as well as through the Canadian Arctic Archipelago via Baffin Bay (Jakobsson et al., 2012; Bluhm et al., 2015).

The AO is a nearly landlocked ocean surrounded by the landmasses – Eurasia, North America and Greenland. It is often referred to as Arctic Mediterranean (Figure 1). The AO is the shallowest ocean (on average ~1201 m) with large continental shelves (Jakobsson, 2002; Jakobsson et al., 2012). In total, the continental shelf area of the AO comprises ~52.7% of the total area. The continental shelves, are some of the most productive areas in the region (Carmack and Wassmann, 2006) and ice-free regions often experience intense seasonal blooms of phytoplankton owing to their favourable nutrient and light conditions (Hill and Cota, 2005).

The oceanography of the AO is unique by virtue of characteristic features. It is dominated by high latitude climate characterized by strong seasonality of atmospheric temperature and solar radiation, the formation and seasonal melting of sea ice and by strong stratification (Johannessen et al., 1994). The AO acts as a heat sink, as it absorbs the heat from the North Atlantic thermohaline circulation producing the colder denser waters that sink into the deep North Atlantic to supply the North Atlantic Deep Water (Aagaard et al., 1985). The Arctic sea ice plays an important role in controlling heat interactions with the atmosphere, determine

albedo and light availability to the underlying waters (Perovich, 2011; Perovich and Polashenski, 2012).

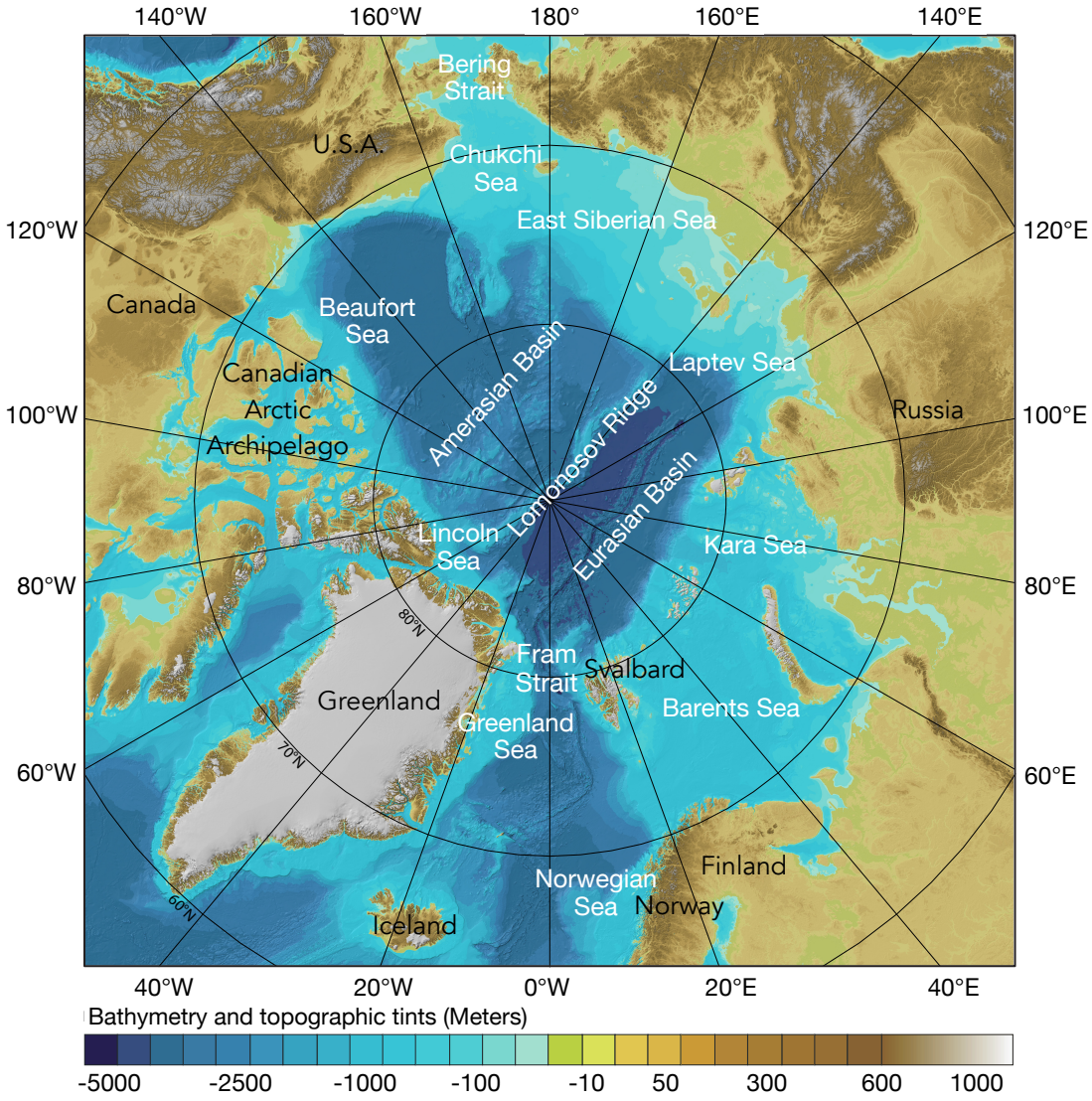

Figure 1. Bathymetric map of the Arctic Ocean, main corresponding Seas and Straits. Modified from the International Bathymetric Chart of the Arctic Ocean (IBCAO) Version 3.0 (Jakobsson et al., 2012).

1.2 Water masses and circulation

Water flows into the AO from the North Atlantic and North Pacific oceans. Inflow into the AO of Pacific water occurs into the Chukchi Sea and outflows through the Canadian Arctic Archipelago and Fram Strait (Rudels et al., 2012). The Pacific water, which enters through the very shallow Bering Strait (~50 m) is less saline (hence less dense) than the Atlantic Water (AW) and resides in the upper ~300 m in the water column (Figure 2.A), thus provides a density barrier between the warm AW and the surface sea ice. Pacific water provides a source

of nutrients and brings high concentrations of silicate and phosphate to the Arctic (Walsh et al., 1989; Torres-Valdés et al., 2013), and constitutes a third of the Arctic freshwater inflow (Woodgate and Aagaard, 2005). Most of the AO water originates in the North Atlantic Ocean, which provides a substantial portion of upper waters and almost all of the mid-depth and the thick homogeneous deep waters layers (~1000 m) that reach the seafloor (Jones, 2001; Rudels and Carmack, 2022) (Figure 2.B). Exchange between the North Atlantic Ocean and the AO occurs through Fram Strait between Greenland and Svalbard and through the Barents Sea. Fram Strait is the only deep passage (sill depth of ~ 2600 m) and the only one with a two-way exchange (Rudels, 2015). The West Spitsbergen Current (WSC) carries warm, saline, and nitrate-rich AW that enter the AO. The Atlantic water deep layers in the Fram Strait preserve the warm core losing less heat to the atmosphere unlike the AW branch in the Barents Sea (Rudels and Carmack, 2022). Outflow of less saline upper water layers and ice occurs through the narrow Straits in the Canadian Arctic Archipelago and in the western part of Fram Strait carried by the East Greenland Current (EGC) and waters above the Greenland shelf (Beszczynska-Moeller et al., 2011).

1.3 Stratification

The AO is stratified by salinity not by temperature (Rudels and Carmack, 2022). Stratification and water mass formation in the AO are regulated by sea ice. Meltwater in summer creates a low-salinity surface layer with strongly reduced density, in addition to river input of freshwater and organic matter (Dittmar and Kattner, 2003), the resulting strong salt-stratification is a dominant characteristic of the AO (Aagaard et al., 1985; Carmack, 2007). The water column of the AO is characterized by a low salinity polar mixed layer in the upper 10 cm and separated by a cold halocline from the layers below (Rudels et al., 1996). The surface mixed layer and the stratified halocline form a low-salinity layer of cold water constraining the heat fluxes from the underlying the thicker, more saline, and warmer inflow from the Atlantic allowing for the persistence of ice cover in winter (Rudels et al., 2012; Polyakov et al., 2013b; Carmack et al., 2015), hence, they play an indirect role in keeping the planetary ice/albedo feedback effects (Aagaard and Carmack, 1989). Three freshwater sources maintain the halocline: river runoff, sea ice meltwater, and the low-salinity Pacific

water entering the AO through the Bering Strait (Ekwurzel et al., 2001). Warmer surface waters weaken the cold halocline layer, increasing the influx of Atlantic heat that amplifies the reduction of the sea ice cover (Polyakov et al., 2017).

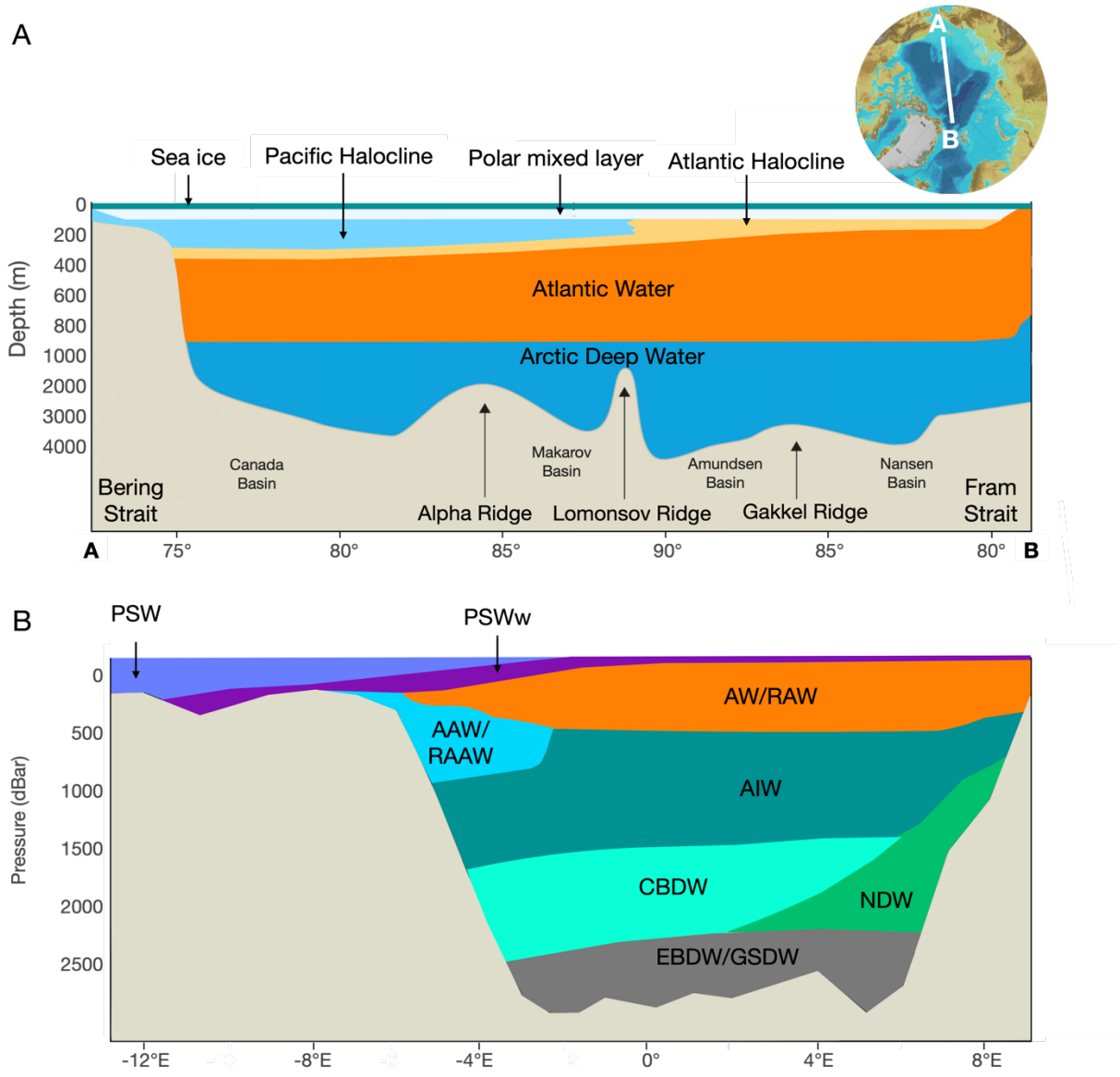

Figure 2. A) Schematics of different water masses in the Arctic Ocean emphasizing on vertical stratification. Modified after (Meltofte et al., 2013). B) Main Water masses in Fram Strait (~79°N): Polar Surface Water (PSW) flows southwards along the EGC and originates from the polar mixed layer and the halocline in the Arctic. PSW is defined as having a potential temperature below 0°C and a potential density lower than 27.7 kg m^{-3} (Rudels et al., 1996; Rudels, 2015). Warm Polar Surface Water (PSWw) is formed when PSW is warmed and freshened and originates with sea ice melting on warmer Atlantic water. Unlike PSW the potential temperature of PSWw is > 0°C (Rudels et al., 2002) and corresponds to up to 50% of freshwater export through Fram Strait (Inall et al., 2014). Atlantic Water/Recirculating Atlantic Water (AW/RAW). AW is carried into the Arctic via the WSC and is a significant source of heat to the Arctic Basins. Deeper water masses of the mesopelagic and bathypelagic include the Arctic Atlantic Water (AAW)/Return Atlantic Water (RAAW) located at the warm core of the East Greenland Current and includes the Arctic Ocean thermocline increasing. The Arctic Intermediate Water (AIW), Canadian Basin Deep Water (CBDW), Eurasian Basin Deep Water (EBDW)/Greenland Sea Deep Water

(GSDW), Atlantic Water/Recirculating Atlantic Water (AW/RAW), and Nordic Seas Deep Water (NDW). Modified after (Stöven et al., 2016).

1.4 Sea ice

The most defining feature of the AO and adjacent seas is its sea ice cover, which expands and decreases with the seasons and changes in extent and thickness over longer times scales (Polyak et al., 2010). Sea ice freezing and melting affects stratification of the water column. As ice forms during the winter, brine rejection reduces stratification, replenishing nutrients in the upper water column. When sea ice melts as a result of increases in solar radiation and water temperature, a strong stratification of the upper water column occurs (Korhonen et al., 2013; Thomas, 2017). Greatest sea ice loss occurs between June and October, and sea ice extent reaches its seasonal minimum in September. Sea ice cover distinctly influences the marine ecosystem, oceanic circulation and surface albedo (Aagaard and Carmack, 1989; Perovich and Polashenski, 2012). Sea ice cover determines primary productivity as it restricts light availability to the underlying surface waters. It provides a habitat, nursery ground and a refuge for a vast variety of species of all domains of life (Arrigo, 2014; Boetius et al., 2015; Thomas, 2017). The sea ice and its microbiota mediate particulate fluxes from the sea ice to the water column and benthos, and it is thus a key component of benthic-pelagic coupling in the AO (Wassmann and Reigstad, 2011; Wiedmann et al., 2020). Observations of accelerating sea ice retreat and thinning of the Arctic sea ice cover are evidence of global climate change (Comiso et al., 2008; Polyak et al., 2010; Gao et al., 2015). It is estimated that the AO may experience sea ice-free summers within the next 20-30 years (Boé et al., 2009; Wang and Overland, 2012; Jahn et al., 2016; Screen and Deser, 2019). The continuing decline in sea ice, (e.g., Stroeve and Notz, 2018), and the changes associated with the increase of Atlantic heat flux into the AO or "Atlantification" (e.g., Polyakov et al., 2017) will continue to substantially affect the marine ecosystem (Wassmann, 2015; Lewis et al., 2020; Frey et al., 2021) and the geophysical and biogeochemical components of the AO system.

1.5 Fram Strait and LTER site HAUSGARTEN

Fram Strait, between Greenland and Svalbard, is the AO only deep connection to the World Ocean (Jakobsson et al., 2003). Geographically, the Fram Strait lies between 77°N and 81°N latitudes, and is centred around 0° longitude. The Strait is approximately ~ 450 km wide and a maximum depth of ~ 5600 m at the Molloy Hole (Klenke and Schenke, 2002). Long considered the most important link between the AO and the Atlantic, the Fram Strait acts as a fundamental gateway through which water masses, nutrients, heat, freshwater, and sea ice from the Transpolar Drift are exchanged between the AO and the North Atlantic via the characteristic opposing water currents of the WSC and the EGC. Hence, the Fram Strait can host distinct water masses in the upper water column with distinct oceanographic conditions in opposing regions across the Strait. Fram Strait is also home to the HAUSGARTEN observatory - the only open ocean long-term ecological research (LTER) site in the Arctic that tracks the impacts of environmental changes in the Arctic as one of the key areas regarding investigations ongoing changes in the AO ecosystem (Soltwedel et al., 2005).

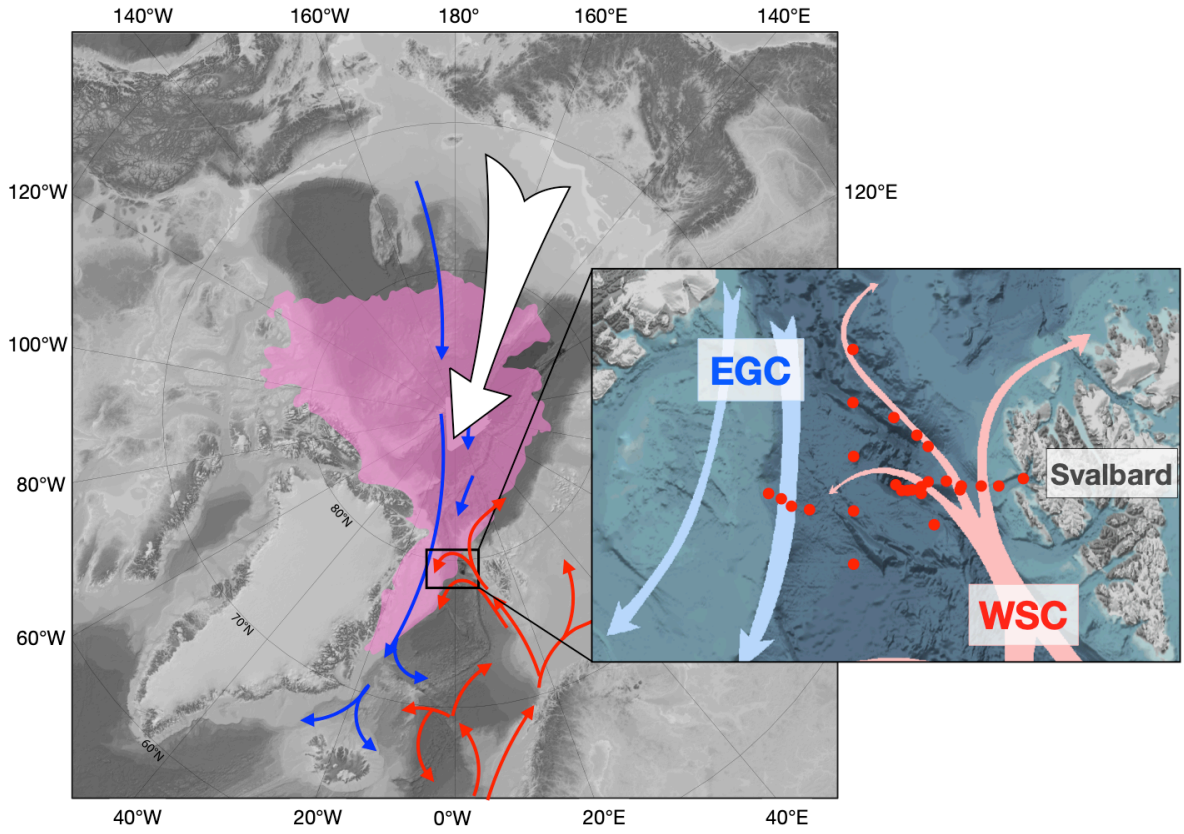

Figure 3. Map of the LTER HAUSGARTEN in the Arctic Ocean. Warm Atlantic water currents are indicated by red arrows, cold less saline polar water current by blue arrows and the transpolar drift that carries sea ice from the Laptev Sea and the East Siberian Sea towards Fram Strait is depicted by the white arrow. The sea ice minimum in 2012, the absolute lowest sea ice extent to date, is shown in pink. The section map represents the HAUSGARTEN observatory stations depicted by the red dots,

the blue arrow represents the EGC and the red arrow the WSC. Map: AWI/ Laura Hehemann, Ingo Schewe.

1.6 The biological carbon pump in the Arctic Ocean

1.6.1 Primary production

The biological carbon pump (BCP), refers to the net biological sequestration of atmospheric CO_2 into the ocean (Volk and Hoffert, 1985). In the upper ocean the fixation of CO_2 is done by photoautotrophic organisms in a process known as primary production (PP). Through photosynthesis, primary producers use sunlight, carbon dioxide and water to produce oxygen and organic compounds, forming the base of the marine food chain. Photoautotrophic organisms inhabiting the sea ice (sympagic algae) and the water column (pelagic phytoplankton) are the main primary producers in the AO. Overall, primary producers are single-celled microbial eukaryotes with different communities in the sea ice and the water column including diatoms, dinoflagellates, rhizarians, haptophytes and chlorophytes (Lovejoy et al., 2006; Lovejoy and Potvin, 2011; Poulin et al., 2011). Diatoms typically dominate sea ice phytoplankton blooms, while others like flagellates, dinoflagellates, and picoeukaryotes usually dominate in summer (Fernández-Méndez et al., 2018; van Leeuwe et al., 2018; Liu et al., 2021).

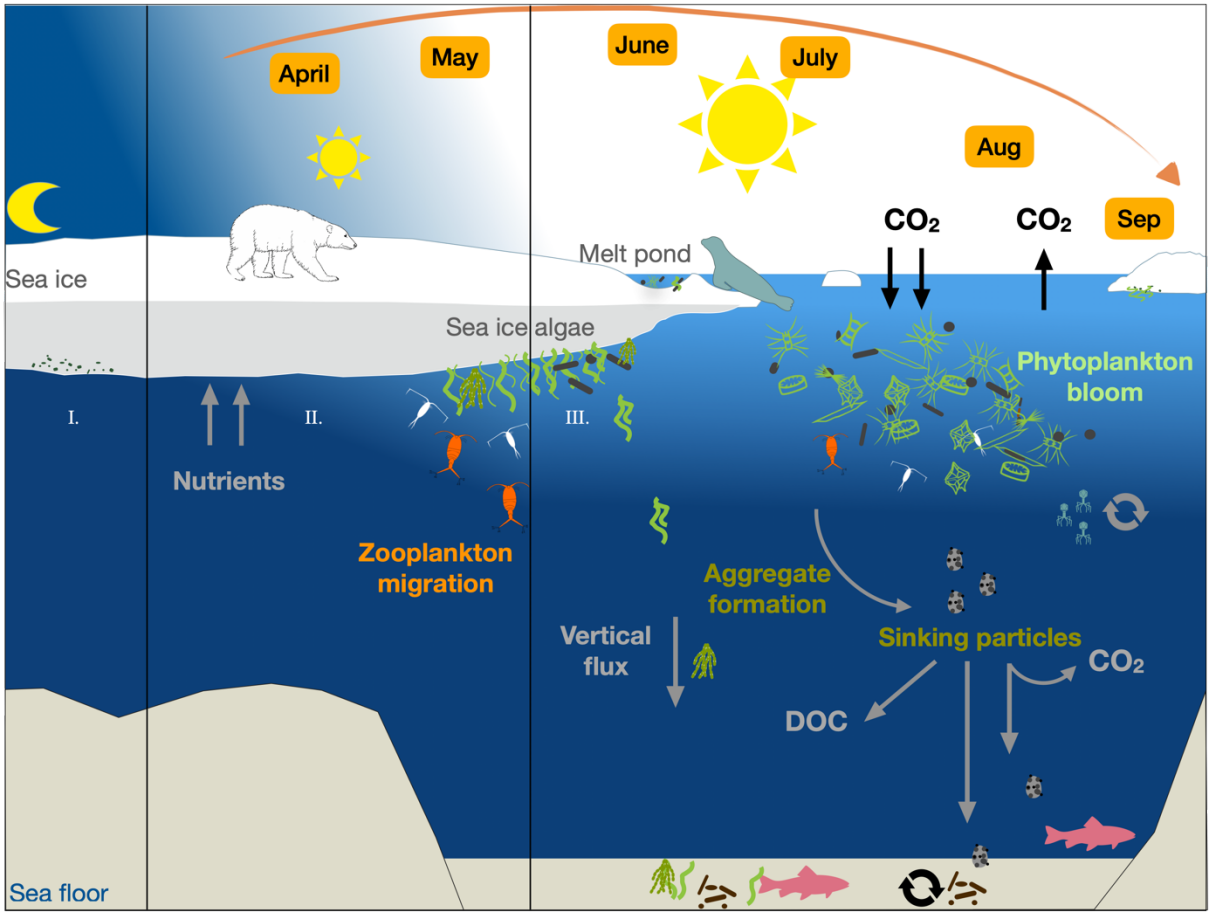

Figure 4. Schematic representation of the biological carbon pump in the Arctic Ocean. The seasonal development of the sea ice algae and phytoplankton blooms in the water column are depicted in the numbered panels in the euphotic zone at the epipelagic (0 to ~ 200 m): I. Low-light and winter conditions are characterized by low ice temperatures, low algae biomass and lack of sympagic-pelagic interaction, yet rather little is known about this period. During this time sea ice formation allows for dormant diatoms cells to be incorporated into the ice (Różańska et al., 2008). Under the sea ice most of the biomass is transformed through the heterotrophic microbial loop (Riedel et al., 2008). In winter, sea ice formation and brine rejection allow for vertical mixing in the water column to replenish the nutrients in the surface (Korhonen et al., 2013). II. During the winter to spring transition, the increasing solar angle and daylight allows for light penetration into the sea ice and the first blooms from low-light adapted algae, usually pennate diatoms (Różańska et al., 2008; Kauko et al., 2018), at the bottom of the ice takes place and the migration of zooplankton species to the sea ice commences (Basedow et al., 2018) particularly copepods (Hop et al., 2021). III: As the season progresses the phytoplankton bloom in the water column increases in productivity. The increases in temperature and light availability characterize the productive season and sympagic-pelagic-benthic coupling is stronger and no longer limited. Towards the latest stages flagellates dominate the phytoplankton bloom (Nöthig et al., 2015). Organic matter produced by phytoplankton is processed by microbes mainly by heterotrophic bacteria together with the viral shunt releasing nutrients back to the water column at the euphotic zone via the "microbial loop", as well as repacked into fecal pellets of zooplankton and higher consumers. Organic matter in the form of marine snow and POC is exported to deeper layers via sinking particles and vertical migration of zooplankton. As particles are exported microbial degradation continues to release nutrients making them available to higher trophic leves. At depth, attenuation of export flux continues, and POC and DOC consumption and repackaging by higher species occurs (Turner, 2015). A smal fraction of the carbon reaches the seafloor where is long-term sequestered for centuries to millennia.

The Arctic experiences extreme seasonality in light conditions with two main seasons from permanent darkness (winter) to continuous light (summer), equal in duration. In winter, vertical mixing replenishes the photic zone with nutrients (Popova et al., 2010). Whereas in spring, increasing light availability triggers phytoplankton blooms (Leu et al., 2015). The PP in the AO thus depends mainly on seasonal light availability and nutrients, which are essential for phytoplankton growth (Popova et al., 2012) and limited to a few months of the year. The different communities that inhabit the sea ice and water column differ not only in composition, but also in the timing of their bloom. Sea ice algae bloom earlier in the year due to photoadaptation to low light conditions that occur under sea ice (Arrigo, 2003; Hancke et al., 2018), acting as a carbon source for both pelagic and benthic communities (Gradinger, 2009). These early blooms provide a food source for metazoan grazers including actively swimming species of meso- and zooplankton (Darnis and Fortier, 2014; Hop et al., 2021), and when not immediately grazed, sea algae sink and provide a food source for benthic organisms (Boetius et al., 2013). Sea ice algae growth can contribute up to 57 % of the total water column and sea ice primary production in the AO (Gosselin et al., 1997). Phytoplankton and sympagic ice algae productivity in and underneath the sea ice have been shown to vary greatly from 1 to 25 g C m^{-2} yr^{-1} (Boetius et al., 2013) (averaging 5 – 10 g C m^{-2} $year^{-1}$ (Leu et al., 2011)), however the contribution of sympagic ice algae productivity shows large variability (0 – 80%) (Boetius et al., 2013; Arrigo, 2017; Lalande et al., 2019; Campbell et al., 2022).

With the increasing availability of light as sea ice recedes, the springtime bloom that started in sea ice continues in the water column under thinning sea ice and in ice-free areas (Arrigo et al., 2012; Leu et al., 2015). As the season progresses, a deep chlorophyll maximum (DCM) forms in a trade-off between light, nutrients and stratification (Martin et al., 2010) and often representing peaks in abundance of phytoplankton. The pelagic phytoplankton bloom estimated production is in most cases larger than production by sea ice algae and varies from 12 to 50 g C m^2 yr^{-1} (Leu et al., 2011; Wiedmann et al., 2020). The PP by sea ice algae has only been found to be higher than pelagic production in areas with very dense ice cover (> 90%) (Fernández-Méndez et al., 2015).

1.6.2 Export of organic matter

The magnitude of carbon that the BCP exports is estimated to be between 5 and 12 Pg C yr^{-1} globally (Boyd and Trull, 2007; Henson et al., 2011; Siegel et al., 2016; DeVries and Weber, 2017). The ocean absorbs about 30 – 40 % of atmospheric CO_2 since industrialization, thus it acts as an important sink for anthropogenically released CO_2 (Takahashi et al., 2002; DeVries et al., 2019; Gruber et al., 2019). The majority of carbon fixed by primary producers in the upper ocean is usually rapidly transformed through microbial processes, grazing by zooplankton, and only a small fraction will be exported to the deep sea in the form of sinking particles (Turner, 2015) (Figure 4). Heterotrophic microbial activity is key in the maintenance of nutrient cycling (Azam and Malfatti, 2007). They degrade organic material, remineralise into CO_2 and release back nutrients to the environment making them available for other trophic levels fueling primary production in a process known as the "microbial loop" (Azam et al., 1983). The photosynthetically fixed carbon becomes inaccessible to the atmosphere mainly in the form of particulate organic carbon (POC) that sinks or dissolved organic carbon (DOC). It is estimated that the carbon exported by the BCP below 1000 m varies from 1.2 – 2.4 % of the annual PP (Legendre et al., 2015), approximately 0.2 – 0.7 PgC yr^{-1} (Guidi et al., 2015), where it is stored for thousands of years.

1.6.3 Export of biogenic matter to the deep sea via sinking particles

The biomass produced by phytoplankton in the sea ice and water column will be transformed by heterotrophic microbes and viruses (Cho and Azam, 1988; Bratbak et al., 1994; Jiao et al., 2010). A small portion of the particulate organic matter (POM) escapes to the deeper layers in the form of sinking particles that originated in the photic zone, providing a source of energy and nutrients to deeper ecosystems (Ducklow et al., 2001; De La Rocha and Passow, 2007; Turner, 2015). These sinking particles usually consist of a diverse mix of organic (and inorganic) matter as marine snow formed by phytoplankton, detritus, zooplankton cells, fecal pellets and ballast minerals (Wassmann et al., 2004; Iversen and Ploug, 2010; Turner, 2015), as well as associated microbial communities (Simon et al., 2002). Particle formation and the subsequent export of POM to the deep ocean is mainly driven by the composition of primary

producers and zooplankton in the sea ice and water (Ducklow et al., 2001; Herndl and Reinthaler, 2013), and the environment at the surface during formation (Simon et al., 2002; Guidi et al., 2009). The dynamics of vertical flux of biogenic matter have been studied in the AO (Wassmann et al., 2004; Soltwedel et al., 2005; Bauerfeind et al., 2009; Lalande et al., 2013; Nöthig et al., 2020), and other oceanographic regions over the past two decades (e.g., Kawakami and Honda, 2007; Fontanez et al., 2015; Smith et al., 2018). The quality and quantity of the sinking particles that reach the benthos depend on seasonality, geography and vertical distribution of the organisms that mediate the distribution and transformation of the particles as they reach the deep sea (Alldredge and Silver, 1988; Henson et al., 2012). The microbial composition of sinking particles has been observed mostly in tropical and subtropical regions (Boeuf et al., 2019; Preston et al., 2020; Poff et al., 2021). However, long-term changes in the microbial composition of sinking particles in higher latitudes marked by a strong seasonality have not been addressed. Recent studies identified the role of changing sea ice conditions in the efficiency of vertical export and microbial composition of sinking particles in the AO (Fadeev et al., 2021a; von Appen et al., 2021), suggesting that a decline in sea ice may reduce export of organic matter. However, seasonal, regional and inter-annual dynamics of microbial communities associated to particles key to understand biological transformations in the AO remain largely understudied.

1.7 Microbial communities, structure and functional diversity in the Arctic Ocean

1.7.1 The sea ice ecosystem

The sea ice matrix provides a wide range of habitats for a variety of organisms, including sea ice algae and microeukaryotes (< 20 µm) (Lizotte, 2003; Piwosz et al., 2013), multicellular organisms such as meiofauna (e.g., nematodes and zooplankton) (Gradinger, 2001; Bluhm et al., 2018), and members of the domains Bacteria and Archaea and viruses (Collins and Deming, 2011; Deming and Collins, 2017; Sazhin et al., 2019). The sympagic foob web and associated communities play a key role in pelagic-benthic coupling by facilitating vertical dispersal of biomass and thus of carbon and associated microbial communities to the water column promoting a strong vertical connectivity (Lizotte, 2003; Fadeev et al., 2021a). Traditionally studied, diatoms are among the main primary producers in sea ice and are

significant contributors of biomass recognizable by the naked eye as pigmented bands in the ice. Although the sea ice environment experiences a high degree of temporal and spatial heterogeneity that can result in differences in microbial community structure (Bowman et al., 2012), dominant eukaryotic species found in sea ice include pennate, centric, and chain-forming species of the diatoms *Fragilariopsis*, *Nitzschia*, *Eucampia* and *Melosira*, as well as the prymnesiophyte *Phaeocystis*, members of dinoflagellates, chlorophytes, xanthophytes and chrysophytes are among the most reported groups (Bowman, 2013; Hop et al., 2020). Particularly, two species are found in high abundances in Arctic sea ice; *Melosira arctica* and *Nitzschia frigida* (Olsen et al., 2017; Hop et al., 2020). The accumulation of algal biomass of *Melosira* at the bottom of the sea ice and their subsequent fast export as aggregates can provide large amounts of organic matter to the seafloor (Boetius et al., 2013).

Microbial communities can be entrained in the sea ice during freeze-up, trapped at the bottom of the sea ice in sub-surface waters or invade through existing brine channels and fissures (Caron et al., 2017; Petrich and Eicken, 2017). Bacteria and archaea are incorporated into the growing sea ice carried by algae or attached to organic and inorganic particles (Gradinger and Ikävalko, 1998; Weissenberger and Grossmann, 1998), or from open water areas by winds and aerosol deposition (Ewert and Deming, 2013). During sea ice formation microorganisms and other compounds like dissolved organic matter (DOM) or extracellular polymeric substances (EPS) produced by algae and bacteria (Decho and Gutierrez, 2017), are rejected by the growing ice lattice and released to the water within the ice. Therefore, brine channels, pores and liquid inclusions are the inhabited fraction of the sea ice (Junge et al., 2001), where the microbes experience high concentrations of nutrients and are protected from fluctuations in the sea ice and grazing. Sea ice that survives no more than one winter is denominated first-year ice (FYI), whereas thicker and older ice (> 0.3 m) which survived at least two summers' melt is categorized as multi-year ice (MYI). These ice types differ in structural and physicochemical characteristics (Eicken et al., 1995; Petrich and Eicken, 2017), as well as in microbial community composition (Bowman et al., 2012; Hatam et al., 2014; Boetius et al., 2015). MYI can host distinct bacterial communities at different depths (Hatam et al., 2014), but the diversity and volume of cells and diversity of bacterial assemblages is usually higher in the bottom ice. Bacterial cell densities can reach up to ~ 10^7 cells/mL in MYI and FYI (Junge et al., 2002; Hatam et al., 2014). Moreover, the lower section of the sea ice

(~ < 30 cm) contains the majority of chlorophyll content and bacterial biomass, and is where most of the exchange with the underlying sea water occurs (Bowman, 2013).

Most commonly identified bacterial and archaeal orders in sea ice studies include members of the *Gammaproteobacteria* (the orders: *Alteromonadales*, *Oceanospirillales*, and *Pseudomonadales*), *Bacteroidetes* (*Flavobacteriales*), *Alphaproteobacteria* (*Rhodobacterales* and *Rickettsiales*) and *Thaumarchaeota* (*Nitrosopumilales*), and with less abundance *Verrucomicrobia* and *Bacilli* and, although rare, cyanobacteria have also been detected but only in ice-melt waters (Harding et al., 2018). Among the dominant genera are heterotrophic cold-adapted bacteria capable to efficiently exploit the high concentrations of EPS and DOM (Bowman et al., 2012; Hatam et al., 2014). Such taxa include *Pseudoalteromonas*, *Shewanella*, *Polaribacter*, *Psychrobacter*, *Psychroflexus, Flavobacterium, Glaciecola*, *Colwellia, Marinobacter, Marinomonas, Octadecabacter, Sulfitobacter* and the archaea *Marine Group I* (Boetius et al., 2015; Deming and Eric Collins, 2017; Rapp et al., 2018). As for viruses, only bacterial phages of the *Siphoviridae* and *Myoviridae* double-stranded DNA viruses have been ascribed to sea ice (Deming and Eric Collins, 2017). In the sea ice, nutrient regeneration occurs primarily in the autochthonous microbial loop (Figure 4). Bacteria, archaea, heterotrophic eukaryotes and viruses transform organic matter, mainly in the form of dead cells, EPS, DOM, POC and DOC produced by photosynthesis, to nutrients supporting primary production and higher trophic levels (Lizotte, 2003; Bowman, 2013).

During sea ice formation and ice melt, rejected DOM and EPS are released to the underlying seawater, supplying a significant amount of labile carbon (Thomas et al., 2009), and with it associated microbial communities, but this mechanism of microbial inoculation is poorly understood.

1.7.2 The pelagic ecosystem

Marked by strong seasonal variation in light, nutrients and temperature, the water column of the AO harbours different eukaryotic, bacterial and archaeal communities throughout the year. The summer phytoplankton community is usually dominated by diatoms (*Thalassiosira*, *Chaetoceros* and *Fragilariopsis*), coccolithophores mainly *Emiliania huxleyi*, flagellates

(*Phaeocystis)*, dinoflagellates and nanoflagellates (Nöthig et al., 2015). Whereas mainly copepods, amphipods and chaetognaths dominate the zooplankton community in spring and summer (Nöthig et al., 2015; Schröter et al., 2019; Ramondenc et al., 2022). However, long-term changes in species composition and elemental matter fluxes were observed within the last decade (Lalande et al., 2013; Nöthig et al., 2015). Previous studies of summer Fram Strait communities, based on sequencing of the 16S rRNA and 18S rRNA genes, indicated that bacterial community structure was driven by the eukaryotic phytoplankton bloom stage reflected by the different communities in ice-free and ice-covered regions of the Strait. In the eastern Fram Strait where the ice is the absent for much of the year, bacterial taxa of the *Bacteroidetes* (*Flavobacteriales*), *Gammaproteobacteria* and *Alphaproteobacteria* (*Rhodobacterales*), and for the eukaryotes mainly diatoms of the *Bacillariophyta* and heterotrophic protists (plankton affiliated with marine stramenopiles (MAST)), prevailed in surface waters following phytoplankton blooms (Wilson et al., 2017; Fadeev et al., 2018; Wietz et al., 2021). Picoeukaryotes are also part of the phytoplankton community and are represented by *Micromonas* and *Bathycoccus,* particularly in the warmer WSC (Kilias et al., 2013, 2014). Surface waters in the EGC experience a higher influence of sea ice, which also affects the microbial composition of the water column and the export of carbon (Fadeev et al., 2021a). Summer assemblages of the EGC are mostly represented by SAR11, SAR202, SAR406, SAR324, *Bdellovibrionaceae, Colwelliaceae* and alveolates (*Syndiniales*) (Fadeev et al., 2018; Wietz et al., 2021). Generally, with depth, the relative abundance of archaea increases along with lesser-known clades: SAR202, SAR406 and members of the former *Deltaproteobacteria* order (i.e. SAR324) (Wilson et al., 2017; Müller et al., 2018; Fadeev et al., 2021a).

In the Arctic pelagic ecosystem, cell abundances of bacteria and archaea vary differently with depth, a similar pattern observed in other regions (Karner et al., 2001; Herndl et al., 2005; Kirchman et al., 2007). Compared to bacteria, proportions of the most common Arctic archaea, i.e. *Thaumarchaeota* were seen to increase to 40% at the epipelagic of these waters (Kirchman et al., 2007). The most commonly found archaeal taxa in the AO water column is the *Thaumarchaeota* (Alonso-Sáez et al., 2008; Müller et al., 2018). Ubiquitous in the deeper waters of the world's oceans, in part because they comprise of ammonia-oxidizing archaea (AOA) (Pester et al., 2011; Zhong et al., 2020), the abundance of *Thaumarchaeota* displays a

seasonal pattern in polar oceans (Church et al., 2003; Alonso-Sáez et al., 2008; Christman et al., 2011). Proportions of *Thaumarchaeota* increase in the winter and decline during summer (Alonso-Sáez et al., 2008). Based on 16S rRNA gene sequencing and qPCR analyses in Atlantic water off the Northwest of Svalbard, the abundance of *Thaumarchaeota* was reported to reach 44% of the community during the winter and less than 2% during the summer (Müller et al., 2018). The authors also suggested a role of the different water masses in shaping the distribution and dispersal of *Thaumarchaeota.* The relevance of *Thaumarchaeota* taxa (the order *Nitrosopumilales*) was also recently observed in the eastern Fram Strait during the winter months when the water column enters a regenerative state (Wietz et al., 2021). *Nitrosopumilales* strongly dominated archaeal assemblages in the first 50 m of a station in the WSC. These observations suggest that ecological role of AOA in nutrient cycling in the water column should be further explored.

1.8 Ecological alterations due to global climate change in the AO ecosystem

1.8.1 Climate change impacts in the AO

Global climate change is amplified in the AO, manifesting in increasing air and water temperatures that result from multiple feedback mechanisms associated with increases in atmospheric CO_2 levels (Serreze et al., 2009). The increases in near-surface air temperatures are 2 to 3 times faster than in other regions, a phenomenon recognized as "Arctic Amplification" (Serreze and Barry, 2011). The warming of the AO has been increasingly faster than any other region, almost four times as previously predicted (Rantanen et al., 2022) and the subsequent rapid decline in sea ice extent has led to measurable changes in the Arctic ecosystem (Wassmann et al., 2011). Today the significant loss of sea ice is recognized as a signature of anthropogenic warming (Meredith and Sommerkorn, 2022). Recent model predictions based on a selection of climate models that best represented the Arctic sea ice state and northward ocean heat transport, suggest that the AO will experience an ice-free summer as early as in 13 years (Docquier and Koenigk, 2021), and well within the first half of this century (Overland and Wang, 2013).

The AO has experienced a strengthened inflow of an increasingly warmer AW (Tsubouchi et al., 2021), a process referred to as "Atlantification" (Polyakov et al., 2017). The advection of anomalous Atlantic and Pacific waters into the Arctic Ocean interior is referred to as "borealization" (Polyakov et al., 2020a). The changes are most pronounced in the surface ocean (Polyakov et al., 2020b) with effects on primary productivity and cascading effects to higher consumer levels (Ardyna and Arrigo, 2020). Changes in primary production in the sea ice and water column have become evident (Lewis et al., 2020).

Recent pan-Arctic long-term assessments of chlorophyll *a*, sea surface temperature (SST) and sea ice concentration from 1998-2018 observed an increase of phytoplankton net primary production (NPP) due to more open water and a higher influx of nutrients (Lewis et al., 2020). The reported increase of NPP based on satellite measurements is ~57% for the AO (Lewis et al., 2020) much more than previously reported (Arrigo and van Dijken, 2015). Such changes were attributed to changes in climate-related events including more storm-induced upwelling (Zhang et al., 2010), enhanced wind mixing (Zhang et al., 2004), shelf break upwelling (Tremblay et al., 2011) and higher influx of nutrients from riverine discharge (McClelland et al., 2006) and higher terrestrial input of nutrients (Terhaar et al., 2021). Since 2009 the rate of open water area in the Fram Strait region has increased considerably compared to other regions of the AO (Lewis et al., 2020). Alternatively, localized studies in different areas of the AO suggest a reduction in the primary production mainly as a result of the freshwater flux from sea ice melt, higher river runoff (Nummelin et al., 2016), glacial discharge (Hopwood et al., 2020) and decreased light availability due to higher cloud formation (Bélanger et al., 2013). For instance, a stronger stratification of the water column could limit nutrient supply to the surface limiting the growth of phytoplankton (McLaughlin and Carmack, 2010). Thus, how climate change and associated changes across the Arctic will affect primary producers and associated microbial communities at the base of the food web, remains a topic of scientific debate.

1.8.2 Ecological alterations in the Fram Strait

At the eastern Fram Strait, a warm water anomaly (WWA) event was recorded between late 2004, reaching a peak in 2006, and persisting until its descent in 2008 (Beszczynska-Möller

et al., 2012). This period was defined as the WWA of 2005-2007, and was characterized by an increase of the mean temperature at the core of the WSC reaching 4.4°C (exceeding the range of 3 -3.5 °C core temperature of the AW) (Beszczynska-Möller et al., 2012). Furthermore, it was observed that the winter export of sea ice through Fram Strait, which is connected to an increase in the Transpolar Drift velocity (Krumpen et al., 2019), is influenced by the Arctic dipole (AD) (Smedsrud et al., 2017).

During this period, a shift in phytoplankton composition and zooplankton occurrences was observed (Weydmann et al., 2014; Nöthig et al., 2015; Soltwedel et al., 2016; Schröter et al., 2019; Ramondenc et al., 2022). The most remarkable sign of change was the transition from diatom- to flagellate-dominated (*Phaeocystis* spp) phytoplankton communities (Nöthig et al., 2015). Diatom-dominated aggregates related to sea ice presence can drive higher carbon export (Fadeev et al., 2021a), whereas the small buoyant colonies that *Phaeocystis* forms sink slower, with consequences for carbon export (Lalande et al., 2013), and lower microbial vertical connectivity (Fadeev et al., 2021a). Moreover, the AD showed a strong long-time correlation with changes in zooplankton composition and carbon export in the eastern Fram Strait (Ramondenc et al., 2022). Such changes are expected to continue affecting carbon export (Vernet et al., 2017), as well as microbial communities.

1.9 Thesis objectives

The thesis focused on understanding the composition, distribution and function of bacteria, archaea and eukaryotic communities in Fram Strait across different spatial and temporal scales. Samples included in this dissertation covered a variety of habitats; sea ice, seawater and sinking particles to be able to address functions and niches of different bacterial groups. Samples were obtained in the framework of the Long-Term Ecological Research (LTER) site HAUSGARTEN and the FRontiers in Marine Monitoring (FRAM) program. The aim of the thesis was to elucidate compositional and functional dynamics of microbial communities in different regions of Fram Strait and their relationship to environmental conditions. The ultimate goal was to identify signature groups and key factors of change, to provide a baseline to the effects of climate change and sea ice retreat. The following questions were addressed in this thesis:

i. Do gene expression and distribution (standing stocks) of key taxonomic groups in the water column differ across different regions of Fram Strait and why?

The examination and assessment of composition and metabolic diversity of microbial communities is essential to better understand ecosystem functioning. To date, the majority of Arctic microbial community studies are performed using high-throughput sequencing of the 16S and 18S rRNA genes. Yet, molecular analysis at the transcriptional level are key to defining metabolic pathways and adaptations of the active Arctic microbiome. Moreover, primer-based studies provide information about diversity and community composition, however the abundances in such datasets are not representations of absolute standing stocks due to the use of polymerase chain reaction (PCR), primers and other quantitative biases. In Chapters I and II I aimed to provide a comprehensive base knowledge of gene expression and distribution in abundance of the communities at the surface and at depth in different regions of Fram Strait influenced by either of the main water currents, and thus characterized by different temperature and sea ice conditions. Chapter I offers a first overview of genomic expression and key functional repertoire of microbial communities in surface (15 m – 25 m) and epipelagic (100 – 200m) waters, and explore the factors driving the genomic expression. In Chapter II, I used CARD-FISH and semi-automated cell counting to quantify the standing stocks of previously identified key *Bacteria* and *Archaea* taxonomic groups in the water column and their association with the ecosystem state in the two major regions of Fram Strait.

ii. Which factors govern variations in the bacterial and eukaryotic composition of sinking particles in Fram Strait over a time frame of 12 years?

The documented increases in seawater temperature between 2005 and 2007 and the elevated sea ice export through Fram Strait have been accompanied by changes in the development of phytoplankton blooms and migration patterns of zooplankton (Nöthig et al., 2015; Ramondenc et al., 2022). These shifts in the phytoplankton and zooplankton communities were reflected in the composition of particle export fluxes (Lalande et al., 2013). More recent studies identified that larger particle sizes and higher sinking rates in the presence of sea ice in Fram Strait led to stronger vertical microbial connectivity (Fadeev et

al., 2021a; von Appen et al., 2021). Therefore, in Chapter III, I used molecular and statistical techniques to address the interannual variability in the microbial composition of sinking particles during peak export phases, together with biogeochemical export fluxes during high carbon export events in spring and summer, and evaluated their correlation to a warm-water anomaly event between 2005 and 2007. Furthermore, I explored the impacts of varying environmental and oceanographic conditions on the seasonality of the sinking particles by comparing spring and summer communities.

iii. How do sympagic and pelagic bacterial and eukaryotic communities respond to ice melt in a microcosm experiment?

A key feature of global climate change is the rapid sea ice decline of the AO. Sea ice provides a habitat for all domains of life. Microbial communities inhabiting the bottom sea ice are important in mediating carbon export from the sea ice to surface water. The presence of sea ice has shown to influence the microbial composition of the surrounding surface and under-ice seawaters of the central Arctic (Hardge et al., 2017; Rapp et al., 2018), but was yet to be explored at the marginal ice zone in Fram Strait. In Chapter IV I aimed at providing a better understanding of the microbial connectivity between sea ice and the surrounding water during ice melt conditions using a microcosm experiment. The ship-based experimental approach offered a unique opportunity to assess bacterial and eukaryotic communitiy dynamics under short time scales and controlled experimental conditions. Chapter IV provided insights into potential bacterial and eukaryotic responses to accelerated sea ice melt.

1.10 Publication outline

Chapter I

Functional gene expression of microbial communities in different water masses during an Arctic late summer phytoplankton bloom

Magda G. Cardozo-Miño, Harald Gruber-Vodicka, Alexandra Kraberg, Anabel von Jackowski, Katja Metfies, Sinhué Torres-Valdés, Anja Engel, Christina Bienhold, Antje Boetius and Massimiliano Molari

Publication in preparation.

This study was conducted to provide a comprehensive picture of active microbial communities and variations in gene expression in different regions of Fram Strait. We obtained metatranscriptomic data from surface and deep waters of Fram Strait during the seasonal sea ice minimum and explored how active microbial communities and gene transcription change in accordance to water masses and environmental conditions. We identified microbial responses to a decaying phytoplankton bloom at the surface whereas deep waters were governed by chemoautotrophic activities. This study offers novel insight into active taxa and the diverse ecological niches they fulfil at surface and with depth.

Contributions: MC-M and MM designed the study. MC-M conducted the sampling and RNA extraction of the samples. AK provided the microscopy overview of eukaryotic groups. AJ and AE provided the carbohydrate and amino acids data. STV provided the nutrient data. MC-M analyzed the data and wrote the manuscript with the guidance of all co-authors.

Chapter II

Spatial Distribution of Arctic Bacterioplankton Abundance Is Linked to Distinct Water Masses and Summertime Phytoplankton Bloom Dynamics (Fram Strait, 79°N)

Magda G. Cardozo- Miño, Eduard Fadeev, Verena Salman-Carvalho and Antje Boetius

Published in Frontiers in Microbiology 12, 1067. doi:10.3389/fmicb.2021.658803.

This study focused on the assessment of the standing stocks of key taxonomic groups and their association with phytoplankton bloom conditions in summer ice-free and ice-covered regions of the Fram Strait. Using CARD-FISH and high-throughput cell counting, we quantified 14 ecologically relevant groups of bacterioplankton (*Bacteria* and *Archaea*) from surface down to deep waters. We observed, that cell abundances were driven by variations in phytoplankton bloom conditions across the Strait. This study provided the first extensive quantification of bacterioplankton community standing stocks down to the deep Arctic water column (> 500 m). Our results suggest that predicted longer seasonal phytoplankton blooms, and the Atlantification of the AO will lead to major changes in the composition and

distribution of key taxonomic groups in surface Arctic waters. This publication provided insights into factors structuring pelagic bacterioplankton communities free of quantitative bias as a baseline to better assess future changes in the region.

Contributions: MC-M, EF, and VS-C designed and conducted the study, and wrote the manuscript with guidance from AB. MC-M performed the hybridizations, cell counting, data and statistical analysis with guidance from VS-C and EF.

Chapter III

12 years of microbial community dynamics on sinking particles in the eastern Fram Strait

Magda G. Cardozo-Miño, Ian Salter, Eva-Maria Nöthig, Katja Metfies, Simon Ramondenc, Claudia Wekerle, Thomas Krumpen, Antje Boetius and Christina Bienhold

Publication in preparation.

This study covered a timeframe of more than a decade (2000-2012), studying microbial dynamics in sinking particles during high carbon export events. We applied next generation sequencing of the 18S and 16S rRNA genes to archived sediment trap samples deployed around 200 m in the water column of Fram Strait. We studied the eukaryotic and bacterial community composition and structure, and their relationship with environmental parameters marked by a warm water anomaly between 2005 and 2007. We observed that microbial composition suggested the development of a more effective retention system at the time of the warm anomaly. This study highlights the relevance of long-term studies to better understand and predict microbiome and ecosystem dynamics. Ultimately, this will help us to formulate expected consequences for the long-term Arctic biological carbon pump.

Contributions: IS, EMN, KM, CB and AB conceived and designed the study. KM and IS conducted Illumina sequencing of the samples. EMN provided background and data for the sediment trap time-series. SR determined the distance to the sea ice edge from remote sensing data products. CW obtained the catchment area from a backward Lagrangian model. IS, TK and CW provided weighted means of sea ice coverage, SST and chlorophyll. MC-M analyzed the data and wrote the manuscript with guidance from CB, IS, EMN and AB.

Chapter IV

Ice-seawater connectivity of eukaryotes, bacteria and metabolites

Magda G. Cardozo-Miño, Julian Merder, Silvia Vidal-Melgosa, Katja Metfies, Thorsten Dittmar, Jan-Hendrik Hehemann, and Matthias Wietz

Publication in preparation.

In this chapter we focused on microbial connectivity between sea ice and the underlying seawater. We conducted a microcosm experiment performed on board of R/V Polarstern PS121. Sea ice cores at the MZI of Fram Strait were inoculated in the surrounding seawater and the changes in microbial composition tracked using next-generation sequencing of the 18S and 16S rRNA genes. We identified a large exchange of eukaryotic and bacterial communities between habitats, and the seeding of sea ice diatom species to the surrounding water, as well as the increase in abundance of *Flavobacteriales* coincided to the seeding of diatoms. Sequence abundance of the *Verrucomicrobiae* and *Rhodobacterales* were linked to substrate sourced from ice. Our results highlight the relevance of experimental approaches to understand microbial responses to accelerated ice melt.

Contributions: MW and MC-M conceived and designed the study. KM and conducted Illumina sequencing of the samples. JM conducted the molecular analysis of DOM via FT-ICR-MS with the support of TD. SVM conducted the extraction of monosaccharides. MC-M analyzed the data and wrote the manuscript with guidance from MW, JD, KM and AB.

Chapter I

Functional gene expression of microbial communities in different water masses during an Arctic late summer phytoplankton bloom

Magda G. Cardozo-Miño[1,2,3], *Harald Gruber-Vodicka*[1], *Alexandra Kraberg*[2], *Anabel von Jackowski*[4], *Katja Metfies*[2], *Sinhué Torres-Valdés*[2], *Anja Engel*[4], *Christina Bienhold*[1,2], *Antje Boetius*[1,2,3,5] *and Massimiliano Molari*[1]

[1]Max Planck Institute for Marine Microbiology, Bremen, Germany
[2]Alfred Wegener Institute, Helmholtz Center for Polar and Marine Research, Bremerhaven, Germany
[3]Faculty of Geosciences, University of Bremen, Bremen, Germany
[4]GEOMAR Helmholtz Centre for Ocean Research Kiel, Kiel, Germany
[5]MARUM, University of Bremen, Bremen, Germany

Keywords: Fram Strait, Arctic Ocean, water column, metatranscriptomics, differential expression

Publication in preparation.

Abstract

The Arctic Ocean is continuing to experience loss in sea ice cover and increasing water temperatures as part of ongoing global climate change. Fram Strait, the only deep-water connection between the Arctic and the Atlantic Ocean offers a unique opportunity to study future Arctic scenarios due to the opposing water currents that carry different water masses that are characterized by differences in sea ice cover, water temperature and nutrient concentrations. Previous studies have provided first insights into regional and temporal patterns of microbial communities and their metabolic potential. However, no studies have yet provided molecular analyses at the transcriptional level, to investigate patterns of the active microbiome. Here, we studied metatranscriptomes from surface waters at the deep chlorophyll maximum (15 m – 25 m) and from epipelagic waters (100 m – 200 m), targeting different water masses during the seasonal sea ice minimum. We observed that, at the time of sampling, gene transcription is accorded with a decaying phytoplankton bloom dominated by *Skeletonema*, *Fragilariopsis* and *Eucampia* in the eastern Strait and by *Chaetoceros* in the western Strait. Active functions allowed us to create a complete picture of the active microbiome by also identifying phages (*Myoviridae* and *Siphoviridae*) and archaeal groups, which are often overlooked in other studies by inherent primer biases. Enrichment analyses of key functions and main taxonomic groups highlighted the activity of particle-associated *Bacteroidetes*, *Gammaproteobacteria* and *Alphaproteobacteria* in surface waters of the Polar Surface Water (PSW) and Warm Polar Surface Water (PSWw) responding to the progression of the phytoplankton bloom, whereas ammonia-oxidizing archaea (*Nitrosopumilales* and unclassified *Thaumarchaeota*) were significantly more active in deeper Atlantic waters (AW). Free-living bacteria *Marinimicrobia* (SAR406), SAR324 and *Thalassobaculales* were active in both water masses (AW and PSWw). SAR202 was significantly more active in the epipelagic PSW. Our results provide the first comprehensive insights into the active functions and key groups shaping the ecosystem during the warmest season of the changing Arctic Ocean.

Introduction

The Arctic Ocean is undergoing rapid changes in sea ice and temperature driven by global climate, warming and amplifying feedback mechanisms (Serreze et al., 2009; Lannuzel et al., 2020; Belter et al., 2021; Tepes et al., 2021). Today, the Arctic Ocean is recognized as the most sensitive region to climatic changes than any other oceanic region (Comiso et al., 2008), with a substantial retreat of sea ice since the late 20th century as one of the signatures of anthropogenic warming (Meredith and Sommerkorn, 2022). Currently, the Arctic Ocean is also continuously impacted by a strengthened inflow of warmer Atlantic Water (Tsubouchi et al., 2021), a term referred to as "Atlantification" (Polyakov et al., 2017). Atlantification and the counterpart "Pacification" constitute the "Borealization" of the Arctic Ocean (Polyakov et al., 2020a), and are especially noticeable in the upper 200 m of the Artic water column (Polyakov et al., 2020b). The inflow of warmer Atlantic Water occurs through Fram Strait, the main gateway to the Arctic Ocean. The Fram Strait is a hydrographically complex area with two dynamic opposing currents, the East Greenland Current (EGC) flowing southward, and the West Spitsbergen Current (WSC) flowing northward and feeding the warm Atlantic Water into the Arctic Ocean (Beszczynska-Möller et al., 2012).

The progression of anomalies from the Atlantic sector through Fram Strait may impact the circulation pathways of specific water masses that will determined the availability of nutrients in the Arctic Ocean (Polyakov et al., 2020a) with consequences on climate, ecosystem functioning, primary productivity (Lewis et al., 2020) and food web configuration (Kortsch et al., 2015). Furthermore, the overall warming of the Arctic has increased the sea ice export through Fram Strait at a higher rate since the last decade (Behnam et al., 2019). These environmental changes have already impacted the pelagic system in Fram Strait. Time series studies indicated a shift in the species composition of the summer phytoplankton bloom, from diatom-dominated towards more buoyant and abundant flagellate species of *Phaeocystis* and small pico-and nanoplankton species (Nöthig et al., 2015), with consequences for carbon export, and vertical connectivity of microorganisms (Fadeev et al., 2020). Furthermore, sea ice dynamics in the Fram Strait linked to Arctic Oscillation and the Arctic Dipole have also shown effects on zooplankton migration and export patterns (Ramondenc et al., 2022).

The microbial diversity and function of the Arctic communities in the water column of Fram Strait have been studied in the context of environmental conditions associated to water temperature and the presence and absence of sea ice cover in the marginal ice zone (MIZ) (Nöthig et al., 2015; Fadeev et al., 2018; Cardozo-Mino et al., 2021) that underline the importance to study microbial dynamics in the region (Soltwedel et al., 2016). Previous studies of summer Fram Strait communities, based on sequencing of the 16S rRNA and 18S rRNA genes, indicated that differences in bacterial community structure were driven by the eukaryotic phytoplankton bloom stage reflected by the different communities in ice-free and ice-covered regions of the Strait (Fadeev et al., 2018). In the eastern Fram Strait where the ice is absent longest throughout the year, *Bacteroidetes* (*Flavobacteriales*), *Gammaproteobacteria* and *Alphaproteobacteria* (*Rhodobacterales*), diatoms of the *Bacillariophyta* class and protists prevailed in surface waters following a phytoplankton bloom (Fadeev et al., 2018; Wietz et al., 2021). Moreover, potential-cross domain associations between bacteria and eukaryotes have been envisioned to shift with substantial changes in the overall microbial community structure (Fadeev et al., 2018). However, the linkages between bacteria, primary producers and even the role of viruses remains larger understudied in the Arctic region. Bacterial taxa that are part of the "microbial dark matter" in this area (Rinke et al., 2013) include the SAR202 clade and *Marinimicrobia* (SAR406 clade), which are associated with Arctic winter conditions at the ice-covered EGC (Fadeev et al., 2018). With depth, the consistency of SAR202, *Marinimicrobia* and SAR324 in cell abundances further suggest significant roles in the ecological system (Cardozo-Mino et al., 2021). Moreover, archaeal sequences are abundant in the Arctic deep waters, comprising ~20% of the sequences in mesopelagic waters (> 200 m) (Wilson et al., 2017; Müller et al., 2018; Fadeev et al., 2021a). Particularly, the *Nitrosopumilales* are among the taxa that mark the end of the productive season, likely contributing to nutrient replenishment (Wietz et al., 2021). More recently, the phylogenetic and functional diversity of key bacterial groups were analysed via metagenomics in the EGC and WSC that are characterized by different sea ice conditions (Priest et al., 2022), and several common bacterial taxa could be associated with potential pathways in the local carbon and nitrogen cycling, however and to what extent these pathways are actively transcribed remains unknown. Moreover, the microbial community in the marine water column is comprised of a complex network of eukaryotes,

bacteria, archaea, and viruses, underlining the need to understand the totality of groups at play, to gain a robust view of the active ecosystem.

Gene expression of microbial communities is key to understand current biogeochemical and ecological processes to project activities in the future ice-free Artic. In this study, we sampled in the upper 200 m at the MIZ of Fram Strait at the Long-Term Ecological Research (LTER) site HAUSGARTEN, because the seasonality and oceanographic characteristics that mark the phytoplankton bloom (light availability, extend of stratification, nutrient and water temperature) mostly fluctuate here (von Appen et al., 2021). The sampling period occurred in the late summer season of 2019, approaching the time when Arctic sea ice extent reached its seasonal minimum and the ice margin was notably further North than in previous years. In fact, by September 2019, the decadal trend of sea ice decline reached ~13% and the sea ice extend was the second lowest after 2012 (Melsheimer and Spreen, 2019; Yadav et al., 2020). Furthermore, we targeted stations located at the EGC and WSC to target microbial communities under different environmental conditions and water masses with the aim to investigate and provide a comprehensive picture of the active microbial communities and gene expression in different regions of Fram Strait. We hypothesized that 1) different water masses harboured different active taxa that allowed for ecosystem state evaluation, 2) active communities and gene transcriptions of bacteria and archaea groups were linked to phytoplankton bloom states and conditions, and that 3) key active functional groups showed significant differences with size fraction and depth.

Materials and Methods

Sampling and remote sensing data

Sampling was performed during the RV Polarstern expedition PS121 to Fram Strait (10th August – 13th September 2019) at the end of the summer season. Samples were retrieved at the Long-Term Ecological Research (LTER) site HAUSGARTEN from 5 stations targeting different sea ice conditions and water masses (Figure 1A). To investigate the different communities and functions expressed by microbial communities in different size fractions (> 10, 10 – 3 and 3 – 0.2) under different environmental conditions, in-situ pumps (Large Volume

Pump WTS-LV, McLane Research Laboratories Inc., East Falmouth, MA, USA) were deployed at two water depths targeting the surface deep chlorophyll maximum (DCM) (15 m – 25 m) and the epipelagic at 100 m (Figure 1). The in-situ pumps were deployed along the Conductivity-Temperature-Depth (CTD) rosette (Sea-Bird Electronics Inc. SBE 911 plus probe, Bellevue, WA, USA) winch system. The CTD rosette was equipped with temperature, pressure and conductivity sensors, a chlorophyll fluorometer, an altimeter and a transmissometer. Hydrographic data including temperature and salinity of PS121 were retrieved from PANGAEA (Metfies et al., 2021). The DCM was determined based on chlorophyll *a* fluorescence during the downcast. Samples were obtained during the upcast, however, due to an error during deployment, the pump deployed at EGI 100 m started filtration already at 200 m, filtering for 20 minutes during the upcast as the pump travelled to 100 m, but later once the pump reached the targeted depth it filtered water for 2 hours. At the surface, the in-situ pumps filtered 100 – 200 L water through successive polycarbonate Nucleopore Track-Etch filters (Whatman, Buckinghamshire, UK) with the pore sizes of 10 µm, 3 µm and 0.2 µm (142 mm diameter each). At 100 m in the epipelagic, the in-situ pumps filtered water through filters with the pore sizes of 3 µm and 0.2 µm. Upon recovery, the filters were quickly removed from the pumps, cut in half with sterile and ethanol-rinse scalpels and immediately frozen in liquid N_2. All samples were stored at -80°C until further processing in the home laboratory. The sampling map, biogeochemical and physical parameters profiles were produced using Ocean Data View v 5.6.2 (Schlitzer, 2018).

Distance of the sea ice edge (defined at 15% sea ice concentration) to the mooring site and ice concentration at each station (EGI, N4, HGI and F4) using a 12 km radius were determined from remote sensing data. Satellite images of daily sea ice measurements were obtained from NSIDC/NOAA (http://nsidc.org/data/nsidc-0051). The images were generated using the NASA Team algorithm (Cavalieri, 2003) and mapped to a 25 x 25 km grid. This satellite data set was derived from brightness and temperature data generated from Scanning Multichannel Microwave Radiometer and Sensor Microwave Imager and Sounder equipped on the Nimbus-7 satellite and the Defence Meteorological Satellite Program, respectively. The sea ice concentration product was provided by CERSAT and is available on a 12.5 x 12.5 km grid (Ezraty et al., 2007).

Fractionated chlorophyll *a*, nutrients, carbohydrates and amino acids

Chlorophyll *a* concentrations were obtained with the niskin bottles of the CTD and used as a proxy for phytoplankton biomass and were obtained from 3 µm and 0.4 µm polycarbonate Nucleopore Track-Etch filters (Whatman, Buckinghamshire, UK), then processed following the protocol described by (Nöthig et al., 2020).

To further understand the ecosystem state and the phytoplankton phase we analysed nutrient concentrations, carbon and nitrogen sources in the water column in the different regions of the strait. For this, raw nutrient concentrations (silica (SiO_3), nitrate (NO_3), phosphate (PO_4) and ammonium (NH_4)) were obtained from samples collected from the CTD cast. Water samples were collected in 50 mL Falcon tubes from selected depths and stored frozen at -20°C for later analysis at the AWI following the protocol of (Torres-Valdés et al., 2013). Dissolved organic carbon (DOC) was sampled at the station and depths covered in this study. Duplicate samples were filtered through 0.45 µm GMF GD/X filters (Whatman, GE Healthcare Life Sciences, UK) and collected in combusted glass ampoules (8 h, 450°C), acidified and stored at 4°C until further processing as in (Engel and Galgani, 2016).

Duplicate samples for high-molecular- weight (> 1 kDa) dissolved combined carbohydrates (DCCHO) were filtered through 0.45 µm Acrodisk filters (Pall Corporation, USA), collected in combusted glass vials (8 h, 450°C) and frozen (-20°C) until analysis. DCCHO analysis was conducted by high-performance anion-exchange chromatography coupled with pulsed amperometric detection (HPAEC-PAD, ICS 3000, Dionex, USA) with a detection limit of 10 nmol L^{-1} (Engel and Händel, 2011). HPAEC-PAD classified 6 neutral sugar monomers: arabinose, fucose, galactose, glucose, rhamnose, and co-elute mannose and xylose. Additionally, HPAEC-PAD classified the amino acids galactosamine and glucosamine as well as the acidic sugars galacturonic acid and glucuronic acid.

Duplicate samples for dissolved hydrolysable amino acids (DHAA) were filtered through 0.45 µm Acrodisk filters (Pall Corporation, USA), collected in combusted glass vials (8 h, 450°C) and frozen (-20°C) until analysis. DHAA were measured with ortho-phthaldialdehyde derivatization by high-performance liquid chromatography (HPLC, Agilent Technologies,

USA) equipped with a C18 column (Phenomenex, USA) with a precision of less than 5% and detection limit of 2 nmol L^{-1} (Lindroth and Mopper, 1979; Dittmar et al., 2009). The analysis classified 8 essential amino acid monomers: alanine, isoleucine, glycine, leucine, phenylalanine, threonine, tyrosine, and valine. Furthermore, analysis classified 5 non-essential amino acid monomers: arginine, aspartic acid, glutamic acid, gamma-aminobutyric acid (GABA), and serine.

RNA extraction and sequencing

Total RNA was extracted from the half filters using the mirVana™ miRNA Isolation Kit (Ambion Inc, Austin, TX, USA). Prior to extraction, the filter pieces were embedded in the Lysis/Binding Buffer and homogenised by cutting the filter section in several pieces and vortexing for about 30 seconds in 10 second intervals. After sample homogenization and cell lysis, RNA was extracted by including an organic extraction step with a volume of Acid-Phenol Chloroform. The extraction continued according to the manufacturer's instructions. DNA was removed using the TURBO DNA-free™ Kit (Ambion Inc, Austin, TX, USA) based on the manufacturer's instructions. RNA was purified and concentrated with the RNeasy® MinElute® Cleanup kit (Qiagen GmbH, Hilden, Germany). The final product was eluted in 30 µl of RNAsecure™ reagent (Ambion Inc, Austin, TX, USA) 1x pre-heated at 60°C and cooled down at room temperature. RNA extracts were stored at -80°C.

RNA library preparation and sequencing

The integrity of RNA extracts was reviewed and quantified in a fragment analyser (Agilent Technologies, Santa Clara, CA, USA). Multiple extractions were pooled to obtain approximately 100 ng of RNA per sample. Library preparation and sequencing was conducted at the Max-Planck-Genome-Centre in Cologne, Germany. An Illumina-compatible RNAseq library was produced with the NEBNext Ultra™ II Directional RNA Library Prep Kit for Illumina (New England Biolabs, Ipswich, MA, USA) with total RNA as an input. Libraries were then sequenced by sequencing-by-synthesis on a HiSeq 3000 device in 2 x 150 bp paired end read mode followed by data trimming to 1 x 150 bp to obtain 80 to 100 million reads per library/sample (Table S1).

Metatranscriptomic read processing, assembly, annotation and analyses

Sequencing adapters and contaminants if present were removed with BBDuck from BBmap (BBMap – Bushnell B., https://sourceforge.net/projects/bbmap/) (v. 38.79) with a kmer size of 27. Overall quality of the reads was assessed with FastQC (v. 0.11.9) (https://www.bioinformatics.babraham.ac.uk/projects/fastqc/) and checked for primarily sequence length distribution, per-base sequence quality and per sequence quality scores. The sequences were quality filtered using Trimmomatic (v. 0.39) (Bolger et al., 2014) with a headcrop of 10 bp, a sliding window of 4:25 and a minimum length of 100 bp. The reads were then filtered to separate rRNA from non-rRNA using SortMeRna (v. 2.0) (Kopylova et al., 2012). The rRNA sequences (3 million reads) were used to reconstruct the small-subunit rRNA (SSU rRNAs) with phyloFlash (v. 3.4) (Gruber-Vodicka et al., 2020). The SSU rRNAs sequences were taxonomically classified using the SILVA 16S rRNA gene non-redundant reference database release 138 (Quast et al., 2013) and the PR2 (v. 4.14) 18S rRNA database (Guillou et al., 2013).

To compare microbial community structure between the stations at individual SSU rRNAs, all the reconstructed sequences of SSUs rRNAs were first concatenated and then clustered at 100% identity to remove the redundancy (VSEARCH v. 2.15.1) (Rognes et al., 2016). The SSUs rRNA representatives for each cluster were used to build a SSU rRNAs catalogue. The transcriptomic reads (50 million reads per sample) were mapped to the SSU rRNAs catalogue using BBmap (v. 38.79) and converted in counts per gene (Table S2). A Mantel test (with 999 permutations) was carried out to test the correlations between similarity of the microbial communities based on single reads and reconstructed SSU rRNAs (Figure S1). The rarefaction curves were calculated to check that the SSU rRNAs catalogue covered the microbial diversity.

Non-rRNA reads were de novo assembled with rnaSPAdes (v. 3.14.1) (Bushmanova et al., 2019). To maximise the reconstruction of contigs, the reads were assembled in different ways: single-library assembling for each sample, co-assembling of multiple-libraries from all the samples and from subsets of samples i.e. based on depth or size fraction to potentially recover genes with too low abundance to be assembled in the individual samples. Quality of

the single assemblies and co-assemblies was checked via rnaQUAST (v. 2.2.2) (Bushmanova et al., 2016). All assemblies and co-assemblies were used to construct gene catalogue, similarly as described for SSU rRNAs. Contigs were then concatenated, the redundancy removed with VSEARCH (v. 2.15.1) by identifying sequences that were at least 100% identical and the output clustered to obtain the longest representative sequence via CD-HIT v4.8.1 (Fu et al., 2012) based on 100% identity and standard parameters. We analysed the frequency of number of the contigs at different lengths and kept sequences that were longer than 500 bp in the final contigs catalogue (Figure S2). The gene catalogue consisted of 664,792 contigs with a sequence length between 501 bp and 38294 bp. To examine the coverage of contigs catalogue, metatranscriptomic reads recruitment was done with BBmap (v. 38.79). The mapped reads were also used to obtain the reads per kilobase (RPK) and transcripts per kilobase million (TPM) values (Figure S3). After removal of low count reads and the centred log-ratio (clr) transformation, differential expression analyses were performed using the edgeR (v. 3.39.3) and Aldex2 (v. 1.29.1) R-packages.

Based on the output of the differential expression analysis, a selection of transcripts from the contigs catalogue were selected for annotation. MetaErg was used to obtain the amino acid sequence file of the protein coding genes. MetaErg is a fully automated metagenome and metaproteome annotation pipeline that uses Prodigal for gene prediction and relies on both Blast and hidden Markov model HMM databases (Dong and Strous, 2019). InterProScan (v. 5.55-88.0) was used to detect putative protein domains by searching against the PFAM (v. 35) database with default settings (Zdobnov and Apweiler, 2001). Genes involved in carbohydrate and protein metabolism degradation, as well as in substrate uptake were identified by performing a BLASTx search against the Carbohydrate-Active enZymes (CAZy) Database (v. 2021-09-24) (Drula et al., 2022), the MEROPS peptidase database (v. 12.4) (Rawlings et al., 2018). For membrane transport proteins we searched against the Transporter Classification Database (TCDB) (Saier et al., 2021) and the database of sulfatases SulfAtlas (Barbeyron et al., 2016). For BLASTx searches we used DIAMOND (v. 2.0.12), in sensitive mode and with a maximum e-value of 0.00001 for fast but reliable high throughput sequence alignment (Buchfink et al., 2015). The Eggnog-mapper 5.0 (Huerta-Cepas et al., 2019) provided the COG (Cluster of Orthologous Groups), and GO (Gene Ontology) annotations and to all detected genes. We further determine the predicted metabolic pathways, with the

Kyoto Encyclopedia of Genes and Genomes (KEGG) data base (Ogata et al., 1999). Annotations were compared to MetaErg, ordered by bitscore and e-value. All the statistical analyses were conducted using in R (v. 4.2.1) (www.r-project.org) and RStudio (v. 2022.07.1). Statistical analyses and clr-transformation were done using the r-packages "vegan" (v. 2.6-2) (Oksanen et al., 2013), and "tidyverse" (v. 1.3.2) (Wickham et al., 2019), and plots were generated with "ggplot2" (v. 3.3.2) (Wickham, 2016).

Results and Discussion

The physicochemical ecosystem at the late phytoplankton bloom state with less-than-usual ice cover

We sampled 5 stations (25 samples in total) located in the Fram Strait targeting the surface at the deep chlorophyll maximum (DCM) (ranging from 15 m to 25 m) and the epipelagic of each station (depths range from 100 to 200 m). Based on established definitions of water masses (Rudels et al., 2012) and physical characteristics of the water column obtained from CTD sensors (Figure 1, Table 1), we identified three distinct water masses in the two main regions of the Strait: the eastern Fram Strait was characterised by the WSC that carried water of Atlantic origin northwards, and the western Fram Strait was characterised by the EGC that carried less saline water and sea ice southwards. The surface layer (0-50 m) in the eastern part of the Strait in the WSC (stations HGIV, N4, HGI and F4) was denoted as Warm Polar Surface Water (PSWw) known to form from sea ice melting on top of the warm Atlantic water (AW). AW was identified anywhere below the ~50 m warm water layer, and hence formed the epipelagic in the eastern Strait (Figure 1A). In the western part of the Strait (at station EGI), a strong pycnocline was identified, indicating a lack of mixing. Cold Polar Surface Water (PSW) with a PSU of < 34 was located at the surface down to ~100 m, Figure 1B).

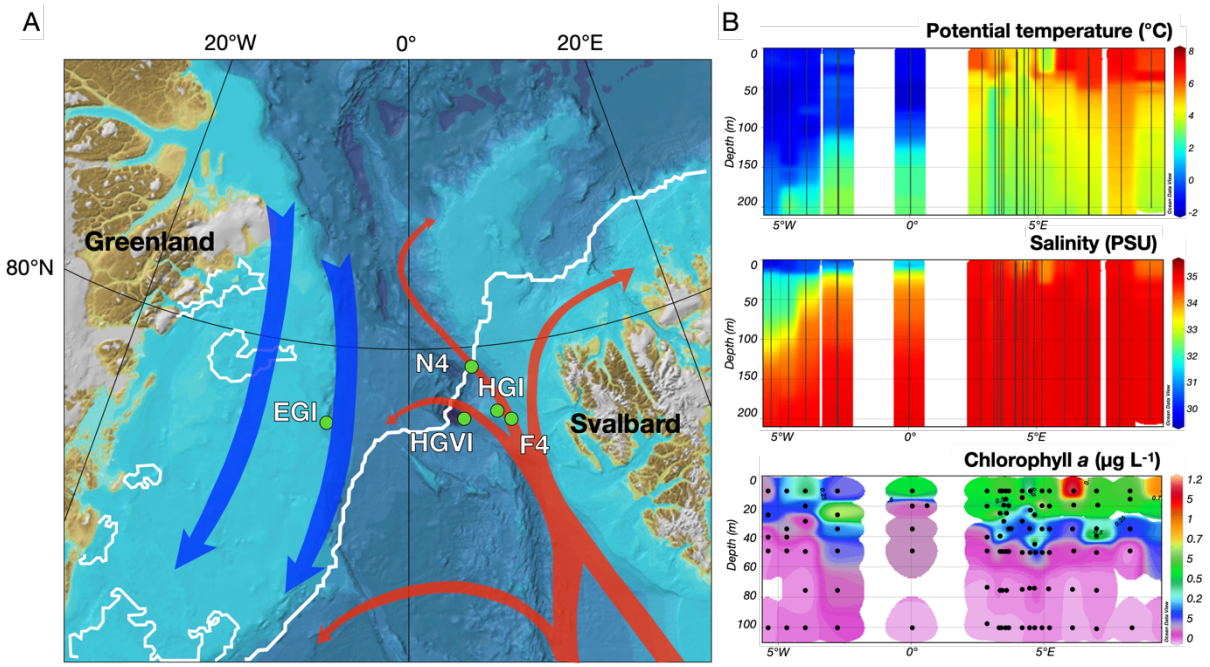

Figure 1. A) Map of the Fram Strait area depicting the sampling stations (green circles) at the HAUSGARTEN observatory (~79°00 N, ~04°20 W). Main currents are indicated by the red (WSC) and blue arrows (EGC). The white line represents the sea ice monthly median edge of August 2019. B) Main physico-chemical parameters of the water column (0 to 100 m & 200 m) obtained from CTD measurements are indicated in the panels, black lines and dots in the panels indicate the positions of the CTD profiles and sampling points for chlorophyll *a*. The map was created using ArcGIS based on the International Bathymetric Chart of the Arctic Ocean (IBCAO) Version 3.0 (Jakobsson et al., 2012). Sea ice data and station locations were exported from maps produced by AWI: https://maps.awi.de. Panel plots were generated using Ocean Data View (v. 5.6.2).

Sea ice revealed great spatial variability across sampling sites (Table 1). Arctic sea ice usually reaches its minimum extent towards September, hence none of the stations were significantly ice-covered (>15% sea ice). The ice edge was well above 79°N as the season progressed (Figure 1A). The station EGI was closest to the sea ice edge (17 km), and it was the only station with reported ice cover of 27% one week prior to sampling (Figure S4). EG stations are usually ice covered for longer times during summer, with ecological implications for the structure and composition of microbial communities (Fadeev et al., 2018; Cardozo-Mino et al., 2021). The easternmost station F4, a station at the core of the WSC, was 146 km from the sea ice edge. Other stations in the PSWw and AW were 67 – 57 km from the sea ice edge. In-situ water temperatures varied greatly across the transect. The temperature was overall colder in the epipelagic and at EGI and N4 stations (-1 – 4°C) and substantially warmer at the surface of stations F4 and HGI (6 – 7°C) (Table 1).

Chlorophyll *a* measurements obtained from the CTD sensors were overall low across the 79°N (Figure 1B), indicating the end phase of the phytoplankton bloom. We corroborated this information from fractionated chlorophyll *a* measurements, hereafter referred to as chlorophyll *a*. Higher values of chlorophyll *a* were present at the surface waters of the WSC (PSWw: 0.07 – 0.50 µg L^{-1}), as compared to the surface waters of EGC (PSW: 0.07 – 0.16 µg L^{-1}). Lowest values were observed in the epipelagic of AW (0.003 – 0.008 µgL^{-1}) and PSW (0.005 – 0.017 µg L^{-1}). The overall values of chlorophyll *a* were consistent with autumn values previously observed in surface waters of Fram Strait (von Jackowski et al., 2020; Wietz et al., 2021). Moreover, microscopic examination of surface stations detected an abundant presence of small nanoflagellates and heterotrophic dinoflagellates, coccolithophores, ciliates and tintinnids occurring together with diatoms like *Proboscia*, *Rhizosolenia* large *Phaeoceros* and *Pseudo-nitzschia* (Data not shown). These data suggest that the phytoplankton community reflected a typical late summer/fall community in this area.

Furthermore, depth profiles of inorganic nutrient concentrations in the water column, i.e silica (SiO_3), nitrate (NO_3), phosphate (PO_4) and ammonium (NH_4), indicated a depleted state, but with some higher concentrations towards the WSC (Table1, Figure S5). In PSWw, NO_3 was on average 8.86 µmol L^{-1} and SiO_3 5.31 µmol L^{-1}. Similarly, in AW, NO_3 was on average 12.69 µmol L^{-1} and SiO_3 6.61 µmol L^{-1}. Concentrations of nutrients were 3-fold lower in PSW, and traces of NH_4 were only present above 50 m in AW and were on average 0.63 µmol L^{-1} in PSWw. An upwelling event was present between HGIV and HGI (Figure S5), that coincided with peak concentrations of nutrients, particularly of NO_3 and SiO_3 at the surface of HGI (15.23 µmol L^{-1} and 11.61 µmol L^{-1}, respectively) and in the epipelagic of HGIV (14.61 µmol L^{-1} and 11.61 µmol L^{-1}, respectively), suggesting a small but localised, and at the time still active, regional bloom in the area. Low concentrations of nutrients aligned with chlorophyll *a* observations that reflected the late-bloom stage. Late summer conditions of the surface water in the Arctic are characterised by a strong halocline from melting sea ice buoyant on top of the regular seawater, which results in overall low (depleted and/or diluted) nutrient concentrations (Codispoti et al., 2013; Stratmann et al., 2017).

Conversely, DOC concentrations were higher in PSW (average 100 µmol L^{-1}) as compared to PSWw (72.95 µmol L^{-1}) and AW (63.13 µmol L^{-1}). In general, the observed values lie within the

range of previously determined DOC concentrations across the Fram Strait (Amon et al., 2003; Engel et al., 2019). In contrary, DOC concentrations were low in the WSC stations, suggesting an end phase of the summer bloom, when bioavailable semi-labile DOC (SLDOC) becomes rapidly remineralised again by microbial surface water communities in early autumn (von Jackowski et al., 2020). The organic matter present in PSW could therefore be considered as being at a more refractory state. Total dissolved combined carbohydrates (dCCHO) and total dissolved hydrolysable amino acids (dHAA) were highest in PSWw, peaking at the HGI and HGIV stations (157.89 – 193.53 nmol L^{-1}). Particularly dCCHO such as mannose and xylose were previously associated to diatoms (Haug and Myklestad, 1976), and at the end of a growth season large amounts of bioavailable DOM are being released (Ittekkot et al., 1981; Engel and Händel, 2011; von Jackowski et al., 2020), which could explain the elevated concentrations of dCCHO and dHAA in PSWw (Table 1).

Table 1. Overview of samples stations and environmental parameters. Lat: latitude. Lon: longitude. Temp: Temperature. Sal: Salinity. Frac. Chl. a: Fractionated chlorophyll a. PSWw: Warm Polar Surface Water. AW: Atlantic Water. PSW: Polar Surface Water. DOC: Dissolved organic carbon. DCCHO: dissolved combined carbohydrates. DHAA: dissolved hydrolysable amino acids.

PANGAEA Event ID	Water mass	Station	Lat (°N)	Lon (°E)	Depth (m)	Size fraction (µm)	Temp (°C)	Sal	Pot. Density	Water layer	Frac. Chl a (µg L^{-1})	Distance to ice edge (km)	PO_4 (µmol L^{-1})	SiO_3 (µmol L^{-1})	NO_3 (µmol L^{-1})	NH_4 (µmol L^{-1})	DOC (µmol L^{-1})	Total DCCHO (nmol L^{-1})	Total DHAA (nmol L^{-1})
PS121-5-3	PSWw	HGI	79.13	6.09	20	10	6.89	34.77	27.25	DCM	-	67	1.00	11.61	15.23	1.37	75.11	515.55	270.97
PS121-5-3	PSWw	HGI	79.13	6.09	20	3	6.89	34.77	27.25	DCM	0.15	67	1.00	11.61	15.23	1.37	75.11	515.55	270.97
PS121-5-3	PSWw	HGI	79.13	6.09	20	2	6.89	34.77	27.25	DCM	0.50	67	1.00	11.61	15.23	1.37	75.11	515.55	270.97
PS121-5-3	AW	HGI	79.13	6.09	100	3	4.16	35.03	27.80	EPI	0.003	67	0.79	4.83	11.13	0.03	62.05	236.27	104.77
PS121-5-3	AW	HGI	79.13	6.09	100	2	4.16	35.03	27.80	EPI	0.004	67	0.79	4.83	11.13	0.03	62.05	236.27	104.77
PS121/007-3	PSWw	HGIV	79.06	4.19	15	10	4.54	34.53	27.35	DCM	-	57	0.8	4.91	12.14	0.61	70.21	473.75	385.63
PS121/007-3	PSWw	HGIV	79.06	4.19	15	3	4.54	34.53	27.35	DCM	0.31	57	0.8	4.91	12.14	0.61	70.21	473.75	385.63
PS121/007-3	PSWw	HGIV	79.06	4.19	15	2	4.54	34.53	27.35	DCM	0.41	57	0.8	4.91	12.14	0.61	70.21	473.75	385.63
PS121/007-3	AW	HGIV	79.06	4.19	100	3	3.66	34.98	27.80	EPI	0.006	57	1.03	11.61	14.61	0.3	57.77	256.79	134.35
PS121/007-3	AW	HGIV	79.06	4.19	100	2	3.66	34.98	27.80	EPI	0.004	57	1.03	11.61	14.61	0.3	57.77	256.79	134.35
PS121/035-3	PSW	EGI	78.98	-5.37	25	10	-1.14	31.83	25.59	DCM	-	17	0.58	4.19	1.73	0.00	108.05	400.30	200.82
PS121/035-3	PSW	EGI	78.98	-5.37	25	3	-1.14	31.83	25.59	DCM	0.16	17	0.58	4.19	1.73	0.00	108.05	400.30	200.82
PS121/035-3	PSW	EGI	78.98	-5.37	25	2	-1.14	31.83	25.59	DCM	0.07	17	0.58	4.19	1.73	0.00	108.05	400.30	200.82
PS121/035-3	PSW	EGI	78.98	-5.37	100	3	-1.39	33.09	26.62	EPI	0.017	17	0.68	6.70	5.92	0.00	87.5	306.59	156.28
PS121/035-3	PSW	EGI	78.98	-5.37	100	2	-1.39	33.09	26.62	EPI	0.005	17	0.68	6.70	5.92	0.00	87.5	306.59	156.28
PS121/052-6	PSWw	F4	79.02	6.70	25	10	6.37	34.87	27.40	DCM	-	146	2.90	2.08	2.72	0.26	76.96	374.04	267.73
PS121/052-6	PSWw	F4	79.02	6.70	25	3	6.37	34.87	27.40	DCM	0.28	146	2.90	2.08	2.72	0.26	76.96	374.04	267.73
PS121/052-6	PSWw	F4	79.02	6.70	25	2	6.37	34.87	27.40	DCM	0.32	146	2.90	2.08	2.72	0.26	76.96	374.04	267.73
PS121/052-6	AW	F4	79.02	6.70	100	3	4.53	35.04	27.76	EPI	0.008	146	0.78	5.01	12.66	0.00	64.82	295.04	126.13
PS121/052-6	AW	F4	79.02	6.70	100	2	4.53	35.04	27.76	EPI	0.004	146	0.78	5.01	12.66	0.00	64.82	295.04	126.13
PS121/043-7	PSWw	N4	79.73	4.47	25	10	3.71	34.35	27.29	DCM	-	64	0.45	2.66	5.34	0.29	69.5	396.89	246.32
PS121/043-7	PSWw	N4	79.73	4.47	25	3	3.71	34.35	27.29	DCM	0.07	64	0.45	2.66	5.34	0.29	69.5	396.89	246.32
PS121/043-7	PSWw	N4	79.73	4.47	25	2	3.71	34.35	27.29	DCM	0.08	64	0.45	2.66	5.34	0.29	69.5	396.89	246.32
PS121/043-7	AW	N4	79.73	4.47	100	3	3.45	34.99	27.84	EPI	0.003	64	0.77	4.98	12.35	0.01	67.87	232.37	163.77
PS121/043-7	AW	N4	79.73	4.47	100	2	3.45	34.99	27.84	EPI	0.007	64	0.77	4.98	12.35	0.01	67.87	232.37	163.77

Activity pattern of *Bacteria*, *Archaea* and eukaryotes across the East-West transect and in different size fractions

We reconstructed the SSU rRNAs from the metatranscriptome data to obtain a first overview of the taxonomic differences of the active microbial communities in the different water samples, with a wholistic view on all three domains – *Bacteria*, *Archaea* and microbial eukaryotes. The composition of active communities was significantly different across samples of differing water mass origins and size fraction, both in the surface and at 100 m depth (PERMANOVA test; $F_{5,19}$ = 6.12, R^2 = 0.62, p = 0.001) (Figure 2). Surface samples from AW separated stronger from each other based on their size fractions as compared to the surface samples originating from PSWw (Figure 2). To further investigate differences between the active taxa in the different size fractions in each water mass, we conducted differential expression analyses (Aldex2 and edgeR) on the RPK reads mapped back to the reconstructed SSUs with the Benjamini–Hochberg correction applied to the *p*-value of the Kruskal–Wallis test ($p < 0.05$) (Figure S6). In total, 639 SSU rRNAs showed significant differences between size fractions ($p < 0.05$) in AW (Table 2), and 455 SSU rRNAs differed between the two larger fractions combined (>10 µm and 10 – 3 µm) and the smallest fraction of PSWw (3 – 0.2 µm). Differences in expression were driven mainly by *Bacteria* and eukaryotes in the PSWw, and by *Archaea*, *Bacteria* and eukaryotes in the AW (Table 3). The reconstructed SSU rRNAs of eukaryotes that showed a positive log2 fold change and a significant effect size based on Aldex (BH-corrected Welch's t-test and BH-corrected Wilcoxon test *p*-values <0.05) in both water masses matched the known minimum size of small and larger eukaryotes including diatoms, metazoans, dinoflagellates and ciliates (Massana, 2011). Bacterial orders that were significantly active in both large size fractions in the PSWw (>10 µm and 10 – 3 µm) and in the large size fraction of the AW (>3 µm), were represented by well-known particle-associated *Bacteroidia* and *Gammaproteobacteria* (Fadeev et al., 2018, 2021b), including *Cytophagales*, *Chitinophagales* and *Flavobacteriales*. The smallest size fraction of the PSWw included pelagic taxa such as *Marinimicrobia* (SAR406 clade), *Thalassobaculales* and the SAR11 clade (*Alphaproteobacteria*) as the main orders with the highest log2 fold change. The highly active taxa in AW were the archaeal order *Nitrosopumilales* (*Nitrososphaeria*), followed by *Marinimicrobia* (SAR406 clade), *Opitutales*, and the SAR202 clade.

Late eukaryotic phytoplankton bloom activity in PSWw was dominated by *Bacillariophyta*

Among the active eukaryotic phytoplankton, diatoms were the most active taxonomic groups, particularly in the surface samples. *Bacillariophyta* was the diatom class with the overall highest 18S read counts and activity. In the PSWw samples, *Bacillariophyta* exhibited an absolute mean log2 fold change of 3.6 in the two larger fractions combined (>10 µm and 3 – 10 µm). In the AW samples, the absolute mean log2 fold change was 3.3 (size fraction 10 – 3 µm) (Figure 3, Table 2). Furthermore, of the *Bacillariophyta* centric and pennate genera such as *Skeletonema*, *Fragilariopsis* and *Eucampia* were active in both water masses. The presence of diatoms coincided with the relative distribution pattern of chlorophyll *a* and nutrients in the water column of the WSC, and serves as an indication of a still active phytoplankton bloom in the surface waters of PSWw. Identifying *Eucampia* is likewise consistent with later stages of phytoplankton communities of the northern Barents Sea shelf (Pautova et al., 2021). *Skeletonema*, however, is not regarded as a dominant diatom in Arctic waters (Lovejoy et al., 2006; Nöthig et al., 2015; Fadeev et al., 2018), because it prefers warmer temperatures (Degerlund and Eilertsen, 2010). We speculate that temperature and the far retreated sea ice cover creates conditions that now support a higher activity of *Skeletonema* in Fram Strait waters at this time of the year. *Fragilariopsis* is a common sea ice diatom (Hop et al., 2020), and may have been released into the water upon sea ice melting in the region during the summer months. These observations further supported the hypothesis that the microbial community was in a very late stage of the phytoplankton bloom, and that the depletion of nutrients in the upper water layers drove the termination of the diatom bloom.

The centric diatom *Chaetoceros* showed considerably higher read counts in the surface of PSW (14 clr-transformed counts) as compared to the PSWw (3 – 9 clr-transformed counts) (Figure 3), thus displaying likely a stronger activity in the western waters (PSW) of the Strait. *Chaetoceros* is a predominantly pelagic diatom that can also be found in summer sea ice communities and seawater communities (Nöthig et al., 2015; Kauko et al., 2018). The presence of sea ice just a few weeks prior to sampling around station EGI (Figure S4) might therefore explain the source of *Chaetoceros* at the surface of PSW, because *Chaetoceros* is

typically abundant during late summer in surface waters and in bottom sea ice communities (Hardge et al., 2017).

Small chlorophytes (< 2 µm) were significantly enriched in the smallest size fraction of the eastern PSWw with a log2 fold change of -3, but were overall underrepresented in the AW underneath, with the exception of a few read counts at HGI (2 clr-transformed counts) (Figure 3). Chlorophytes were mainly represented by the order *Mamiellales* (average 7 clr-transformed counts). Other green algae SSU rRNAs were mainly assigned to *Bathycoccus* and *Micromonas*, which are also very common pelagic taxa in Arctic waters (Metfies et al., 2016; Hardge et al., 2017). *Micromonas* is the most common Chl *b*-containing picoeukaryote in the Arctic, and is known to positively respond to warmer conditions (Balzano et al., 2012; Hoppe et al., 2018; Demory et al., 2019). In the west of the Strait, *Pyramimonadales* (comprised only by *Pyramimonas*) showed higher read counts than in the east (average 5 clr-transformed counts at PSW surface compared to -0.6 clr-transformed counts at PSWw). *Pyramimonas* are common in the Arctic (Niemi et al., 2011) with higher presence in surface, nutrient-depleted waters associated with sea ice retreat (Schanke et al., 2021). At the end-phase of a phytoplankton bloom, *Micromonas* dominance might also be the response of picoplankton adaptation to lower nutrient concentrations (Li et al., 2009). Thus, the distribution of the dominant chlorophyte species across the transect, highlights their significant role and contribution in the seasonal transition of the eukaryotic microbial community into a late bloom phase.

SSU rRNAs assigned to haptophytes did not show significant differences in expression between the different size fractions ($p > 0.05$). However, high read counts of SSU rRNAs of *Phaeocystales*, and *Phaeocystaleplas* (dominated by the flagellate *Phaeocystis*), were distributed in all size fractions of the PSWw and contributed significantly to the active community of the PSWw (averaged across size fractions: 19 clr-transformed counts) (Figure 3). In AW, *Phaeocystales*, and *Phaeocystaleplas* were mostly present in the smallest size fraction (average: 10 clr-transformed counts) (Figure 3). *Phaeocystis* typically dominate late-stage summer phytoplankton blooms (Fadeev et al., 2018), and prefer the warm waters of the WSC (Nöthig et al., 2015). Coccolithophores SSU rRNAs of *Isochrysidaleplas* assigned to the coccolithophore *Gephyrocapsa* were only present at the epipelagic of the PSW and AW

(average 2 clr-transformed counts) and did not show significant differences based on size fraction since *Gephyrocapsa* coccoliths size can vary between 3.5 to 6 µm (Young et al., 2003).

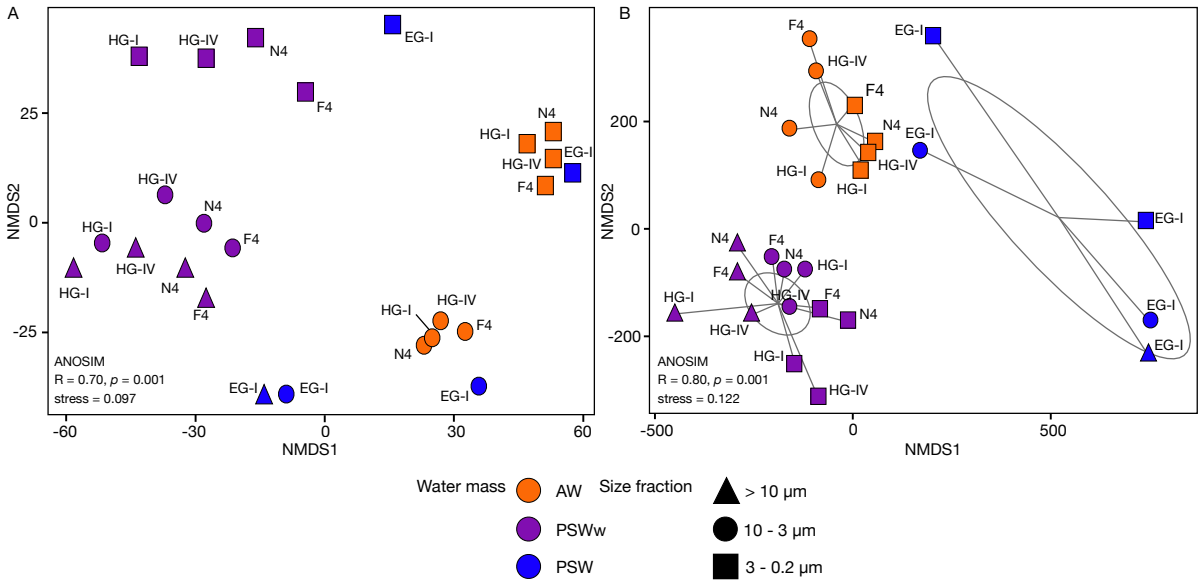

Figure 2. A) Two-dimensional NMDS ordination plot of RPK dissimilarities of eukaryotic and bacterial SSU rRNAs. B) Two-dimensional NMDS ordination plot of microbial TPM dissimilarities. Dissimilarity matrices and ANOSIM tests for size fraction were calculated based on Euclidean distances on clr-transformed data. Ellipses around sample groupings indicated 95% dispersion limits for each water mass. Samples are connected to the centroid through a spider diagram Water masses clusters are depicted in the different colours: blue for PSW, purple for PSWw and orange for AW, and shapes indicate the different size fractions.

Concurrence of grazers marked the end of the phytoplankton bloom

We encountered significantly active heterotrophic and mixotrophic protists in the larger fractions of in both, PSWw (>10 µm and 10 – 3 µm) and AW (>3 µm) ($p < 0.05$). The representation of heterotrophic and mixotrophic protists was overall higher in the AW samples as compared to the PSWw samples (Table 3), and included members of *Telonemia*, cryptomonads of the class *Cryptophyceae*, members of the *Filosa-Thecofilosea*, metazoans and dinoflagellates (*Syndiniales* and *Dinophyceae*). Ciliates and dinoflagellates (*Dinophyceae*) and were the most active hetero- and mixotrophic groups identified in the larger fractions of PSWw. Dinoflagellates (*Dinophyceae*) have previously been found abundant in summer 18S amplicon surveys of the DCM of Fram Strait (Metfies et al., 2017), and remain also dominant during the post-bloom state (Kilias et al., 2013). Able to display mixotrophy in the Arctic Ocean (Levinsen and Nielsen, 2002), photosynthetic dinoflagellates might also feed on prey such as diatoms (Sherr and Sherr, 2007; Flynn et al., 2019).

Dinophyceae included two orders: *Peridiniales* that were mainly in the PSW, and *Gymnodiniales* (dominated by *Gyrodinium*) dominating in PSWw and AW. *Gyrodinium* is a major consumer of diatoms and small autotrophs (Saito et al., 2006), matching their increased activity in the diatom bloom waters of the PSWw. *Telonemia*, choanoflagellates (*Acanthoecida*), *Katablepharidales*, and *Picozoa*, as well as the ciliates *Strombidiida* and OLIGO5 were highly present across our datasets (Figure 3). These heterotrophs participate in the carbon cycle by grazing upon a wide range of bacteria and on small phytoplankton. In return, they represent a food source for zooplankton and higher trophic levels. Moreover, in addition to prey availability, abiotic factors associated to water masses can also drive the composition of heterotrophic flagellates in the Arctic Ocean water column (Monier et al., 2013). Hence, the significant active presence of heterotrophs and mixotrophs serves as indicators of the late phytoplankton bloom, and suggests their diverse roles in the food network of the different water masses in Fram Strait.

Metazoans are larger than protists, multicellular, and the next link in the food chain. We identified a high log2 fold change of 3.4 in PSWw as compared to 2.1 in the AW (Table 2). Metazoan SSU rRNAs were represented primarily by the orders *Crustacea* and *Gastropoda* in PSWw, and by members of the *Ctenophora* in the surface of PSW. In AW, metazoans decreased in abundance with depth, however, in PSW *Ctenophora* read counts doubled from the surface towards the epipelagic (Figure 3). Likely, metazoan read counts indicated the presence of zooplankton that actively feed on phytoplankton particularly diatoms as a preferable food source (Falk-Petersen et al., 2002; Cleary et al., 2017), as well as heterotrophic flagellates. Amphipods and copepods are the most dominant zooplankton in summer to early autumn, while sea ice dynamics and water temperatures affect their abundance and distribution patterns masses in Fram Strait (Ramondenc et al., 2022), and explains why we identify the activity of different orders in the different water masses as well. Altogether, the strong expression of SSU rRNAs of heterotrophs, mixotrophs and zooplankton that comprised a substantially part of the eukaryotic community highlights the important ecological role of these taxonomic groups at the end of a phytoplankton bloom.

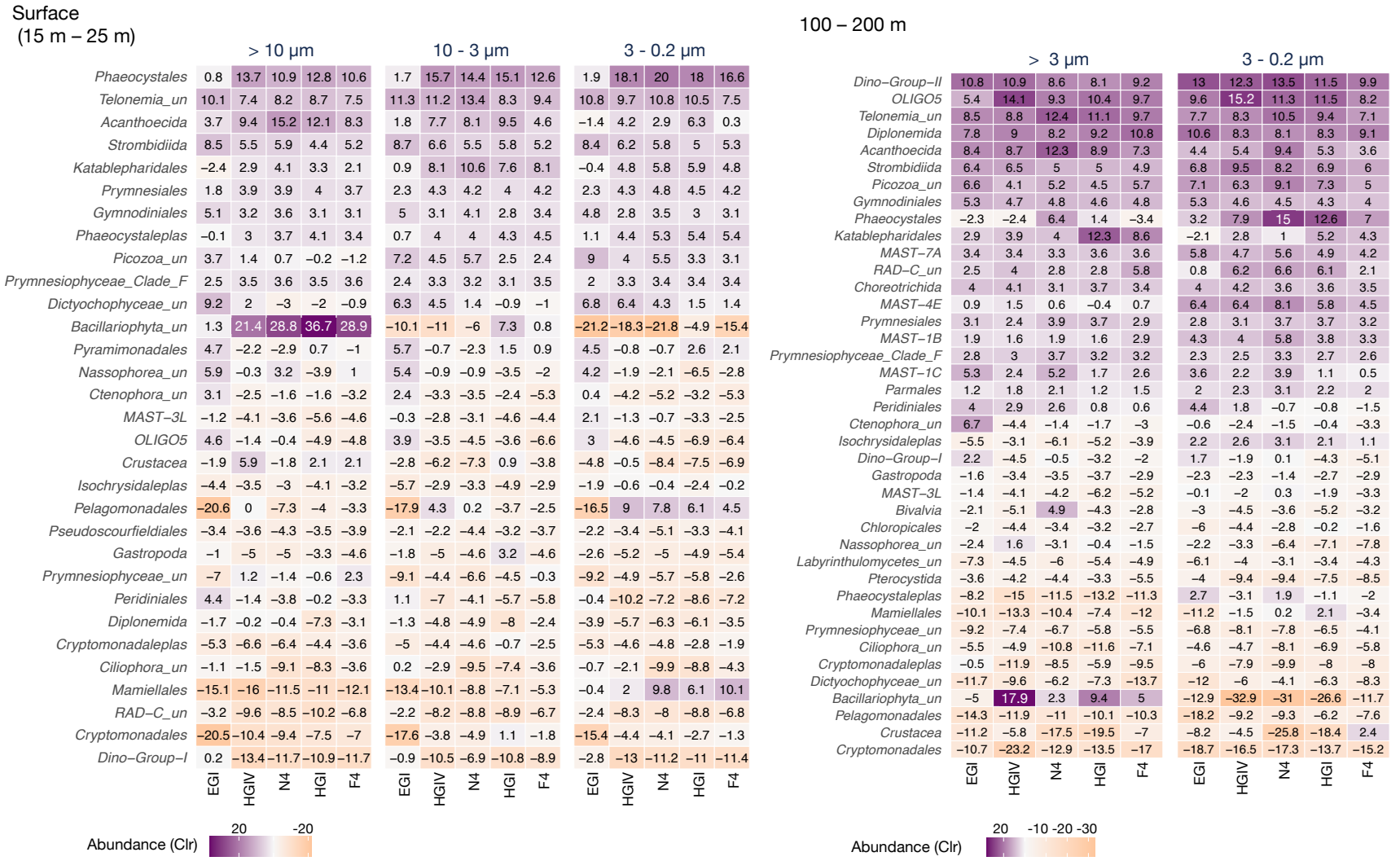

Figure 3. Heatmap of main eukaryotic orders identified based on the reconstructed SSU rRNAs based on clr-transformed counts in the different size fractions. Displayed positive values in purple shades indicate enrichment of the corresponding taxonomic orders and negative values in light orange indicate underrepresented orders. Stations are organized based on the longitude coordinates from west to east. Station EGI represents the PSW, stations HGIV to F4 represent on the surface PSWw and at the epipelagic AW located in the eastern Fram Strait.

Table 2. Summary of differential expression analysis for the different eukaryotic and bacterial reconstructed SSU rRNAs in PSWw and taxonomical classification summarized at the order level for eukaryotes and family level for bacteria. Only SSUs with n >1 and significant *p*-value were included ($p < 0.05$).

Log2 Fold Change	Log CPM	Effect size	Group	Kingdom	Phylum/Supergroup	Class/Division	Order/Class	Family/Order	SSU rRNAs (n)
3.85	7.31	-1.40	>10 & 10-3 µm	*Bacteria*	*Proteobacteria*	*Gammaproteobacteria*	*Cellvibrionales*	*Spongiibacteraceae*	8
4.49	6.25	-1.61	>10 & 10-3 µm	*Bacteria*	*Bacteroidota*	*Bacteroidia*	*Chitinophagales*	*Saprospiraceae*	4
3.08	7.21	-1.76	>10 & 10-3 µm	*Bacteria*	*Verrucomicrobiota*	*Verrucomicrobiae*	*Verrucomicrobiales*	*Rubritaleaceae*	6
3.19	7.06	-2.81	>10 & 10-3 µm	*Bacteria*	*Planctomycetota*	*Phycisphaerae*	*Phycisphaerales*	*Phycisphaeraceae*	4
2.87	3.96	-1.45	>10 & 10-3 µm	*Bacteria*	*Planctomycetota*	OM190	OM190_un	OM190_un	3
2.63	5.91	-1.99	>10 & 10-3 µm	*Bacteria*	*Bacteroidota*	*Bacteroidia*	*Flavobacteriales*	NS9 marine group	4
2.90	5.60	-2.52	>10 & 10-3 µm	*Bacteria*	*Bacteroidota*	*Bacteroidia*	*Flavobacteriales*	NS7 marine group	3
3.28	3.83	-2.37	>10 & 10-3 µm	*Bacteria*	NB1-j	NB1-j_un	NB1-j_un	NB1-j_un	13
3.43	10.31	-1.60	>10 & 10-3 µm	*Eukaryota*	*Opisthokonta*	*Metazoa*	*Metazoa_un*	*Metazoa_un*	10
2.04	6.29	-2.31	>10 & 10-3 µm	*Eukaryota*	*Alveolata*	*Ciliophora*	*Intramacronucleata*	*Intramacronucleata_un*	4
3.46	6.76	-1.79	>10 & 10-3 µm	*Bacteria*	*Bacteroidota*	*Bacteroidia*	*Flavobacteriales*	*Flavobacteriaceae*	10
2.11	10.66	-2.15	>10 & 10-3 µm	*Eukaryota*	*Alveolata*	*Dinoflagellata*	*Dinophyceae*	*Dinophyceae_un*	5
3.37	4.70	-2.44	>10 & 10-3 µm	*Bacteria*	*Desulfobacterota*	*Desulfobacterota_un*	*Desulfobacterota_un*	*Desulfobacterota_un*	2
4.88	6.23	-1.76	>10 & 10-3 µm	*Bacteria*	*Bacteroidota*	*Bacteroidia*	*Cytophagales*	*Cyclobacteriaceae*	13
3.96	7.66	-2.13	>10 & 10-3 µm	*Bacteria*	*Bacteroidota*	*Bacteroidia*	*Flavobacteriales*	*Cryomorphaceae*	9
3.13	6.66	-1.84	>10 & 10-3 µm	*Bacteria*	*Bacteroidota*	*Bacteroidia*	*Flavobacteriales*	*Crocinitomicaceae*	8
3.81	6.63	-1.84	>10 & 10-3 µm	*Bacteria*	*Proteobacteria*	*Gammaproteobacteria*	*Alteromonadales*	*Colwelliaceae*	5
4.01	8.24	-1.36	>10 & 10-3 µm	*Bacteria*	*Proteobacteria*	*Gammaproteobacteria*	*Cellvibrionales*	*Cellvibrionaceae*	4
3.38	5.74	-2.13	>10 & 10-3 µm	*Bacteria*	*Bdellovibrionota*	*Bdellovibrionia*	*Bacteriovoracales*	*Bacteriovoracaceae*	23
3.62	10.89	-1.61	>10 & 10-3 µm	*Eukaryota*	*Stramenopiles*	*Ochrophyta*	*Bacillariophyta*	*Bacillariophyta_un*	18
-2.46	2.91	1.58	3 - 0.2 µm	*Bacteria*	*Proteobacteria*	*Gammaproteobacteria*	UBA10353 marine group	UBA10353 marine group_un	5
-3.15	5.72	2.31	3 - 0.2 µm	*Bacteria*	*Proteobacteria*	*Gammaproteobacteria*	*Thiotrichales*	*Thiotrichaceae*	2
-3.08	5.05	3.66	3 - 0.2 µm	*Bacteria*	*Proteobacteria*	*Gammaproteobacteria*	*Thiomicrospirales*	*Thioglobaceae*	9
-2.79	5.51	2.62	3 - 0.2 µm	*Bacteria*	*Proteobacteria*	*Gammaproteobacteria*	SAR86 clade	SAR86 clade_un	25
-3.48	3.02	2.57	3 - 0.2 µm	*Bacteria*	SAR324 clade	SAR324 clade_un	SAR324 clade_un	SAR324 clade_un	5
-2.82	1.32	1.41	3 - 0.2 µm	*Bacteria*	*Chloroflexi*	*Dehalococcoidia*	SAR202 clade	SAR202 clade_un	2

-2.68	5.57	1.96	3 - 0.2 µm	*Bacteria*	*Proteobacteria*	*Alphaproteobacteria*	*Puniceispirillales*	SAR116 clade	17
-2.60	7.11	3.21	3 - 0.2 µm	*Bacteria*	*Proteobacteria*	*Alphaproteobacteria*	*Rhodobacterales*	*Rhodobacteraceae*	20
-3.62	5.50	2.19	3 - 0.2 µm	*Bacteria*	*Verrucomicrobiota*	*Verrucomicrobiae*	*Opitutales*	*Puniceicoccaceae*	5
-2.64	5.82	3.04	3 - 0.2 µm	*Bacteria*	*Proteobacteria*	*Gammaproteobacteria*	*Oceanospirillales*	*Pseudohongiellaceae*	14
-2.16	6.00	2.05	3 - 0.2 µm	*Bacteria*	*Proteobacteria*	*Gammaproteobacteria*	*Cellvibrionales*	*Porticoccaceae*	8
-3.02	5.35	3.18	3 - 0.2 µm	*Bacteria*	*Proteobacteria*	*Gammaproteobacteria*	OM182 clade	OM182 clade_un	7
-2.81	6.59	3.04	3 - 0.2 µm	*Bacteria*	*Proteobacteria*	*Alphaproteobacteria*	*Parvibaculales*	OCS116 clade	3
-3.54	4.90	2.24	3 - 0.2 µm	*Bacteria*	*Proteobacteria*	*Gammaproteobacteria*	*Burkholderiales*	*Nitrosomonadaceae*	3
-3.84	6.66	5.49	3 - 0.2 µm	*Bacteria*	*Proteobacteria*	*Alphaproteobacteria*	*Thalassobaculales*	*Nisaeaceae*	3
-3.01	4.44	2.61	3 - 0.2 µm	*Bacteria*	*Proteobacteria*	*Gammaproteobacteria*	*Burkholderiales*	*Methylophilaceae*	9
-4.51	3.92	3.46	3 - 0.2 µm	*Bacteria*	*Marinimicrobia*	*Marinimicrobia_un*	*Marinimicrobia_un*	*Marinimicrobia_un*	30
-2.50	6.40	2.64	3 - 0.2 µm	*Archaea*	*Thermoplasmatota*	*Thermoplasmata*	*Marine Group II*	*Marine Group II_un*	9
-2.96	6.40	2.20	3 - 0.2 µm	*Eukaryota*	*Archaeplastida*	*Chlorophyta*	*Mamiellophyceae*	*Mamiellales*	2
-2.65	4.88	2.99	3 - 0.2 µm	*Bacteria*	*Proteobacteria*	*Alphaproteobacteria*	*Rhodospirillales*	*Magnetospiraceae*	23
-2.08	4.64	1.82	3 - 0.2 µm	*Bacteria*	*Proteobacteria*	*Gammaproteobacteria*	*Oceanospirillales*	*Litoricolaceae*	2
-2.13	4.81	1.99	3 - 0.2 µm	*Bacteria*	*Proteobacteria*	*Gammaproteobacteria*	KI89A clade	KI89A clade_un	6
-3.15	3.35	3.07	3 - 0.2 µm	*Bacteria*	*Proteobacteria*	*Gammaproteobacteria*	*Gammaproteobacteria_un*	*Gammaproteobacteria_un*	7
-1.98	7.00	1.96	3 - 0.2 µm	*Bacteria*	*Bacteroidota*	*Bacteroidia*	*Flavobacteriales*	*Flavobacteriaceae*	6
-2.54	4.04	2.84	3 - 0.2 µm	*Bacteria*	*Proteobacteria*	*Alphaproteobacteria*	*Defluviicoccales*	*Defluviicoccales_un*	5
-3.09	6.48	3.03	3 - 0.2 µm	*Bacteria*	*Bacteroidota*	*Bacteroidia*	*Cytophagales*	*Cyclobacteriaceae*	2
-2.63	6.13	2.16	3 - 0.2 µm	*Bacteria*	*Proteobacteria*	*Alphaproteobacteria*	SAR11 clade	Clade IV	4
-2.72	6.82	2.31	3 - 0.2 µm	*Bacteria*	*Proteobacteria*	*Alphaproteobacteria*	SAR11 clade	Clade II	3
-3.17	13.50	2.75	3 - 0.2 µm	*Bacteria*	*Proteobacteria*	*Alphaproteobacteria*	SAR11 clade	Clade I	3
-2.50	5.78	2.23	3 - 0.2 µm	*Bacteria*	*Proteobacteria*	*Alphaproteobacteria*	AT-s3-44	AT-s3-44_un	2
-2.61	3.65	2.24	3 - 0.2 µm	*Bacteria*	*Proteobacteria*	*Alphaproteobacteria*	*Alphaproteobacteria_un*	*Alphaproteobacteria_un*	4
-3.04	4.41	3.14	3 - 0.2 µm	*Bacteria*	*Proteobacteria*	*Alphaproteobacteria*	*Rhodospirillales*	AEGEAN-169 *marine group*	9
-2.96	5.04	4.75	3 - 0.2 µm	*Bacteria*	*Proteobacteria*	*Gammaproteobacteria*	*Steroidobacterales*	*Woeseiaceae*	4

Table 3. Summary of differential expression analysis for the different eukaryotic and bacterial reconstructed SSU rRNAs at the AW and taxonomical classification summarized at the order level for eukaryotes and family level for bacteria. Only SSUs with n >1 and significant *p*-value were included ($p < 0.05$).

Log2 Fold Change	Log CPM	Effect size	Group	Kingdom	Phylum/Supergroup	Class/Division	Order/Class	Family/Order	SSU rRNAs (n)
3.26	8.98	3.82	> 3 µm	*Eukaryota*	*Stramenopiles*	*Ochrophyta*	*Bacillariophyta*	*Bacillariophyta_un*	19
1.62	6.98	2.61	> 3 µm	*Bacteria*	*Bdellovibrionota*	*Bdellovibrionia*	*Bacteriovoracales*	*Bacteriovoracaceae*	5
2.43	8.35	3.61	> 3 µm	*Bacteria*	*Bdellovibrionota*	*Bdellovibrionia*	*Bdellovibrionales*	*Bdellovibrionaceae*	29
2.67	10.30	3.92	> 3 µm	*Eukaryota*	*Alveolata*	*Ciliophora*	*Ciliophora_un*	*Ciliophora_un*	8
2.59	7.19	3.91	> 3 µm	*Bacteria*	*Bacteroidota*	*Bacteroidia*	*Flavobacteriales*	*Crocinitomicaceae*	8
2.52	6.17	2.78	> 3 µm	*Bacteria*	*Bacteroidota*	*Bacteroidia*	*Flavobacteriales*	*Cryomorphaceae*	14
2.43	9.58	2.30	> 3 µm	*Eukaryota*	*Hacrobia*	*Cryptophyta*	*Cryptophyceae*	*Cryptomonadales*	7
2.00	4.84	2.71	> 3 µm	*Bacteria*	*Bacteroidota*	*Bacteroidia*	*Cytophagales*	*Cyclobacteriaceae*	11
1.72	11.18	6.05	> 3 µm	*Eukaryota*	*Alveolata*	*Dinoflagellata*	*Syndiniales*	*Dino-Group-II*	5
1.99	11.55	6.27	> 3 µm	*Eukaryota*	*Alveolata*	*Dinoflagellata*	*Dinophyceae*	*Dinophyceae_un*	7
2.20	8.54	3.56	> 3 µm	*Eukaryota*	*Rhizaria*	*Cercozoa*	*Filosa-Thecofilosea*	*Filosa-Thecofilosea_un*	8
2.13	6.16	3.38	> 3 µm	*Bacteria*	*Bacteroidota*	*Bacteroidia*	*Flavobacteriales*	*Flavobacteriaceae*	15
2.41	7.12	3.75	> 3 µm	*Bacteria*	*Planctomycetota*	*Planctomycetes*	*Planctomycetales*	*Gimesiaceae*	3
2.74	8.67	3.88	> 3 µm	*Bacteria*	*Proteobacteria*	*Gammaproteobacteria*	*Cellvibrionales*	*Halieaceae*	3
2.78	12.38	2.69	> 3 µm	*Eukaryota*	*Stramenopiles*	*Opalozoa*	*MAST-3*	*MAST-3I*	4
2.07	9.70	2.68	> 3 µm	*Eukaryota*	*Opisthokonta*	*Metazoa*	*Metazoa_un*	*Metazoa_un*	6
3.33	7.76	5.90	> 3 µm	*Bacteria*	NB1-j	NB1-j_un	NB1-j_un	NB1-j_un	19
2.62	6.01	5.40	> 3 µm	*Bacteria*	*Bacteroidota*	*Bacteroidia*	*Flavobacteriales*	*NS7 marine group*	6
2.03	6.32	3.68	> 3 µm	*Bacteria*	*Bacteroidota*	*Bacteroidia*	*Flavobacteriales*	*NS9 marine group*	6
2.72	7.87	2.64	> 3 µm	*Bacteria*	*Planctomycetota*	OM190	OM190_un	OM190_un	7
3.30	10.25	4.83	> 3 µm	*Bacteria*	*Planctomycetota*	*Phycisphaerae*	*Phycisphaerales*	*Phycisphaeraceae*	4
2.50	6.40	3.83	> 3 µm	*Bacteria*	*Planctomycetota*	*Planctomycetes*	*Pirellulales*	*Pirellulaceae*	3
2.05	5.90	2.49	> 3 µm	*Bacteria*	*Proteobacteria*	*Alphaproteobacteria*	*Rickettsiales*	*Rickettsiales_un*	5
3.94	10.05	5.13	> 3 µm	*Bacteria*	*Planctomycetota*	*Planctomycetes*	*Planctomycetales*	*Rubinisphaeraceae*	3
1.97	6.41	4.95	> 3 µm	*Bacteria*	*Verrucomicrobiota*	*Verrucomicrobiae*	*Verrucomicrobiales*	*Rubritaleaceae*	3
2.68	5.05	2.27	> 3 µm	*Bacteria*	*Bacteroidota*	*Bacteroidia*	*Chitinophagales*	*Saprospiraceae*	5
2.38	9.86	3.29	> 3 µm	*Bacteria*	*Proteobacteria*	*Gammaproteobacteria*	*Cellvibrionales*	*Spongiibacteraceae*	10

2.33	10.94	2.84	> 3 µm	*Eukaryota*	*Hacrobia*	*Telonemia*	*Telonemia_un*	*Telonemia_un*	4
-3.16	6.54	-3.92	3 - 0.2 µm	*Bacteria*	*Proteobacteria*	*Alphaproteobacteria*	*Rhodospirillales*	AEGEAN-169 marine group	12
-3.22	7.37	-3.80	3 - 0.2 µm	*Bacteria*	*Proteobacteria*	*Alphaproteobacteria*	*Alphaproteobacteria_un*	*Alphaproteobacteria_un*	4
-3.11	9.35	-6.88	3 - 0.2 µm	*Bacteria*	*Verrucomicrobiota*	*Verrucomicrobiae*	Arctic97B-4 marine group	Arctic97B-4 marine group_un	3
-2.78	12.16	-3.43	3 - 0.2 µm	*Bacteria*	*Proteobacteria*	*Alphaproteobacteria*	SAR11 clade	Clade I	3
-2.23	8.82	-2.98	3 - 0.2 µm	*Bacteria*	*Proteobacteria*	*Alphaproteobacteria*	SAR11 clade	Clade II	3
-2.50	6.15	-3.91	3 - 0.2 µm	*Bacteria*	*Proteobacteria*	*Alphaproteobacteria*	SAR11 clade	Clade IV	4
-2.62	6.26	-4.49	3 - 0.2 µm	*Bacteria*	*Bacteroidota*	*Bacteroidia*	*Cytophagales*	*Cyclobacteriaceae*	3
-3.63	7.05	-6.13	3 - 0.2 µm	*Bacteria*	*Proteobacteria*	*Alphaproteobacteria*	*Defluviicoccales*	*Defluviicoccales_un*	9
-2.53	6.59	-2.48	3 - 0.2 µm	*Bacteria*	*Proteobacteria*	*Gammaproteobacteria*	*Gammaproteobacteria_un*	*Gammaproteobacteria_un*	6
-2.40	6.50	-4.76	3 - 0.2 µm	*Bacteria*	*Proteobacteria*	*Gammaproteobacteria*	HgCo23	HgCo23_un	4
-1.68	6.37	-3.30	3 - 0.2 µm	*Bacteria*	*Proteobacteria*	*Gammaproteobacteria*	KI89A clade	KI89A clade_un	3
-3.22	7.67	-5.64	3 - 0.2 µm	*Bacteria*	*Proteobacteria*	*Alphaproteobacteria*	*Rhodospirillales*	*Magnetospiraceae*	28
-3.18	8.72	-4.96	3 - 0.2 µm	*Archaea*	*Thermoplasmatota*	*Thermoplasmata*	*Marine Group II*	*Marine Group II_un*	11
-3.28	7.11	-4.25	3 - 0.2 µm	*Archaea*	*Thermoplasmatota*	*Thermoplasmata*	*Marine Group III*	*Marine Group III_un*	4
-4.86	7.25	-5.69	3 - 0.2 µm	*Bacteria*	*Marinimicrobia*	*Marinimicrobia_un*	*Marinimicrobia_un*	*Marinimicrobia_un*	40
-3.18	6.68	-3.24	3 - 0.2 µm	*Bacteria*	*Proteobacteria*	*Gammaproteobacteria*	*Burkholderiales*	*Methylophilaceae*	7
-2.58	7.86	-8.50	3 - 0.2 µm	*Bacteria*	*Actinobacteriota*	*Acidimicrobiia*	*Microtrichales*	*Microtrichaceae*	4
-3.96	9.40	-5.85	3 - 0.2 µm	*Bacteria*	*Proteobacteria*	*Alphaproteobacteria*	*Thalassobaculales*	*Nisaeaceae*	3
-2.91	6.00	-3.40	3 - 0.2 µm	*Bacteria*	*Proteobacteria*	*Gammaproteobacteria*	*Burkholderiales*	*Nitrosomonadaceae*	6
-4.98	10.04	-6.89	3 - 0.2 µm	*Archaea*	*Crenarchaeota*	*Nitrososphaeria*	*Nitrosopumilales*	*Nitrosopumilaceae*	8
-3.54	11.34	-3.89	3 - 0.2 µm	*Bacteria*	*Nitrospinota*	*Nitrospinia*	*Nitrospinales*	*Nitrospinaceae*	10
-2.74	7.01	-3.91	3 - 0.2 µm	*Bacteria*	*Proteobacteria*	*Alphaproteobacteria*	*Parvibaculales*	OCS116 clade	4
-2.64	7.00	-2.56	3 - 0.2 µm	*Bacteria*	*Proteobacteria*	*Gammaproteobacteria*	OM182 clade	OM182 clade_un	9
-3.33	8.05	-3.63	3 - 0.2 µm	*Bacteria*	PAUC34f	PAUC34f_un	PAUC34f_un	PAUC34f_un	7
-1.95	9.72	-2.44	3 - 0.2 µm	*Bacteria*	*Verrucomicrobiota*	*Verrucomicrobiae*	*Pedosphaerales*	*Pedosphaeraceae*	3
-2.64	7.11	-3.53	3 - 0.2 µm	*Bacteria*	*Proteobacteria*	*Gammaproteobacteria*	*Cellvibrionales*	*Porticoccaceae*	8
-2.50	6.95	-3.78	3 - 0.2 µm	*Bacteria*	*Proteobacteria*	*Gammaproteobacteria*	*Oceanospirillales*	*Pseudohongiellaceae*	10
-4.18	7.96	-3.24	3 - 0.2 µm	*Bacteria*	*Verrucomicrobiota*	*Verrucomicrobiae*	*Opitutales*	*Puniceicoccaceae*	10
-3.39	7.80	-5.55	0.2 µm	*Bacteria*	*Proteobacteria*	*Alphaproteobacteria*	*Rhodobacterales*	*Rhodobacteraceae*	16
-2.45	5.68	-3.04	0.2 µm	*Bacteria*	*Proteobacteria*	*Alphaproteobacteria*	*Puniceispirillales*	SAR116 clade	17

-4.01	6.46	-3.65	0.2 µm	*Bacteria*	*Chloroflexi*	*Dehalococcoidia*	SAR202 clade	SAR202 clade_un	27
-3.24	8.18	-4.55	0.2 µm	*Bacteria*	SAR324 clade	SAR324 clade_un	SAR324 clade_un	SAR324 clade_un	6
-3.30	6.82	-4.96	0.2 µm	*Bacteria*	*Proteobacteria*	*Gammaproteobacteria*	SAR86 clade	SAR86 clade_un	23
-3.65	8.32	-4.98	0.2 µm	*Bacteria*	*Proteobacteria*	*Gammaproteobacteria*	*Thiomicrospirales*	*Thioglobaceae*	10
-3.10	6.01	-3.97	0.2 µm	*Bacteria*	*Proteobacteria*	*Gammaproteobacteria*	*Thiotrichales*	*Thiotrichaceae*	4
-2.89	8.41	-5.03	0.2 µm	*Bacteria*	*Proteobacteria*	*Gammaproteobacteria*	UBA10353 marine group	UBA10353 marine group_un	8
-3.17	7.65	-7.15	0.2 µm	*Bacteria*	*Proteobacteria*	*Gammaproteobacteria*	*Steroidobacterales*	*Woeseiaceae*	6

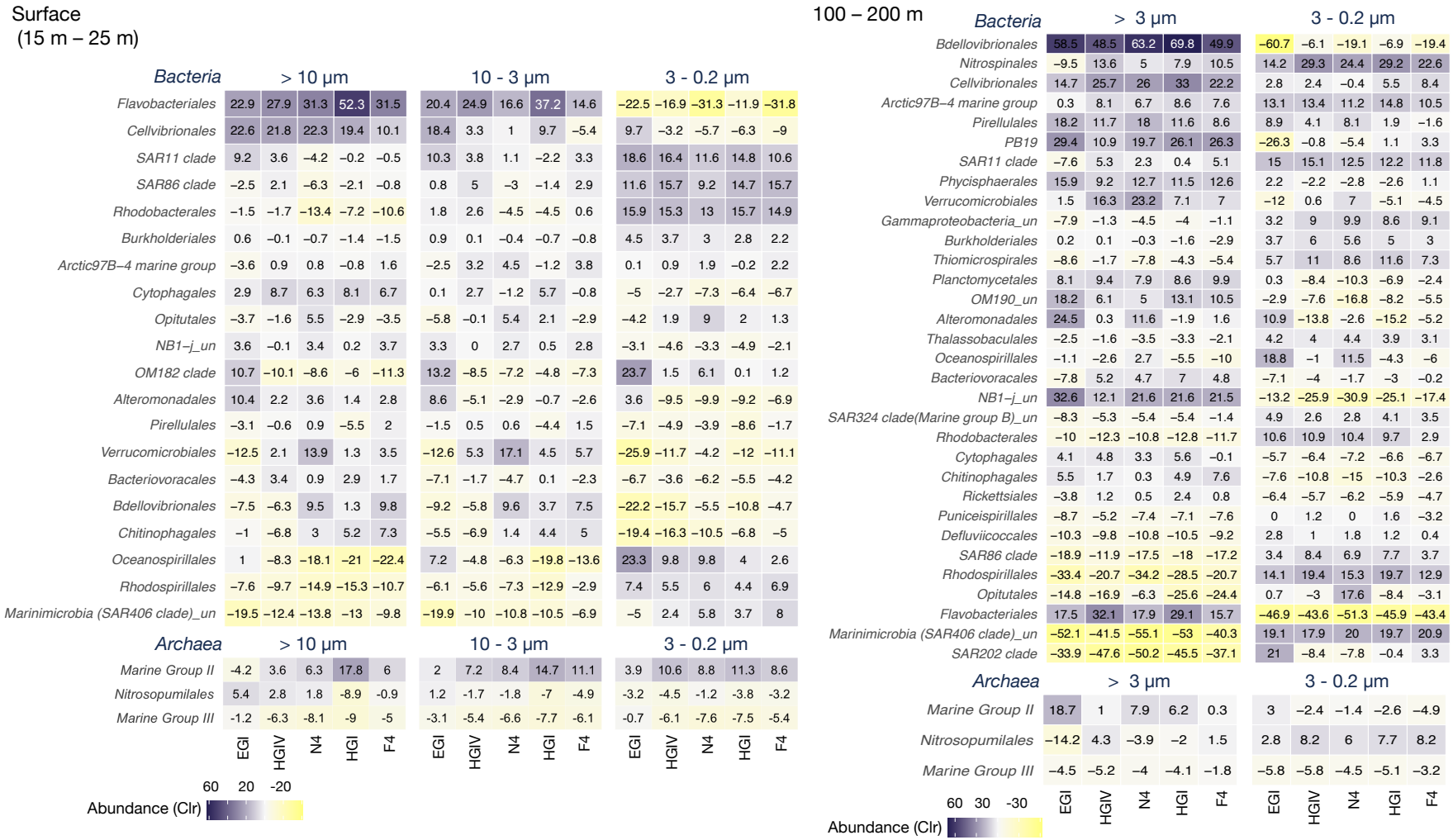

Figure 4. Heatmap of main bacterial and archaeal orders identified based on the reconstructed SSU rRNAs based on clr-transformed counts in the different size fractions. Positive values in dark blue shades indicate enrichment of the corresponding taxonomic orders and negative values in light yellow indicate underrepresented orders. Stations are organized based on the longitude coordinates from west to east. Station EGI represents the PSW, stations HGIV to F4 represent on the surface PSWw and at the epipelagic AW located in the eastern Fram Strait.

Active particle-associated *Bacteria* co-occurring with the active diatom bloom

SSU rRNAs assigned to the class *Bacteroidia* showed the highest log2 fold change (4 – 4.9) in the combined larger fractions of PSWw (>10 µm and 10 – 3 µm) (Table 2), which are associated with aggregate-forming or particle-attached bacterial community. The top active families in these larger size fractions were *Cyclobacteriaceae (Cytophagales), Saprospiraceae* (*Chitinophagales*) and *Cryomorphaceae* (*Flavobacteriales*). In general, the phylum *Bacteroidetes* is among the dominant responders to phytoplankton blooms in Fram Strait (Fadeev et al., 2018; von Appen et al., 2021; Wietz et al., 2021), together with *Gammaproteobacteria* and *Alphaproteobacteria*, because of their ability to decompose high-molecular-weight organic matter (Kirchman, 2002), including also diatom-derived polysaccharides (Krüger et al., 2019). Many *Bacteroidia* are associated with particles and diatoms, and were also identified in larger fractions studied at a river-to-sea interphase in the western central Arctic (Unfried et al., 2018; Bowman, 2020; Morency et al., 2022). The elevated activity of these taxa might be associated with the strong concurring activity of diatoms in the PSWw, as well as in the PSW (Figure 4). In addition, the highly active gammaproteobacterial families *Cellvibrionaceae, Spongiibacteraceae and Colwelliaceae* were also active at the surface (log2 fold change around 4). The obligate predatory bacteria (Davidov and Jurkevitch, 2004) belonging to the family *Bacteriovoracaceae* of the class *Bdellovibrionia* were also active in the larger fraction of PSWw (Table 2).

At depth, particle-associated bacteria of the *Planctomycetota* phylum were most active in the AW with a log2 fold change of 2.5 – 3.9, and represented by families such as *Rubinisphaeraceae, Phycisphaeraceae, Pirellulaceae* as well as the OM190 cluster. *Pirellulales*, *Planctomycetales* and OM190 have shown enrichment in particle-associated communities in ice-free and ice-covered regions of the Fram Strait (Fadeev et al., 2021b). These observations coincide with the similar abundances of read counts of *Pirellulales*, *Planctomycetales* OM190 in the epipelagic of PSW compared to the AW (Figure 4). *Planctomycetota* species participate in carbon and nitrogen cycling by partaking in the breakdown of complex polysaccharides (Glöckner et al., 2003). Genome analysis of *Planctomycetes* indicate a repertoire of necessary genes for the degradation of complex nitrogen-containing polysaccharides in the sediment of Svalbard fjords (Vipindas et al., 2020).

Planctomycetota is an important taxonomic group that includes taxa involved in the removal of nitrogen and the transformation of complex molecules releasing nutrients to the deep water of Fram Strait. Other known particle-associated taxa with a significant log2 fold change in the larger fraction of the AW included the NB1-j and *Flavobacteriales*, which were also active at the surface.

Distribution of free-living *Bacteria* and *Archaea* across water masses

Microbial groups without cultured representatives and limited availability of any lab-based physiological information are generally described as "microbial dark matter" (Rinke et al., 2013). In the eastern Arctic water column (PSWw and AW), we identified many of these microorganisms in the active smallest size fraction. The bacterial groups *Marinimicrobia* (SAR406), SAR324, *Thalassobaculales* (*Alphaproteobacteria*), *Opitutales* (*Verrucomicrobiae*), and the archaeal group Marine Group II (MGII) and the order *Nitrosopumilales* all had a log2 fold change (Table 2, Table 3). Read counts of *Marinimicrobia* were highest in the AW (average 20 clr-transformed read counts) as compared to the PSWw (average 5 clr-transformed read counts) (Figure 4). *Marinimicrobia* was previously reported as a relevant taxonomic group in the ice-covered EGC during a summer bloom (Fadeev et al., 2018), but can also be present in the WSC and EGC waters in the transition to winter (Wilson et al., 2017; Wietz et al., 2021). Thus, the elevated activity of *Marinimicrobia* in the first 100 m of the water column across the Strait, but especially in the east (Figure 4), supports the late summer bloom state of the ecosystem and indicates the biological transition towards winter. Although *Thalassobaculales* and SAR324 are not main taxonomic groups in Fram Strait waters in amplicon sequence studies e.g (Wilson et al., 2017; Fadeev et al., 2018; Wietz et al., 2021), the active expression of SSU rRNAs and the high abundance of read counts in the PSW and AW (Figure 4) suggest an important ecological role of these bacterial groups in the water column. *Thalassobaculales* may be involved in the degradation of complex aromatic compounds (Grevesse et al., 2022), while the role for SAR324 remains unclear because it displays wide metabolic diversity (Malfertheiner et al., 2022). *Verrucomicrobiae* is capable to transform complex polysaccharides such as fucose-containing sulphated polysaccharides from diatoms and brown macroalgae. Degradation products and the stored intracellular carbon later sink as particles to the deep sea (Vidal-Melgosa et al., 2021). Our results confirm

the presence of a specific microbial community, active toward the end of the phytoplankton bloom, with likely specific functions in the degradation of organic matter.

Archaeal SSUs in the smaller fraction of the PSWw were represented by the planktonic MGII with a log2 fold change of -2.5 in the PSWw, and high abundances of read counts of MGII were observed in all size fractions of the PSWw (average 9 clr-transformed read counts) (Figure 4). In AW, MGII and *Nitrosopumilales* were significantly represented in the smaller fraction with a log2 fold change < -3.2 (Table 3), which highlights the relevance of archaeal taxa in both water masses. Our results fit with recent metagenomic surveys of the photic layer of oceanographic regions covered during the Tara Ocean's expeditions, where it was indicated that the archaeal group MGII presence is widely distributed in ocean surface waters (Pereira et al., 2019), and may be metabolically diverse. MGII also occurs particle-attached (Orsi et al., 2015), where they can actively participate in degradation of marine particles via anaerobic metabolism (Rinke et al., 2019), or anaerobic respiration of dimethylsulphoxide (DMSO) (Martin-Cuadrado et al., 2008), and feed on algal produced carbon in warmer temperatures (Orsi et al., 2015).

SAR202 was significantly active in the small fraction at epipelagic of PSW (21 clr-transformed read counts) and underrepresented in other water masses. This elevated activity in the top 200 m is surprising since previous DNA-based studies found that SAR202 is typically abundant below the photic zone at the meso- and bathypelagic of Fram Strait (Cardozo-Mino et al., 2021), the Canadian Basin (Colatriano et al., 2018), and in other oceanographic regions (Morris et al., 2004; Landry et al., 2017). SAR202 has been associated with the oxidation of organic compounds rendered largely resistant to microbial degradation (Landry et al., 2017; Colatriano et al., 2018; Saw et al., 2020). Thus, the activity of SAR202 in the epipelagic of PSW implies the increased presence of refractory compounds in concert with the bloom activity in these waters (Table 1).

Key metabolic activities in the different water masses and evidence for an ongoing bacteriophage infection

With a final catalogue of 664,792 contigs, we also studied the expression spectrum of functional genes in the microbial communities along the Fram Strait transect. Overall, the

transcripts showed a significant separation according to water masses and size fractions (Figure 2B). Similar to the distribution of the reconstructed SSU rRNAs, the separation between water masses and the size fraction within each water mass cluster was found significant (PERMANOVA test; $F_{5,19}$ = 6.53, R^2 = 0.63, p = 0.001). Differential expression analyses across the different water masses revealed that the largest size fraction (10 – 3 µm) of PSWw contained the largest amount (2531 total genes) with significantly elevated expression ($p < 0.05$, Figure S7), of which 2254 transcripts were associated with known proteins and only 277 to hypothetical proteins. In AW, only 486 genes were identified as being differentially expressed across the different size fractions, however, 60% corresponded to hypothetical proteins.

In PSWw, most of the differentially expressed genes (with a negative log2 fold change less than -8) compared to the AW were involved with the maintenance of basic cellular functions in bacteria and eukaryotes, including genes encoding for ribosomal proteins, chaperons, cell division proteases, ATP-dependent Clp protease, and protease subunits. We further identified many transcripts involved in carbohydrate and amino acid metabolism, as well with substrate uptake. For example, ABC transporters showed a log2 fold change between -4.3 and -9 in the PSWw, were mostly associated with transport systems (substrate-binding proteins) (Figure 5) for L-amino acids, monosaccharides (glucose, mannose and xylose), iron (III), and glycerol. ABC transporters were affiliated with *Rhodobacteraceae* (*Alphaproteobacteria*) and *Pseudomonadales* (*Gammaprotoebacteria*). ABC transporters are fundamental for carbon and DOC metabolism in marine microbial communities (Sowell et al., 2009; Poretsky et al., 2010). The particular configuration of ABC transporters, for example in *Roseobacter* and SAR11, can indicate an organism's preference for carbohydrate-based DOC over nitrogen-based DOC respectively (Jiao and Zheng, 2011), and thus play a significant role in carbon partitioning and in carbon cycling. Other abundant transcripts related to transport were genes for putative spermidine/putrescine and peptide/nickel transport systems. Genes for spermidine/putrescine transform spermidine for both energy generation and biosynthesis and part of the machinery for polyamine transformation (Mou et al., 2010). The abundance of spermidine/putrescine could also explain the high concentration of serine in the DHAA fraction at the eastern part of the Strait. Transcripts involved in sulphur metabolism were also identified with a log2 fold change between -8.5 and -6.9, and were

associated to the taurine transport system binding proteins, adenylylsulfate reductases and methanethiol oxidases. These were associated with members of *Gammaproteobacteria* and *Bacilli*. In general, the distribution of transporters is an abundant component of the surface metaproteome, especially under low nutrient conditions (Sowell et al., 2009), and are known to vary in distribution with depth (DeLong et al., 2006).

Transcripts encoding the photosystems PSI and PSII were also highly abundant in the PSWw compared to the AW, and were associated mainly with small eukaryotes of the *Chlorophyta* as well as diatoms of the *Bacillariophyta*. As part of PSII, we found transcripts for the P680 reaction center D2, PsbZ, oxygen-evolving enhancer, CP47 chlorophyll apoprotein, and cytochrome b559 subunit alpha proteins. As part of PSI, we found transcripts of the P700 chlorophyll *a* apoprotein A2 and A1 as well as other subunit proteins (Figure 5A). Other significantly expressed transcripts in the smaller size fraction related to photosynthesis were associated with cytochrome b6 and light-harvesting complex proteins. Transcripts of genes involved in photosynthetic electron transport in photosystem II as well as transcripts encoding the photosynthetic CO_2-fixing enzyme ribulose-1,5-bisphosphate carboxylase/oxygenase (Rubisco) were also expressed in the larger fractions, although they did not show a significant log2 fold change (p-value > 0.05). These transcripts were associated to diatoms of the *Bacillariophyta* and had a significant log2 fold change of -8 compared to the AW, demonstrating that the ongoing diatom bloom at the surface was active at the surface.

Transcription of genes associated with chlorophytes involved in energy production and conversion included genes of the oxidative phosphorylation pathway (Figure 5). Abundant transcripts furthermore coded for F-type H+-transporting ATPase subunits, NADH-ubiquinone oxidoreductase, F-type H+/Na+-transporting ATPase subunit alpha and cytochrome c oxidase subunits. Other less abundant but significantly expressed functions in eukaryotes were transcripts for genes involved in phagocytosis, ribosome biogenesis, TCA cycle, and glyoxylate and dicarboxylate metabolism (mainly encoding for the ribulose-bisphosphate carboxylase large and small chain proteins).

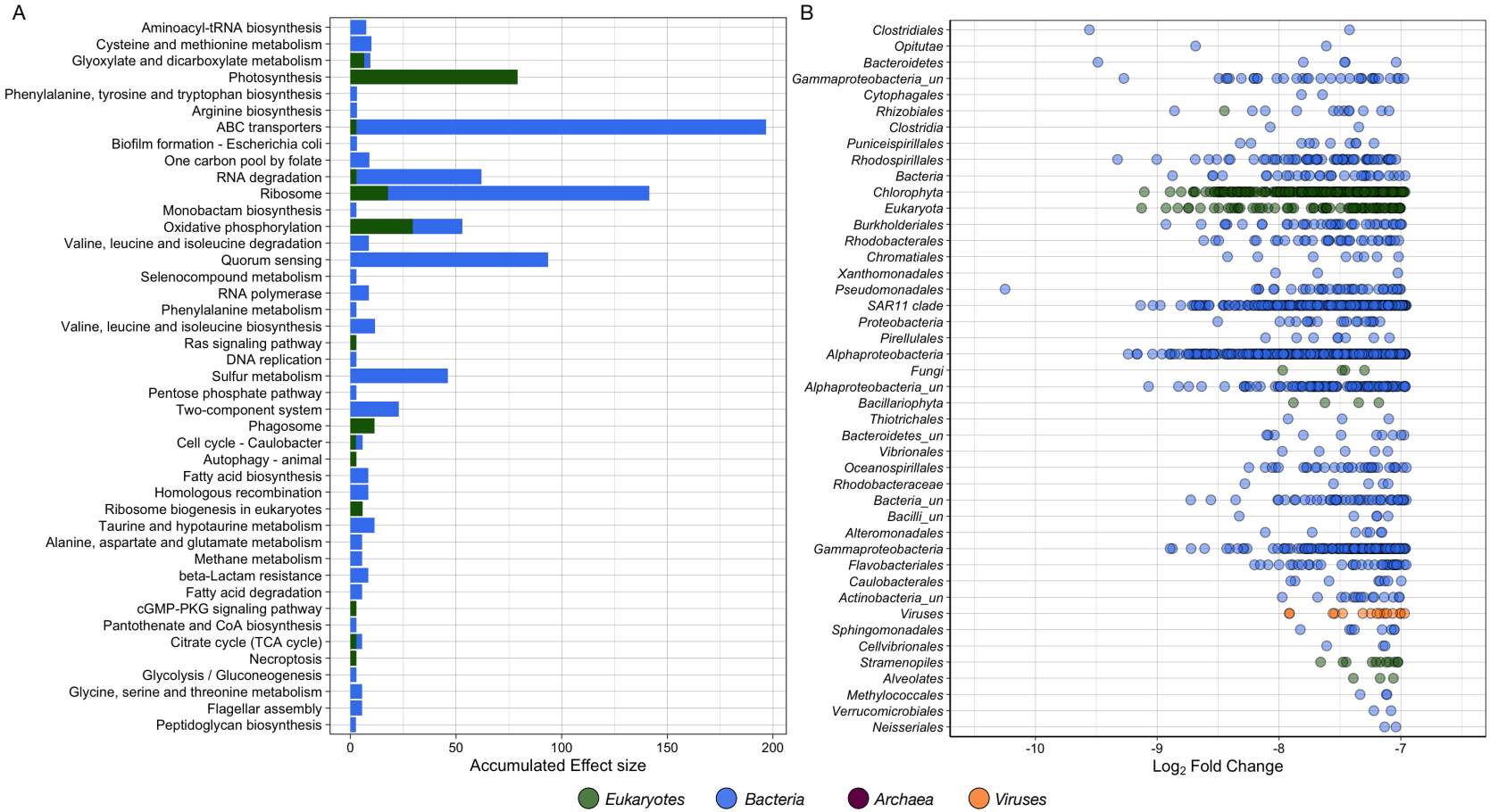

Figure 5. Representation of the main predicted metabolic pathways of transcripts annotated with the KEGG data base and of taxonomical classification in the PSWw. A) Main significant predicted metabolic pathways of transcripts (BH-corrected Welch's t-test and BH-corrected Wilcoxon test *p*-values <0.05). Only transcripts with a mean effect size higher than 2.5 were included. B) Differential representation of transcripts (*p*-value < 0.05) classified at the order taxonomic rank for bacteria and class for eukaryotes. The x-axis represents values of log2 fold change. Negative values indicate enrichment in the larger fractions.

We identified a pool of 40 transcribed genes in the PSWw large fraction (log2 fold change from -7.9 to -6.4) encoding for viral proteins associated to the double-stranded DNA phage families *Myoviridae* and *Siphoviridae* (Figure 5B), however only 24 were successfully annotated. Based on the identification of protein family (PFAM) domains, the most highly expressed genes were capsid proteins (Major capsid protein Gp23), peptidases, recombination proteins and DNA binding proteins (Table 4). No transcripts were identified for specific metabolic functions. *Myoviridae* and *Siphoviridae* are commonly found in the water column, sediments sea ice and brine (Hurwitz and Sullivan, 2013; Zhong et al., 2020; Heyerhoff et al., 2022). The interactions between phages and their bacterial targets is typically host-specific and through auxiliary metabolic genes improved the fitness of the virus or enhance metabolism of the host (Williamson et al., 2008). A number of phages of *Myoviridae* and *Siphoviridae* that target sea ice and seawater bacteria have been isolated from Arctic environments, including those specific to *Colwellia*, *Flavobacteriales* and other species of *Bacteroidetes* (Borriss et al., 2003, 2007; Wells and Deming, 2006; Collins and Deming, 2011; Zhong et al., 2020). In Arctic sea ice common host of *Myoviridae* and *Siphoviridae* phages were *Marinobacter*, *Glaciecola*, and *Colwellia*, and were found to encoded fatty acid desaturase (*FAD*) genes that likely helped their hosts overcome cold and salt stress (Zhong et al., 2020). Metagenomic analysis of *Myoviridae* and *Siphoviridae* obtained from seawater and sediments from the Baltic sea were found to procure auxiliary metabolic genes specific for photosynthesis, genes involved in nutrient cycling pathways such as sulfur, and to evade host restriction mechanisms through methylation (Heyerhoff et al., 2022). These findings indicate an ongoing lytic viral infection occurred at the time of sampling, and highlights the importance of viral infections in the contribution to the dissolved organic matter pool to the Artic water column (Fuhrman, 1999; Breitbart et al., 2018). Future studies, should address implication on bacterial and eukaryotic abundances as well as interactions between phages and their bacterial hosts to understand the role in the different water masses.

Table 4. Differential expression and functional description of viral transcripts obtained in the PSWw. Transcripts were classified by viral family. PFAM: protein families. COG: Clusters of Orthologous Groups of proteins. n.d: data not available.

Transcript	Family	Functional Description	PFAM	Effect size	Log2 Fold Change
NODE_938_length_2448_cov_7.833544_g476_i0	*Myoviridae*	Major capsid protein Gp23	PF07068	2.27	-6.53
NODE_6367_length_1641_cov_7.889313_g4792_i0	*Myoviridae*	Major capsid protein Gp23	PF07068	2.01	-6.71
NODE_4266_length_3493_cov_12.835572_g2502_i0	*Myoviridae*	Pfam: Peptidase_S77	n.d	2.84	-7.91
NODE_4266_length_3493_cov_12.835572_g2502_i0	*Myoviridae*	Major capsid protein Gp23	PF07068	2.84	-7.91
NODE_40141_length_1169_cov_4.461818_g32509_i0	*Myoviridae*	Major capsid protein Gp23	PF07068	2.25	-6.97
NODE_35985_length_1597_cov_9.786649_g26789_i0	*Siphoviridae*	Putative transcription factor D5	n.d	2.39	-6.59
NODE_342_length_2083_cov_4.177756_g283_i0	*Myoviridae*	Major capsid protein Gp23	PF07068	2.33	-6.93
NODE_31422_length_1724_cov_8.908157_g22994_i0	*Siphoviridae*	NAD-dependent DNA ligase adenylation domain	PF01653	2.12	-6.57
NODE_29555_length_1372_cov_4.168074_g23255_i0	*Myoviridae*	Major capsid protein Gp23	PF07068	2.24	-6.96
NODE_28632_length_897_cov_5.746377_g23957_i0	*Siphoviridae*	Putative transcription factor D5	n.d	2.20	-6.92
NODE_246461_length_546_cov_5.029350_g225837_i0	*Siphoviridae*	Putative transcription factor D5	n.d	2.65	-7.17
NODE_23835_length_2030_cov_6.505864_g16871_i0	*Myoviridae*	recA bacterial DNA recombination protein	PF00154	2.55	-7.25
NODE_230938_length_566_cov_7.098592_g210389_i0	*Myoviridae*	gp32 DNA binding protein like	PF08804	2.62	-7.56
NODE_21234_length_1615_cov_4.924321_g16080_i0	*Myoviridae*	Major capsid protein Gp23	PF07068	2.50	-6.93
NODE_2101_length_2889_cov_10.603901_g1132_i0	*Podoviridae*	P22 coat protein - gene protein 5	n.d	2.37	-6.60
NODE_14603_length_2758_cov_5.953142_g9728_i0	*Myoviridae*	Major capsid protein Gp23	PF07068	2.53	-6.80
NODE_14569_length_1937_cov_4.226981_g10502_i0	*Myoviridae*	Major capsid protein Gp23	PF07068	2.34	-6.77
NODE_143255_length_739_cov_1.741791_g124160_i0	*Myoviridae*	Phage tail sheath protein	PF04984	1.97	-6.41
NODE_142734_length_740_cov_3.442623_g123654_i0	*Myoviridae*	Major capsid protein Gp23	PF07068	2.28	-6.54
NODE_14031_length_2833_cov_18.200434_g9305_i0	*Siphoviridae*	DNA ligase (NAD+)	n.d	2.66	-7.54
NODE_108530_length_862_cov_3.223203_g91154_i0	*Myoviridae*	n.d	n.d	2.50	-7.20
NODE_107930_length_682_cov_7.021207_g96548_i0	*Myoviridae*	gp32 DNA binding protein like	PF08804	2.55	-6.81
NODE_10425_length_3536_cov_12.928180_g6716_i0	*Myoviridae*	Major capsid protein Gp23	PF07068	2.84	-7.92
NODE_10144_length_1418_cov_3.385471_g7463_i0	*Siphoviridae*	Putative transcription factor D5	n.d	2.01	-6.67

Most archaeal activity (i.e the order *Nitrosopumilales* and unclassified *Thaumarchaeota*, 80% of the most differentially expressed transcripts (fold change > 4) was observed in the smallest size fraction of the AW (Figure 6). The *Thaumarchaeota* comprised a large group of ammonia-oxidizing archaea (AOA) (Hatzenpichler, 2012), and one of the most abundant archaeal group found in the oceanic water column (Salazar et al., 2016).

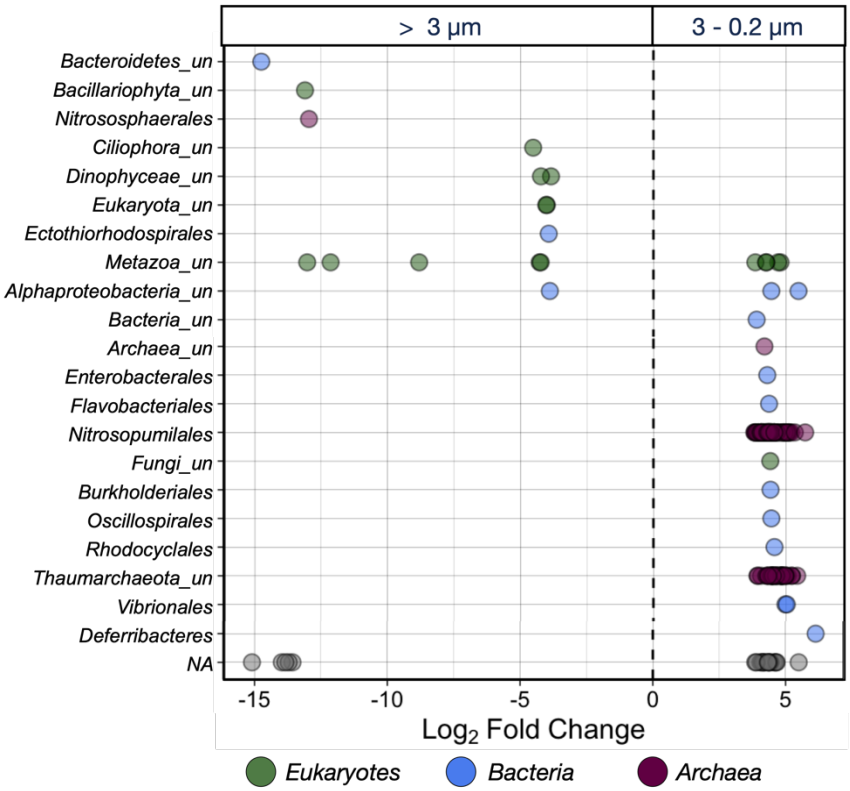

Figure 6. Differential representation of transcripts (*p*-value < 0.05) in the AW classified at the order taxonomic rank for Bacteria and Archaea and class for eukaryotes. The x-axis represents values of log2 fold change. Positive values represent transcripts enriched in the small size fraction (3 – 0.2 µm) and negative values indicate enrichment in the larger fraction (> 3 µm).

Abundance of archaeal transcribed functional genes matched with our observations of active archaeal groups (MGII and *Nitrosopumilales*) in the epipelagic of AW based on reconstructed 16S rRNA (Figure 4). *Thaumarchaeota* abundances based on cell counts were also highest at 100 m in the ice-free region of the WSC during a late phytoplankton bloom, where they formed half of the total archaeal community (Cardozo-Mino et al., 2021). We observed *Thaumarchaeota*-associated gene transcripts for the AmoC and AmoA subunits of ammonia monooxygenase with high levels of expression (log2 fold change > 5) in AW (Figure 6). *Thaumarchaeota* and MGII have been described to co-occur at depth on the basis of the AmoA gene of *Thaumarchaeota* (Parada and Fuhrman, 2017; Pereira et al., 2019), and the detection of AOA also coincided with higher concentrations of NH_4 in AW during the time of sampling (Figure S5). It can be speculated that AOA might persist in AW until NH_4 and other nutrient sources deplete, the water stratifies or light inhibition occurs (Parada and Fuhrman, 2017). We also encountered a high number of archaeal transcripts for subunits of superoxide dismutase and for proteins involved in iron and ammonium transport, as well as

for maintenance functions in DNA recombination and repair. Thus, we expand previous findings that *Archaea* comprise key players in the recycling of nutrients in the Arctic water column with key enzymes being actively transcribed that mainly affect the nitrogen cycle at the surface and with depth.

Conclusion

We provided the first close view on Fram Strait microbial communities during a summer bloom based on their activity profiles. In the two opposing currents EGC and WSC, with differing physicochemical, nutritional, and biological conditions. We encountered significantly different active community members harboured by different water masses. We identified an active, late-stage phytoplankton bloom dominated by diatoms in the WSC, where *Bacteria* of the *Bacteroidetes* (*Flavobacteriales*, *Cytophagales*, and *Chitinophagales)* were most active in the surface layer (PSWw). The most abundant transcripts of functional genes in the location were ABC transporters and fundamental cellular functions supporting the high microbial activity in carbon and nitrogen cycling in surface waters, whereas deeper waters were characterized by a strong presence of AOA activity. Moreover, viral activities could be reported for the first time in the context of an ongoing phytoplankton bloom. We identified active phages of *Colwellia* and *Flavobacteriales* that likely contributed to the regulation of these and other bacterial activities in these surface waters. The waters of the EGC (PSW) on the other hand were characterized by lower nutrient concentrations, based on measurements, and likely higher amounts of refractory organic compounds, based on finding increased activity of SAR202 in this location. Here we present a wholistic view of the active fraction of the Arctic surface water microbiome during the warmest time of the year that permits an informative portrayal of the key players at the entrance of the Arctic Ocean highly impacted by global change.

References

Amon, R. M. W., Budéus, G., and Meon, B. (2003). Dissolved organic carbon distribution and origin in the Nordic Seas: Exchanges with the Arctic Ocean and the North Atlantic. *J. Geophys. Res. Ocean.* 108. doi:10.1029/2002JC001594.

Balzano, S., Gourvil, P., Siano, R., Chanoine, M., Marie, D., Lessard, S., et al. (2012). Diversity of cultured photosynthetic flagellates in the northeast Pacific and Arctic Oceans in summer. *Biogeosciences* 9, 4553–4571. doi:10.5194/bg-9-4553-2012.

Barbeyron, T., Brillet-Guéguen, L., Carré, W., Carrière, C., Caron, C., Czjzek, M., et al. (2016). Matching the Diversity of Sulfated Biomolecules: Creation of a Classification Database for Sulfatases Reflecting Their Substrate Specificity. *PLoS One* 11, e0164846. doi:10.1371/journal.pone.0164846.

Behnam, Krumpen, T., Smedsrud, L. H., and Gerdes, R. (2019). Fram Strait sea ice export affected by thinning: comparing high-resolution simulations and observations. *Clim. Dyn.* 53, 3257–3270. doi:10.1007/s00382-019-04699-z.

Belter, H. J., Krumpen, T., von Albedyll, L., Alekseeva, T. A., Birnbaum, G., Frolov, S. V, et al. (2021). Interannual variability in Transpolar Drift summer sea ice thickness and potential impact of Atlantification. *Cryosph.* 15, 2575–2591. doi:10.5194/tc-15-2575-2021.

Beszczynska-Möller, A., Fahrbach, E., Schauer, U., and Hansen, E. (2012). Variability in Atlantic water temperature and transport at the entrance to the Arctic Ocean, 19972010. *ICES J. Mar. Sci.* 69, 852–863. doi:10.1093/icesjms/fss056.

Bolger, A. M., Lohse, M., and Usadel, B. (2014). Trimmomatic: a flexible trimmer for Illumina sequence data. *Bioinformatics* 30, 2114–2120. doi:10.1093/bioinformatics/btu170.

Borriss, M., Helmke, E., Hanschke, R., and Schweder, T. (2003). Isolation and characterization of marine psychrophilic phage-host systems from Arctic sea ice. *Extremophiles* 7, 377–384. doi:10.1007/s00792-003-0334-7.

Borriss, M., Lombardot, T., Glöckner, F. O., Becher, D., Albrecht, D., and Schweder, T. (2007). Genome and proteome characterization of the psychrophilic Flavobacterium bacteriophage 11b. *Extremophiles* 11, 95–104. doi:10.1007/s00792-006-0014-5.

Bowman, J. P. (2020). Out From the Shadows – Resolution of the Taxonomy of the Family Cryomorphaceae. *Front. Microbiol.* 11. doi:10.3389/fmicb.2020.00795.

Breitbart, M., Bonnain, C., Malki, K., and Sawaya, N. A. (2018). Phage puppet masters of the marine microbial realm. *Nat. Microbiol.* 3, 754–766. doi:10.1038/s41564-018-0166-y.

Buchfink, B., Xie, C., and Huson, D. H. (2015). Fast and sensitive protein alignment using DIAMOND. *Nat. Methods* 12, 59–60. doi:10.1038/nmeth.3176.

Bushmanova, E., Antipov, D., Lapidus, A., and Prjibelski, A. D. (2019). rnaSPAdes: a de novo transcriptome assembler and its application to RNA-Seq data. *Gigascience* 8, giz100. doi:10.1093/gigascience/giz100.

Bushmanova, E., Antipov, D., Lapidus, A., Suvorov, V., and Prjibelski, A. D. (2016). rnaQUAST: a quality assessment tool for de novo transcriptome assemblies. *Bioinformatics* 32, 2210–2212. doi:10.1093/bioinformatics/btw218.

Cardozo-Mino, M. G., Fadeev, E., Salman-Carvalho, V., and Boetius, A. (2021). Spatial Distribution of Arctic Bacterioplankton Abundance Is Linked to Distinct Water Masses and Summertime Phytoplankton Bloom Dynamics (Fram Strait, 79°N). *Front. Microbiol.* 12, 1067. doi:10.3389/fmicb.2021.658803.

Cavalieri, D. J. (2003). Sea ice concentrations from Nimbus-7 SMMR and DMSP SSM/I passive microwave data. *Boulder, Color. USA, NASA Natl. Snow Ice Data Cent. Distrib. Act. Arch. Center, doi* 10. Available at: http://home.earthlink.net/~tech_comm/SupportFiles/Portfolio/NSIDC/nsidc0051_gsfc_seaice.gd.pdf.

Cleary, A. C., Søreide, J. E., Freese, D., Niehoff, B., and Gabrielsen, T. M. (2017). Feeding by Calanus glacialis in a high arctic fjord: potential seasonal importance of alternative prey.

ICES J. Mar. Sci. 74, 1937–1946.

Codispoti, L. A., Kelly, V., Thessen, A., Matrai, P., Suttles, S., Hill, V., et al. (2013). Synthesis of primary production in the Arctic Ocean: III. Nitrate and phosphate based estimates of net community production. *Prog. Oceanogr.* 110, 126–150. doi:10.1016/j.pocean.2012.11.006.

Colatriano, D., Tran, P. Q., Guéguen, C., Williams, W. J., Lovejoy, C., and Walsh, D. A. (2018). Genomic evidence for the degradation of terrestrial organic matter by pelagic Arctic Ocean Chloroflexi bacteria. *Commun. Biol.* 1, 90. doi:10.1038/s42003-018-0086-7.

Collins, R. E., and Deming, J. W. (2011). Abundant dissolved genetic material in Arctic sea ice Part II: Viral dynamics during autumn freeze-up. *Polar Biol.* 34, 1831–1841. doi:10.1007/s00300-011-1008-z.

Comiso, J. C., Parkinson, C. L., Gersten, R., and Stock, L. (2008). Accelerated decline in the Arctic sea ice cover. *Geophys. Res. Lett.* 35. doi:10.1029/2007GL031972.

Davidov, Y., and Jurkevitch, E. (2004). Diversity and evolution of Bdellovibrio-and-like organisms (BALOs), reclassification of Bacteriovorax starrii as Peredibacter starrii gen. nov., comb. nov., and description of the Bacteriovorax–Peredibacter clade as Bacteriovoracaceae fam. nov. *Int. J. Syst. Evol. Microbiol.* 54, 1439–1452. doi:10.1099/ijs.0.02978-0.

Degerlund, M., and Eilertsen, H. C. (2010). Main Species Characteristics of Phytoplankton Spring Blooms in NE Atlantic and Arctic Waters (68–80° N). *Estuaries and Coasts* 33, 242–269. doi:10.1007/s12237-009-9167-7.

DeLong, E. F., Preston, C. M., Mincer, T., Rich, V., Hallam, S. J., Frigaard, N.-U., et al. (2006). Community Genomics among Stratified Microbial Assemblages in the Ocean's Interior. *Science (80-.).* 311, 496–503.

Demory, D., Baudoux, A.-C., Monier, A., Simon, N., Six, C., Ge, P., et al. (2019). Picoeukaryotes of the Micromonas genus: sentinels of a warming ocean. *ISME J.* 13, 132–146. doi:10.1038/s41396-018-0248-0.

Dittmar, T., Cherrier, J., and Ludwichowski, K.-U. (2009). "The analysis of amino acids in seawater," in *Practical guidelines for the analysis of seawater* (CRC Press), 79–90.

Dong, X., and Strous, M. (2019). An Integrated Pipeline for Annotation and Visualization of Metagenomic Contigs. *Front. Genet.* 10. doi:10.3389/fgene.2019.00999.

Drula, E., Garron, M.-L., Dogan, S., Lombard, V., Henrissat, B., and Terrapon, N. (2022). The carbohydrate-active enzyme database: functions and literature. *Nucleic Acids Res.* 50, D571–D577. doi:10.1093/nar/gkab1045.

Engel, A., Bracher, A., Dinter, T., Endres, S., Grosse, J., Metfies, K., et al. (2019). Inter-annual variability of organic carbon concentrations in the eastern Fram Strait during summer (2009-2017). *Front. Mar. Sci.* 6, 187. doi:10.3389/fmars.2019.00187.

Engel, A., and Galgani, L. (2016). The organic sea-surface microlayer in the upwelling region off the coast of Peru and potential implications for air-sea exchange processes. *Biogeosciences* 13, 989–1007. doi:10.5194/bg-13-989-2016.

Engel, A., and Händel, N. (2011). A novel protocol for determining the concentration and composition of sugars in particulate and in high molecular weight dissolved organic matter (HMW-DOM) in seawater. *Mar. Chem.* 127, 180–191. doi:10.1016/j.marchem.2011.09.004.

Ezraty, R., Girard-Ardhuin, F., Piollé, J., Kaleschke, L., and Heygster, G. (2007). Arctic and Antarctic Sea Ice Concentration and Arctic Sea Ice Drift Estimated from Special Sensor Microwave Imager Data. *User's manual, Version* 2.

Fadeev, E., Cardozo-Mino, M. G., Rapp, J. Z., Bienhold, C., Salter, I., Salman-Carvalho, V., et al. (2021a). Comparison of Two 16S rRNA Primers (V3–V4 and V4–V5) for Studies of Arctic Microbial Communities. *Front. Microbiol.* 12, 283. Available at: https://www.frontiersin.org/articles/10.3389/fmicb.2021.637526/full.

Fadeev, E., Rogge, A., Ramondenc, S., Nöthig, E.-M., Wekerle, C., Bienhold, C., et al. (2020). Sea-ice retreat may decrease carbon export and vertical microbial connectivity in the Eurasian Arctic basins. *Nat. Res.* doi:10.21203/rs.3.rs-101878/v1.

Fadeev, E., Rogge, A., Ramondenc, S., Nöthig, E.-M., Wekerle, C., Bienhold, C., et al. (2021b). Sea ice presence is linked to higher carbon export and vertical microbial connectivity in the Eurasian Arctic Ocean. *Commun. Biol.* 4, 1255. doi:10.1038/s42003-021-02776-w.

Fadeev, E., Salter, I., Schourup-Kristensen, V., Nöthig, E. M., Metfies, K., Engel, A., et al. (2018). Microbial communities in the east and west fram strait during sea ice melting season. *Front. Mar. Sci.* 5, 429. doi:10.3389/fmars.2018.00429.

Falk-Petersen, S., Dahl, T. M., Scott, C. L., Sargent, J. R., Gulliksen, B., Kwasniewski, S., et al. (2002). Lipid biomarkers and trophic linkages between ctenophores and copepods in Svalbard waters. *Mar. Ecol. Prog. Ser.* 227, 187–194.

Flynn, K. J., Mitra, A., Anestis, K., Anschütz, A. A., Calbet, A., Ferreira, G. D., et al. (2019). Mixotrophic protists and a new paradigm for marine ecology: where does plankton research go now? *J. Plankton Res.* 41, 375–391. doi:10.1093/plankt/fbz026.

Fu, L., Niu, B., Zhu, Z., Wu, S., and Li, W. (2012). CD-HIT: accelerated for clustering the next-generation sequencing data. *Bioinformatics* 28, 3150-3152 NP–3. doi:10.1093/bioinformatics/bts565.

Fuhrman, J. A. (1999). Marine viruses and their biogeochemical and ecological effects. *Nature* 399, 541–548. doi:10.1038/21119.

Glöckner, F. O., Kube, M., Bauer, M., Teeling, H., Lombardot, T., Ludwig, W., et al. (2003). Complete genome sequence of the marine planctomycete Pirellula sp. strain 1. *Proc. Natl. Acad. Sci.* 100, 8298–8303. doi:10.1073/pnas.1431443100.

Grevesse, T., Guéguen, C., Onana, V. E., and Walsh, D. A. (2022). Degradation pathways for organic matter of terrestrial origin are widespread and expressed in Arctic Ocean microbiomes. *bioRxiv*, 2022.08.13.503825. doi:10.1101/2022.08.13.503825.

Gruber-Vodicka, H. R., Seah, B. K. B., Pruesse, E., Arumugam, M., and Kato, S. (2020). phyloFlash: Rapid Small-Subunit rRNA Profiling and Targeted Assembly from Metagenomes. *mSystems* 5, e00920-20. doi:10.1128/mSystems.00920-20.

Guillou, L., Bachar, D., Audic, S., Bass, D., Berney, C., Bittner, L., et al. (2013). The Protist Ribosomal Reference database (PR2): A catalog of unicellular eukaryote Small Sub-Unit rRNA sequences with curated taxonomy. *Nucleic Acids Res.* 41, D597–D604. doi:10.1093/nar/gks1160.

Hardge, K., Peeken, I., Neuhaus, S., Lange, B. A., Stock, A., Stoeck, T., et al. (2017). The importance of sea ice for exchange of habitat-specific protist communities in the Central Arctic Ocean. *J. Mar. Syst.* 165, 124–138. doi:10.1016/j.jmarsys.2016.10.004.

Hatzenpichler, R. (2012). Diversity, Physiology, and Niche Differentiation of Ammonia-Oxidizing Archaea. *Appl. Environ. Microbiol.* 78, 7501–7510. doi:10.1128/AEM.01960-12.

Haug, A., and Myklestad, S. (1976). Polysaccharides of marine diatoms with special reference to Chaetoceros species. *Mar. Biol.* 34, 217–222. doi:10.1007/BF00388798.

Heyerhoff, B., Engelen, B., and Bunse, C. (2022). Auxiliary Metabolic Gene Functions in

Pelagic and Benthic Viruses of the Baltic Sea. *Front. Microbiol.* 13. doi:10.3389/fmicb.2022.863620.

Hop, H., Vihtakari, M., Bluhm, B. A., Assmy, P., Poulin, M., Gradinger, R., et al. (2020). Changes in Sea-Ice Protist Diversity With Declining Sea Ice in the Arctic Ocean From the 1980s to 2010s. *Front. Mar. Sci.* 7. doi:10.3389/fmars.2020.00243.

Hoppe, C. J. M., Flintrop, C. M., and Rost, B. (2018). The Arctic picoeukaryote Micromonas pusilla benefits synergistically from warming and ocean acidification. *Biogeosciences* 15, 4353–4365. doi:10.5194/bg-15-4353-2018.

Hsieh, T. C., Ma, K. H., and Chao, A. (2016). iNEXT: an R package for rarefaction and extrapolation of species diversity (H ill numbers). *Methods Ecol. Evol.* 7, 1451–1456.

Huerta-Cepas, J., Szklarczyk, D., Heller, D., Hernández-Plaza, A., Forslund, S. K., Cook, H., et al. (2019). eggNOG 5.0: a hierarchical, functionally and phylogenetically annotated orthology resource based on 5090 organisms and 2502 viruses. *Nucleic Acids Res.* 47, D309–D314. doi:10.1093/nar/gky1085.

Hurwitz, B. L., and Sullivan, M. B. (2013). The Pacific Ocean Virome (POV): A Marine Viral Metagenomic Dataset and Associated Protein Clusters for Quantitative Viral Ecology. *PLoS One* 8, e57355. doi:10.1371/journal.pone.0057355.

Ittekkot, V., Brockmann, U., Michaelis, W., and Degens, E. T. (1981). Dissolved Free and Combined Carbohydrates During a Phytoplankton Bloom in the Northern North Sea. *Mar. Ecol. Prog. Ser.* 4, 299–305.

Jakobsson, M., Mayer, L., Coakley, B., Dowdeswell, J. A., Forbes, S., Fridman, B., et al. (2012). The international bathymetric chart of the Arctic Ocean (IBCAO) version 3.0. *Geophys. Res. Lett.* 39. doi:10.1029/2012GL052219.

Jiao, N., and Zheng, Q. (2011). The Microbial Carbon Pump: from Genes to Ecosystems. *Appl. Environ. Microbiol.* 77, 7439–7444. doi:10.1128/AEM.05640-11.

Kauko, H. M., Olsen, L. M., Duarte, P., Peeken, I., Granskog, M. A., Johnsen, G., et al. (2018). Algal Colonization of Young Arctic Sea Ice in Spring. *Front. Mar. Sci.* 5. Available at: https://www.frontiersin.org/article/10.3389/fmars.2018.00199.

Kilias, E., Wolf, C., Nöthig, E.-M., Peeken, I., and Metfies, K. (2013). Protist distribution in the Western Fram Strait in summer 2010 based on 454-pyrosequencing of 18S rDNA. *J. Phycol.* 49, 996–1010. doi:10.1111/jpy.12109.

Kirchman, D. L. (2002). The ecology of Cytophaga–Flavobacteria in aquatic environments. *FEMS Microbiol. Ecol.* 39, 91–100. doi:10.1111/j.1574-6941.2002.tb00910.x.

Kopylova, E., Noé, L., and Touzet, H. (2012). SortMeRNA: fast and accurate filtering of ribosomal RNAs in metatranscriptomic data. *Bioinformatics* 28, 3211–3217. doi:10.1093/bioinformatics/bts611.

Kortsch, S., Primicerio, R., Fossheim, M., Dolgov, A. V, and Aschan, M. (2015). Climate change alters the structure of arctic marine food webs due to poleward shifts of boreal generalists. *Proceedings. Biol. Sci.* 282, 20151546. doi:10.1098/rspb.2015.1546.

Krüger, K., Chafee, M., Francis, T. Ben, Del Rio, T. G., Becher, D., Schweder, T., et al. (2019). In marine Bacteroidetes the bulk of glycan degradation during algae blooms is mediated by few clades using a restricted set of genes. *ISME J.* 13, 2800–2816. doi:10.1038/s41396-019-0476-y.

Landry, Z., Swa, B. K., Herndl, G. J., Stepanauskas, R., and Giovannoni, S. J. (2017). SAR202 genomes from the dark ocean predict pathways for the oxidation of recalcitrant dissolved organic matter. *MBio* 8, e00413-17. doi:10.1128/mBio.00413-17.

Lannuzel, D., Tedesco, L., van Leeuwe, M., Campbell, K., Flores, H., Delille, B., et al. (2020).

The future of Arctic sea-ice biogeochemistry and ice-associated ecosystems. *Nat. Clim. Chang.* 10, 983–992. doi:10.1038/s41558-020-00940-4.

Levinsen, H., and Nielsen, T. G. (2002). The trophic role of marine pelagic ciliates and heterotrophic dinoflagellates in arctic and temperate coastal ecosystems: A cross-latitude comparison. *Limnol. Oceanogr.* 47, 427–439. doi:10.4319/lo.2002.47.2.0427.

Lewis, K. M., Van Dijken, G. L., and Arrigo, K. R. (2020). Changes in phytoplankton concentration now drive increased Arctic Ocean primary production. *Science (80-.).* 369, 198–202. doi:10.1126/science.aay8380.

Li, W. K. W., McLaughlin, F. A., Lovejoy, C., and Carmack, E. C. (2009). Smallest algae thrive as the arctic ocean freshens. *Science (80-.).* 326, 539. doi:10.1126/science.1179798.

Lindroth, P., and Mopper, K. (1979). High performance liquid chromatographic determination of subpicomole amounts of amino acids by precolumn fluorescence derivatization with o-phthaldialdehyde. *Anal. Chem.* 51, 1667–1674. doi:10.1021/ac50047a019.

Lovejoy, C., Massana, R., and Pedrós-Alió, C. (2006). Diversity and Distribution of Marine Microbial Eukaryotes in the Arctic Ocean and Adjacent Seas. *Appl. Environ. Microbiol.* 72, 3085–3095. doi:10.1128/AEM.72.5.3085-3095.2006.

Malfertheiner, L., Martínez-Pérez, C., Zhao, Z., Herndl, G. J., and Baltar, F. (2022). Phylogeny and Metabolic Potential of the Candidate Phylum SAR324. *Biology (Basel).* 11. doi:10.3390/biology11040599.

Martin-Cuadrado, A.-B., Rodriguez-Valera, F., Moreira, D., Alba, J. C., Ivars-Martínez, E., Henn, M. R., et al. (2008). Hindsight in the relative abundance, metabolic potential and genome dynamics of uncultivated marine archaea from comparative metagenomic analyses of bathypelagic plankton of different oceanic regions. *ISME J.* 2, 865–886. doi:10.1038/ismej.2008.40.

Massana, R. (2011). Eukaryotic picoplankton in surface oceans. *Annu. Rev. Microbiol.* 65, 91–110.

Melsheimer, C., and Spreen, G. (2019). AMSR2 ASI sea ice concentration data, Arctic, version 5.4 (NetCDF) (July 2012 - December 2019). doi:10.1594/PANGAEA.898399.

Meredith, M. P., and Sommerkorn, M. (2022). "Polar Regions," in *The Ocean and Cryosphere in a Changing Climate: Special Report of the Intergovernmental Panel on Climate Change*, ed. Intergovernmental Panel on Climate Change (IPCC) (Cambridge: Cambridge University Press), 203–320. doi:DOI: 10.1017/9781009157964.005.

Metfies, K., Bauerfeind, E., Wolf, C., Sprong, P., Frickenhaus, S., Kaleschke, L., et al. (2017). Protist communities in moored long-term sediment traps (Fram Strait, Arctic)-preservation with mercury chloride allows for PCR-based molecular genetic analyses. *Front. Mar. Sci.* 4, 301. doi:10.3389/fmars.2017.00301.

Metfies, K., Hoppmann, M., Tippenhauer, S., and Rohardt, G. (2021). Continuous thermosalinograph oceanography along RV POLARSTERN cruise track PS121. doi:10.1594/PANGAEA.930022.

Metfies, K., von Appen, W.-J., Kilias, E., Nicolaus, A., and Nöthig, E.-M. (2016). Biogeography and photosynthetic biomass of arctic marine pico-eukaroytes during summer of the record sea ice minimum 2012. *PLoS One* 11, e0148512.

Monier, A., Terrado, R., Thaler, M., Comeau, A., Medrinal, E., and Lovejoy, C. (2013). Upper Arctic Ocean water masses harbor distinct communities of heterotrophic flagellates. *Biogeosciences* 10, 4273–4286. doi:10.5194/bg-10-4273-2013.

Morency, C., Jacquemot, L., Potvin, M., and Lovejoy, C. (2022). A microbial perspective on

the local influence of Arctic rivers and estuaries on Hudson Bay (Canada). *Elem. Sci. Anthr.* 10, 9. doi:10.1525/elementa.2021.00009.

Morris, M., Rappé, S., Urbach, E., Connon, A., and Giovannoni, J. (2004). Prevalence of the Chloroflexi-Related SAR202 Bacterioplankton Cluster throughout the Mesopelagic Zone and Deep Ocean. *Appl. Environ. Microbiol.* 70, 2836–2842. doi:10.1128/AEM.70.5.2836-2842.2004.

Mou, X., Sun, S., Rayapati, P., and A, M. M. (2010). Genes for transport and metabolism of spermidine in Ruegeria pomeroyi DSS-3 and other marine bacteria. *Aquat. Microb. Ecol.* 58, 311–321. doi:10.3354/ame01367.

Müller, O., Wilson, B., Paulsen, M. L., Ruminska, A., Armo, H. R., Bratbak, G., et al. (2018). Spatiotemporal dynamics of ammonia-oxidizing Thaumarchaeota in Distinct Arctic water masses. *Front. Microbiol.* 9, 24. doi:10.3389/fmicb.2018.00024.

Niemi, A., Michel, C., Hille, K., and Poulin, M. (2011). Protist assemblages in winter sea ice: setting the stage for the spring ice algal bloom. *Polar Biol.* 34, 1803–1817. doi:10.1007/s00300-011-1059-1.

Nöthig, E. M., Bracher, A., Engel, A., Metfies, K., Niehoff, B., Peeken, I., et al. (2015). Summertime plankton ecology in fram strait-a compilation of long-and short-term observations. *Polar Res.* 34, 23349. doi:10.3402/polar.v34.23349.

Nöthig, E. M., Ramondenc, S., Haas, A., Hehemann, L., Walter, A., Bracher, A., et al. (2020). Summertime Chlorophyll a and Particulate Organic Carbon Standing Stocks in Surface Waters of the Fram Strait and the Arctic Ocean (1991–2015). *Front. Mar. Sci.* 7. doi:10.3389/fmars.2020.00350.

Ogata, H., Goto, S., Sato, K., Fujibuchi, W., Bono, H., and Kanehisa, M. (1999). KEGG: Kyoto Encyclopedia of Genes and Genomes. *Nucleic Acids Res.* 27, 29–34. doi:10.1093/nar/27.1.29.

Oksanen, J., Blanchet, F. G., Kindt, R., Legendre, P., Minchin, P. R., O'hara, R. B., et al. (2013). Community ecology package. *R Packag. version* 2.

Orsi, W. D., Smith, J. M., Wilcox, H. M., Swalwell, J. E., Carini, P., Worden, A. Z., et al. (2015). Ecophysiology of uncultivated marine euryarchaea is linked to particulate organic matter. *ISME J.* 9, 1747–1763. doi:10.1038/ismej.2014.260.

Parada, A. E., and Fuhrman, J. A. (2017). Marine archaeal dynamics and interactions with the microbial community over 5 years from surface to seafloor. *ISME J.* 11, 2510–2525. doi:10.1038/ismej.2017.104.

Pautova, L. A., Silkin, V. A., Kravchishina, M. D., Yakubenko, V. G., Kudryavtseva, E. A., Klyuvitkin, A. A., et al. (2021). Pelagic Ecosystem of the Nansen Basin under the Influence of Variable Atlantic Water Inflow: The Mechanism Forming Diatom Bloom in the Marginal Ice Zone. *Dokl. Earth Sci.* 499, 590–594. doi:10.1134/S1028334X21070138.

Pereira, O., Hochart, C., Auguet, J. C., Debroas, D., and Galand, P. E. (2019). Genomic ecology of Marine Group II, the most common marine planktonic Archaea across the surface ocean. *Microbiologyopen* 8, e00852. doi:10.1002/mbo3.852.

Polyakov, I. V., Pnyushkov, A. V., Alkire, M. B., Ashik, I. M., Baumann, T. M., Carmack, E. C., et al. (2017). Greater role for Atlantic inflows on sea-ice loss in the Eurasian Basin of the Arctic Ocean. *Science (80-.).* 356, 285–291. doi:10.1126/science.aai8204.

Polyakov, I. V, Alkire, M. B., Bluhm, B. A., Brown, K. A., Carmack, E. C., Chierici, M., et al. (2020a). Borealization of the Arctic Ocean in Response to Anomalous Advection From Sub-Arctic Seas. *Front. Mar. Sci.* 7. doi:10.3389/fmars.2020.00491.

Polyakov, I. V, Rippeth, T. P., Fer, I., Alkire, M. B., Baumann, T. M., Carmack, E. C., et al.

(2020b). Weakening of Cold Halocline Layer Exposes Sea Ice to Oceanic Heat in the Eastern Arctic Ocean. *J. Clim.* 33, 8107–8123. doi:10.1175/JCLI-D-19-0976.1.

Poretsky, R. S., Sun, S., Mou, X., and Moran, M. A. (2010). Transporter genes expressed by coastal bacterioplankton in response to dissolved organic carbon. *Environ. Microbiol.* 12, 616–627. doi:10.1111/j.1462-2920.2009.02102.x.

Priest, T., Appen, W.-J. von, Oldenburg, E., Popa, O., Torres-Valdés, S., Bienhold, C., et al. (2022). Variations in Atlantic water influx and sea-ice cover drive taxonomic and functional shifts in Arctic marine bacterial communities. *bioRxiv*, 2022.08.12.503524. doi:10.1101/2022.08.12.503524.

Quast, C., Pruesse, E., Yilmaz, P., Gerken, J., Schweer, T., Yarza, P., et al. (2013). The SILVA ribosomal RNA gene database project: Improved data processing and web-based tools. *Nucleic Acids Res.* 41, D590–D596. doi:10.1093/nar/gks1219.

Ramondenc, S., Nöthig, E.-M., Hufnagel, L., Bauerfeind, E., Busch, K., Knüppel, N., et al. (2022). Effects of Atlantification and changing sea-ice dynamics on zooplankton community structure and carbon flux between 2000 and 2016 in the eastern Fram Strait. *Limnol. Oceanogr.* n/a. doi:10.1002/lno.12192.

Rawlings, N. D., Barrett, A. J., Thomas, P. D., Huang, X., Bateman, A., and Finn, R. D. (2018). The MEROPS database of proteolytic enzymes, their substrates and inhibitors in 2017 and a comparison with peptidases in the PANTHER database. *Nucleic Acids Res.* 46, D624–D632. doi:10.1093/nar/gkx1134.

Rinke, C., Rubino, F., Messer, L. F., Youssef, N., Parks, D. H., Chuvochina, M., et al. (2019). A phylogenomic and ecological analysis of the globally abundant Marine Group II archaea (Ca. Poseidoniales ord. nov.). *ISME J.* 13, 663–675. doi:10.1038/s41396-018-0282-y.

Rinke, C., Schwientek, P., Sczyrba, A., Ivanova, N. N., Anderson, I. J., Cheng, J.-F., et al. (2013). Insights into the phylogeny and coding potential of microbial dark matter. *Nature* 499, 431–437. doi:10.1038/nature12352.

Rognes, T., Flouri, T., Nichols, B., Quince, C., and Mahé, F. (2016). VSEARCH: a versatile open source tool for metagenomics. *PeerJ* 4, e2584–e2584. doi:10.7717/peerj.2584.

Rudels, B., Schauer, U., Björk, G., Korhonen, M., Pisarev, S., Rabe, B., et al. (2012). Observations of water masses and circulation in the Eurasian Basin of the Arctic Ocean from the 1990s to the late 2000s. *Ocean Sci. Discuss.* 9, 2695–2747. doi:10.5194/osd-9-2695-2012.

Saier, M. H., Reddy, V. S., Moreno-Hagelsieb, G., Hendargo, K. J., Zhang, Y., Iddamsetty, V., et al. (2021). The Transporter Classification Database (TCDB): 2021 update. *Nucleic Acids Res.* 49, D461–D467. doi:10.1093/nar/gkaa1004.

Saito, H., Ota, T., Suzuki, K., Nishioka, J., and Tsuda, A. (2006). Role of heterotrophic dinoflagellate Gyrodinium sp. in the fate of an iron induced diatom bloom. *Geophys. Res. Lett.* 33. doi:10.1029/2005GL025366.

Salazar, G., Cornejo-Castillo, F. M., Benítez-Barrios, V., Fraile-Nuez, E., Álvarez-Salgado, X. A., Duarte, C. M., et al. (2016). Global diversity and biogeography of deep-sea pelagic prokaryotes. *ISME J.* 10, 596–608. doi:10.1038/ismej.2015.137.

Saw, J., Nunoura, T., Hirai, M., Takaki, Y., Parsons, R., Michelsen, M., et al. (2020). Pangenomics Analysis Reveals Diversification of Enzyme Families and Niche Specialization in Globally Abundant SAR202 Bacteria. *MBio* 11, e02975-19. doi:10.1128/mBio.02975-19.

Schanke, N. L., Bolinesi, F., Mangoni, O., Katlein, C., Anhaus, P., Hoppmann, M., et al. (2021). Biogeochemical and ecological variability during the late summer–early autumn

transition at an ice-floe drift station in the Central Arctic Ocean. *Limnol. Oceanogr.* 66, S363–S382. doi:10.1002/lno.11676.

Schlitzer, R. (2018). Ocean Data View. Available at: https://odv.awi.de.

Serreze, M. C., Barrett, A. P., Stroeve, J. C., Kindig, D. N., and Holland, M. M. (2009). The emergence of surface-based Arctic amplification. *Cryosph.* 3, 11–19. doi:10.5194/tc-3-11-2009.

Sherr, E., and Sherr, F. (2007). Heterotrophic dinoflagellates: a significant component of microzooplankton biomass and major grazers of diatoms in the sea. *Mar. Ecol. Prog. Ser.* 352, 187–197. doi:10.3354/meps07161.

Soltwedel, T., Bauerfeind, E., Bergmann, M., Bracher, A., Budaeva, N., Busch, K., et al. (2016). Natural variability or anthropogenically-induced variation? Insights from 15 years of multidisciplinary observations at the arctic marine LTER site HAUSGARTEN. *Ecol. Indic.* 65, 89–102. doi:10.1016/j.ecolind.2015.10.001.

Sowell, S. M., Wilhelm, L. J., Norbeck, A. D., Lipton, M. S., Nicora, C. D., Barofsky, D. F., et al. (2009). Transport functions dominate the SAR11 metaproteome at low-nutrient extremes in the Sargasso Sea. *ISME J.* 3, 93–105. doi:10.1038/ismej.2008.83.

Stratmann, T., Lund-Hansen, L. C., Sorrell, B. K., and Markager, S. (2017). Concentrations of organic and inorganic bound nutrients and chlorophyll a in the Eurasian Basin, Arctic Ocean, early autumn 2012. *Reg. Stud. Mar. Sci.* 9, 69–75. doi:10.1016/j.rsma.2016.11.008.

Tepes, P., Nienow, P., and Gourmelen, N. (2021). Accelerating Ice Mass Loss Across Arctic Russia in Response to Atmospheric Warming, Sea Ice Decline, and Atlantification of the Eurasian Arctic Shelf Seas. *J. Geophys. Res. Earth Surf.* 126, e2021JF006068. doi:10.1029/2021JF006068.

Torres-Valdés, S., Tsubouchi, T., Bacon, S., Naveira-Garabato, A. C., Sanders, R., McLaughlin, F. A., et al. (2013). Export of nutrients from the Arctic Ocean. *J. Geophys. Res. Ocean.* 118, 1625–1644. doi:https://doi.org/10.1002/jgrc.20063.

Tsubouchi, T., Våge, K., Hansen, B., Larsen, K. M. H., Østerhus, S., Johnson, C., et al. (2021). Increased ocean heat transport into the Nordic Seas and Arctic Ocean over the period 1993–2016. *Nat. Clim. Chang.* 11, 21–26. doi:10.1038/s41558-020-00941-3.

Unfried, F., Becker, S., Robb, C. S., Hehemann, J.-H., Markert, S., Heiden, S. E., et al. (2018). Adaptive mechanisms that provide competitive advantages to marine bacteroidetes during microalgal blooms. *ISME J.* 12, 2894–2906. doi:10.1038/s41396-018-0243-5.

Vidal-Melgosa, S., Sichert, A., Francis, T. Ben, Bartosik, D., Niggemann, J., Wichels, A., et al. (2021). Diatom fucan polysaccharide precipitates carbon during algal blooms. *Nat. Commun.* 12, 1150. doi:10.1038/s41467-021-21009-6.

Vipindas, P. V, Krishnan, K. P., Rehitha, T. V, Jabir, T., and Dinesh, S. L. (2020). Diversity of sediment associated Planctomycetes and its related phyla with special reference to anammox bacterial community in a high Arctic fjord. *World J. Microbiol. Biotechnol.* 36, 107. doi:10.1007/s11274-020-02886-3.

von Appen, W.-J., Waite, A. M., Bergmann, M., Bienhold, C., Boebel, O., Bracher, A., et al. (2021). Sea-ice derived meltwater stratification slows the biological carbon pump: results from continuous observations. *Nat. Commun.* 12, 1–16.

von Jackowski, A., Grosse, J., Nöthig, E.-M., and Engel, A. (2020). Dynamics of organic matter and bacterial activity in the Fram Strait during summer and autumn. *Philos. Trans. R. Soc. A Math. Phys. Eng. Sci.* 378, 20190366. doi:10.1098/rsta.2019.0366.

Wells, L. E., and Deming, J. W. (2006). Characterization of a cold-active bacteriophage on

two psychrophilic marine hosts. *Aquat. Microb. Ecol.* 45, 15–29.
Wickham, H. (2016). "Getting Started with ggplot2," in *ggplot2* (Springer), 11–31. doi:10.1007/978-3-319-24277-4_2.
Wickham, H., Averick, M., Bryan, J., Chang, W., McGowan, L., François, R., et al. (2019). Welcome to the Tidyverse. *J. Open Source Softw.* 4, 1686. doi:10.21105/joss.01686.
Wietz, M., Bienhold, C., Metfies, K., Torres-Valdés, S., von Appen, W.-J., Salter, I., et al. (2021). The polar night shift: seasonal dynamics and drivers of Arctic Ocean microbiomes revealed by autonomous sampling. *ISME Commun.* 1, 76. doi:10.1038/s43705-021-00074-4.
Williamson, S. J., Rusch, D. B., Yooseph, S., Halpern, A. L., Heidelberg, K. B., Glass, J. I., et al. (2008). The Sorcerer II Global Ocean Sampling Expedition: Metagenomic Characterization of Viruses within Aquatic Microbial Samples. *PLoS One* 3, e1456. doi:10.1371/journal.pone.0001456.
Wilson, B., Müller, O., Nordmann, E. L., Seuthe, L., Bratbak, G., and Øvreås, L. (2017). Changes in marine prokaryote composition with season and depth over an Arctic polar year. *Front. Mar. Sci.* 4, 95. doi:10.3389/fmars.2017.00095.
Yadav, J., Kumar, A., and Mohan, R. (2020). Dramatic decline of Arctic sea ice linked to global warming. *Nat. Hazards* 103, 2617–2621. doi:10.1007/s11069-020-04064-y.
Young, J. R., Geisen, M., Cros, L., Kleijne, A., Sprengel, C., Probert, I., et al. (2003). A guide to extant coccolithophore taxonomy. *J. Nannoplankt. Res. Spec. Issue* 1, 1–132.
Zdobnov, E. M., and Apweiler, R. (2001). InterProScan--an integration platform for the signature-recognition methods in InterPro. *Bioinformatics* 17, 847–848. doi:10.1093/bioinformatics/17.9.847.
Zhong, Z.-P., Rapp, J. Z., Wainaina, J. M., Solonenko, N. E., Maughan, H., Carpenter, S. D., et al. (2020). Viral ecogenomics of arctic cryopeg brine and sea ice. *Msystems* 5, e00246-20. doi:10.1128/mSystems.00246-20.

Supplementary Material

Table S1. Overview of metatranscriptomic sequencing and read processing output. The table consists of stations sampled during RV Polarstern expedition PS121, as well as bioinformatic steps.

PANGAEA station ID	Station name	Long. (°E)	Lat. (°N)	Sampling date	Depth	Size fraction (µm)	No of sequences								
							Raw	After removing adapter	% retained after removing adapter	After quality trimming	% retained after trimming	non-rRNA		rRNA	
												No. Of sequences	%	No. Of sequences	%
PS121/052-6	F4	6.99	79.02	10-09-2019	DCM	10	82031320	82031303	99.99	69538300	95.93	5839835	8.40	63698465	91.60
PS121/052-6	F4	6.99	79.02	10-09-2019	DCM	3	74568597	74568577	99.99	63212410	95.93	6598743	10.44	56613667	89.56
PS121/052-6	F4	6.99	79.02	10-09-2019	DCM	0.2	82387195	82387173	99.99	68562571	95.50	5566335	8.12	62996236	91.88
PS121/052-6	F4	6.99	79.02	10-09-2019	100M	3	82770628	82770606	99.99	67139672	95.02	10078978	15.01	57060694	84.99
PS121/052-6	F4	6.99	79.02	10-09-2019	100M	0.2	82643126	82643105	99.99	68865725	95.45	4842956	7.03	64022769	92.97
PS121-5-3	HGI	6.08	79.13	17-08-2019	DCM	10	82088119	82088085	99.99	69903218	96.03	6629974	9.48	63273244	90.52
PS121-5-3	HGI	6.08	79.13	17-08-2019	DCM	3	87812025	87812003	99.99	66971387	93.72	6498147	9.70	60473240	90.30
PS121-5-3	HGI	6.08	79.13	17-08-2019	DCM	0.2	90675181	90675154	99.99	76380714	95.79	5865741	7.68	70514973	92.32
PS121-5-3	HGI	6.08	79.13	17-08-2019	100M	3	81855018	81854983	99.99	68845205	95.79	10539457	15.31	58305748	84.69
PS121-5-3	HGI	6.08	79.13	17-08-2019	100M	0.2	70000931	70000920	99.99	58818385	95.70	4809686	8.18	54008699	91.82
PS121/043-7	N4	4.47	79.73	06-09-2019	DCM	10	86620526	86620500	99.99	73299884	95.86	7192780	9.81	66107104	90.19
PS121/043-7	N4	4.47	79.73	06-09-2019	DCM	3	86710971	86710945	99.99	73516471	95.89	8472619	11.52	65043852	88.48
PS121/043-7	N4	4.47	79.73	06-09-2019	DCM	0.2	80074140	80074107	99.99	67414228	95.74	5348856	7.93	62065372	92.07
PS121/043-7	N4	4.47	79.73	06-09-2019	100M	3	90640056	90640021	99.99	76549516	95.80	8629144	11.27	67920372	88.73

PS121/043-7	N4	4.47	79.73	06-09-2019	100M	0.2	85901660	85901647	99.99	72306722	95.68	6141432	8.49	66165290	91.51
PS121/007-3	HGIV	4.19	79.06	18-08-2019	DCM	10	90799996	90799953	99.99	76881539	95.84	7016040	9.13	69865499	90.87
PS121/007-3	HGIV	4.19	79.06	18-08-2019	DCM	3	82332017	82331990	99.99	69407365	95.82	7422342	10.69	61985023	89.31
PS121/007-3	HGIV	4.19	79.06	18-08-2019	DCM	0.2	76932681	76932651	99.99	58514913	93.76	4588554	7.84	53926359	92.16
PS121/007-3	HGIV	4.19	79.06	18-08-2019	100M	3	82179003	82178903	99.99	67025530	95.42	18893221	28.19	48132309	71.81
PS121/007-3	HGIV	4.19	79.06	18-08-2019	100M	0.2	89415805	89415769	99.99	75059489	95.68	5883239	7.84	69176250	92.16
PS121/035-3	EGI	-5.37	78.98	01-09-2019	DCM	10	92435945	92435889	99.99	77356572	95.67	7558514	9.77	69798058	90.23
PS121/035-3	EGI	-5.37	78.98	01-09-2019	DCM	3	95644590	95644547	99.99	80653231	95.82	8443884	10.47	72209347	89.53
PS121/035-3	EGI	-5.37	78.98	01-09-2019	DCM	0.2	77223925	77223900	99.99	64782242	95.69	5729912	8.84	59052330	91.16
PS121/035-3	EGI	-5.37	78.98	01-09-2019	100M	3	88291478	88291378	99.99	74220467	95.75	8076748	10.88	66143719	89.12
PS121/035-3	EGI	-5.37	78.98	01-09-2019	100M	0.2	80861877	80861843	99.99	68640886	95.93	6014605	8.76	62626281	91.24

Table S2. Coverage of reconstructed SSU per sample.

Station name	Size	Depth	Coverage	Num reads
F4	10µm	DCM	35.02 %	17511642
F4	3µm	DCM	34.77 %	17386211
F4	0.2µm	DCM	35.50 %	17751337
F4	3µm	100M	33.88 %	16939391
F4	0.2µm	100M	34.30 %	17150834
HGI	10µm	DCM	35.90 %	17949513
HGI	3µm	DCM	34.94 %	17471730
HGI	0.2µm	DCM	35.53 %	17763238
HGI	3µm	100M	35.00 %	17500771
HGI	0.2µm	100M	34.50 %	17247540
N4	10µm	DCM	36.27 %	18135477
N4	3µm	DCM	34.23 %	17114422
N4	0.2µm	DCM	35.13 %	17564255
N4	3µm	100M	35.82 %	17911688
N4	0.2µm	100M	35.52 %	17758084
HGIV	10µm	DCM	34.40 %	17201296
HGIV	3µm	DCM	34.32 %	17160126
HGIV	0.2µm	DCM	34.87 %	17433487
HGIV	3µm	100M	36.83 %	17728201
HGIV	0.2µm	100M	34.08 %	17039457
EGI	10µm	DCM	31.61 %	15806672
EGI	3µm	DCM	31.52 %	15759749
EGI	0.2µm	DCM	32.54 %	16270944
EGI	3µm	100M	31.54 %	15767954
EGI	0.2µm	100M	33.71 %	16853653

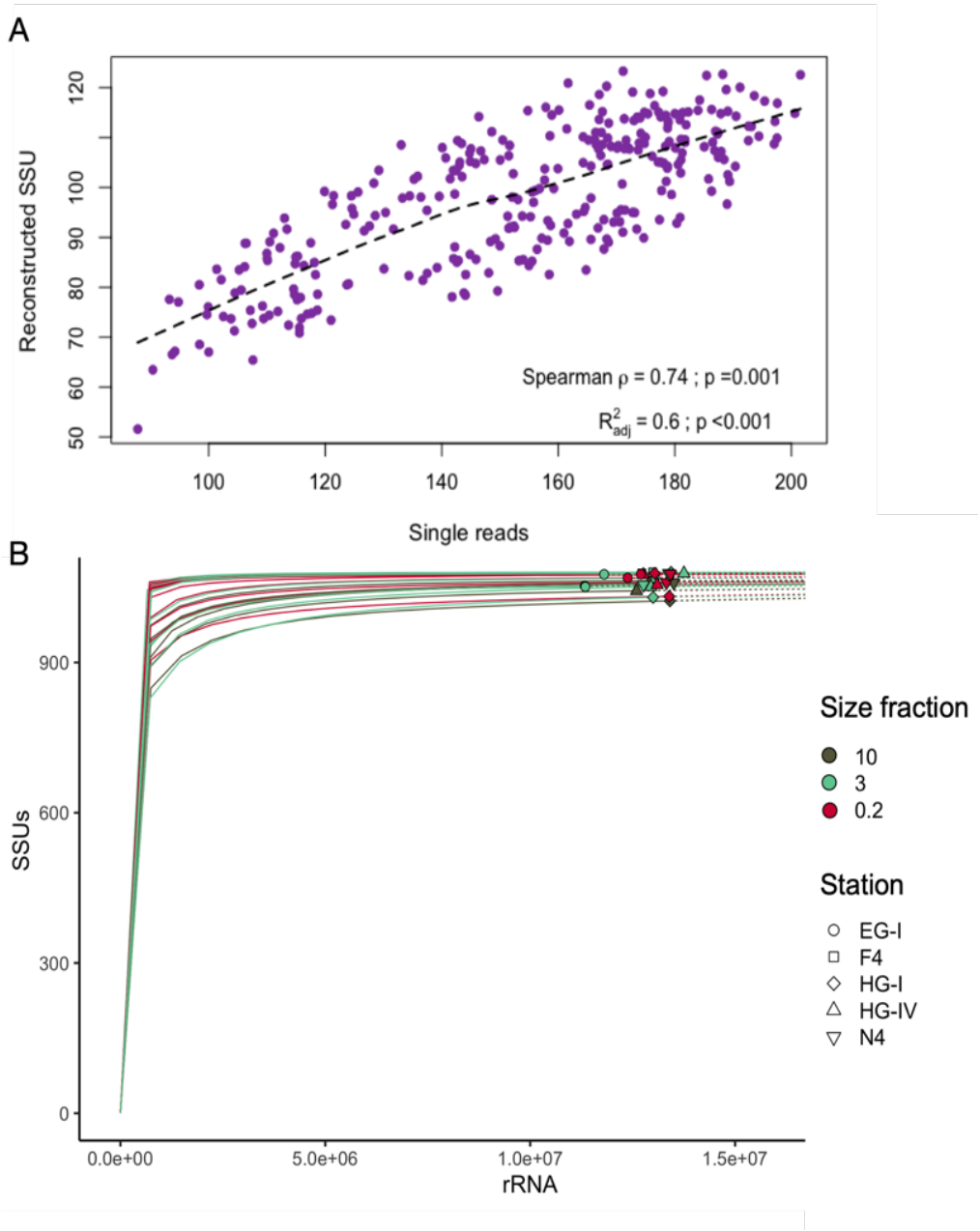

Figure S1. A) Comparison of single reads and reconstructed SSU based on non-parametric Mantel test based on the Spearman correlation coefficient (significance assessed based on 999 Monte Carlo permutations). Linear model's R2, Spearman's rho correlation and their significance indicated consensus between reads and SSUs. B) Rarefaction curves of reconstructed SSUs depicted in each sample. The solid lines represent the observed accumulation of reads (interpolation) and the dashed lines the accumulation (extrapolation) of double the number of reads. Rarefaction curves were created using the iNEXT package v2.0.12 (Hsieh et al., 2016).

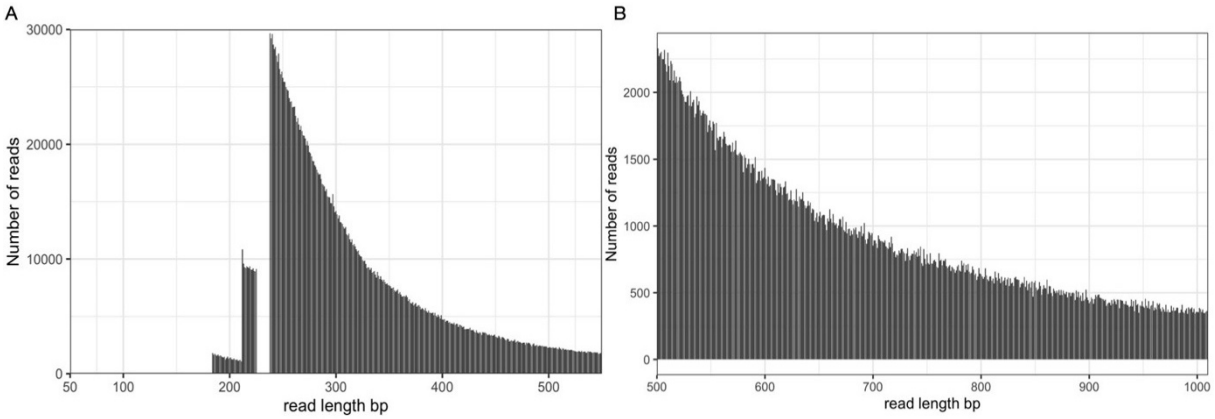

Figure S2. Frequency distribution of sequencing read lengths in A) the gene catalogue and in B) the gene catalogue after a cutoff of 500 bp in read length.

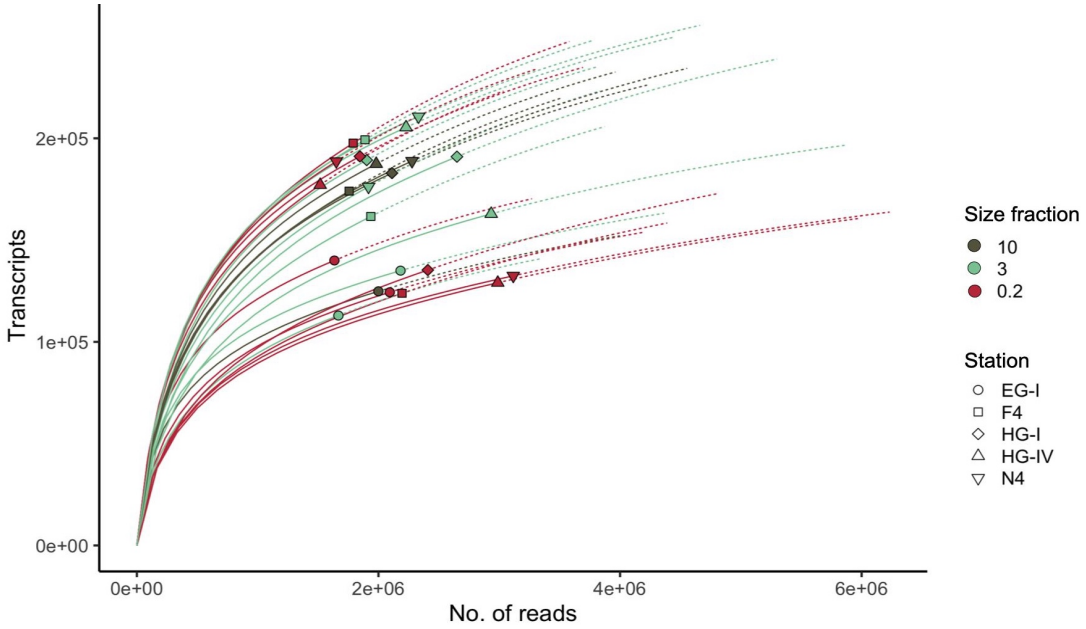

Figure S3. Rarefaction curves of number of transcripts per sample. The solid lines represent the observed accumulation of reads (interpolation) and the dashed lines the accumulation (extrapolation) of double the number of reads. Rarefaction curves were created using the iNEXT package v2.0.12 (Hsieh et al., 2016).

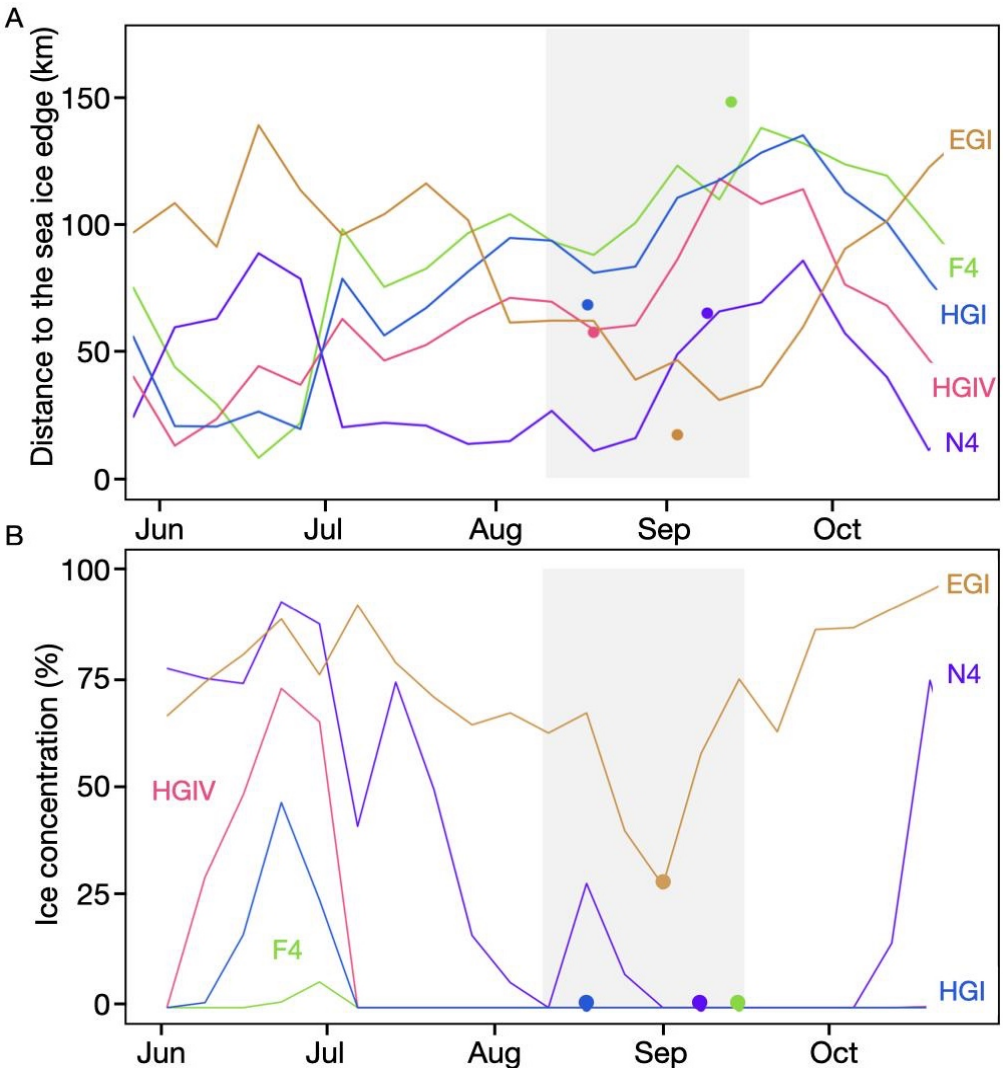

Figure S4. A) Distance to the sea ice edge (km) and B) ice cover (%) at the sampling sites depicted for the period from June to October 2019. The sampling date for each station is noted by the colored circles. Lines correspond to weekly calculated values. The light grey area indicates the sampling period during PS121.

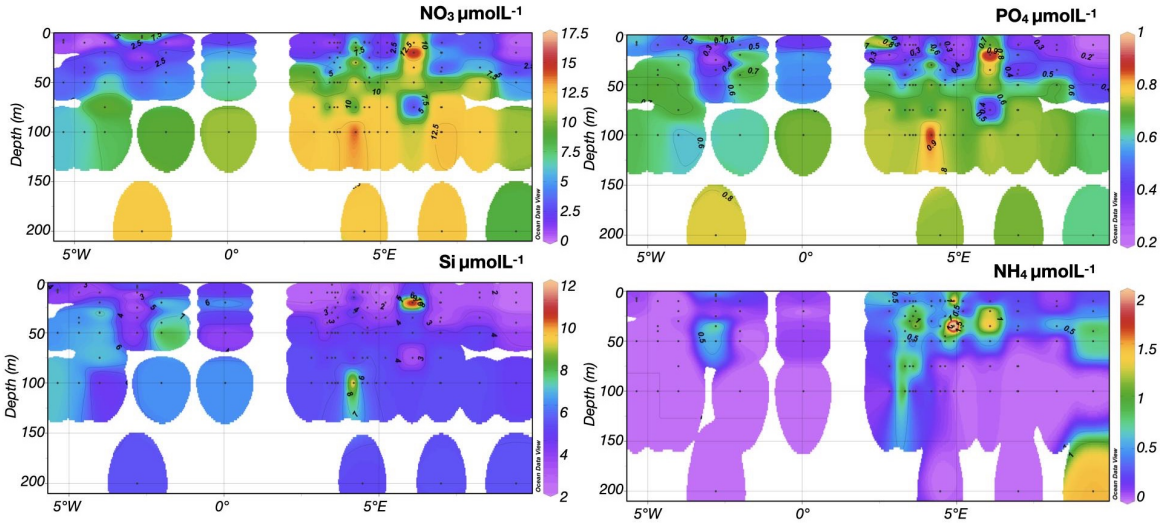

Figure S5. Nutrient profile at the ~ 79°N transect (79.7°N - 78.7°N) measured in-situ at the uppermost 200 m during PS121 expedition to Fram Strait, black dots represent sampled depth.

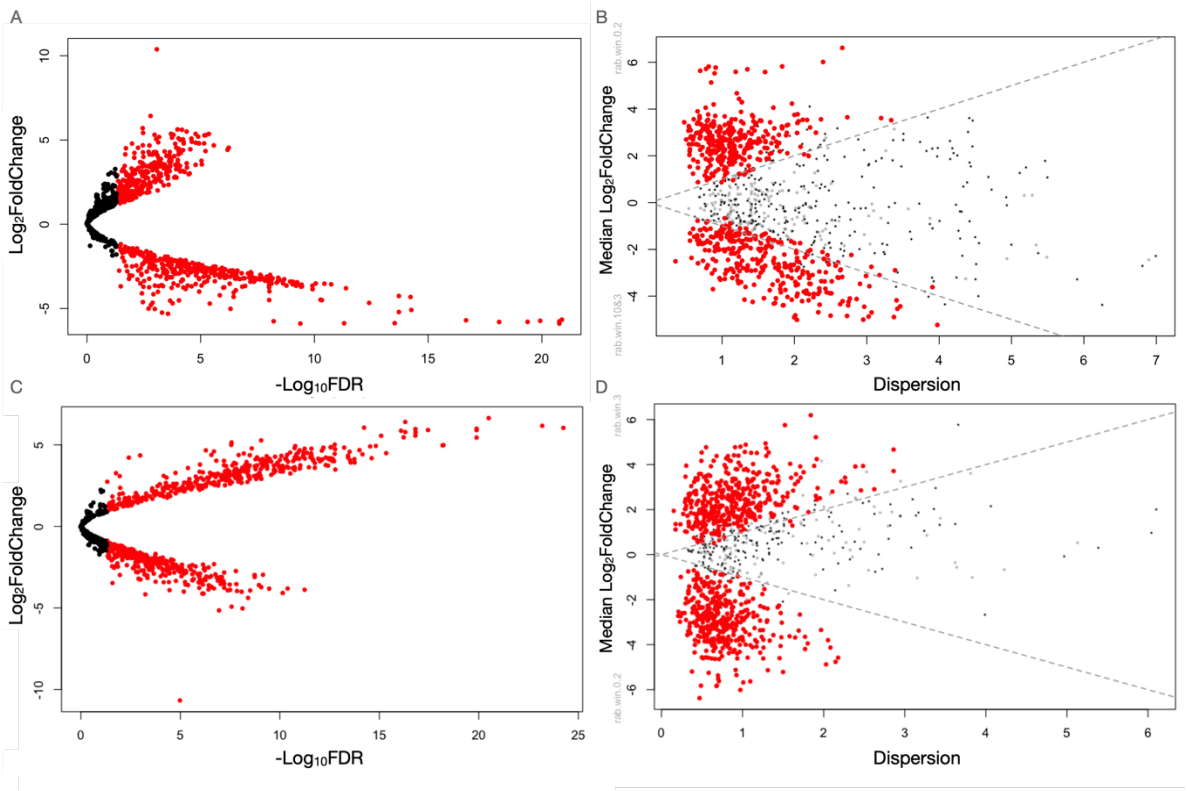

Figure S6. Volcano plot (A & C) and effect size plots of Aldex (B & D) for PSWw (A & B) and AW (C & D) water masses. Plots features differential abundance between reconstructed SSU rRNAs. B) & D) Red dots are SSUs with a <0.1 Benjamini-Hochberg false discovery rate from the Wilcoxon rank sum test performed with Aldex

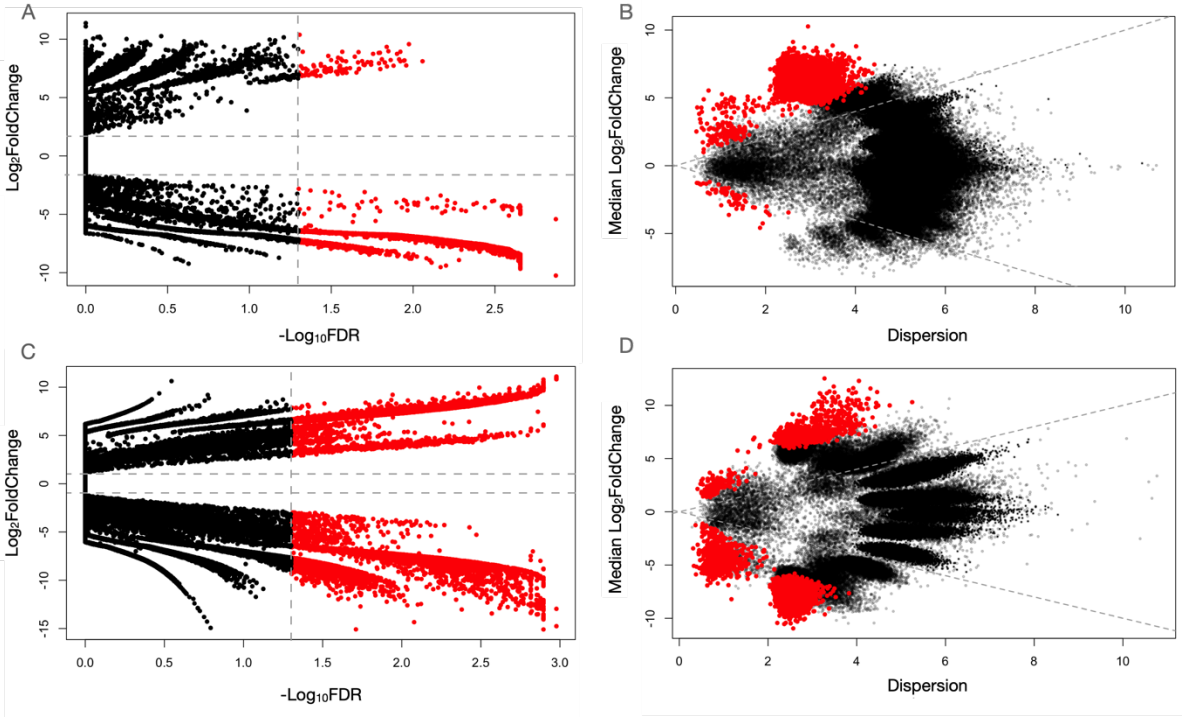

Figure S7. Volcano plot (A & C) and effect size plots of ALDEX2 (B & D) for PSWw (A & B) and AW (C & D) water masses. Plots features differential abundance between transcripts. B) & D) Red dots are transcripts with a <0.1 Benjamini-Hochberg false discovery rate from the Wilcoxon rank sum test performed with Aldex.

Chapter II

Spatial distribution of Arctic bacterioplankton abundance is linked to distinct water masses and summertime phytoplankton bloom dynamics (Fram Strait, 79°N) bloom

Magda G. Cardozo-Miño [1,2*†], *Eduard Fadeev* [1,2,3†], *Verena Salman-Carvalho*[1,2,4], *Antje Boetius*[1,2,5]

[1]Max Planck Institute for Marine Microbiology, Bremen, Germany
[2]Alfred Wegener Institute, Helmholtz Center for Polar and Marine Research, Bremerhaven, Germany
[3]Current affiliation: Department of Functional and Evolutionary Ecology, University of Vienna, Vienna, Austria
[4]Current affiliation: Microbiology Department, University of Massachusetts Amherst, Massachusetts, MA, United States of America
[5]MARUM, University of Bremen, Bremen, Germany
† - equal contribution

Keywords: Arctic Ocean, Fram Strait, bacterioplankton, CARD-FISH, water column

Published in Frontiers in Microbiology 12, 1067. doi:10.3389/fmicb.2021.658803.

Abstract

The Arctic is impacted by climate warming faster than any other oceanic region on Earth. Assessing the baseline of microbial communities in this rapidly changing ecosystem is vital for understanding the implications of ocean warming and sea ice retreat on ecosystem functioning. Using CARD-FISH and semi-automated counting, we quantified 14 ecologically relevant taxonomic groups of bacterioplankton (*Bacteria* and *Archaea*) from surface (0-30 m) down to deep waters (2500 m) in summer ice-covered and ice-free regions of the Fram Strait, the main gateway for Atlantic inflow into the Arctic Ocean. Cell abundances of the bacterioplankton communities in surface waters varied from 10^5 cells mL^{-1} in ice-covered regions to 10^6 cells mL^{-1} in the ice-free regions. Observations suggest that these were overall driven by variations in phytoplankton bloom conditions across the Strait. The bacterial groups *Bacteroidetes* and *Gammaproteobacteria* showed several-fold higher cell abundances under late phytoplankton bloom conditions of the ice-free regions. Other taxonomic groups, such as the *Rhodobacteraceae*, revealed a distinct association of cell abundances with the surface Atlantic waters. With increasing depth (> 500 m), the total cell abundances of the bacterioplankton communities decreased by up to two orders of magnitude, while largely unknown taxonomic groups (e.g., *SAR324* and *SAR202* clades) maintained constant cell abundances throughout the entire water column (ca. 10^3 cells mL^{-1}). This suggests that these enigmatic groups may occupy a specific ecological niche in the entire water column. Our results provide the first quantitative spatial variations assessment of bacterioplankton in the summer ice-covered and ice-free Arctic water column, and suggest that further shift towards ice-free Arctic summers with longer phytoplankton blooms can lead to major changes in the associated standing stock of the bacterioplankton communities.

Introduction

Atmospheric and oceanic warming has a substantial impact on the Arctic Ocean already today (Dobricic et al., 2016; Sun et al., 2016; Dai et al., 2019). The strong decline in sea ice coverage (Peng and Meier, 2018; Dai et al., 2019) and heat transfer by the Atlantic water inflow (Beszczynska-Möller et al., 2012; Rudels et al., 2012; Walczowski et al., 2017) will affect stratification of the water column and can lead to an increase in upward mixing of the Atlantic core water, a process also termed "Atlantification" (Polyakov et al., 2017). The main inflow of Atlantic water into the Arctic Ocean occurs through the Fram Strait (Beszczynska-Möller et al., 2011), making it a sentinel region for observing the ongoing changes in the Arctic marine ecosystem (Soltwedel et al., 2005, 2016). The Fram Strait is also the main deep-water gateway between the Atlantic and the Arctic Ocean. It hosts two distinct hydrographic regimes; the West Spitsbergen Current (WSC) that carries relatively warm and saline Atlantic water northwards along the Svalbard shelf (Beszczynska-Möller et al., 2012; von Appen et al., 2015), and the East Greenland Current (EGC) that transports cold polar water and sea ice southwards from the Arctic Ocean along the ice-covered Greenland shelf (de Steur et al., 2009; Wekerle et al., 2017).

Sea ice conditions have a strong impact on the seasonal ecological dynamics in Fram Strait and the whole Arctic Ocean (Wassmann and Reigstad, 2011), affecting light availability and stratification in the water column. The presence of sea ice and snow cover can suppress the seasonal phytoplankton bloom in the water column through light limitation (Mundy et al., 2005; Leu et al., 2011), or change its timing, e.g. by increasing stratification of the surface waters once the ice melts (Korhonen et al., 2013). Also, sea-ice algae can make up a significant proportion of the annual productivity (Leu et al., 2011; Boetius et al., 2013; Fernández-Méndez et al., 2014). Previous summer observations in the Fram Strait already suggested that total cell abundances and productivity of bacterioplankton communities in surface waters are driven by environmental parameters associated with phytoplankton bloom dynamics (Fadeev et al., 2018), such as the availability and composition of organic matter (Piontek et al., 2015; Engel et al., 2019), with differences between ice-covered and ice-free regions (Piontek et al., 2014; Fadeev et al., 2018).

Long-term summer observations in the region, conducted in the framework of the Long-Term Ecological Research site HAUSGARTEN, revealed strong ecological variations associated

with the Atlantic Meridional Overturning Circulation (Soltwedel et al., 2016). Warming events during the past decades influenced seasonal phytoplankton blooms by causing a slow but continuous increase in biomass, and a shift from diatom- to flagellate-dominated communities (Nöthig et al., 2015; Engel et al., 2017; Basedow et al., 2018). It has been recently observed that phytoplankton blooms show an increasing partitioning of the produced organic carbon into the dissolved phase (Engel et al., 2019), which may result in a more active microbial loop in the upper ocean and less export of particulate matter (Vernet et al., 2017; Fadeev et al., 2020). In times of a rapidly changing Arctic ecosystem, investigating structure and dynamics of bacterioplankton communities remains a key component to the understanding of current changes in this environment. However, so far, an assessment of associated responses of the key bacterial taxa responsible for an increased recycling is missing, especially with regard to shifts in standing stocks.

To date, the majority of Arctic bacterioplankton studies are performed using high-throughput sequencing of the 16S rRNA gene, which cannot be directly converted to absolute standing stock abundances of specific taxonomic groups due to polymerase chain reaction (PCR) primers selection (Fadeev et al., 2021), as well as other quantitative biases (Gloor et al., 2017; Kumar et al., 2017; Piwosz et al., 2020). Here we used semi-automatic CAtalyzed Reporter Deposition-Fluorescence In Situ Hybridization (CARD-FISH; Pernthaler et al., 2002). The power of this technique lies in the ability to acquire absolute abundance of the targeted taxonomic groups free of compositional effect (Amann et al., 1990). Besides the ability to target and quantify specific taxonomic groups, the retrieval of a positive hybridization signal furthermore indicates that the analyzed cell was alive and active before fixation (Amann et al., 1990; DeLong et al., 1999). Automatization of the microscopic examination and counting procedure can reach a high-throughput standard (Schattenhofer et al., 2009; Teeling et al., 2012; Bižić-Ionescu et al., 2015; Bennke et al., 2016).

Using CARD-FISH and semi-automated cell counting, we quantified bacterial and archaeal cell abundances of 12 taxonomic groups selected based on a 16S rRNA gene survey of water column microbial communities during the same summer expedition in the Fram Strait (Fadeev et al., 2020) (Table S1). Samples were collected from 11 stations at 4 different depths, targeting previously defined layers of the water column in the Fram Strait (Rudels et

al., 2012): surface mixed layer (0-30 m; seasonally mixed layer of Atlantic and Arctic waters), epipelagic (100 m; mainly modified Atlantic water), deep mesopelagic (500-1000 m; intermediate water), and bathypelagic (1200-2500 m; Eurasian Basin deep waters; Table 1). The main objective of this study was to assess the standing stocks of key taxonomic groups in the summer bacterioplankton across the Fram Strait. Using high-throughput cell counts data of bacterioplankton cell abundances we tested the following hypotheses: 1) in surface waters, the abundances of different bacterioplankton taxonomic groups are associated with phytoplankton bloom conditions, and, are linked to the abundances of specific phytoplankton populations; 2) water depth structures the bacterioplankton communities, and 3) differences between communities in ice-covered and ice-free regions decrease with increasing water depth.

Results and Discussion

Hydrographic and biogeochemical conditions across the Fram Strait

Based on the known hydrography of the Strait (Rudels et al., 2012) and the observed sea-ice conditions, we sampled three distinct regions of the Fram Strait (Figure 1): the ice-free eastern part of the Strait ("HG" stations) associated with the WSC (Beszczynska-Möller et al., 2012), the ice-covered western part of the Strait ("EG" stations) associated with the EGC (de Steur et al., 2009), and the partially ice-covered north-eastern part of the Strait ("N" stations) that represents a highly productive ice-margin zone (Hebbeln and Wefer, 1991; Perrette et al., 2011).

At the time of sampling in June-July 2016, the low level of inorganic nutrients above the seasonal pycnocline, and the chlorophyll *a* concentrations, suggested a late stage of the phytoplankton bloom across the Strait (Table 1). Microscopic analyses of phyto- and protozooplankton communities previously conducted in representative stations of each region (LTER HAUSGARTEN stations EG1, EG4, N5, N4, HG4 and S3) at the chlorophyll *a* maximum- 10-28 m depth), revealed that the communities at the time of sampling in the ice-covered EG and the ice-margin N stations had a higher abundance of diatoms, in contrast to the ice-free HG stations that had a higher abundance of *Phaeocystis* spp., (Fadeev et al.,

2020). These locally defined conditions correspond to an interannual trend of distinct phytoplankton bloom conditions observed in the western ice-covered EGC and the eastern ice-free WSC (Nöthig et al., 2015; Fadeev et al., 2018).

Table 1. Environmental parameters measured at different stations and microscopy counts (cells mL^{-1}) of diatoms and *Phaeocystis* spp. Chl. *a*: chlorophyll *a*. EGC: East Greenland current region, N: North region, WSC: West Spitsbergen Current region. SUR: surface mixed water, EPI: epipelagic, MES: mesopelagic, and BAT: bathypelagic zone. Lat: latitude. Lon: longitude. Temp: Temperature. Sal: Salinity. Diatoms and *Phaeocystis* spp.

Region	Station	PANGAEA Event ID	Water layer	Lat (°N)	Lon (°E)	Depth (m)	Temp (°C)	Sal	Chl *a* (µg L^{-1})	NO_3 (µmol L^{-1})	ΔNO_3 (µmol L^{-1})	PO_4 (µmol L^{-1})	ΔPO_4 (µmol L^{-1})	N:P	NH_4 (µmol L^{-1})	ΔNH_4 (µmol L^{-1})	SiO_3 (µmol L^{-1})	ΔSiO_3 (µmol L^{-1})	Diatoms (pennate and centric)	*Phaeocystis* spp.
EGC	EG1	PS99/051-2	SUR	78.99	-5.42	13	-1.51	33.17	1.66	3.75 ± 0.01	3.55 ± 0.01	0.46 ± 0.00	0.13 ± 0.00	8.15	0 ± 0.00	0.00	4.50 ± 0.00	0.14 ± 0.02	148	163
EGC	EG1	PS99/051-2	EPI	78.99	-5.42	100	-1.11	34.23		8.44 ± 0.04		0.63 ± 0.00		13.40	0 ± 0.01		4.04 ± 0.00			
EGC	EG1	PS99/051-2	MES	78.99	-5.42	971	-0.14	34.89		12.62 ± 0.03		0.85 ± 0.00		14.85	0 ± 0.03		7.00 ± 0.04			
EGC	EG4	PS99/048-11	SUR	78.82	-2.73	24	-1.17	34.48	1.52	4.92 ± 0.02	6.34 ± 0.01	0.50 ± 0.00	0.35 ± 0.00	9.84	0 ± 0.02	0.08 ± 0.01	2.44 ± 0.14	2.38 ± 0.34	65	13178
EGC	EG4	PS99/048-11	EPI	78.82	-2.73	100	3.86	35.05		10.97 ± 0.07		0.81 ± 0.00		13.54	0 ± 0.02		4.83 ± 0.17			
EGC	EG4	PS99/048-1	MES	78.82	-2.73	1000	-0.24	34.91		13.77 ± 0.04		0.94 ± 0.02		14.65	0 ± 0.01		7.10 ± 0.01			
EGC	EG4	PS99/048-1	BAT	78.82	-2.73	2527	-0.76	34.91		14.97 ± 0.09		1.06 ± 0.01		14.12	0 ± 0.01		12.07 ± 0.19			
N	N3	PS99/054-1	SUR	79.58	5.17	34	3.28	34.40	0.95	8.09 ± 0.06	5.23 ± 0.01	0.72 ± 0.00	0.31 ± 0.00	11.24	1.29 ± 0.00	0.00	3.19 ± 0.05	1.02 ± 0.03		
N	N3	PS99/054-1	EPI	79.58	5.17	100	4.25	35.10		10.11 ± 0.04		0.78 ± 0.00		12.96	0.47 ± 0.01		3.29 ± 0.04			
N	N3	PS99/054-1	MES	79.58	5.17	1000	-0.33	34.10		13.51 ± 0.02		1.05 ± 0.00		12.87	0 ± 0.00		7.25 ± 0.00			
N	N3	PS99/054-1	BAT	79.58	5.17	2500	-0.72	34.92		14.81 ± 0.05		1.09 ± 0.00		13.59	0 ± 0.00		10.74 ± 0.03			
N	N4	PS99/055-1	SUR	79.74	4.51	22	2.66	33.99	2.21	3.33 ± 0.01	6.80 ± 0.01	0.53 ± 0.01	0.49 ± 0.01	6.28	0.29 ± 0.03	0.00	1.65 ± 0.00	2.06 ± 0.01	119	4047
N	N4	PS99/055-1	EPI	79.74	4.51	100	3.94	35.08		10.64 ± 0.00		1.00 ± 0.03		10.64	0.42 ± 0.01		3.90 ± 0.00			
N	N4	PS99/055-7	MES	79.74	4.51	1000	-0.41	34.91		13.96 ± 0.08		0.92 ± 0.00		15.17	0 ± 0.01		9.07 ± 0.19			
N	N4	PS99/055-7	BAT	79.74	4.51	2500	-0.74	34.92		14.47 ± 0.02		0.86 ± 0.00		16.83	0 ± 0.00		11.24 ± 0.14			
N	N5	PS99/053-2	SUR	79.92	3.06	19	0.75	33.59	7.40	0.97 ± 0.01	8.21 ± 0.01	0.51 ± 0.04	0.66 ± 0.02	1.90	0 ± 0.04	1.56 ± 0.01	0.71 ± 0.01	2.34 ± 0.04	14	9401
N	N5	PS99/053-2	EPI	79.92	3.06	100	4.27	35.10		10.05 ± 0.05		1.10 ± 0.06		9.14	0.42 ± 0.01		3.22 0.08			

N	N5	PS99/053-2	MES	79.92	3.06	1000	-0.23	34.91		13.04 ± 0.12		1.34 ± 0.01		9.73	0 ± 0.00		6.50 ± 0.02			
N	N5	PS99/053-2	BAT	79.92	3.06	2427	-0.74	34.92		14.29 ± 0.04		1.59 ± 0.00		8.99	0 ± 0.01		10.79 ± 0.01			
WSC	HG1	PS99/066-2	SUR	79.14	6.09	17	6.27	35.33	3.42											
WSC	HG1	PS99/066-5	EPI	79.14	6.09	100	4.38	35.09												
WSC	HG1	PS99/066-5	MES	79.14	6.09	500	1.46	34.95												
WSC	HG1	PS99/066-5	BAT	79.14	6.09	1253	-0.81	34.91												
WSC	HG2	PS99/057-1	SUR	79.13	4.91	22	2.30	34.90	2.23	6.15 ± 0.01	5.30 ± 0.01	0.89 ± 0.00	0.55 ± 0.02	6.91	0.94 ± 0.00	0.00	2.74 ± 0.02	1.36 ± 0.05		
WSC	HG2	PS99/057-1	EPI	79.13	4.91	100	3.60	35.04		10.84 ± 0.01		1.30 ± 0.01		8.34	0 ± 0.01		3.88 ± 0.11			
WSC	HG2	PS99/057-1	MES	79.13	4.91	1000	-0.58	34.91		14.15 ± 0.09		1.69 ± 0.01		8.37	0 ± 0.01		9.33 ± 0.06			
WSC	HG2	PS99/057-1	BAT	79.13	4.91	1492	-0.81	34.91		14.95 ± 0.02		1.78 ± 0.07		8.40	0 ± 0.00		12.35 ± 0.02			
WSC	HG4	PS99/042-11	SUR	79.07	4.19	28	0.41	34.44	3.54	5.79 ± 0.04	6.42 ± 0.04	0.66 ± 0.02	0.41 ± 0.02	8.77	0.56 ± 0.01	0.17 ± 0.01	2.66 ± 0.02	2.11 ± 0.03	29	4007
WSC	HG4	PS99/042-11	EPI	79.07	4.19	100	3.51	35.04		10.88 ± 0.07		0.87 ± 0.06		12.51	0 ± 0.01		4.16 ± 0.12			
WSC	HG4	PS99/042-1	MES	79.06	4.19	1000	-0.35	34.91		13.71 ± 0.04		0.96 ± 0.01		14.28	0 ± 0.01		7.70 ± 0.02			
WSC	HG4	PS99/042-1	BAT	79.06	4.19	2462	-0.73	34.92		14.67 ± 0.05		1.01 ± 0.00		14.52	0 ± 0.00		11.59 ± 0.03			
WSC	HG5	PS99/044-1	SUR	79.07	3.66	25	1.74	32.363	4.24	5.1 ± 0.03	7.08 ± 0.02	0.53 ± 0.00	0.37 ± 0.00	9.62	0.50 ± 0.02	0.00	3.19 ± 0.01	1.96 ± 0.06		
WSC	HG5	PS99/044-1	EPI	79.07	3.66	100	3.94	35.089		11.26 ± 0.03		0.80 ± 0.00		14.08	0 ± 0.01		4.75 ± 0.03			
WSC	HG5	PS99/044-1	MES	79.07	3.66	2600	-0.73	34.924												
WSC	HG5	PS99/044-1	BAT	79.07	3.66	3038	-0.70	34.925												
WSC	HG7	PS99/046-1	SUR	79.05	3.53	35	3.73	33.957	4.46	5.24 ± 0.01	2.61 ± 0.05	0.51 ± 0.00	0.09 ± 0.00	10.27	0.48 ± 0.00	0.00	2.84 ± 0.20	1.68 ± 0.08		
WSC	HG7	PS99/046-1	EPI	79.05	3.53	100	3.35	35.016		10.35 ± 0.04		0.74 ± 0.00		13.99	0.09 ± 0.00		4.21 ± 0.02			
WSC	HG7	PS99/046-1	MES	79.05	3.53	1005	-0.28	34.908												
WSC	HG7	PS99/046-1	BAT	79.05	3.53	3772	-0.63	34.924												
WSC	HG9	PS99/059-2	SUR	79.13	2.84	24	-1.24	35.089	1.90	1.74 ± 0.04	6.58 ± 0.01	0.67 ± 0.00	0.58 ± 0.13	2.60	0 ± 0.02	0.73 ± 0.21	1.72 ± 0.02	1.96 ± 0.01		
WSC	HG9	PS99/059-2	EPI	79.13	2.84	100	3.92	35.047		10.97 ± 0.01		1.12 ± 0.05		9.79	0.47 ± 0.28		3.70 ± 0.03			
WSC	HG9	PS99/059-2	MES	79.13	2.84	1000	-0.19	34.897		13.59 ± 0.02		1.17 ± 0.17		11.62	0.00 ± 0.17		6.82 ± 0.01			
WSC	HG9	PS99/059-2	BAT	79.13	2.84	2499	-0.72	34.919		15.23 ± 0.01		1.27 ± 0.03		11.99	0.00 ± 0.00		11.11 ± 0.03			

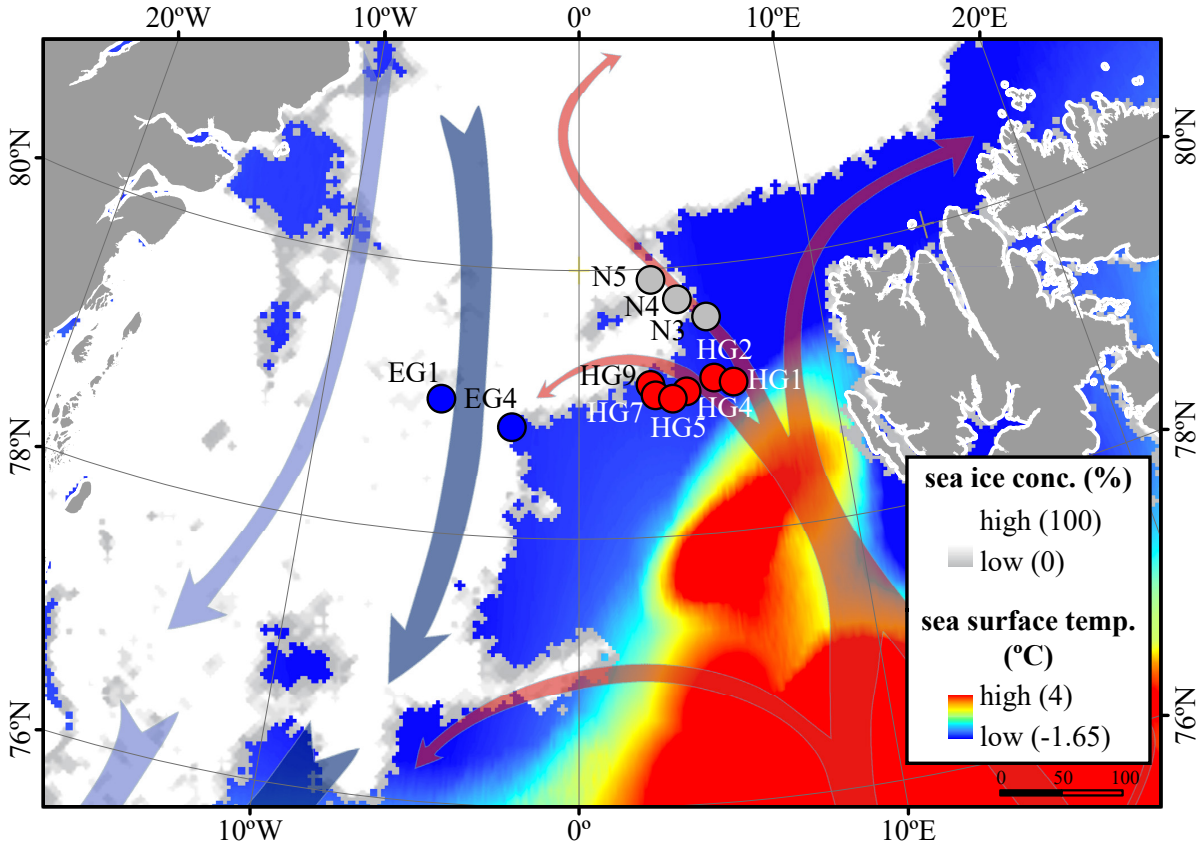

Figure 1. Oceanographic overview of the Fram Strait, including the monthly mean of sea-ice cover and sea surface temperature during July 2016. The sea ice concentration is represented by inverted grayscale (gray=low, white=high). Arrows represent general directions of the WSC (in red) and the EGC (in blue). Stations of water column sampling are indicated and colored according to their sea-ice conditions: ice-covered EGC (EG) stations – blue, ice-margin N stations – gray, ice-free WSC (HG) stations – red. The map was modified from (Fadeev et al., 2020).

Surface water bacterioplankton communities are affected by distinct phytoplankton bloom conditions

Phytoplankton blooms in surface waters generally lead to an increased cell abundance of heterotrophic bacteria that are specialized in the degradation of organic matter from algal exudates and phytodetritus (Buchan et al., 2014; Teeling et al., 2016). Previous observations in Fram Strait revealed a strong influence of the summer phytoplankton bloom conditions on the composition and structure of bacterioplankton communities (Wilson et al., 2017; Müller et al., 2018b), differing also between the ice-covered and ice-free regions of the Strait (Fadeev et al., 2018). We observed significantly higher total cell abundances of the bacterioplankton (i.e. all DAPI-stained bacterial and archaeal cells) in the surface water of the HG and N stations (6-17×10^5 cells mL^{-1}; Table S2), as compared to the EG stations (3 ×10^5 cells mL^{-1}; Kruskal-Wallis test; Chi square=81.85, df=2, *p*-value < 0.01). The communities

were dominated by bacterial cells that comprised 8-11×10^5 cells mL^{-1} in the HG and N stations, and 2×10^5 cells mL^{-1} in the EG stations (Figure 2, Table S2).

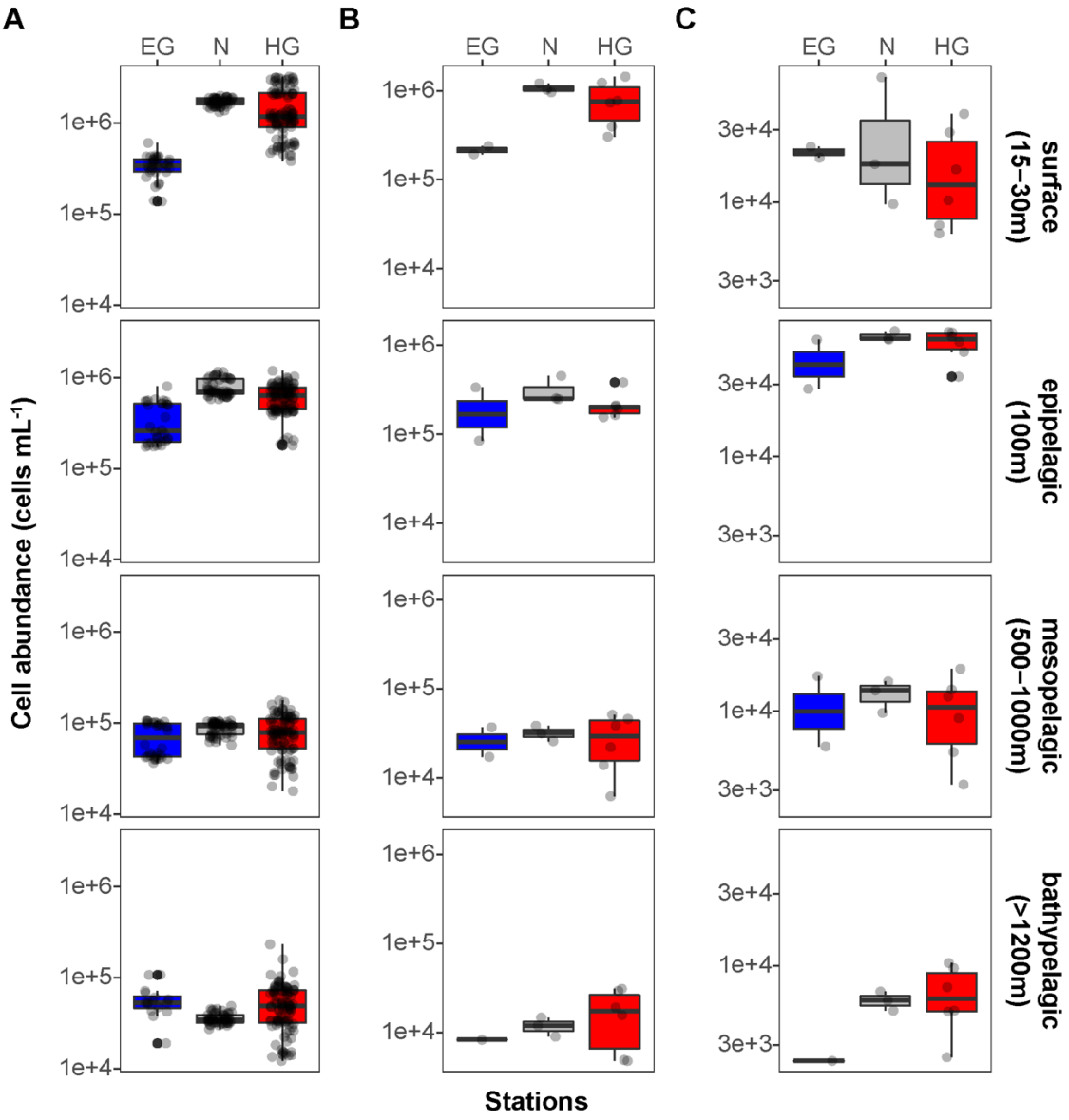

Figure 2. Mean bacterioplankton cell abundances calculated in the different regions of the Fram Strait: Total bacterioplankton (A); *Bacteria* (B); and *Archaea* (C). Box plots were calculated based on cell abundance. Note the different scale of the cell abundances for *Archaea*. The different regions are indicated by color: ice-covered EGC – blue (EG stations), ice-margin N – gray (N stations), ice-free WSC – red (HG stations). The asterisks represent levels of statistical significance of difference between all three regions per depth and domain: * < 0.05, ** < 0.01, *** < 0.001.

The bacterial communities exhibited high abundance of the classes *Bacteroidetes* (2.1×10^5 cells mL^{-1}) in the HG and N stations, followed by *Gammaproteobacteria* (from 1.6 to 2.1×10^5 cells mL^{-1}) and *Verrucomicrobia* (from 1.6 to 2.1×10^5 cells mL^{-1}), with a several-fold higher cell

abundance, compared to the EG stations (where together they comprised between 0.1 and 0.3×10^5 cells mL^{-1}) (Figure 3; Table S3).

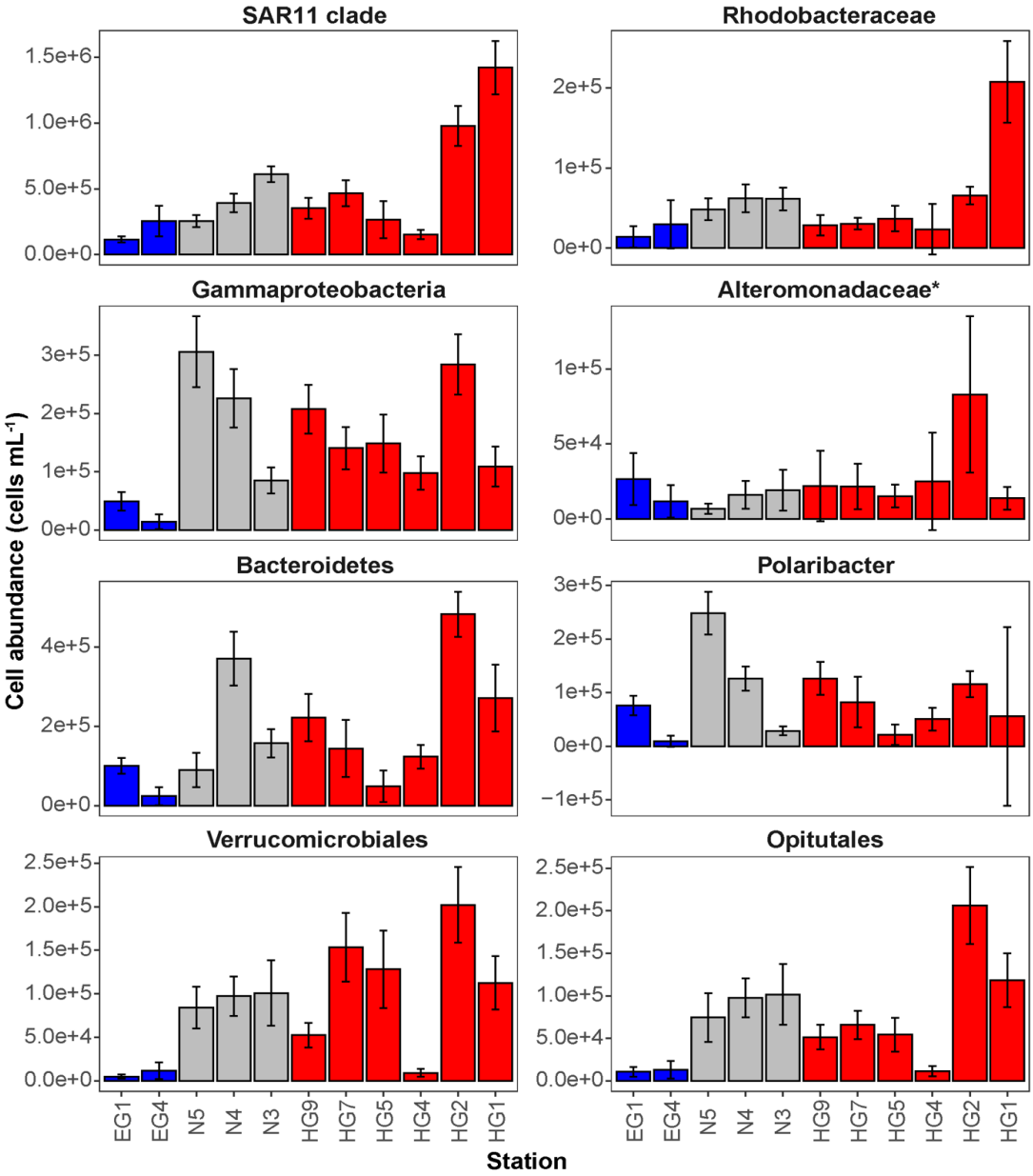

Figure 3. Mean cell abundances of selected taxonomic groups at each station in surface (15-30 m) waters (cells mL^{-1}). The different regions are indicated by color: ice-covered EGC- blue, ice-margin N - gray, ice-free - red.

These taxonomic groups were previously suggested to be associated with the seasonal phytoplankton blooms in the region (Fadeev et al., 2018, Wilson et al., 2017). Previous molecular studies also have shown that various taxonomic groups had higher sequence proportion in surface waters of ice-covered, compared to ice-free, regions of the Fram Strait, and are likely associated with Arctic water masses and winter communities in the Fram Strait

(Wilson et al., 2017; Fadeev et al., 2018, 2020; Müller et al., 2018b). Our microscopy data showed that while *Thaumarchaeota* and the *SAR202* clade had only little variations between the different regions, the class *Deltaproteobacteria* and the *SAR324* clade exhibited much higher cell abundances in the ice-covered EG stations, as compared to the ice-free HG and ice-margin N stations (Figure 4; Table S3). Hence, the observed patterns in surface water bacterioplankton communities seem to be driven by differences in environmental conditions across the Fram Strait.

In our study, the relative abundance of *Bacteroidetes*, *Gammaproteobacteria* and *Verrucomicrobia* were consistent with in 16S rRNA gene observations of size-fractionated bacterioplankton communities (i.e., free-living and particle-associated) conducted during the same expedition (> 75%) (Fadeev et al., 2020). However, other taxonomic groups (e.g., *Alteromonadaceae*) showed two- to three-fold lower relative abundance in the molecular study (Figure S1). These discrepancies can be explained by previously conducted direct methodological comparison between 16S rRNA gene observations and CARD-FISH counts (Fadeev et al., 2021), which suggested potential over-representation of the *SAR11* clade in the microscopy counts that could affect the proportional representation of other taxonomic groups in the dataset. Alternatively, the potentially higher cellular activity (and thus higher ribosomal content) of phytoplankton bloom-associated taxonomic groups (e.g., Bacteroidetes) may have altered their representation in the PCR-based 16S rRNA gene dataset (Rosselli et al., 2016), and thus potentially lower sequence proportion of other taxonomic groups. The methodology applied in this study avoids this compositionality effect and allows for the direct determination of absolute cell abundances of each targeted taxonomic group.

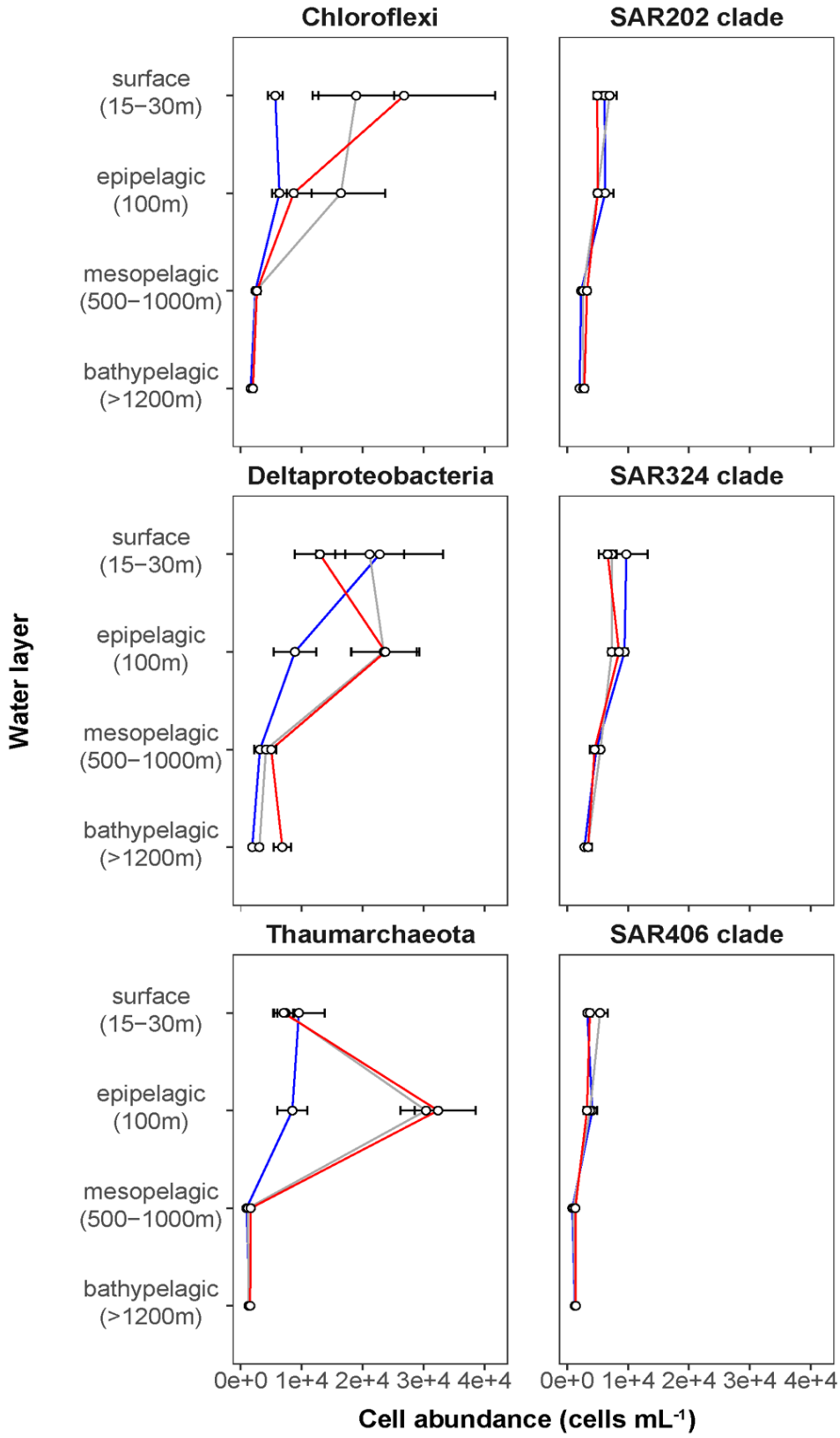

Figure 4. Depth profiles of mean cell abundances of selected taxonomic groups (cells mL^{-1}) calculated for the different Fram Strait regions. The different regions are indicated by color: ice-covered EGC – blue (EG stations), ice-margin N – gray (N stations), ice-free WSC – red (HG stations).

To test the hypothesis that environmental conditions across the Strait shape bacterioplankton communities, we examined a set of key physicochemical environmental parameters that represent the distinct water masses (temperature and salinity) and the different phytoplankton bloom conditions (categorized based on chlorophyll *a* concentration and consumed inorganic nutrients) across the Strait. We did not find significant correlations between these physical and biogeochemical parameters, which suggest to some extent their independent effect on the bacterioplankton communities (Figure S2). Based on this assumption we conducted specific correlation tests between each of these environmental parameters and cell abundances of various taxonomic groups (Table S4). Cell abundances of *Verrucomicrobia* and its order *Opitutales*, as well as of the *SAR11* clade and the family *Rhodobacteraceae* (both members of the class *Alphaproteobacteria*), showed significant positive correlations to water temperature (Pearson's correlation; $r > 0.5$, p-value < 0.05; Table S4), suggesting an association with the warmer Atlantic waters of the eastern Fram Strait. The *Verrucomicrobia* has been previously shown to be a major polysaccharide-degrading bacterial taxonomic group in the north-western Svalbard fjord Smeerenburgfjord (Cardman et al., 2014), and therefore may also be associated with the outflow from the Svalbard fjords (e.g., Kongsfjord) into the Atlantic waters of the WSC (Cottier et al., 2005) sampled for this study. The *SAR11* clade and the *Rhodobacteraceae* have both been previously shown to correlate with temperature at high latitudes (Giebel et al., 2011; Tada et al., 2013), and are known to have distinct phylotypes in water masses with different temperatures (Selje et al., 2004; Sperling et al., 2012; Giovannoni, 2017). However, the *Rhodobacteraceae* are also known for their broad abilities in utilizing organic compounds (Buchan et al., 2014; Luo and Moran, 2014). Thus, one cannot rule out that their higher cell abundances in warmer waters of the HG and N stations are associated with the late stage of the phytoplankton bloom and their exudates. In addition, the *SAR324* clade (*Deltaproteobacteria*) showed strong positive correlation with statistical significance to salinity (Pearson's correlation; $r > 0.5$, p-value < 0.05; Table S4). During the summer, with increased melting of sea ice, a low-salinity water layer is formed in surface waters, and the strong stratification of this water layer enhances the development of the phytoplankton bloom (Fadeev et al., 2018). Consequently, the correlation of *SAR324* with higher salinity suggests that their cell abundances are lower in surface waters where, in turn, we observe a strong phytoplankton bloom (e.g., in WSC).

The distinct surface water masses in the region differ not only in their physical but also in their biogeochemical characteristics (Wilson and Wallace, 1990; Fadeev et al., 2018), with higher concentrations of inorganic nitrogen and phosphate in the Atlantic, compared to the Arctic water masses. At the time of sampling, the typical Redfield ratio between inorganic nitrogen (mainly nitrate NO_3) and inorganic phosphate (PO_4) was below 16 (Redfield, 1963; Goldman et al., 1979). This suggests that surface waters across all three regions were nitrogen limited (Table 1) due to the progressing phytoplankton growth (Nöthig et al., 2015). In order to disentangle the effect of biological consumption of nutrients from water mass-specific nutrient signatures, we calculated the seasonal net consumption of inorganic nutrients, as the proxy for phytoplankton bloom conditions (Table 1). Consumed nitrate (ΔNO_3) and phosphate **(**ΔPO_4**)** revealed a very strong positive correlation with statistical significance (Pearson's correlation; r=0.86, *p*-value < 0.05; Table S4). The consumed silica (ΔSiO_3), used by diatoms, did not show a significant correlation to ΔPO_4 and ΔNO_3. This further supports the impact of different phytoplankton populations across the Strait (i.e., diatoms vs. *Phaeocystis*; Fadeev et al., 2020). Phytoplankton bloom-associated environmental parameters (chlorophyll *a* concentration and the consumed inorganic nutrients) revealed weaker relationships with cell abundances of different taxonomic groups (Table S4). Furthermore, we did not observe significant positive correlations of the cell abundances of diatoms or *Phaeocystis* spp., with the quantified bacterioplankton taxa. This might be explained by time lags and local differences in the dynamic development of phytoplankton blooms across the entire Strait (Wilson et al., 2017; Fadeev et al., 2018).

Bacterioplankton communities strongly change in cell abundance and composition with depth

The complexity of Fram Strait surface waters with different ice-coverages, a dynamic ice-melt water layer and mesoscale mixing events of Atlantic and Polar water masses by eddies (Wekerle et al., 2017), challenges the identification of specific associations between microbial cell abundances and environmental parameters. Some taxonomic groups (e.g., *SAR11* clade) were potentially more influenced by the physical processes such as the presence of ice and distinct Arctic water masses (Kraemer et al., 2020). Likely the mixture of all these environmental variables shaped the observed bacterioplankton communities. We found that

cell abundances of some taxonomic groups (e.g., *Gammaproteobacteria*) were higher in some stations with more advanced phytoplankton bloom conditions. However, as we have only limited observations of phytoplankton for this study, we cannot test previous hypotheses of direct associations between the abundances of specific phytoplankton groups and bacterioplankton taxa (Fadeev et al., 2018). Nonetheless, the here observed patterns could represent an enhanced growth of the bacterioplankton on algal exudates (Tada et al., 2011; Teeling et al., 2012). Alternatively, considering the advection of Atlantic waters (Wekerle et al. 2017), it is also possible that some of the observed trends represent lateral transport of phytoplankton or bacterioplankton, or both, from the southern part of the Strait.

In surface waters of all stations, ca. 60% of the total bacterioplankton community was covered by the *Bacteria*-specific probes (EUB388 I-III) and up to 8% was covered by the *Archaea*-specific probe (ARCH915; Table S2). At depth (> 100 m), the coverage of total cells by the *Bacteria*-specific probes strongly decreased to 16-40% of DAPI-stained cells (ANOVA; F_3=15.39, $p < 0.01$), while the coverage by the *Archaea*-specific probe significantly increased up to 17% of DAPI-stained cells (ANOVA; F_3=34.31, $p < 0.01$; Table S2). A similar decrease in detectability of the *Bacteria*-specific probes was previously observed in other bacterioplankton microscopy studies (Karner et al., 2001; Herndl et al., 2005; Varela et al., 2008), and reasons may lie in a ribosomal nucleic acid concentration decrease within the bacterial cells (i.e., lower activity) towards the oligotrophic depths. In addition, there is a potential increase with greater water depths of microbial phylogenetic groups that are not captured by the currently existing probes (Hewson et al., 2006; Galand et al., 2009a; Agogué et al., 2011; Welch and Huse, 2011; Salazar et al., 2016).

We found that in all three regions, total cell abundances of the entire bacterioplankton community were highest at surface with 10^5-10^6 cells mL^{-1}, and significantly decreased with depth down to 10^4 cells mL^{-1} at meso- and bathypelagic depths (Figure 2a; Table S3; Kruskal-Wallis test; Chi square=554.39, df=3, *p*-value < 0.01). Members of the domain *Bacteria* dominated the communities throughout the entire water column, with highest cell abundances in surface waters (10^5-10^6 cells mL^{-1}), and significantly lower 10^4 cells mL^{-1} at depth (Figure 2b; Kruskal-Wallis test; Chi square=35.27, df=3, *p*-value < 0.01). Archaeal cells

had an overall lower abundance than bacterial cells by an order of magnitude throughout the entire water column, ranging from 10^4 cells mL^{-1} at surface down to 10^3 cells mL^{-1} in bathypelagic waters (Figure 2c). However, unlike *Bacteria*, archaeal communities doubled their absolute cell abundances from ca. 3×10^4 cells mL^{-1} at surface to ca. 6×10^4 cells mL^{-1} at 100 m depth, followed by a significant decrease in cell abundance at meso- and bathypelagic depths (Kruskal-Wallis test; Chi square=29.04, df=3, *p*-value < 0.01). Compared to the stronger decline in bacterial cell numbers, this pattern mirrors the known global trend of relative archaeal enrichment in epipelagic waters (Karner et al., 2001; Herndl et al., 2005; Kirchman et al., 2007; Varela et al., 2008; Schattenhofer et al., 2009), and was also observed in other regions of the Arctic Ocean (Amano-Sato et al., 2013). Altogether, the here observed bacterioplankton cell abundances in surface waters were well within the range of previous observations in the Fram Strait waters, conducted by flow cytometry (Piontek et al., 2014; Fadeev et al., 2018; Engel et al., 2019). However, compared to recent CARD-FISH based observations in eastern Fram Strait (Quero et al., 2020), our cell abundances were consistently one order of magnitude lower along the entire water column. The discrepancy might be associated with methodological differences, such as shorter staining times and the usage of an automated over a manual counting approach in our study. Nevertheless, both studies showed a similar pattern of a strong decrease in bacterioplankton cell abundances with depth, which also matches observations in other oceanic regions (Karner et al., 2001; Church et al., 2003; Teira et al., 2004; Schattenhofer et al., 2009; Dobal-Amador et al., 2016).

Enigmatic microbial lineages increase in cell abundance towards the deep ocean

The deep waters of the Fram Strait basin (> 500 m) have a rather homogeneous hydrography (von Appen et al., 2015), and are less affected by the seasonal dynamics that govern the surface layers (Wilson et al., 2017). Previous molecular observations of the deep water bacterioplankton communities showed high sequence abundances of largely unknown taxonomic groups, such as the *SAR202* (class *Dehalococcoidia*), *SAR324* (class *Deltaproteobacteria*), and *SAR406* (phylum *Marinimicrobia*) (Wilson et al., 2017; Fadeev et al., 2020; Quero et al., 2020). There was also higher archaeal sequence abundance at depth,

with the class *Nitrososphaeria* (i.e., *Thaumarchaeota*) reaching up to 15% of the sequences in mesopelagic waters (> 200 m) (Wilson et al., 2017; Müller et al., 2018b; Fadeev et al., 2020). However, it has also been recently shown that in ice-covered regions of the Strait surface-dominant taxonomic groups, such as *Gammaproteobacteria* and *Nitrososphaeria*, are exported via fast-sinking aggregates from surface to the deep ocean (> 1000 m), where they may realize an ecological niche (Fadeev et al., 2020). We observed that in all meso- and bathypelagic waters across all analyzed regions the total cell abundances of the bacterioplankton communities were in the range of 10^4 cells mL^{-1} (Figure 2), reflecting observations made in Arctic mesopelagic waters (Wells et al., 2006, Quero et al., 2020). Bacterial taxonomic groups that dominated the surface water communities (e.g., *Bacteroidetes*, *Gammaproteobacteria* and *Verrucomicrobia*), in both ice-free and ice-covered regions of the Strait, decreased by two orders of magnitude in their cell abundances at meso- and bathypelagic depths (Kruskal-Wallis test; *p*-value < 0.01; Figure 3, Table S3). This trend strongly correlated with the total bacterioplankton cell abundances along the general water column (Pearson's correlation; r > 0.8, *p*-value < 0.05; Table S4). In contrast, other bacterial groups, such as the *SAR202* and *SAR324* clades, proportionally increased in cell abundances with depth and maintained overall constant cell abundances of ca. 0.5×10^4 cells mL^{-1} until the deep basin (Table S3). Previous molecular studies of bacterioplankton communities in the Fram Strait suggested a proportional increase of these largely understudied bacterial lineages in the deep ocean, which were previously found to be associated with winter (surface) bacterioplankton (Wilson et al., 2017; Fadeev et al., 2020). The cell abundances presented here indicate that their increasing proportional abundance at depth is due to stronger decrease in the cell abundances of other groups (Figure 4; Table S3). Very little is currently known about these two taxonomic groups, but previous genetic observations suggest that they possess distinct metabolic capabilities, and may be involved in the degradation of recalcitrant organic matter (*SAR202* clade; Landry et al., 2017; Colatriano et al., 2018; Saw et al., 2019), or, in sulfur oxidation (*SAR324* clade; Swan et al., 2011; Sheik et al., 2014). Their homogeneous distribution from the stratified surface to the homogenous deep ocean suggests that through high functional plasticity these enigmatic bacterial groups fulfil various ecological niches throughout the water column (Saw et al., 2019; Wei et al., 2020), and thus may play important roles in oceanic nutrient cycling.

With depth, the decrease of archaeal cell abundances was less than that of members of the domain *Bacteria* (Figure 4; Table S3), meaning that members of the *Archaea* were proportionally increasing in the total microbial deep-water communities. The *Thaumarchaeota* strongly correlated with the pattern of the archaeal cell abundances (Pearson's correlation; r=0.76, *p*-value < 0.05; Table S4), showing a two-fold increase in cell abundance from surface to epipelagic depth (100 m), followed by a substantial decrease towards meso- and bathypelagic waters (Figure 4; Table S3). This two-fold increase towards the epipelagic depths corresponds to previous observations of *Thaumarchaeota* in the north Atlantic (Müller et al., 2018b), and a further increase in their cell abundances at higher depths (> 1000 m) was also observed in other oceanic regions (Karner et al., 2001; Church et al., 2003; Herndl et al., 2005; Teira et al., 2006; Galand et al., 2009b). It has been shown in molecular studies that *Thaumarchaeota* comprise a large proportion of the bacterioplankton communities in the Fram Strait, especially in the epipelagic waters (Wilson et al., 2017; Müller et al., 2018b; Fadeev et al., 2020). In our study, the *Thaumarchaeota* exhibited their highest cell abundances at 100 m in the ice-free HG, and at the ice-margin N stations (3×10^4 cells mL^{-1}), where they comprised half of the total archaeal community (Figure 4; Table S3). The strong absolute decrease of *Thaumarchaeota* cell abundances towards the meso- and bathypelagic waters suggests a decrease in cell number or activity with depth (Herndl et al., 2005; Kirchman et al., 2007; Alonso-Sáez et al., 2012), and thus lower cell detectability. In deeper water layers, other pelagic archaeal groups, such as the phylum *Euryarchaeota* that was not quantified in this study, may increase in abundance and form the bulk of total archaeal cells here (Galand et al., 2010; Fadeev et al., 2020).

Conclusions

Using state-of-the-art semi-automatic microscopy cell counting, we quantified the absolute cell abundance of 12 key taxonomic groups in summer bacterioplankton communities of both ice-free and ice-covered regions of the Fram Strait. We found that in surface waters some taxonomic groups were associated with the distinct water masses of the Strait (e.g., *Rhodobacteraceae* with the Atlantic waters). Surface water bacterioplankton communities were dominated by *Gammaproteobacteria*, *Bacteroidetes* and *Verrucomicrobia*, which

corresponded with biogeochemical conditions in the ongoing seasonal phytoplankton bloom. This suggests that currently predicted longer seasonal phytoplankton blooms, as well as the increasing Atlantic influence on the Arctic Ocean (i.e., "Atlantification"), may have a strong impact on the composition and biogeographical distribution of certain bacterioplankton taxonomic groups in the surface Arctic waters. This study also provides the first extensive quantification of bacterioplankton community standing stocks in the deep Arctic water column (> 500 m). With depth, some taxonomic groups, such as the *SAR202* clade, maintained similar abundances throughout the entire water column (2500 m depth), where other taxa decline by several-fold. The observation of a homogenous abundance further supports the previously established hypothesis that through high functional plasticity these taxonomic groups are realizing various ecological niches throughout the entire water column. Altogether, our quantitative data on cell abundances of ecologically relevant taxonomic bacterioplankton groups provide insights into factors structuring pelagic bacterioplankton communities from surface to the deep waters of the Arctic Ocean, and add to a baseline to better assess future changes in a rapidly warming region.

Materials and Methods

Sampling and environmental data collection

Sampling was carried out during the RV Polarstern expedition PS99.2 to the Long-Term Ecological Research (LTER) site HAUSGARTEN in Fram Strait (June 24th – July 16th, 2016). Sampling was carried out with 12 L Niskin bottles mounted on a CTD rosette (Sea-Bird Electronics Inc. SBE 911 plus probe) equipped with temperature and conductivity sensors, a pressure sensor, altimeter, and a chlorophyll fluorometer. In ice-covered regions the samples were collected through holes in the ice kept open by the research vessel. On board, the samples were fixed with formalin in a final concentration of 2% for 10 – 12 hours, then filtered onto 0.2 µm polycarbonate Nucleopore Track-Etched filters (Whatman, Buckinghamshire, UK), and stored at -20°C for further analysis. Hydrographic data of the seawater including temperature and salinity were retrieved from PANGAEA (Schröder and Wisotzki, 2014), along with measured chlorophyll *a* concentration (Nöthig et al., 2018; Fadeev et al., 2020) (Table 1).

Relative abundance of relevant 16S rRNA as well as data on microscopic abundances of microbial eukaryotes in phytoplankton blooms of the sample location was obtained from (Fadeev et al., 2020).

Catalyzed reporter deposition-fluorescence in situ hybridization (CARD-FISH)

We quantified absolute cell abundances of 12 key bacterioplankton groups (Table S1), members of the *Bacteria* and *Archaea*, based on their relatively high sequence abundance and recurrences in previous molecular studies of Arctic waters (Bowman et al., 2012; Wilson et al., 2017; Müller et al., 2018b; Fadeev et al., 2020). The selected probes covered a variety of taxonomic entities to address standing stocks at different taxonomic levels. All probes were checked for specificity and coverage of their target groups against the SILVA database release 132 (Quast et al., 2013). CARD-FISH was applied based on the protocol established by (Pernthaler et al., 2002), using horseradish-peroxidase (HRP)–labelled oligonucleotide probes (Biomers.net, Ulm, Germany). All filters were embedded in 0.2% low-gelling-point agarose, and treated with 10 mg mL^{-1} lysozyme solution (Sigma-Aldrich Chemie GmbH, Hamburg, Germany) for 1 h at 37°C. Filters for enumerating *Archaea* and *Thaumarchaeota* were treated for an additional 30 min in 36 U mL^{-1} achromopeptidase (Sigma-Aldrich Chemie GmbH, Hamburg, Germany) and 15 µg mL^{-1} proteinase K at 37°C. Subsequently, endogenous peroxidases were inactivated by submerging the filter pieces in 0.15% H_2O_2 in methanol for 30 min before rinsing in Milli-Q water and dehydration in 96% ethanol. Then, the filters were covered in hybridization buffer and a probe concentration of 0.2 ng $µL^{-1}$. Hybridization was performed at 46°C for 2.5 h, followed by washing in pre-warmed washing buffer at 48°C for 10 min, and 15 min in 1x PBS. Signal amplification was carried out for 45 min at 46°C with amplification buffer containing either tyramide-bound Alexa 488 (1 µg/mL) or Alexa 594 (0.33 µg mL^{-1}). Afterwards, the cells were counterstained in 1 µg/mL DAPI (4',6-diamidino-2-phenylindole; Thermo Fisher Scientific GmbH, Bremen, Germany) for 10 min at 46°C. After rinsing with Milli-Q water and 96% ethanol, the filter pieces were embedded in a 4:1 mix of Citifluor (Citifluor Ltd, London, United Kingdom) and Vectashield (Vector Laboratories, Inc., Burlingame, United States), and stored overnight at -20°C for later microscopy evaluation.

Automated image acquisition and cell counting

The filters were evaluated microscopically under a Zeiss Axio Imager.Z2 stand (Carl Zeiss MicroImaging GmbH, Jena, Germany), equipped with a multipurpose fully automated microscope imaging system (MPISYS), a Colibri LED light source illumination system, and a multi-filter set 62HE (Carl Zeiss MicroImaging GmbH, Jena, Germany). Pictures were taken via a cooled charged-coupled-device (CCD) camera (AxioCam MRm; Carl Zeiss AG, Oberkochen, Germany) with a 63× oil objective, a numerical aperture of 1.4, and a pixel size of 0.1016 µm/pixel, coupled to the AxioVision SE64 Rel.4.9.1 software (Carl Zeiss AG, Oberkochen, Germany) as described by (Bennke et al., 2016). Exposure times were adjusted after manual inspection with the AxioVision Rel.4.8 software coupled to the SamLoc 1.7 software (Zeder et al., 2011), which was also used to define the coordinates of the filters on the slides. For image acquisition, channels were defined with the MPISYS software, and a minimum of 55 fields of view with a minimum distance of 0.25 mm were acquired of each filter piece by recoding a z-stack of 7 images in autofocus.

Cell enumeration was performed with the software Automated Cell Measuring and Enumeration Tool (ACMETool3, 2018-11-09; M. Zeder, Technobiology GmbH, Buchrain, Switzerland). Total bacterioplankton cells were determined as the total amount of DAPI-stained cells. Counts for each taxonomic group included only cells that were simultaneously stained by DAPI and the taxa-specific FISH probe.

Calculation of consumed inorganic nutrients

Following (Fadeev et al., 2018) the nutrient consumption (Δ) at each station was calculated by subtracting the mean value of all collected measurements above 50 m from the mean value of all collected measurements between 50 and 100 m (below the seasonal pycnocline).

Statistical analyses

All statistical analyses and calculations in this study were performed using R (v4.0.2) (www.r-project.org) in RStudio (v1.3.1056), i.e. statistical tests for normality, ANOVA and Kruskal-Wallis. Post-hoc Wilcoxon test and Pearson's rank correlation coefficient were conducted

with the R-package "rstatix" (v0.6.0) (Kassambara, 2020). Plots were generated using the R-package "ggplot2" (v3.3.2) (Wickham, 2016) and "tidyverse" (v1.3.0) (Wickham et al., 2019).

Data availability

All data is accessible via the Data Publisher for Earth & Environmental Science PANGAEA (www.pangaea.de): cell abundances under doi:10.1594/PANGAEA.905212, and inorganic nutrient measurements under doi:10.1594/PANGAEA.906132. Scripts for processing the data can be accessed at https://github.com/edfadeev/FramStrait-counts.

Conflict of Interest

The authors declare that the research was conducted in the absence of any commercial or financial relationships that could be construed as a potential conflict of interest.

Author contributions

MC-M, EF and VS-C designed and conducted the study. MC-M performed the hybridizations, cell counting, data and statistical analysis with guidance from VS-C (probe selection, CARD-FISH application and counting) and EF (data and statistical analysis). MC-M, EF and VS-C wrote the manuscript with guidance from AB. All authors critically revised the manuscript and gave their approval of the submitted version.

Funding

This project has received funding from the European Research Council (ERC) under the European Union's Seventh Framework Program (FP7/2007-2013) research project ABYSS (Grant Agreement no. 294757) to AB. Additional funding came from the Helmholtz

Association, specifically for the FRAM infrastructure, from the Max Planck Society, from the Hector Fellow Academy, and from the Austrian Science Fund (FWF) grant no. M-2797 to EF. This publication is Eprint ID 51358 of the Alfred Wegener Institute Helmholtz Center for Polar and Marine Research, Bremerhaven, Germany.

Acknowledgements

We thank the captain and crew of RV Polarstern expedition PS99.2, as well as the chief scientist Thomas Soltwedel for support with work at sea. We also thank Pier Offre for assistance in sampling, Greta Reintjes for designing the probe Opi346, Mareike Bach for technical support, Sinhue Torres-Valdes and Laura Wischnewski for conducting the inorganic nutrient measurements. We thank Andreas Ellrott for the support with the automated microscope from the Max Planck Institute for Marine Microbiology. This work was conducted in the framework of the HGF Infrastructure Program FRAM of the Alfred-Wegener-Institute Helmholtz Center for Polar and Marine Research.

References

Agogué, H., Lamy, D., Neal, P. R., Sogin, M. L., and Herndl, G. J. (2011). Water mass-specificity of bacterial communities in the North Atlantic revealed by massively parallel sequencing. Mol. Ecol. 20, 258–274. doi:10.1111/j.1365-294X.2010.04932.x.

Alonso-Sáez, L., Waller, A. S., Mende, D. R., Bakker, K., Farnelid, H., Yager, P. L., et al. (2012). Role for urea in nitrification by polar marine Archaea. Proc. Natl. Acad. Sci. U. S. A. 109, 17989–17994. doi:10.1073/pnas.1201914109.

Amann, R., and Fuchs, B. M. (2008). Single-cell identification in microbial communities by improved fluorescence in situ hybridization techniques. Nat. Rev. Microbiol. 6, 339–348. doi: 10.1038/nrmicro1888

Amann, R. I., Binder, B. J., Olson, R. J., Chisholm, S. W., Devereux, R., and Stahl, D. A. (1990). Combination of 16S rRNA-targeted oligonucleotide probes with flow cytometry for analyzing mixed microbial populations. Appl. Environ. Microbiol. 56, 1919–1925. doi:10.1128/aem.56.6.1919-1925.1990.

Amano-Sato, C., Akiyama, S., Uchida, M., Shimada, K., and Utsumi, M. (2013). Archaeal distribution and abundance in water masses of the Arctic Ocean, Pacific sector. Aquat. Microb. Ecol. 69, 101–112. doi:10.3354/ame01624.

Basedow, S. L., Sundfjord, A., von Appen, W. J., Halvorsen, E., Kwasniewski, S., and Reigstad, M. (2018). Seasonal variation in transport of zooplankton Into the Arctic basin through the Atlantic gateway, Fram Strait. Front. Mar. Sci. 5, 194. doi:10.3389/fmars.2018.00194.

Bennke, C. M., Reintjes, G., Schattenhofer, M., Ellrott, A., Wulf, J., Zeder, M., et al. (2016). Modification of a high-throughput automatic microbial cell enumeration system for shipboard analyses. Appl. Environ. Microbiol. 82, 3289–3296. doi:10.1128/AEM.03931-15.

Beszczynska-Möller, A., Fahrbach, E., Schauer, U., and Hansen, E. (2012). Variability in Atlantic water temperature and transport at the entrance to the Arctic Ocean, 19972010. ICES J. Mar. Sci. 69, 852–863. doi:10.1093/icesjms/fss056.

Beszczynska-Möller, A., Woodgate, R. A., Lee, C., Melling, H., and Karcher, M. (2011). A synthesis of exchanges through the main oceanic gateways to the Arctic Ocean. Oceanography 24, 83–99. doi:10.5670/oceanog.2011.59.

Bižić-Ionescu, M., Zeder, M., Ionescu, D., Orlić, S., Fuchs, B. M., Grossart, H. P., et al. (2015). Comparison of bacterial communities on limnic versus coastal marine particles reveals profound differences in colonization. Environ. Microbiol. 17, 3500–3514. doi:10.1111/1462-2920.12466.

Boetius, A., Albrecht, S., Bakker, K., Bienhold, C., Felden, J., Fernández-Méndez, M., et al. (2013). Export of algal biomass from the melting arctic sea ice. Science (80-.). 339, 1430–1432. doi:10.1126/science.1231346.

Bowman, J. S., Rasmussen, S., Blom, N., Deming, J. W., Rysgaard, S., and Sicheritz-Ponten, T. (2012). Microbial community structure of Arctic multiyear sea ice and surface seawater by 454 sequencing of the 16S RNA gene. ISME J. 6, 11–20. doi:10.1038/ismej.2011.76.

Buchan, A., LeCleir, G. R., Gulvik, C. A., and González, J. M. (2014). Master recyclers: features and functions of Bacteria associated with phytoplankton blooms. Nat. Rev. Microbiol. 12, 686–698. doi:10.1038/nrmicro3326.

Cardman, Z., Arnosti, C., Durbin, A., Ziervogel, K., Cox, C., Steen, A. D., et al. (2014). Verrucomicrobia are candidates for polysaccharide-degrading bacterioplankton in an Arctic fjord of Svalbard. Appl. Environ. Microbiol. 80, 3749–3756. doi:10.1128/AEM.00899-14.

Church, M. J., DeLong, E. F., Ducklow, H. W., Karner, M. B., Preston, C. M., and Karl, D. M. (2003). Abundance and distribution of planktonic Archaea and Bacteria in the waters west of the Antarctic Peninsula. Limnol. Oceanogr. 48, 1893–1902. doi:10.4319/lo.2003.48.5.1893.

Colatriano, D., Tran, P. Q., Guéguen, C., Williams, W. J., Lovejoy, C., and Walsh, D. A. (2018). Genomic evidence for the degradation of terrestrial organic matter by pelagic Arctic Ocean Chloroflexi bacteria. Commun. Biol. 1, 90. doi:10.1038/s42003-018-0086-7.

Cottier, F., Tverberg, V., Inall, M., Svendsen, H., Nilsen, F., and Griffiths, C. (2005). Water mass modification in an Arctic fjord through cross-shelf exchange: The seasonal hydrography of Kongsfjorden, Svalbard. J. Geophys. Res. Ocean. 110, 1–18. doi:10.1029/2004JC002757.

Dai, A., Luo, D., Song, M., and Liu, J. (2019). Arctic amplification is caused by sea-ice loss under increasing CO_2. Nat. Commun. 10, 121. doi:10.1038/s41467-018-07954-9.

de Steur, L., Hansen, E., Gerdes, R., Karcher, M., Fahrbach, E., and Holfort, J. (2009). Freshwater fluxes in the East Greenland Current: A decade of observations. Geophys. Res. Lett. 36, L23611. doi:10.1029/2009GL041278.

DeLong, E. F., Taylor, L. T., Marsh, T. L., and Preston, C. M. (1999). Visualization and enumeration of marine planktonic Archaea and Bacteria by using polyribonucleotide probes and fluorescent in situ hybridization. Appl. Environ. Microbiol. 65, 5554–5563. doi:10.1128/aem.65.12.5554-5563.1999.

Dobal-Amador, V., Nieto-Cid, M., Guerrero-Feijoo, E., Hernando-Morales, V., Teira, E., and Varela-Rozados, M. M. (2016). Vertical stratification of bacterial communities driven by multiple environmental factors in the waters (0-5000 m) off the Galician coast (NW Iberian margin). Deep. Res. Part I Oceanogr. Res. Pap. 114, 1–11. doi:10.1016/j.dsr.2016.04.009.

Dobricic, S., Vignati, E., and Russo, S. (2016). Large-scale atmospheric warming in winter and the Arctic sea ice retreat. J. Clim. 29, 2869–2888. doi:10.1175/JCLI-D-15-0417.1.

Engel, A., Bracher, A., Dinter, T., Endres, S., Grosse, J., Metfies, K., et al. (2019). Inter-annual variability of organic carbon concentrations in the eastern Fram Strait during summer (2009-2017). Front. Mar. Sci. 6, 187. doi:10.3389/fmars.2019.00187.

Engel, A., Piontek, J., Metfies, K., Endres, S., Sprong, P., Peeken, I., et al. (2017). Inter-annual variability of transparent exopolymer particles in the Arctic Ocean reveals high sensitivity to ecosystem changes. Sci. Rep. 7, 4129. doi:10.1038/s41598-017-04106-9.

Fadeev, E., Cardozo-Mino, M. G., Rapp, J. Z., Bienhold, C., Salter, I., Salman-Carvalho, V., et al. (2021). Comparison of Two 16S rRNA Primers (V3–V4 and V4–V5) for Studies of Arctic Microbial Communities. Front. Microbiol. 12, 283. doi: 10.3389/fmicb.2021.637526.

Fadeev, E., Rogge, A., Ramondenc, S., Nöthig, E.-M., Wekerle, C., Bienhold, C., et al. (2020). Sea-ice retreat may decrease carbon export and vertical microbial connectivity in the Eurasian Arctic basins. Nat. Res. doi:10.21203/rs.3.rs-101878/v1.

Fadeev, E., Salter, I., Schourup-Kristensen, V., Nöthig, E. M., Metfies, K., Engel, A., et al. (2018). Microbial communities in the east and west fram strait during sea ice melting season. Front. Mar. Sci. 5, 429. doi:10.3389/fmars.2018.00429.

Fernández-Méndez, M., Wenzhöfer, F., Peeken, I., Sørensen, H. L., Glud, R. N., and Boetius, A. (2014). Composition, buoyancy regulation and fate of ice algal aggregates in the Central Arctic Ocean. PLoS One 9, e107452–e107452. doi:10.1371/journal.pone.0107452.

Galand, P. E., Casamayor, E. O., Kirchman, D. L., and Lovejoy, C. (2009a). Ecology of the rare microbial biosphere of the Arctic Ocean. Proc. Natl. Acad. Sci. U. S. A. 106, 22427–22432. doi:10.1073/pnas.0908284106.

Galand, P. E., Casamayor, E. O., Kirchman, D. L., Potvin, M., and Lovejoy, C. (2009b). Unique archaeal assemblages in the Arctic Ocean unveiled by massively parallel tag sequencing. ISME J. 3, 860–869. doi:10.1038/ismej.2009.23.

Galand, P. E., Potvin, M., Casamayor, E. O., and Lovejoy, C. (2010). Hydrography shapes bacterial biogeography of the deep Arctic Ocean. ISME J. 4, 564–576. doi:10.1038/ismej.2009.134.

Giebel, H. A., Kalhoefer, D., Lemke, A., Thole, S., Gahl-Janssen, R., Simon, M., et al. (2011). Distribution of Roseobacter RCA and SAR11 lineages in the North Sea and characteristics of an abundant RCA isolate. ISME J. 5, 8–19. doi:10.1038/ismej.2010.87.

Giovannoni, S. J. (2017). SAR11 Bacteria: The Most Abundant Plankton in the Oceans. Ann. Rev. Mar. Sci. 9, 231–255. doi:10.1146/annurev-marine-010814-015934.

Gloor, G. B., Macklaim, J. M., Pawlowsky-Glahn, V., and Egozcue, J. J. (2017). Microbiome datasets are compositional: And this is not optional. Front. Microbiol. 8, 2224. doi:10.3389/fmicb.2017.02224.

Goldman, J. C., McCarthy, J. J., and Peavey, D. G. (1979). Growth rate influence on the chemical composition of phytoplankton in oceanic waters. Nature 279, 210–215. doi:10.1038/279210a0.

Gómez-Pereira, P. R., Hartmann, M., Grob, C., Tarran, G. A., Martin, A. P., Fuchs, B. M., et

al. (2013). Comparable light stimulation of organic nutrient uptake by SAR11 and Prochlorococcus in the North Atlantic subtropical gyre. ISME J. 7, 603–614. doi:10.1038/ismej.2012.126.

Hebbeln, D., and Wefer, G. (1991). Effects of ice coverage and ice-rafted material on sedimentation in the Fram Strait. Nature 350, 409–411. doi:10.1038/350409a0.

Herndl, G. J., Reinthaler, T., Teira, E., Van Aken, H., Veth, C., Pernthaler, A., et al. (2005). Contribution of Archaea to total prokaryotic production in the deep Atlantic Ocean. Appl. Environ. Microbiol. 71, 2303–2309. doi:10.1128/AEM.71.5.2303-2309.2005.

Hewson, I., Steele, J. A., Capone, D. G., and Fuhrman, J. A. (2006). Remarkable heterogeneity in meso- and bathypelagic bacterioplankton assemblage composition. Limnol. Oceanogr. 51, 1274–1283. doi:10.4319/lo.2006.51.3.1274.

Karner, M. B., Delong, E. F., and Karl, D. M. (2001). Archaeal dominance in the mesopelagic zone of the Pacific Ocean. Nature 409, 507–510. doi:10.1038/35054051.

Kassambara, A. (2020). rstatix: Pipe-friendly framework for basic statistical tests. R package version 0.5.0.999. R Packag. version 0.6.0, https://rpkgs.datanovia.com/rstatix/.

Kirchman, D. L., Elifantz, H., Dittel, A. I., Malmstrom, R. R., and Cottrell, M. T. (2007). Standing stocks and activity of Archaea and Bacteria in the western Arctic Ocean. Limnol. Oceanogr. 52, 495–507. doi:10.4319/lo.2007.52.2.0495.

Korhonen, M., Rudels, B., Marnela, M., Wisotzki, A., and Zhao, J. (2013). Time and space variability of freshwater content, heat content and seasonal ice melt in the Arctic Ocean from 1991 to 2011. Ocean Sci. 9, 1015–1055. doi:10.5194/os-9-1015-2013.

Kraemer, S., Ramachandran, A., Colatriano, D., Lovejoy, C., and Walsh, D. A. (2020). Diversity and biogeography of SAR11 bacteria from the Arctic Ocean. ISME J. 14, 79–90. doi:10.1038/s41396-019-0499-4.

Kumar, M. S., Slud, E. V., Okrah, K., Hicks, S. C., Hannenhalli, S., and Bravo, H. C. (2017). Analysis and correction of compositional bias in sparse sequencing count data. bioRxiv 19, 799. doi:10.1101/142851.

Landry, Z., Swa, B. K., Herndl, G. J., Stepanauskas, R., and Giovannoni, S. J. (2017). SAR202 genomes from the dark ocean predict pathways for the oxidation of recalcitrant dissolved organic matter. MBio 8, e00413-17. doi:10.1128/mBio.00413-17.

Leu, E., Søreide, J. E., Hessen, D. O., Falk-Petersen, S., and Berge, J. (2011). Consequences of changing sea-ice cover for primary and secondary producers in the european Arctic shelf seas: timing, quantity, and quality. Prog. Oceanogr. 90, 18–32. doi:10.1016/j.pocean.2011.02.004.

Luo, H., and Moran, M. A. (2014). Evolutionary ecology of the marine Roseobacter clade. Microbiol. Mol. Biol. Rev. 78, 1–16. doi:10.1128/mmbr.88888-88.

Müller, O., Seuthe, L., Bratbak, G., and Paulsen, M. L. (2018a). Bacterial response to permafrost derived organic matter input in an Arctic Fjord. Front. Mar. Sci. 5. doi:10.3389/fmars.2018.00263.

Müller, O., Wilson, B., Paulsen, M. L., Ruminska, A., Armo, H. R., Bratbak, G., et al. (2018b). Spatiotemporal dynamics of ammonia-oxidizing Thaumarchaeota in Distinct Arctic water masses. Front. Microbiol. 9, 24. doi:10.3389/fmicb.2018.00024.

Mundy, C. J., Barber, D. G., and Michel, C. (2005). Variability of snow and ice thermal, physical and optical properties pertinent to sea ice algae biomass during spring. J. Mar. Syst. 58, 107–120. doi:10.1016/j.jmarsys.2005.07.003.

Nöthig, E.-M., Knüppel, N., and Lorenzen, C. (2018). Chlorophyll *a* measured on water bottle samples during POLARSTERN cruise PS99.2 (ARK-XXX/1.2). PANGAEA

doi:10.1594/PANGAEA.887855.
Nöthig, E. M., Bracher, A., Engel, A., Metfies, K., Niehoff, B., Peeken, I., et al. (2015). Summertime plankton ecology in Fram Strait - a compilation of long-and short-term observations. Polar Res. 34, 23349. doi:10.3402/polar.v34.23349.
Owrid, G., Socal, G., Civitarese, G., Luchetta, A., Wiktor, J., Nöthig, E. M., et al. (2000). Spatial variability of phytoplankton, nutrients and new production estimates in the waters around Svalbard. Polar Res. 19, 155–171. doi:10.1111/j.1751-8369.2000.tb00340.x.
Peng, G., and Meier, W. N. (2018). Temporal and regional variability of Arctic sea-ice coverage from satellite data. Ann. Glaciol. 59, 191–200. doi:10.1017/aog.2017.32.
Pernthaler, A., Pernthaler, J., and Amann, R. (2002). Fluorescence in situ hybridization and catalyzed reporter deposition for the identification of marine Bacteria. Appl. Environ. Microbiol. 68, 3094–3101. doi:10.1128/AEM.68.6.3094-3101.2002.
Perrette, M., Yool, A., Quartly, G. D., and Popova, E. E. (2011). Near-ubiquity of ice-edge blooms in the Arctic. Biogeosciences 8, 515–524. doi:10.5194/bg-8-515-2011.
Piontek, J., Sperling, M., Nöthig, E. M., and Engel, A. (2014). Regulation of bacterioplankton activity in Fram Strait (Arctic Ocean) during early summer: The role of organic matter supply and temperature. J. Mar. Syst. 132, 83–94. doi:10.1016/j.jmarsys.2014.01.003.
Piontek, J., Sperling, M., Nöthig, E. M., and Engel, A. (2015). Multiple environmental changes induce interactive effects on bacterial degradation activity in the Arctic Ocean. Limnol. Oceanogr. 60, 1392–1410. doi:10.1002/lno.10112.
Piwosz, K., Shabarova, T., Pernthaler, J., Posch, T., Šimek, K., Porcal, P., et al. (2020). Bacterial and eukaryotic small-Subunit amplicon data do not provide a quantitative picture of microbial communities, but they are reliable in the context of ecological interpretations. mSphere 5, 1–14. doi:10.1128/msphere.00052-20.
Polyakov, I. V., Pnyushkov, A. V., Alkire, M. B., Ashik, I. M., Baumann, T. M., Carmack, E. C., et al. (2017). Greater role for Atlantic inflows on sea-ice loss in the Eurasian Basin of the Arctic Ocean. Science (80-.). 356, 285–291. doi:10.1126/science.aai8204.
Quast, C., Pruesse, E., Yilmaz, P., Gerken, J., Schweer, T., Yarza, P., et al. (2013). The SILVA ribosomal RNA gene database project: Improved data processing and web-based tools. Nucleic Acids Res. 41, D590–D596. doi:10.1093/nar/gks1219.
Quero, G. M., Celussi, M., Relitti, F., Kovačević, V., Del Negro, P., and Luna, G. M. (2020). Inorganic and organic carbon uptake processes and their connection to microbial diversity in meso- and bathypelagic Arctic waters (eastern Fram Strait). Microb. Ecol. 79, 823–839. doi:10.1007/s00248-019-01451-2.
Redfield, A. C. (1963). "The influence of organisms on the composition of seawater," in The sea (Wiley-Interscience), 26–77.
Rosselli, R., Romoli, O., Vitulo, N., Vezzi, A., Campanaro, S., De Pascale, F., et al. (2016). Direct 16S rRNA-seq from bacterial communities: a PCR-independent approach to simultaneously assess microbial diversity and functional activity potential of each taxon. Sci. Rep. 6, 1–12.
Rudels, B., Schauer, U., Björk, G., Korhonen, M., Pisarev, S., Rabe, B., et al. (2012). Observations of water masses and circulation in the Eurasian Basin of the Arctic Ocean from the 1990s to the late 2000s. Ocean Sci. Discuss. 9, 2695–2747. doi:10.5194/osd-9-2695-2012.
Salazar, G., Cornejo-Castillo, F. M., Benítez-Barrios, V., Fraile-Nuez, E., Álvarez-Salgado, X. A., Duarte, C. M., et al. (2016). Global diversity and biogeography of deep-sea pelagic

prokaryotes. ISME J. 10, 596–608. doi:10.1038/ismej.2015.137.
Saw, J. H. W., Nunoura, T., Hirai, M., Takaki, Y., Parsons, R., Michelsen, M., et al. (2019). Pangenomics reveal diversification of enzyme families and niche specialization in globally abundant SAR202 Bacteria. bioRxiv 11. doi:10.1101/692848.
Schattenhofer, M., Fuchs, B. M., Amann, R., Zubkov, M. V., Tarran, G. A., and Pernthaler, J. (2009). Latitudinal distribution of prokaryotic picoplankton populations in the Atlantic Ocean. Environ. Microbiol. 11, 2078–2093. doi:10.1111/j.1462-2920.2009.01929.x.
Schröder, M., and Wisotzki, A. (2014). Physical oceanography measured on water bottle samples during POLARSTERN cruise PS82 (ANT-XXIX/9). doi:10.1594/PANGAEA.871952.
Selje, N., Simon, M., and Brinkhoff, T. (2004). A newly discovered Roseobacter cluster in temperate and polar oceans. Nature 427, 445–448. doi:10.1038/nature02272.
Sheik, C. S., Jain, S., and Dick, G. J. (2014). Metabolic flexibility of enigmatic SAR324 revealed through metagenomics and metatranscriptomics. Environ. Microbiol. 16, 304–317. doi:10.1111/1462-2920.12165.
Soltwedel, T., Bauerfeind, E., Bergmann, M., Bracher, A., Budaeva, N., Busch, K., et al. (2016). Natural variability or anthropogenically-induced variation? Insights from 15 years of multidisciplinary observations at the Arctic marine LTER site HAUSGARTEN. Ecol. Indic. 65, 89–102. doi:10.1016/j.ecolind.2015.10.001.
Soltwedel, T., Bauerfeind, E., Bergmann, M., Budaeva, N., Hoste, E., Jaeckisch, N., et al. (2005). Hausgarten: Multidisciplinary investigations at a deep-Sea, long-term observatory in the Arctic Ocean. Oceanography 18, 46–61. doi:10.5670/oceanog.2005.24.
Sperling, M., Giebel, H. A., Rink, B., Grayek, S., Staneva, J., Stanev, E., et al. (2012). Differential effects of hydrographic and biogeochemical properties on the SAR11 clade and Roseobacter RCA cluster in the North Sea. Aquat. Microb. Ecol. 67, 25–34. doi:10.3354/ame01580.
Sun, L., Perlwitz, J., and Hoerling, M. (2016). What caused the recent "Warm Arctic, Cold Continents" trend pattern in winter temperatures? Geophys. Res. Lett. 43, 5345–5352. doi:10.1002/2016GL069024.
Swan, B. K., Martinez-Garcia, M., Preston, C. M., Sczyrba, A., Woyke, T., Lamy, D., et al. (2011). Potential for chemolithoautotrophy among ubiquitous Bacteria lineages in the dark ocean. Science (80-.). 333, 1296–1300. doi:10.1126/science.1203690.
Tada, Y., Makabe, R., Kasamatsu-Takazawa, N., Taniguchi, A., and Hamasaki, K. (2013). Growth and distribution patterns of Roseobacter/Rhodobacter, SAR11, and Bacteroidetes lineages in the Southern Ocean. Polar Biol. 36, 691–704. doi:10.1007/s00300-013-1294-8.
Tada, Y., Taniguchi, A., Nagao, I., Miki, T., Uematsu, M., Tsuda, A., et al. (2011). Differing growth responses of major phylogenetic groups of marine Bacteria to natural phytoplankton blooms in the Western North Pacific Ocean. Appl. Environ. Microbiol. 77, 4055–4065. doi:10.1128/AEM.02952-10.
Teeling, H., Fuchs, B. M., Becher, D., Klockow, C., Gardebrecht, A., Bennke, C. M., et al. (2012). Substrate-controlled succession of marine bacterioplankton populations induced by a phytoplankton bloom. Science (80-.). 336, 608–611. doi:10.1126/science.1218344.
Teeling, H., Fuchs, B. M., Bennke, C. M., Krüger, K., Chafee, M., Kappelmann, L., et al. (2016). Recurring patterns in bacterioplankton dynamics during coastal spring algae blooms. Elife 5, e11888. doi:10.7554/eLife.11888.

Teira, E., Lebaron, P., Van Aken, H., and Herndl, G. J. (2006). Distribution and activity of Bacteria and Archaea in the deep water masses of the North Atlantic. Limnol. Oceanogr. 51, 2131–2144. doi:10.4319/lo.2006.51.5.2131.

Teira, E., Reinthaler, T., Pernthaler, A., Pernthaler, J., and Herndl, G. J. (2004). Combining catalyzed reporter deposition-fluorescence in situ hybridization and microautoradiography to detect substrate utilization by Bacteria and Archaea in the deep ocean. Appl. Environ. Microbiol. 70, 4411–4414. doi:10.1128/AEM.70.7.4411-4414.2004.

Varela, M. M., Van Aken, H. M., and Herndl, G. J. (2008). Abundance and activity of Chloroflexi-type SAR202 bacterioplankton in the meso- and bathypelagic waters of the (sub)tropical Atlantic. Environ. Microbiol. 10, 1903–1911. doi:10.1111/j.1462-2920.2008.01627.x.

Vernet, M., Richardson, T. L., Metfies, K., Eva-Maria Nöthig, and Peeken, I. (2017). Models of plankton community changes during a warm water anomaly in Arctic waters show altered trophic pathways with minimal changes in carbon export. Front. Mar. Sci. 4, 160. doi:10.3389/fmars.2017.00160.

von Appen, W. J., Schauer, U., Somavilla, R., Bauerfeind, E., and Beszczynska-Möller, A. (2015). Exchange of warming deep waters across Fram Strait. Deep. Res. Part I Oceanogr. Res. Pap. 103, 86–100. doi:10.1016/j.dsr.2015.06.003.

Walczowski, W., Beszczynska-Möller, A., Wieczorek, P., Merchel, M., and Grynczel, A. (2017). Oceanographic observations in the Nordic Sea and Fram Strait in 2016 under the IO PAN long-term monitoring program AREX. Oceanologia 59, 187–194. doi:10.1016/j.oceano.2016.12.003.

Wassmann, P., and Reigstad, M. (2011). Future Arctic Ocean seasonal ice zones and implications for pelagic-benthic coupling. Oceanography 24, 220–231. doi:10.5670/oceanog.2011.74.

Wei, Z.-F., Li, W.-L., Huang, J.-M., and Wang, Y. (2020). Metagenomic studies of SAR202 bacteria at the full-ocean depth in the Mariana Trench. Deep Sea Res. Part I Oceanogr. Res. Pap. 165, 103396. doi:https://doi.org/10.1016/j.dsr.2020.103396.

Wekerle, C., Wang, Q., von Appen, W. J., Danilov, S., Schourup-Kristensen, V., and Jung, T. (2017). Eddy-Resolving simulation of the Atlantic water circulation in the Fram Strait with focus on the seasonal cycle. J. Geophys. Res. Ocean. 122, 8385–8405. doi:10.1002/2017JC012974.

Welch, D. B. M., and Huse, S. M. (2011). Microbial diversity in the deep sea and the underexplored "rare biosphere." Handb. Mol. Microb. Ecol. II Metagenomics Differ. Habitats 103, 243–252. doi:10.1002/9781118010549.ch24.

Wells, L. E., Cordray, M., Bowerman, S., Miller, L. A., Vincent, W. F., and Deming, J. W. (2006). Archaea in particle-rich waters of the Beaufort Shelf and Franklin Bay, Canadian Arctic: Clues to an allochthonous origin? Limnol. Oceanogr. 51, 47–59. doi:10.4319/lo.2006.51.1.0047.

Wickham, H. (2016). "Getting started with ggplot2," in ggplot2 (Springer), 11–31. doi:10.1007/978-3-319-24277-4_2.

Wickham, H., Averick, M., Bryan, J., Chang, W., McGowan, L., François, R., et al. (2019). Welcome to the Tidyverse. J. Open Source Softw. 4, 1686. doi:10.21105/joss.01686.

Williams, T.J., Wilkins, D., Long, E., Evans, F., DeMaere, M.Z., Raftery, M.J., et al. (2013). The role of planktonic Flavobacteria in processing algal organic matter in coastal East Antarctica revealed using metagenomics and metaproteomics. Environmental

Microbiology 15(5), 1302-1317. doi: 10.1111/1462-2920.12017.
Wilson, B., Müller, O., Nordmann, E. L., Seuthe, L., Bratbak, G., and Øvreås, L. (2017). Changes in marine prokaryote composition with season and depth over an Arctic polar year. Front. Mar. Sci. 4, 95. doi:10.3389/fmars.2017.00095.
Wilson, C., and Wallace, D. W. R. (1990). Using the nutrient ratio NO/PO as a tracer of continental shelf waters in the central Arctic Ocean. J. Geophys. Res. 95, 22193. doi:10.1029/jc095ic12p22193.
Zeder, M., Ellrott, A., and Amann, R. (2011). Automated sample area definition for high-throughput microscopy. Cytom. Part A 79 A, 306–310. doi:10.1002/cyto.a.21034.
Publication in preparation.

Supplementary Material

Table S1. Specificities of publicly available rRNA-targeting oligonucleotide probes used during CARD-FISH for the quantification of pelagic microbial groups in the Fram Strait, and their total sequence proportions in 16S rRNA data of Fadeev et al. (2020). FA - formamide concentration in the hybridization buffer.

*Taxonomic groups in the 16S rRNA data were defined according to SILVA reference database v138 (k - kingdom, p - phylum, c - class, o - order, f - family, g - genus).

Probe name	Targeted group	Sequence proportion*	Sequence (5'-3')	FA (%)	Reference
EUB338 I	*Bacteria*	92% (k: *Bacteria*)	GCT GCC TCC CGT AGG AGT	35	(Amann et al., 1990)
EUB338 II	*Planctomycetales (Bacteria)*	1% (o: *Planctomycetales*)	GCA GCC ACC CGT AGG TGT	35	(Daims et al., 1999)
EUB338 III	*Verrucomicrobia and Bacteria*	9% (p: *Verrucomicrobiae*)	GCT GCC ACC CGT AGG TGT	35	(Daims et al., 1999)
Non338	nonsense probe	-	ACT CCT ACG GGA GGC AGC	35	(Wallner et al., 1993)
ARCH915	*Archaea*	8% (k: *Archaea*)	GTG CTC CCC CGC CAA TTC CT	35	(Amann et al., 1995)
CFX1223	*Chloroflexi*	2% (p: *Chloroflexi*)	CCA TTG TAG CGT GTG TGT MG	35	(Björnsson et al., 2002)
GNSB941	*Chloroflexi*		AAA CCA CAC GCT CCG CT	35	(Gich et al., 2001)
SAR202-312R	*SAR202 clade*	1% (o: *SAR202* clade)	TGT CTC AGT CCC CCT CTG	40	(Morris et al., 2004)
PSA184	*Alteromonadaceae, Colwelliaceae, Pseudoalteromonadaceae*	2% (o: *Alteromonadales*)	CCC CTT TGG TCC GTA GAC	30	(Eilers et al., 2000)
GAM42a	*Gammaproteobacteria*	22% (c: *Gammaproteobacteria*)	GCC TTC CCA CAT CGT TT	35	(Manz et al., 1992)
BET421	*competitor for GAM42a*		GCC TTC CCA CTT CGT TT	35	(Manz et al., 1992)

POL740	*Polaribacter*	11% (g: *Polaribacter*)	CCC TCA GCG TCA GTA CAT ACG T	35	(Malmstrom et al., 2007)
CF968	*Bacteroidetes*	28% (c: *Bacteroidia*)	GGT AAG GTT CCT CGC GTA	55	(Acinas et al., 2015)
Opi346	*Opitutales*	7% (o: *Opitutales*)	TTC GAA ACT GCT GCC ACC C	20	(Reintjes 2017)
Cren554	*Thaumarchaeota*	6% (c: *Nitrososphaeria*)	TTA GGC CCA ATA ATC MTC CT	20	(Massana et al., 1997)
SAR406-97	*SAR406 clade (Marinimicrobia)*	4% (p: *SAR406* clade)	CAC CCG TTC GCC AGT TTA	40	(Fuchs et al., 2005)
DELTA495a	*Deltaproteobacteria*	1% (p: B*dellovibrionota, Desulfobacterota, Myxococcota)*	AGT TAG CCG GTG CTT CCT	35	(Loy et al., 2002)
cDELTA495a	*competitor for DELTA495a*		AGT TAG CCG GTG CTT CTT	35	(Lücker et al., 2007)
DELTA495b	*Deltaproteobacteria*		AGT TAG CCG GCG CTT CCT	35	(Loy et al., 2002)
cDELTA495b	competitor for DELTA495b		AGT TAG CCG GCG CTT CKT	35	(Lücker et al., 2007)
DELTA495c	*Deltaproteobacteria*		AAT TAG CCG GTG CTT CCT	35	(Loy et al., 2002)
cDELTA495c	competitor for DELTA495c		AAT TAG CCG GTG CTT CTT	35	(Lücker et al., 2007)
SAR324-R-625	*SAR324* clade ("Marine group B")	3% (p: *SAR324* clade)	CGA AAG ACC CTC CGG	15	(Wright et al., 1997)
ROS536	*Rhodobacteraceae*	2% (f: *Rhodobacteraceae*)	CAA CGC TAA CCC CCT CCG	35	(Brinkmeyer et al., 2000)
SAR11-152R	*SAR11 clade*	9% (o: *SAR11* clade)	TTAGCACAAGTTTCCYCGTG T	25	(Morris et al. 2002)
SAR11-441R	*SAR11 clade*		TACAGTCATTTTCTTCCCCG AC	25	(Morris et al. 2002)
SAR11-441Rmod	*SAR11 clade*		TACCGTCATTTTCTTCCCCG AC	25	(Gomez-Pereira et al., 2013)

SAR11-542R	*SAR11 clade*		TCCGAACTACGCTAGGTC	25	(Morris et al. 2002)
SAR11-732R	*SAR11 clade*		GTCAGTAATGATCCAGAAA GYTG	25	(Morris et al. 2002)
SAR11-487Rmodif	*SAR11 clade*		CGGACCTTCTTATTCGGG	25	(Gomez-Pereira et al., 2013)
SAR11-487_h3	*SAR11 clade*		CGGCTGCTGGCACGAAGTT AGC	25	(Gomez-Pereira et al., 2013)

Table S2. Average bacterioplankton cell abundances along the water column of ice-covered and ice-free regions of the Fram Strait. The DAPI counts represent total bacterioplankton cell abundances. The proportions (%) of *Archaea* (ARCH) and *Bacteria* (EUB) were calculated based on the total bacterioplankton cell abundances (DAPI stained cells). Sample size 'n' represents the number of counted fields of view. Standard error was not calculated for samples of the EGC located in the bathypelagic zone due to one station located at this depth in the region (NA). EGC: the ice-covered East Greenland Current, EG stations, N: the marginal ice northern stations, WSC: the ice-free West Spitsbergen Current, HG stations. All values are represented in 10^5 cells mL^{-1}.

Region	Water layer	DAPI	*Archaea*	%	n	*Bacteria*	%	n
EGC	Surface	3.4 ± 0.2	0.2 ± 0.0	8	56	2.2 ± 0.2	60	52
EGC	Epipelagic	3.5 ± 1.2	0.4 ± 0.2	14	57	2.1 ± 1.3	55	48
EGC	Mesopelagic	0.7 ± 0.3	0.1 ± 0.1	17	51	0.2 ± 0.1	40	44
EGC	Bathypelagic	0.6 ± NA	0.02 ± NA	12	32	0.1 ± NA	16	32
N	Surface	17.1 ± 0.7	0.3 ± 0.1	2	90	10.7 ± 0.7	62	81
N	Epipelagic	7.9 ± 1.2	0.6 ± 0.0	9	90	3.2 ± 0.7	40	73
N	Mesopelagic	0.9 ± 0.1	0.1 ± 0.0	17	77	0.3 ± 0.0	37	101
N	Bathypelagic	0.4 ± 0.0	0.1 ± 0.0	17	63	0.1 ± 0.0	37	85
WSC	Surface	15.0 ± 3.6	0.2 ± 0.0	1	146	8.1 ± 1.8	59	150
WSC	Epipelagic	6.2 ± 0.7	0.6 ± 0.1	12	217	2.2 ± 0.3	36	175
WSC	Mesopelagic	0.8 ± 0.1	0.1 ± 0.0	13	152	0.3 ± 0.1	34	166
WSC	Bathypelagic	0.5 ± 0.1	0.1 ± 0.0	15	198	0.2 ± 0.0	33	201

Table S3. Cell abundances and proportions of taxonomic groups in the different regions and water layers across the Fram Strait. The proportions (%) were calculated based on the total bacterioplankton cell abundances (DAPI stained cells), 'n' represents the number of counted fields of view. All values are represented in 10^5 cells mL^{-1}. *Alteromonadaceae/Colwelliaceae/Pseudoalteromonadaceae* (ATL), *Bacteroidetes* (BACT), *Chloroflexi* (CFX), *Thaumarchaeota* (THA), *Deltaproteobacteria* (DELTA), *Gammaproteobacteria* (GAM), *Opitutales* (OPI), *Polaribacter* (POL), *Rhodobacteraceae* (ROS), *Verrucomicrobia* (VER), *SAR202, SAR324*, *SAR406* and *SAR11* clades.

Region	Station	Water layer	ALT	%	n	BACT	%	n	CFX	%	n	THA	%	n	DELTA	%	n	GAM	%	n	OPI	%	n
EGC	EG1	SRF	0.27 ± 0.17	6.2	35	1.01 ± 0.20	23.7	31	0.07 ± 0.06	2.4	25	0.05 ± 0.03	1.6	15	0.33 ± 0.20	8.9	42	0.49 ± 0.16	14.6	35	0.11 ± 0.06	2.7	32
EGC	EG1	EPI	0.06 ± 0.04	3.2	28	0.13 ± 0.07	7.5	27	0.05 ± 0.02	2.3	20	0.06 ± 0.03	3.2	32	0.05 ± 0.02	2.7	33	0.11 ± 0.07	6.0	36	0.16 ± 0.12	1.9	26
EGC	EG1	MESO	0.02 ± 0.01	4.2	20	0.01 ± 0.00	2.1	4	0.03 ± 0.01	6.8	28	0.01 ± 0.00	2.1	8	0.02 ± 0.01	5.1	27	0.01 ± 0.00	2.2	5	0.02 ± 0.01	3.7	16
EGC	EG4	SRF	0.12 ± 0.11	8.3	29	0.24 ± 0.23	12.0	35	0.04 ± 0.02	1.1	23	0.14 ± 0.09	4.3	19	0.12 ± 0.17	4.3	15	0.14 ± 0.13	10.4	32	0.13 ± 0.10	2.2	21
EGC	EG4	EPI	0.07 ± 0.05	1.4	33	0.47 ± 0.11	8.5	66	0.08 ± 0.04	1.5	31	0.11 ± 0.06	4.6	43	0.12 ± 0.08	4.9	34	0.24 ± 0.09	4.8	41	0.13 ± 0.08	2.3	44
EGC	EG4	MESO	0.02 ± 0.01	1.5	33	0.01 ± 0.01	1.1	19	0.02 ± 0.01	2.2	29	0.01 ± 0.00	1.0	19	0.04 ± 0.03	3.9	18	0.01 ± 0.00	1.0	22	0.01 ± 0.01	1.5	24
EGC	EG4	BATHY	0.01 ± 0.00	1.9	11	0.01 ± 0.01	1.1	25	0.02 ± 0.01	3.9	18	0.01 ± 0.01	2.1	14	0.02 ± 0.01	3.3	33	0.01 ± 0.00	1.6	5	0.01 ± 0.01	3.2	11
WSC	HG1	SRF	0.14 ± 0.08	0.5	22	2.71 ± 0.84	8.6	20	0.10 ± 0.06	0.4	26	0.14 ± 0.09	0.6	37	0.11 ± 0.05	0.4	16	1.09 ± 0.34	3.8	23	1.18 ± 0.32	3.8	19
WSC	HG1	EPI	0.08 ± 0.05	1.0	34	0.16 ± 0.08	2.4	35	0.05 ± 0.02	0.6	30	0.41 ± 0.14	6.2	51	0.31 ± 0.22	4.2	35	0.11 ± 0.07	1.6	37	0.17 ± 0.07	2.1	42
WSC	HG1	MESO	0.02 ± 0.01	1.4	19	0.02 ± 0.01	1.3	20	0.03 ± 0.02	2.2	40	0.02 ± 0.02	1.6	33	0.06 ± 0.05	3.5	28	0.03 ± 0.01	2.4	24	0.02 ± 0.02	1.7	33
WSC	HG1	BATHY	0.02 ± 0.01	2.9	27	0.02 ± 0.01	1.8	11	0.02 ± 0.01	2.4	33	0.01 ± 0.01	1.9	21	0.11 ± 0.09	4.9	26	0.02 ± 0.01	2.5	27	0.03 ± 0.02	3.6	23
WSC	HG2	SRF	0.83 ± 0.52	4.0	32	4.82 ± 0.57	21.1	29	0.97 ± 0.58	4.6	24	0.08 ± 0.05	0.4	32	0.08 ± 0.05	0.4	25	2.84 ± 0.52	13.6	32	2.06 ± 0.45	10.0	29
WSC	HG2	EPI	0.09 ± 0.05	1.2	33	0.32 ± 0.14	5.6	28	0.15 ± 0.14	2.1	32	0.41 ± 0.14	6.1	40	0.26 ± 0.26	3.3	24	0.20 ± 0.08	3.0	40	0.17 ± 0.08	2.5	38

WSC	HG2	MESO	0.01 ± 0.01	1.7	17	0.02 ± 0.01	2.4	15	0.03 ± 0.02	3.8	54	0.01 ± 0.01	1.9	16	0.06 ± 0.04	5.0	17	0.02 ± 0.01	2.6	29	0.02 ± 0.01	2.2	22
WSC	HG2	BATHY	0.02 ± 0.01	2.2	19	0.01 ± 0.00	1.6	11	0.03 ± 0.02	2.9	42	0.01 ± 0.01	1.8	13	0.11 ± 0.05	10.3	21	0.02 ± 0.02	3.3	23	0.04 ± 0.03	4.4	22
WSC	HG4	SRF	0.25 ± 0.33	5.0	44	1.23 ± 0.30	22.5	31	0.36 ± 0.20	7.9	32	0.07 ± 0.04	0.6	28	0.29 ± 0.17	3.3	26	0.98 ± 0.29	19.6	45	0.11 ± 0.06	1.9	44
WSC	HG4	EPI	0.18 ± 0.14	3.3	38	0.22 ± 0.13	5.2	34	0.20 ± 0.17	5.2	36	0.41 ± 0.10	7.0	42	0.45 ± 0.20	7.1	41	0.22 ± 0.13	4.1	39	0.08 ± 0.05	1.3	39
WSC	HG4	MESO	0.01 ± 0.01	2.0	20	0.02 ± 0.01	1.4	17	0.06 ± 0.05	4.5	24	0.01 ± 0.00	1.1	24	0.06 ± 0.04	4.6	48	0.02 ± 0.01	2.4	17	0.02 ± 0.02	1.5	24
WSC	HG4	BATHY	0.02 ± 0.01	3.6	17	0.01 ± 0.00	2.2	5	0.02 ± 0.01	4.2	32	0.01 ± 0.01	0.9	4	0.06 ± 0.05	8.2	12	0.01 ± 0.00	2.1	8	0.02 ± 0.01	3.9	20
WSC	HG5	SRF	0.15 ± 0.08	1.2	26	0.49 ± 0.40	8.9	20	0.02 ± 0.01	0.5	14	0.04 ± 0.02	0.3	26	0.05 ± 0.04	0.5	14	1.49 ± 0.50	11.6	26	0.54 ± 0.20	4.7	25
WSC	HG5	EPI	0.03 ± 0.01	0.5	38	0.10 ± 0.07	2.1	29	0.03 ± 0.02	0.7	27	0.03 ± 0.02	1.4	17	0.07 ± 0.04	3.7	37	0.11 ± 0.05	2.2	46	0.05 ± 0.02	1.1	42
WSC	HG5	MESO	0.02 ± 0.00	5.9	2	0.01 ± 0.00	2.0	4	0.01 ± 0.01	3.3	23	0.02 ± 0.00	3.2	2	0.03 ± 0.02	9.6	14	0.01 ± 0.00	3.0	4	0.01 ± 0.01	3.7	4
WSC	HG5	BATHY	0.01 ± 0.01	7.7	5	0.01 ± 0.00	4.6	11	0.01 ± 0.00	6.8	24	0.03 ± 0.01	12.1	5	0.02 ± 0.01	10.1	34	0.01 ± 0.00	5.0	4	0.01 ± 0.00	6.1	11
WSC	HG7	SRF	0.22 ± 0.15	1.9	31	1.44 ± 0.72	12.3	29	0.03 ± 0.03	0.2	11	0.05 ± 0.03	0.4	36	0.04 ± 0.03	0.3	18	1.41 ± 0.36	12.2	31	0.66 ± 0.17	5.7	19
WSC	HG7	EPI	0.05 ± 0.03	1.2	27	0.23 ± 0.09	5.1	32	0.04 ± 0.01	0.8	33	0.39 ± 0.10	6.1	53	0.13 ± 0.15	1.9	18	0.15 ± 0.06	3.4	30	0.07 ± 0.04	1.7	45
WSC	HG7	MESO	0.02 ± 0.01	2.4	10	0.01 ± 0.01	1.5	14	0.02 ± 0.01	2.4	35	0.01 ± 0.00	5.6	3	0.02 ± 0.01	6.1	17	0.01 ± 0.00	1.6	19	0.01 ± 0.01	1.7	17
WSC	HG7	BATHY	0.01 ± 0.01	2.7	16	0.01 ± 0.00	1.6	8	0.02 ± 0.01	5.1	24	0.01 ± 0.00	3.4	5	0.06 ± 0.04	12.0	18	0.02 ± 0.01	3.2	29	0.02 ± 0.01	8.0	10
WSC	HG9	SRF	0.22 ± 0.24	2.2	31	2.22 ± 0.59	23.0	34	0.13 ± 0.10	1.3	20	0.05 ± 0.02	0.5	19	0.21 ± 0.21	2.4	22	2.08 ± 0.42	20.5	32	0.52 ± 0.15	5.4	36
WSC	HG9	EPI	0.06 ± 0.03	0.7	16	0.37 ± 0.13	4.8	37	0.05 ± 0.02	0.6	25	0.30 ± 0.13	3.4	43	0.20 ± 0.17	2.2	41	0.24 ± 0.12	3.0	22	0.19 ± 0.08	2.0	32
WSC	HG9	MESO	0.01 ± 0.01	2.9	22	0.01 ± NA	2.0	1	0.02 ± 0.01	2.8	41	0.02 ± 0.01	2.5	8	0.07 ± 0.04	7.4	15	0.02 ± 0.01	3.0	15	0.02 ± 0.01	3.2	10
WSC	HG9	BATHY	0.02 ± 0.01	5.3	18	0.01 ± 0.01	4.4	4	0.02 ± 0.01	5.2	44	0.01 ± 0.01	3.1	6	0.04 ± 0.02	8.0	19	0.01 ± 0.00	3.4	14	0.02 ± 0.01	5.4	24

N	N3	SRF	0.19 ± 0.14	1.0	32	1.57 ± 0.36	8.1	28	0.28 ± 0.33	1.5	35	0.10 ± 0.06	0.7	34	0.32 ± 0.29	2.2	36	0.85 ± 0.22	4.6	32	1.02 ± 0.36	5.4	28
N	N3	EPI	0.31 ± 0.13	3.0	34	0.58 ± 0.22	5.9	35	0.30 ± 0.26	3.2	38	0.27 ± 0.10	2.8	40	0.34 ± 0.28	3.0	42	0.55 ± 0.17	5.3	34	0.29 ± 0.12	2.9	39
N	N3	MESO	0.01 ± 0.00	1.6	23	0.02 ± 0.01	2.2	12	0.03 ± 0.02	4.1	48	0.01 ± 0.01	2.0	6	0.04 ± 0.02	4.7	32	0.02 ± 0.01	2.8	30	0.02 ± 0.01	2.5	27
N	N3	BATHY	0.01 ± 0.00	3.3	9	0.01 ± 0.00	3.3	4	0.02 ± 0.01	6.9	38	0.01 ± 0.00	3.3	14	0.03 ± 0.01	7.6	43	0.01 ± 0.01	3.5	12	0.02 ± 0.01	5.4	18
N	N4	SRF	0.16 ± 0.09	1.0	23	3.71 ± 0.68	22.8	27	0.21 ± 0.19	1.6	29	0.06 ± 0.04	0.4	17	0.17 ± 0.10	0.9	26	2.26 ± 0.50	13.9	23	0.98 ± 0.23	5.6	37
N	N4	EPI	0.06 ± 0.04	0.9	17	0.43 ± 0.20	7.1	34	0.13 ± 0.12	2.2	40	0.34 ± 0.10	5.2	39	0.17 ± 0.19	2.5	15	0.31 ± 0.14	5.3	35	0.13 ± 0.11	2.1	32
N	N4	MESO	0.02 ± 0.01	1.6	24	0.02 ± 0.01	1.9	19	0.02 ± 0.01	2.3	29	0.01 ± 0.00	1.0	7	0.04 ± 0.03	4.5	34	0.02 ± 0.01	2.1	31	0.02 ± 0.01	2.4	24
N	N4	BATHY	0.02 ± 0.01	5.7	28	0.01 ± 0.00	4.1	16	0.02 ± 0.01	5.3	44	0.02 ± 0.01	4.0	13	0.04 ± 0.02	9.0	37	0.02 ± 0.01	6.1	26	0.02 ± 0.01	5.2	21
N	N5	SRF	0.07 ± 0.03	0.4	13	0.90 ± 0.43	5.6	30	0.07 ± 0.08	0.5	6	0.06 ± 0.03	0.4	14	0.14 ± 0.07	0.8	24	3.06 ± 0.61	19.8	23	0.75 ± 0.29	4.9	26
N	N5	EPI	0.12 ± 0.07	1.6	36	0.30 ± 0.12	5.0	33	0.06 ± 0.03	0.8	29	0.31 ± 0.12	4.5	43	0.19 ± 0.16	2.4	37	0.24 ± 0.11	3.5	40	0.10 ± 0.05	1.4	36
N	N5	MESO	0.02 ± 0.01	1.6	26	0.02 ± 0.01	1.9	20	0.02 ± 0.02	2.6	39	0.01 ± 0.01	1.3	15	0.04 ± 0.03	4.4	33	0.02 ± 0.01	2.2	32	0.02 ± 0.01	2.1	23
N	N5	BATHY	0.02 ± 0.01	4.6	16	0.01 ± 0.00	2.6	6	0.02 ± 0.01	5.1	33	0.01 ± 0.01	3.2	12	0.03 ± 0.02	7.7	43	0.01 ± 0.01	3.6	17	0.01 ± 0.01	3.3	13
Region	Station	Water layer	POL	%	n	ROS	%	n	SAR11	%	n	SAR202	%	n	SAR324	%	n	SAR406	%	n	VER	%	n
EGC	EG1	SRF	0.76 ± 0.18	17.9	31	0.14 ± 0.13	3.8	19	1.15 ± 0.22	34.9	28	0.07 ± 0.03	2.4	19	0.06 ± 0.04	1.6	22	0.03 ± 0.00	0.9	2	0.05 ± 0.02	1.5	23
EGC	EG1	EPI	0.04 ± 0.02	2.4	19	0.16 ± 0.13	8.1	21	0.40 ± 0.10	22.5	21	0.05 ± 0.03	2.3	21	0.10 ± 0.06	3.7	23	0.05 ± 0.02	2.3	2	0.04 ± 0.02	2.0	21
EGC	EG1	MESO	0.02 ± 0.01	4.3	17	0.07 ± 0.03	15.4	42	0.10 ± 0.03	23.3	25	0.02 ± 0.02	6.1	42	0.04 ± 0.02	7.2	18	0.01 ± 0.00	1.9	4	0.01 ± 0.01	3.2	14
EGC	EG4	SRF	0.09 ± 0.11	4.4	31	0.30 ± 0.30	10.2	25	2.56 ± 1.16	64.3	25	0.05 ± 0.03	1.2	25	0.13 ± 0.06	3.1	22	0.03 ± 0.00	1.3	11	0.12 ± 0.10	3.5	18

EGC	EG4	EPI	0.12 ± 0.07	2.1	33	0.51 ± 0.35	9.8	39	1.63 ± 0.26	29.8	29	0.08 ± 0.04	1.5	39	0.09 ± 0.06	2.4	16	0.03 ± 0.00	1.2	4	0.08 ± 0.05	1.5	42
EGC	EG4	MESO	0.01 ± 0.01	1.3	30	0.06 ± 0.04	6.7	33	0.21 ± 0.05	20.5	24	0.02 ± 0.01	2.4	33	0.05 ± 0.02	5.6	42	0.01 ± 0.00	0.9	7	0.02 ± 0.01	1.8	23
EGC	EG4	BATHY	0.02 ± 0.01	1.6	29	0.03 ± 0.03	5.1	14	0.07 ± 0.07	13.9	32	0.02 ± 0.02	5.4	14	0.03 ± 0.01	4.7	35	0.01 ± 0.01	2.7	6	0.01 ± 0.01	2.0	11
WSC	HG1	SRF	0.56 ± 1.67	1.8	20	2.08 ± 0.51	6.9	21	14.2 ± 2.03	44.9	22	0.07 ± 0.04	0.2	21	0.13 ± 0.07	0.5	29	0.03 ± 0.00	0.1	8	1.13 ± 0.31	3.5	19
WSC	HG1	EPI	0.06 ± 0.03	0.9	20	0.26 ± 0.13	3.3	46	2.34 ± 0.41	33.2	37	0.06 ± 0.03	0.9	46	0.11 ± 0.06	1.2	21	0.05 ± 0.02	0.6	17	0.07 ± 0.04	0.9	35
WSC	HG1	MESO	0.02 ± 0.01	1.7	29	0.06 ± 0.05	4.2	37	0.25 ± 0.06	22.9	30	0.04 ± 0.02	3.4	37	0.07 ± 0.03	4.2	23	0.01 ± 0.01	0.8	3	0.02 ± 0.01	1.7	30
WSC	HG1	BATHY	0.03 ± 0.02	3.5	28	0.05 ± 0.03	6.7	39	0.10 ± 0.04	12.0	36	0.04 ± 0.02	4.4	39	0.05 ± 0.02	6.9	18	0.01 ± 0.00	1.9	8	0.02 ± 0.01	2.8	18
WSC	HG2	SRF	1.16 ± 0.24	5.1	29	0.66 ± 0.11	2.9	32	9.78 ± 1.50	45.6	26	0.06 ± 0.04	0.3	32	0.08 ± 0.04	0.4	31	0.04 ± 0.02	0.2	11	2.02 ± 0.43	9.7	29
WSC	HG2	EPI	0.07 ± 0.04	1.2	27	0.17 ± 0.13	2.5	38	2.48 ± 0.45	31.5	23	0.04 ± 0.02	0.6	38	0.08 ± 0.04	1.0	30	0.04 ± 0.01	0.5	12	0.16 ± 0.07	2.4	37
WSC	HG2	MESO	0.01 ± 0.01	2.4	20	0.10 ± 0.04	12.5	37	0.17 ± 0.05	18.2	29	0.03 ± 0.01	3.5	37	0.06 ± 0.02	6.4	25	0.01 ± 0.00	1.6	8	0.02 ± 0.01	2.4	25
WSC	HG2	BATHY	0.02 ± 0.01	3.0	27	0.06 ± 0.02	8.0	35	0.13 ± 0.04	16.6	34	0.03 ± 0.02	4.5	35	0.05 ± 0.03	6.1	25	0.01 ± 0.00	1.7	13	0.02 ± 0.01	2.6	19
WSC	HG4	SRF	0.50 ± 0.21	9.2	31	0.23 ± 0.32	4.3	27	1.54 ± 0.36	26.9	25	0.04 ± 0.01	0.8	27	0.05 ± 0.03	0.7	16	0.05 ± 0.02	1.4	5	0.09 ± 0.05	1.5	43
WSC	HG4	EPI	0.08 ± 0.05	1.9	29	0.09 ± 0.03	2.1	37	2.29 ± 0.33	51.2	37	0.06 ± 0.03	1.4	37	0.10 ± 0.08	1.7	54	0.04 ± 0.01	0.7	10	0.06 ± 0.03	0.9	28
WSC	HG4	MESO	0.02 ± 0.01	1.4	27	0.09 ± 0.05	7.8	39	0.22 ± 0.06	21.4	22	0.05 ± 0.04	4.1	39	0.05 ± 0.02	4.7	32	0.02 ± 0.01	1.4	15	0.02 ± 0.02	1.9	25
WSC	HG4	BATHY	0.02 ± 0.01	3.3	21	0.03 ± 0.02	5.9	35	0.08 ± 0.03	17.0	35	0.03 ± 0.02	4.5	35	0.04 ± 0.04	6.2	10	0.02 ± 0.01	1.9	2	0.01 ± 0.01	3.0	13
WSC	HG5	SRF	0.21 ± 0.19	3.7	19	0.37 ± 0.16	2.9	34	2.66 ± 1.41	40.4	25	0.03 ± 0.03	0.7	34	0.03 ± 0.02	0.5	22	0.03 ± 0.02	0.2	17	1.28 ± 0.45	4.7	25
WSC	HG5	EPI	0.05 ± 0.03	1.1	31	0.08 ± 0.05	2.1	25	1.25 ± 0.43	25.8	29	0.04 ± 0.03	0.8	25	0.03 ± 0.03	1.5	18	0.01 ± 0.00	0.8	3	0.14 ± 0.06	1.2	42
WSC	HG5	MESO	0.01 ± 0.00	2.8	16	0.02 ± 0.01	4.4	19	0.04 ± 0.02	12.7	27	0.02 ± 0.01	7.4	19	0.01 ± 0.01	4.5	18	0.01 ± NA	2.0	1	0.01 ± 0.00	3.8	3

WSC	HG5	BATHY	0.01 ± 0.01	5.5	16	0.03 ± 0.02	18.7	42	0.05 ± 0.02	31.4	38	0.01 ± 0.01	8.5	42	0.02 ± 0.01	6.0	25	0.02 ± NA	5.9	1	0.01 ± 0.00	5.7	5
WSC	HG7	SRF	0.82 ± 0.47	7.0	29	0.31 ± 0.07	2.5	24	4.66 ± 0.99	38.6	30	0.04 ± 0.05	0.3	24	0.04 ± 0.02	0.3	25	0.02 ± 0.01	0.2	20	1.53 ± 0.40	5.6	19
WSC	HG7	EPI	0.08 ± 0.04	1.7	32	0.09 ± 0.04	2.0	38	1.30 ± 0.26	31.1	28	0.04 ± 0.02	1.0	38	0.09 ± 0.08	2.3	3	0.02 ± 0.01	0.8	11	0.14 ± 0.09	1.4	45
WSC	HG7	MESO	0.01 ± 0.01	1.8	21	0.04 ± 0.02	5.3	36	0.15 ± 0.04	18.2	23	0.03 ± 0.02	4.0	36	0.03 ± 0.02	6.5	32	0.01 ± 0.00	3.7	3	0.02 ± 0.01	2.7	8
WSC	HG7	BATHY	0.03 ± 0.02	5.9	21	0.04 ± 0.03	27.9	23	0.12 ± 0.04	26.2	25	0.04 ± 0.03	13.1	23	0.03 ± 0.02	5.8	35	0.01 ± 0.01	4.3	9	0.01 ± 0.01	4.2	8
WSC	HG9	SRF	1.26 ± 0.31	13.1	34	0.29 ± 0.13	2.9	27	3.53 ± 0.79	33.2	22	0.06 ± 0.06	0.6	27	0.07 ± 0.04	0.7	23	0.04 ± 0.02	0.5	10	0.53 ± 0.14	5.2	36
WSC	HG9	EPI	0.11 ± 0.05	1.4	37	0.20 ± 0.11	2.4	39	1.78 ± 0.49	19.9	21	0.06 ± 0.05	0.7	39	0.10 ± 0.04	1.0	15	0.04 ± 0.02	0.6	11	0.18 ± 0.08	1.9	32
WSC	HG9	MESO	0.02 ± 0.01	3.1	15	0.03 ± 0.02	6.1	27	0.11 ± 0.04	19.6	35	0.03 ± 0.01	4.4	27	0.05 ± 0.02	6.0	38	0.02 ± 0.02	3.3	7	0.02 ± 0.01	3.1	7
WSC	HG9	BATHY	0.02 ± 0.01	6.6	16	0.05 ± 0.03	15.8	23	0.09 ± 0.03	25.5	33	0.02 ± 0.01	7.7	23	0.03 ± 0.01	6.2	25	0.01 ± 0.00	2.7	12	0.01 ± 0.01	4.3	11
N	N3	SRF	0.29 ± 0.08	1.5	28	0.61 ± 0.14	3.2	29	6.10 ± 0.60	32.1	33	0.07 ± 0.06	0.4	29	0.08 ± 0.04	0.5	32	0.08 ± 0.05	0.4	24	1.01 ± 0.37	5.3	28
N	N3	EPI	0.11 ± 0.05	1.1	33	0.22 ± 0.09	2.0	51	2.71 ± 0.44	28.0	27	0.04 ± 0.02	0.4	51	0.07 ± 0.04	0.6	37	0.04 ± 0.02	0.4	13	0.28 ± 0.12	2.8	39
N	N3	MESO	0.02 ± 0.01	2.0	19	0.12 ± 0.05	17.2	39	0.14 ± 0.05	23.1	41	0.03 ± 0.02	4.4	39	0.05 ± 0.02	6.4	16	0.01 ± 0.00	1.4	3	0.02 ± 0.01	2.9	29
N	N3	BATHY	0.02 ± 0.01	7.3	18	0.06 ± 0.02	17.9	44	0.07 ± 0.03	23.9	31	0.03 ± 0.02	9.6	44	0.03 ± 0.02	6.9	7	0.02 ± 0.01	4.7	11	0.01 ± 0.01	3.6	16
N	N4	SRF	1.26 ± 0.22	7.8	27	0.62 ± 0.17	3.4	32	3.93 ± 0.71	22.8	24	0.09 ± 0.06	0.7	32	0.07 ± 0.04	0.4	30	0.04 ± 0.02	0.2	12	0.97 ± 0.23	5.4	37
N	N4	EPI	0.13 ± 0.05	2.0	32	0.25 ± 0.10	3.6	31	1.64 ± 0.30	23.6	22	0.06 ± 0.03	1.0	31	0.06 ± 0.03	0.9	27	0.04 ± 0.01	0.5	9	0.10 ± 0.06	1.8	29
N	N4	MESO	0.03 ± 0.02	2.8	26	0.10 ± 0.06	9.8	41	0.18 ± 0.05	18.0	21	0.03 ± 0.02	3.1	41	0.06 ± 0.02	5.4	24	0.01 ± 0.00	1.2	8	0.02 ± 0.01	1.9	24
N	N4	BATHY	0.02 ± 0.01	5.2	23	0.07 ± 0.04	22.4	34	0.12 ± 0.05	34.0	22	0.02 ± 0.01	7.1	34	0.05 ± 0.03	9.6	16	0.01 ± 0.01	2.9	19	0.01 ± 0.00	4.2	14
N	N5	SRF	2.48 ± 0.40	15.5	30	0.48 ± 0.13	2.9	31	2.54 ± 0.46	15.6	24	0.05 ± 0.03	0.3	31	0.06 ± 0.04	0.4	18	0.04 ± 0.02	0.3	11	0.84 ± 0.24	4.9	26

N	N5	EPI	0.10 ± 0.05	1.6	33	0.18 ± 0.17	2.5	26	2.39 ± 0.64	35.5	24	0.05 ± 0.02	0.7	26	0.08 ± 0.04	1.1	33	0.03 ± 0.00	0.5	6	0.08 ± 0.04	1.2	30
N	N5	MESO	0.02 ± 0.01	1.9	25	0.13 ± 0.05	12.9	48	0.20 ± 0.06	19.6	39	0.02 ± 0.01	1.9	48	0.06 ± 0.03	6.0	26	0.01 ± 0.00	1.1	7	0.02 ± 0.01	2.0	20
N	N5	BATHY	0.02 ± 0.01	3.6	14	0.07 ± 0.03	19.9	44	0.07 ± 0.02	21.6	32	0.03 ± 0.01	6.5	44	0.03 ± 0.01	6.1	31	0.01 ± 0.00	2.8	7	0.02 ± 0.01	4.7	18

Table S4. Pearson's correlation coefficient (r) tests of investigated bacterioplankton groups with environmental parameters (n=10), and phytoplankton cell abundances (n=5) in surface waters of the Fram Strait. Combinations that show significant correlation are marked with grey shadow. *Bacteria* (EUB), *Archaea* (ARCH), *Alteromonadaceae/Colwelliaceae/Pseudoalteromonadaceae* (ATL), *Bacteroidetes* (BACT), *Chloroflexi* (CFX), *Thaumarchaeota* (THA), *Deltaproteobacteria* (DELTA), *Gammaproteobacteria* (GAM), *Opitutales* (OPI), *Polaribacter* (POL), *Rhodobacteraceae* (ROS), *Verrucomicrobia* (VER), *SAR202, SAR324, SAR406* and *SAR11* clades.

Taxa	Temperature		Salinity		Chlorophyll *a* conc.		ΔNO_3		ΔPO_4		ΔSO_3		Diatoms		*Phaeocystis* spp.	
	r	*p*-value	r	*p*-value	r	*p*-value	r	*p*-value	r	*p*-value	r	*p*-value	r	*p*-value	r	*p*-value
ALT	0.03	0.93	0.28	0.41	-0.28	0.40	-0.12	0.74	0.27	0.44	-0.23	0.519	0.49	0.40	-0.84	0.08
ARCH	0.47	0.14	0.36	0.28	-0.50	0.12	-0.31	0.39	-0.21	0.56	-0.63	0.05	0.87	0.06	-0.15	0.81
BACT	0.41	0.21	0.52	0.10	-0.25	0.46	0.14	0.70	0.56	0.09	0.01	0.98	0.40	0.50	-0.36	0.55
CFX	0.12	0.72	0.40	0.23	-0.25	0.45	0.07	0.85	0.45	0.19	-0.12	0.74	-0.22	0.72	-0.38	0.53
THA	0.35	0.30	0.59	0.06	-0.30	0.37	-0.1	0.79	-0.09	0.80	-0.05	0.90	-0.19	0.76	0.78	0.12
DELTA	-0.4	0.23	0.05	0.89	-0.43	0.18	0.04	0.91	-0.15	0.68	-0.60	0.07	0.38	0.53	-0.89	0.04
EUB	0.60	0.05	0.50	0.12	0.22	0.52	0.17	0.64	0.59	0.07	0.14	0.69	-0.32	0.60	0.19	0.76
GAM	0.14	0.69	0.04	0.91	0.50	0.12	0.42	0.22	0.74	0.01	0.41	0.25	-0.34	0.57	0.08	0.90
OPI	0.61	0.05	0.38	0.25	-0.02	0.94	0.06	0.87	0.49	0.15	-0.02	0.96	-0.01	0.98	0.11	0.85
POL	-0.10	0.78	0.00	0.99	0.59	0.05	0.33	0.36	0.54	0.12	0.25	0.48	-0.30	0.62	0.03	0.96
ROS	0.78	0.00	0.49	0.13	0.06	0.87	0.26	0.47	0.54	0.12	0.09	0.80	-0.13	0.84	0.32	0.60
SAR11	0.79	0.00	0.61	0.04	-0.09	0.78	-0.15	0.69	0.30	0.40	-0.08	0.82	0.02	0.97	0.43	0.47
SAR202	0.16	0.64	0.29	0.39	-0.51	0.11	0.23	0.51	0.33	0.36	-0.37	0.29	0.82	0.09	-0.33	0.59
SAR324	0.14	0.69	0.64	0.03	-0.39	0.24	0.21	0.56	0.22	0.55	0.03	0.93	0.02	0.97	0.77	0.13
SAR406	0.04	0.92	0.26	0.44	-0.33	0.32	0.18	0.62	0.18	0.63	-0.29	0.41	-0.58	0.30	-0.18	0.77
VER	0.68	0.02	0.06	0.86	0.20	0.55	-0.18	0.61	0.20	0.59	0.10	0.78	-0.10	0.87	0.17	0.78

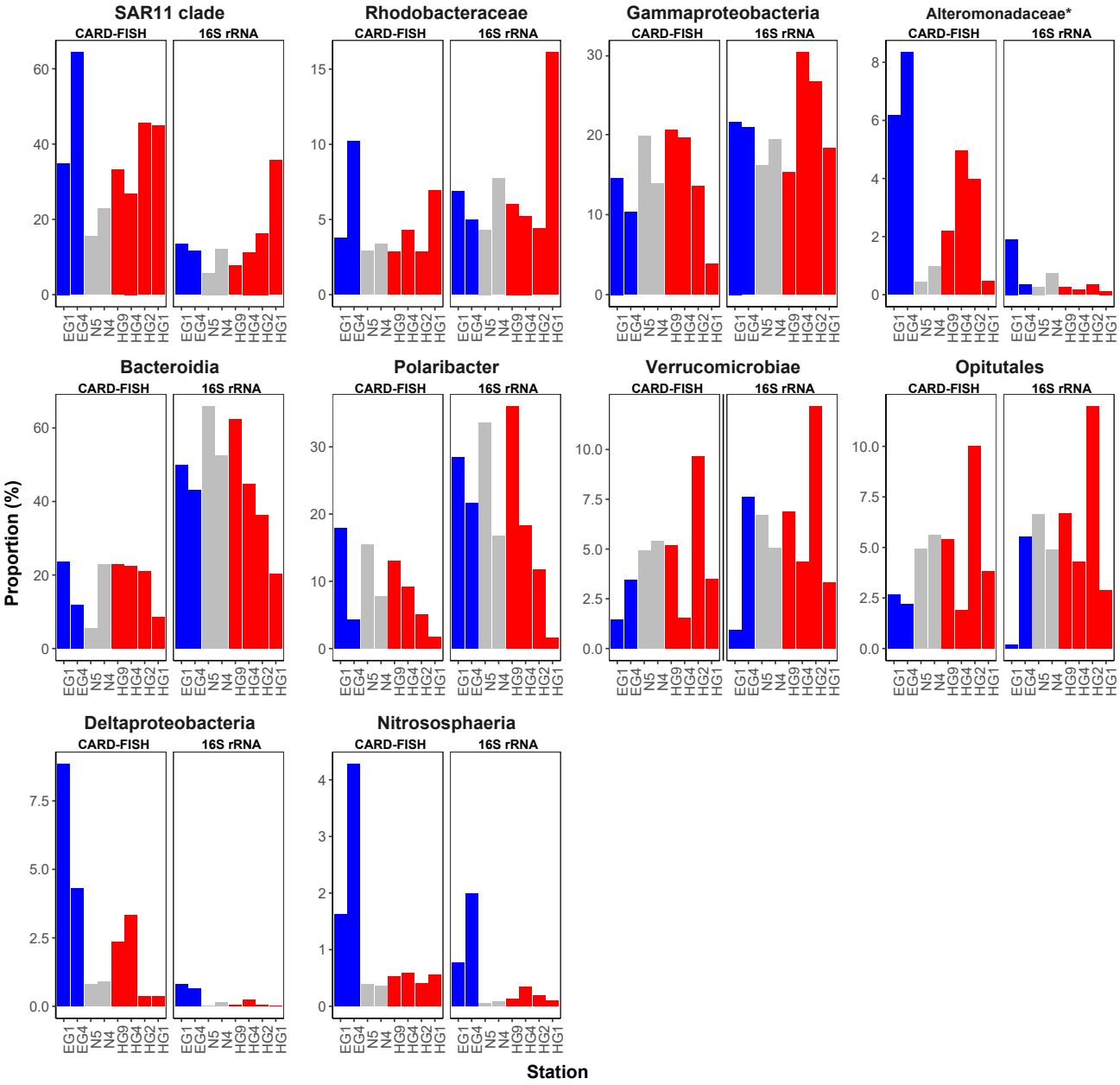

Figure S1. Proportion abundance of the targeted taxonomic groups in CARD-FISH and in high-throughput 16S rRNA gene sequencing performed during PS99.2. The different geographical regions of the Fram Strait are indicated by color: ice-covered EGC – blue, ice-margin N – gray, ice-free WSC – red.

* *Alteromonadaceae/Colwelliaceae/Pseudoalteromonadaceae.*

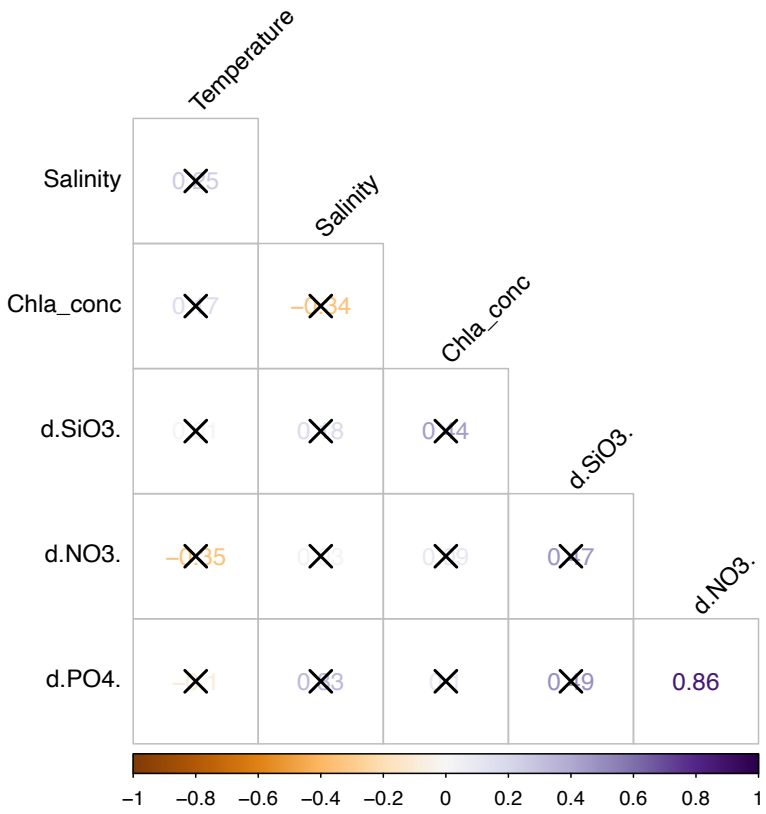

Figure S2. Pearsons's correlation coefficient (r) plot between environmental parameters representing the distinct water masses (temperature and salinity) and the different phytoplankton bloom conditions (chlorophyll *a* concentration and consumed inorganic nutrients) across the Fram Strait. Insignificant correlations are crossed with (X).

Chapter III

12 years of microbial community dynamics on sinking particles in the eastern Fram Strait

Magda G. Cardozo-Miño [1,2,3], *Ian Salter*[1,2,4], *Eva-Maria Nöthig*[2], *Katja Metfies*[2], *Simon Ramondenc*[2], *Claudia Wekerle*[2], *Thomas Krumpen*[2], *Antje Boetius*[1,2,5], *Christina Bienhold*[1,2]

[1]Max Planck Institute for Marine Microbiology, Bremen, Germany
[2]Alfred Wegener Institute for Polar and Marine Research, Bremerhaven, Germany
[3]Faculty of Geosciences, University of Bremen, Bremen, Germany
[4]Current affiliation: Faroe Marine Research Institute, Tórshavn, Faroe Islands
[5]MARUM, University of Bremen, Bremen, Germany

Keywords: Arctic Ocean, marine sinking particles, amplicon sequencing, sea ice, warm anomaly, Atlantic water, time series

Publication in preparation.

Abstract

Marine sinking particles sequester atmospheric carbon dioxide via the biological carbon pump. Understanding how environmental shifts drive changes in the microbial composition of particles and how these affect the export of organic matter from the surface to the deep ocean is critical, especially in the rapidly changing Arctic Ocean. Here, we applied next generation sequencing of the 18S and 16S rRNA genes to archived sediment trap samples from around 200 m water depth in the eastern Fram Strait, covering a timeframe of more than one decade (2000-2012). The aim was to characterize their microbial composition during annual highest particulate organic carbon flux events (HPF). Sequence libraries of sinking particles from HPF events were dominated by diatoms, dinoflagellates and radiolarians. Their bacterial communities were mainly represented by the classes *Gammaproteobacteria*, *Bacteroidia*, and *Alphaproteobacteria.* Using a high-resolution particle backtracking model, we estimated the catchment area of the sediment traps and retrieved relevant remote-sensing data products to assess variations in sea ice cover, sea surface temperature (SST), and chlorophyll concentrations, as well as hydrographic stratification regimes from a sea ice-ocean model. The bimodal annual spring and summer export fluxes were representative of the strong seasonality in the region, with distinct communities that correlated with stratification regimes and daylight. Furthermore, the study period was characterized by considerable interannual variation, especially by a warm water anomaly (WWA) between 2005 and 2007, accompanied by changes in the hydrography and sea ice cover, with measurable impacts on the microbial composition of particles and POC flux. The WWA period was marked by a decrease in diatoms affiliated with *Chaetoceros* an increase of small phytoplankton and an increase of the bacterial taxa *Oceanospirillales*, *Alteromonadales* and *Rhodobacterales* on the particles. The resulting changes in microbial composition and the associated microbial network structure suggested the development of a more developed retention system, with decreased POC flux compared to pre- and post-WWA periods. Our results provide the first long-term assessment of the microbial composition of sinking particles in the Arctic Ocean, and stress the importance of sea ice and hydrography for particle composition and subsequent flux of organic matter to deeper waters.

Introduction

Sinking particles play a key role in the global carbon cycle by transporting particulate organic matter (POM) from the surface to deeper ocean layers in a process called the biological carbon pump (BCP) (De La Rocha and Passow, 2007; Turner, 2015). A large proportion of the sinking particles originate in the photic zone from primary production, either directly by clumping algal blooms, or by grazing. The particles consist of live and dead phytoplankton, zooplankton and bacterioplankton, as well as inorganic components such as mineral grains, zooplankton shells other ballast minerals (calcium carbonate, opal, and lithogenic material), and fecal matter (Alldredge and Silver, 1988; Simon et al., 2002; Jiao et al., 2010; Turner, 2015). Particle composition is strongly determined by the environmental conditions in surface waters where the particles are formed (Simon et al., 2002; Buesseler and Boyd, 2009; Guidi et al., 2009; Bach et al., 2016).

Sinking particles act as "hot spots" of microbial diversity and activity (Azam and Malfatti, 2007). The microbial communities that colonize particles play a key role in the degradation of particulate organic carbon (POC) (Alldredge and Silver, 1988; Grossart et al., 2003; Fontanez et al., 2015), with implications for food web structures, export efficiency (Ducklow et al., 2001), and the flux of nutrients and carbon to deeper water layers (Simon et al., 2002; Iversen and Ploug, 2010; Grabowski et al., 2019). The activity of heterotrophic microbes determines particle remineralization rates across different depth layers of the ocean (Datta et al., 2016). In addition, sinking particles can act as dispersal vectors of viable microbial communities from the surface to the deep ocean (Mestre et al., 2018; Preston et al., 2020; Ruiz-González et al., 2020; Fadeev et al., 2021b), thus influencing the microbial structure and functioning of the deep sea (Gibbons et al., 2013; Cram et al., 2015; Thiele et al., 2015; Rapp et al., 2018). Recent studies have addressed molecular microbial community composition of sinking particles across seasons in other oceanographic regions (Boeuf et al., 2019; Preston et al., 2020). However, we are not aware of any studies that have investigated sinking particle-associated microbial community dynamics over longer time scales, which are of particular relevance when assessing effects of long-term environmental changes on microbial dynamics and POC export. Here, we focused on such dynamics by analysing the microbial community

composition in legacy trap samples of the Arctic Ocean time series at LTER HAUSGARTEN (78.5°N - 80°N, 05°W - 11°E) from 2000-2012.

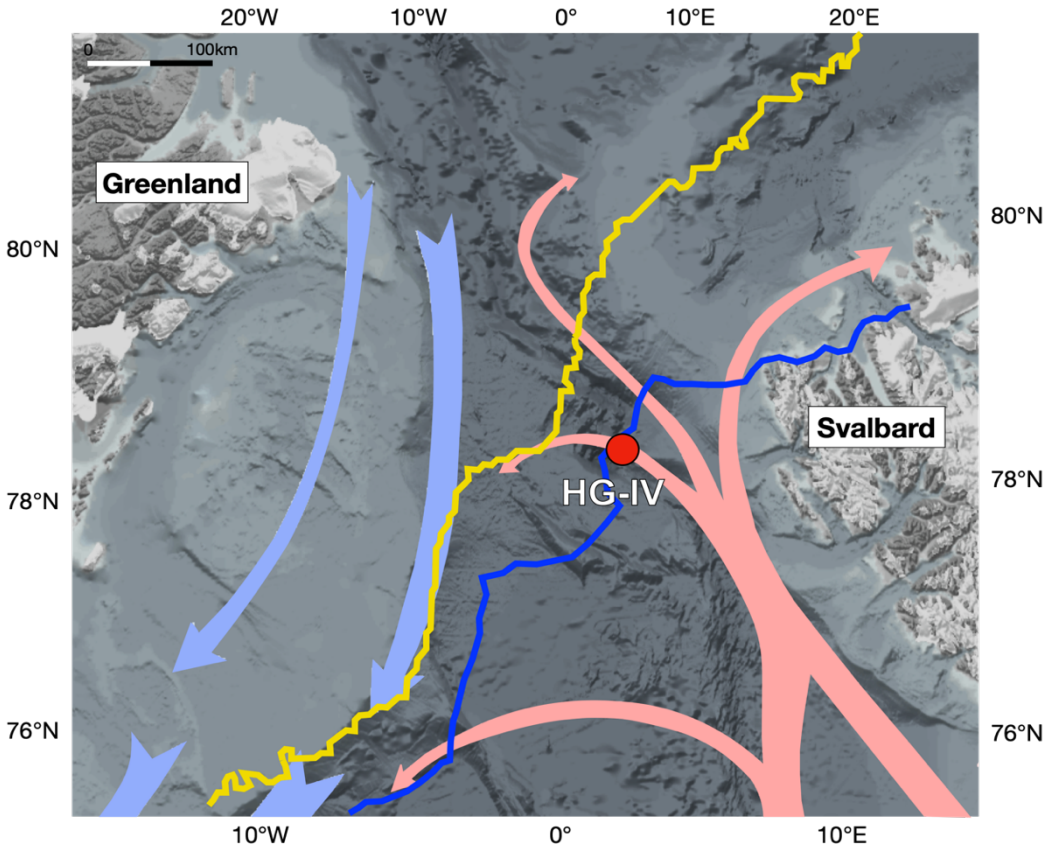

Figure 1. Map of the Fram Strait area depicting the deployment location (~79°00 N, ~04°20 W) of the sediment traps at the central station (HGIV) of the HAUSGARTEN observatory from 2000 to 2012. The red arrows indicate the West Spitsbergen Current carrying Atlantic Water into the region and the blue arrow the East Greenland Current with cold polar water exiting the Arctic Ocean. The monthly median sea ice edge is depicted for June 2006 in dark blue and June 2012 in bright yellow. Visualization and sea ice data were obtained from https://maps.awi.de (Grosfeld et al., 2016).

The Arctic Ocean is one of the most rapidly changing areas of the world, with increases in temperature 2-3 times higher than the global average. Substantial decreases in sea ice extent and thickness (Kwok and Rothrock, 2009; Perovich, 2011) are some of the most prominent manifestations of global warming today (Peng and Meier, 2018; Dai et al., 2019; Lannuzel et al., 2020). These environmental changes already have strong impacts on the pelagic system, including increases in primary production across shelf seas of the Arctic Ocean (Arrigo et al., 2012; Lewis et al., 2020; Nöthig et al., 2020). Arctic warming and sea ice retreat also alter pelagic species composition (Leu et al., 2011; Nöthig et al., 2015; Hop et al., 2019), the composition and structure of sinking particles, fecal pellets and marine snow exported to the

seafloor (Wassmann and Reigstad, 2011; Boetius et al., 2013; Wiedmann et al., 2020), and may weaken pelagic-benthic coupling as sea ice continues to retreat (Fadeev et al., 2021b).

Fram Strait, which is located between Greenland and Spitsbergen (Figure 1), is the main gateway between the Atlantic and Arctic Ocean. It is a hydrographically complex area with two dynamic current systems, the East Greenland Current (EGC) that transports sea ice with the Transpolar Drift out of the Arctic and the West Spitsbergen Current (WSC) that feeds Atlantic water into the Arctic Ocean (Beszczynska-Moeller et al., 2011). Over the past decades, the eastern Fram Strait has seen increased heat flux in the WSC (Walczowski et al., 2017). A particular event was a warm water anomaly (WWA) that occurred between 2005 and 2007 (Beszczynska-Möller et al., 2012). At the same time, winter sea ice area export through Fram Strait increased over the past decades as a result of warming-induced increased Transpolar Drift velocity (Krumpen et al., 2019). Moreover, sea-ice transport from the central Arctic to the Atlantic Ocean via Fram Strait and the Transpolar Drift is influenced by the Arctic dipole (Ramondenc et al., 2022). These changes have been accompanied by shifts in the timing and composition of phytoplankton blooms and zooplankton occurrences (Weydmann et al., 2014; Busch et al., 2015; Nöthig et al., 2015; Soltwedel et al., 2016; Schröter et al., 2019; Ramondenc et al., 2022), e.g., with a transition from diatom- to flagellate-dominated phytoplankton communities (Nöthig et al., 2015), with subsequent changes in the composition of particle export fluxes (Bauerfeind et al., 2009; Lalande et al., 2011, 2013), and the migration behaviour of main zooplankton species with consequences for higher trophic levels (Ramondenc et al., 2022). Only recently, Fadeev et al. (2021) have observed a decline in particle size and sinking rates influencing vertical microbial connectivity in ice-free compared to ice-covered areas of Fram Strait, and hypothesized weakening of pelagic-benthic coupling as sea ice continues to retreat. Another study in the same area has evidenced measurable impacts of variations in sea ice derived meltwater stratification on the biological carbon pump (von Appen et al. 2021). However, it remains largely unknown if or how the changes in sea ice cover, hydrography and pelagic community composition affect the microbial composition of sinking particles, especially over long timescales.

Despite recent advances in understanding temporal dynamics of microbial communities and the impacts on the BCP in the Arctic Ocean, little is known about the microbial community

composition of sinking particles, and effects of varying environmental conditions and shifts over longer periods of time. Here, in the framework of the Long-Term Ecological Research (LTER) site HAUSGARTEN, we utilized archived moored sediment trap samples to compare annual shifts in microbial eukaryotic and bacterial community composition between 2000 and 2012. We selected samples with the highest POC fluxes (HPF) during spring and summer in each year, as the main events driving the export of carbon and associated microbial communities to depths, and analysed them in context of their prevailing environmental conditions. We tested the hypotheses that 1) spring (March to May) and summer (June to September) export events differ in microbial composition, according to the seasonal development of the ecosystem, 2) interannual differences in community composition are linked to environmental shifts in the region, with 3) specific associations between eukaryotes and bacteria during the different periods, and that 4) changes in community composition can be linked with differences in POM export.

Materials and Methods

Sample collection

Sinking particles were sampled with modified automatic Kiel sediment traps with a sampling area of 0.5 m^2 and 20 liquid-tight sampling cups (Kremling et al., 1996), deployed and recovered yearly from 2000 to 2013 at the central LTER HAUSGARTEN station HG-IV (~79.01N, ~4.20E). An electronic failure of the sediment trap prevented the collection of sinking material during the 2003-2004 operational year and from mid-March through July 2002. The depth of the sediment traps ranged between 80 m and 280 m (only one sediment trap from July 2009 to July 2010 was deployed at 80 m) with an average deployment depth of 200 m over the study period, i.e. was at all times below the mixed layer in spring and summer. The sample cups were programmed to collect in intervals of 7 to 31 days depending on the predicted timing of the productive season and POC flux. Sampling cups were filled with filtered North Sea seawater adjusted to a salinity of 40 PSU with NaCl, and poisoned with $HgCl_2$ to a final concentration of 0.14%. After recovery, the samples were refrigerated until further processing in the laboratory. Before splitting of the samples, zooplankton (swimmers) with a size larger than 0.5 mm were carefully picked with forceps under a

dissecting microscope at a magnification of 20 and 50. The samples were split by a wet splitting procedure as described by (Bodungen et al., 1991) and stored as 1/8 volumetric splits in their original preservative at 4°C. For this study we selected samples with the highest POC fluxes in each year. Five samples showed signs of decomposition, regardless of the time of storage (in summer 2002, spring 2003, summer 2004 and in spring 2007), and were removed from the data set. Signs of decomposition observed shortly after recovery of the samples included rotten and sulfidic smell, black color, and signs of zooplankton decomposition, indicating incomplete fixation in the cups after sample collection.

Biogenic fluxes

Subsamples for the analysis of total sedimented matter (DW), and biogenic material (POC, particulate organic nitrogen PON, calcium carbonate $CaCO_3$, and particulate silicon PSi) were filtered, and analysed as described by (Bodungen et al., 1991). Subsamples for POC measurements were filtered on pre-weighted GF/F filter with a pore size of 0.7 µm pre-combusted at 500 °C for 4 h. Before drying for CHN analysis, POC filters were soaked in 0.1 N HCL to remove inorganic carbon, and dried at 60°C (Lalande et al., 2013, 2014). POC was measured using an elemental CHN analyser (Lalande et al., 2013). The total flux and the $CaCO_3$ flux were corrected when organisms containing calcium carbonate, such as pteropods, were present in the sample. The corrections were done by applying a factor of 0.174 mg/ind for DW and 0.167 mg/ind for carbonate (Bauerfeind et al., 2009). Subsamples for PSi were filtered on polycarbonate filters with a pore size of 0.8 µm, pre-treated for 12 h at 85°C in an oven, particulate biogenic silica (PbSi) measurements were obtained by wet-alkaline digestion of the samples and extracted for 2 h at 85°C in a shaking water bath (Bodungen et al., 1991). Particulate flux measurements were retrieved from the Data Publisher for Earth & Environmental Science PANGAEA (www.pangaea.de; Table S1).

Sediment trap catchment area and remote sensing data

A Lagrangian back-tracking model was used to determine the surface origin of particles arriving at 200 m at station HGIV, using the time-dependent velocity field of a high resolution, eddy resolving ocean-sea ice model (Wekerle et al., 2018). Daily particle trajectories were computed assuming a particle sinking velocity of 60 m d^{-1} (Fadeev et al., 2021b). The model

was used to constrain the relative distribution of particle positions within the sediment trap catchment area from all trajectory calculations conducted daily for the time period 2002-2009. Particle distributions were binned into grid-cells to calculate weighted means. Grid cell size was determined from the available resolution of remote-sensing and model data products. Using these probability distributions for calculating weighted means provides a more realistic estimate than simply integrating over the areal extent of the catchment area. The spatial grid bin that was used to calculate weighted means of sea ice coverage, SST and surface chlorophyll.

A sea ice concentration product was provided by CERSAT and is available on a 12.5 x 12.5 km grid (Ezraty et al. 2007). The ESA Ocean Color CCI Remote Sensing Reflectance (merged, bias-corrected) data are used to compute surface chlorophyll-a concentration with a spatial resolution of 1 km^2 using the regional OC5ci chlorophyll algorithms (Wekerle et al. 2018). The chlorophyll data is interpolated to the sea ice grid size of 12.5 x 12.5 km. Model output from the Finite-Element Sea-ice Ocean Model (FESOM) was used to obtain salinity values and Mixed Layer Depth (MLD) (von Appen et al. 2021). Here we use a FESOM configuration adapted to the Fram Strait (Wekerle et al. 2017). Model products were binned into 25 x 25 km grid cells and as for remote-sensing products, weighted means were calculated based on the relative proportion of particle trajectories in each grid cell. Mixed layer and stratified melt-water regimes have been previously defined in the Fram Strait and been shown to determine onset of biological production and export (von Appen et al. 2021). In the present study these regimes were defined in the catchment areas as follows: Unstratified (MLD>50m), mixed layer regime (ML) (MLD <50m and ($S_{100m} - S_{0m}$) <1) and meltwater regime (MW) (MLD <50m and ($S_{100m} - S_{0m}$) >1), where S_{100m} and S_{0m} are salinity values at 100 m and 0 m, respectively. The daily values of catchment area properties described above were integrated over the sediment trap opening period, considering a temporal lag of 4-days to reflect the impact of the changing environment that influenced the formation and export of the particles.

Distance to the sea ice edge

Distance of the sea ice edge (defined at 15% sea ice concentration) to the mooring site at the central HAUSGARTEN station (HGIV) was determined from remote sensing data. Satellite images of daily sea ice measurements were obtained from NSIDC/NOAA (http://nsidc.org/data/nsidc-0051). The images were generated using the NASA Team algorithm (Cavalieri, 2003) and mapped to a 25x25 km grid. This satellite data set was derived from brightness and temperature data generated from Scanning Multichannel Microwave Radiometer and Sensor Microwave Imager and Sounder equipped on the Nimbus-7 satellite and the Defense Meteorological Satellite Program, respectively. Distances to the sea ice edge were averaged for the opening time of the sample cups on the sediment traps and calculated with a 4-day lag.

DNA extraction and Illumina amplicon sequencing

DNA analyses were done with splits of the original sediment trap sample. Samples were sequentially filtered through 10, 3 and 0.2 µm polycarbonate membrane filters (Millipore, Schwalbach, Germany). DNA extraction was carried out using the NucleoSpin Plant Kit II (Machery-Nagel, Germany) following the manufacturer's protocol. The DNA concentration was determined using the Quantus Fluorometer (Promega, United States). DNA extracts from the different fractions were pooled and amplified with a REPLI-g Mini Kit (Qiagen, Hilden, Germany) according to the manufacturer's protocol. Samples were stored at -20 °C. The successful DNA isolation and amplification from mercury chloride-preserved sinking particle samples has been demonstrated previously (Metfies et al., 2017; Liu et al., 2020; Onda et al., 2020; Wietz et al., 2022).

16S and 18S rRNA amplicon sequencing

Library preparations were performed according to the standard instructions of the 16S Metagenomic Sequencing Library Preparation protocol (Illumina, Inc., San Diego, CA, United States). The hypervariable V3–V4 region of the bacterial 16S rRNA gene was amplified using bacterial primers S-D-Bact-0341-b-S-17 (5'-CCT ACG GGN GGC WGC AG-3') and S-D-Bact-0785-a-A-21 (5'-GAC TAC HVG GGT ATC TAA TCC-3' (Klindworth et al., 2013). For microbial eukaryotes, the hypervariable V4 region of the 18S rDNA gene was amplified with the primer set 528iF (5'-GCG GTA ATT CCA GCT CC-3') (Elwood et al., 1985) and 964iR (5'-AC TTT

CGT TCT TGA TYR R-3′ (Onda et al., 2020). Sequencing was performed on the Illumina MiSeq platform in 2 × 300 bp paired-end runs (at CeBiTec, Bielefeld, Germany for bacteria, and at AWI, Bremerhaven, Germany for eukaryotes). Paired-end, primer-trimmed reads were deposited in the European Nucleotide Archive (ENA) at EMBL-EBI (Harrison et al., 2021), under accession numbers PRJEB43086 and PRJEB43576 for bacterial and eukaryotic data, respectively. Data were archived using the brokerage service of the German Federation for Biological Data (GFBio) (Diepenbroek et al., 2014), in compliance with the Minimal Information about any (X) Sequence (MIxS) standard (Yilmaz et al., 2011).

Bioinformatics and statistical analyses

Bacterial and eukaryotic libraries followed similar pipelines. Cutadapt was used to remove primer sequences from paired-end reads (Martin, 2011). The trimmed libraries were further processed using the package "DADA2" v. 1.14.1 (Callahan et al., 2016) in R v. 3.6.1 3 (http://www.Rproject.org/). DADA2 was used to differentiate amplicon sequence variants (ASVs) for both datasets, following the suggested workflow (https://benjjneb.github.io/dada2/tutorial.html). Briefly, after quality trimming and filtering of reads, dereplication was used to identify unique sequences and determine their abundance. The output of the dereplication and the error model were fed into the subsequent denoising step to resolve ASVs of up to one nucleotide difference using the quality score distribution in a probability model. Chimeras and singletons were then filtered out from the dataset. The Silva reference database release 138 was used to assign taxonomy to the bacterial dataset (Quast et al., 2013), and PR v. 4.12.0 for the eukaryotic dataset (Guillou et al., 2013). ASVs unclassified in the highest taxonomic rank were removed, as were ASVs classified as *Mitochondria*, *Chloroplast* and *Craniata*. The final dataset consisted of 2,069,920 sequences; 672,992 18S rRNA sequences, and 1,396,928 16S rRNA sequences, from which 1,122 eukaryotic and 3,398 bacterial unique amplicon sequence variants (ASVs) were identified. Rarefaction curves showed that the sequencing efforts applied were sufficient to describe the majority of the eukaryotic and bacterial diversity (Figure S10).

Statistical analyses and calculations in this study were performed using the R-package "phyloseq" v. 1.36.0 (McMurdie and Holmes, 2013). Alpha-diversity measurements and

rarefaction curves were obtained using the R-packages "phyloseq" and "iNEXT" v. 2.0.20 (Hsieh et al., 2016). Beta-diversity, statistical analyses and clr-transformation of the ASV matrix were done using the "vegan" package v. 2.5-7 (Oksanen et al., 2013), and "tidyverse" v. 1.3.1 (Wickham et al., 2019). The ASVs fold-change between seasons were calculated using the R-package "DEseq2" v. 1.32.0 (Love et al., 2014).

We performed a Weighted gene correlation network analysis (WGCNA) using the R-package v. 1.70.3 (Langfelder and Horvath, 2008) to identify clusters of microbial ASVs by sorting ASV into modules and correlating them with environmental variables (Guidi et al., 2016). Briefly, an ASV matrix was Hellinger-transformed and fed into a network topology analysis function, a signed network was used to preserve positively and negatively correlated nodes. Then, the adjacency matrix was used to create a topological overlap matrix (TOM). For this, adjacencies were calculated using the soft thresholding power of 14 for the eukaryotic data set and 8 for the bacterial data set. Module identification using dynamic tree cut was applied to the final selection of the modules (ME). The first principal component of each module ME (i.e., eigenvalue) was Pearson-correlated with each environmental variable. The minimum size of the ME was 35 for bacteria and 20 for eukaryotes to have a balanced number of ASVs per module. Variables were: SST, Chlorophyll a and sea ice cover from the backward Lagrangian particle tracking model, distance to the sea ice edge, daylight hours, biogenic fluxes (POC, PbSi and $CaCO_3$) and total swimmer flux measured from sediment trap samples (Ramondenc et al., 2022) as a representation of zooplankton occurrence in the water column, and modeled water regime proportions (unstratified, ML, MW regimes as proportions).

Results

Oceanographic setting: general trends of sea ice, chlorophyll *a* concentration, temperature and identification of water stratification regimes from 2000 to 2012

The location investigated here in the eastern Fram Strait is often influenced by the highly productive marginal ice zone (Soltwedel et al., 2016; Figure 1). At the time of the spring and summer HPF events, sea ice coverage remained on average below 2% (range: 0 – 17%).

Higher sea ice coverage was observed in spring (3%) compared to summer (1%) (Table 1, Figure S1). Sea ice coverage displayed great interannual variability, i.e. was lower during the WWA period (0 – 3%) and increased after 2007 (0.3 – 17%). Distances to the sea ice edge varied from 4 km to 116 km. Coinciding with higher sea ice cover in the catchment area, distances to the sea ice edge were shorter (average 38 km) towards the end and after the WWA (2007 – 2011), while they were generally higher during the summer events (average 56 km). SST varied according to seasonality, with warmer values (2 – 4.8°C) in the summer, and colder (0.6 – 1.5°C) during the spring events. Increases in temperature above 1.4°C were recorded during the spring period at the time of the WWA. Chlorophyll values ranged from 0 – 0.56 µg L^{-1} throughout the time-series. Daylight hours varied between 9 h and 24 h (average 20 h) only two spring samples were below 15 h of daylight in 2001 and 2005 (8 and 10 h of daylight, respectively).

The substantial interannual differences in sea ice presence in the catchment area affect the hydrography and lead to different water stratification regimes that were modelled for the region. The water column in the pre-WWA and post-WWA years, when the sea ice cover was higher, was mostly characterized by the MW regime (average: 73% and 51% respectively) (Table 1; Figure S2). In contrast, the period of the WWA was characterized by weaker stratification and rather qualified as ML regime. Unstratified waters were present in our data set early in spring (on average 41% in spring and <1% in summer events). Overall, 2000, 2005 and 2012 shared a higher proportion of unstratified water, but otherwise a combination of ML and MW regimes dominated spring from 2000 to 2012 (Figure S3). Towards the Arctic summer, HPF shared a higher proportion of MW (66%) over ML (33%).

Table 1. Overview of microbial samples collected from sediment trap samples, environmental parameters, water regimes and export fluxes measured from the sediment traps deployed at the central station of the HAUSGARTEN observatory. Ice cover (%), Chlorophyll *a* (Chl *a*; µg L^{-1}) and SST (°C) were obtained from remote sensing products and integrated over sediment trap catchment areas defined with a sinking velocity of 60 m d^{-1} and at 200 m depth (Wekerle et al., 2018). Distance to the ice edge was calculated from satellite images of daily sea ice measurements obtained from NSIDC/NOAA. The distance to the ice edge was defined at the position with at least 15% sea ice concentration. Environmental parameters and water regimes were averaged for the opening time of the sample cups (sampling days) of the sediment traps with a 4-day lag. WWA state grouped samples obtained from sediment traps deployed before (pre-WWA), during (WWA) and after (post-WWA) the warm water anomaly. The proportion of the water regimes (reg. (%)) are indicated per sample. Un: Unstratified.

PANGAEA Station ID	DNA sample	Sed. trap ID	Sample depth (m)	Water depth (m)	Collection period	Long. (°E)	Lat. (°N)	WWA state	SST (°C)	Chl *a* (µg L^{-1})	Ice cover (%)	Distance to the ice edge (km)	POC (mg m^{-2} d^{-1})	PON (mg m^{-2} d^{-1})	PbSi/C	C/N	PbSi (mg m^{-2} d^{-1})	$CaCO_3$ (mg m^{-2} d^{-1})	Total swimmer flux (Ind. m^{-2} d^{-1})	Un. Reg. (%)	Mixed layer reg. (%)	Melt water reg. (%)
PS57/273-1	summer 2000	FEVI 1	280	2549	2000-08-31 / 2000-09-15	4.35	79.03	Pre-WWA	3.68	0.03	0.03	74.20	26.07	3.42	0.61	8.89	37.30	10.07	75	0.00	0.12	0.88
PS57/273-1	spring 2001	FEVI 1	280	2549	2001-03-14 / 2001-03-29	4.35	79.03	Pre-WWA	1.02	0.00	0.95	33.19	9.13	1.11	0.02	9.60	0.32	2.76	71	0.38	0.40	0.22
PS59/101-1	summer 2001	FEVI 2	260	2549	2001-08-14 / 2001-08-31	4.36	79.03	Pre-WWA	3.57	0.01	0.51	40.91	17.73	1.15	0.02	17.99	0.64	16.81	99	0.00	0.15	0.85
PS66/129-1	summer 2004	FEVI 7	280	2584	2004-07-29 / 2004-08-05	4.34	79.02	Pre-WWA	3.72	0.00	1.05	43.80	49.37	7.10	0.30	8.12	35.13	44.88	184	0.00	0.55	0.45
PS66/129-1	spring 2005	FEVI 7	280	2584	2005-02-28 / 2005-03-31	4.34	79.02	WWA	1.48	0.00	0.17	55.54	7.61	0.70	0.02	12.66	0.29	15.31	19	0.73	0.25	0.02
PS68/263-1	summer 2005	FEVI 10	179	2582	2005-09-05 / 2005-09-25	4.34	79.02	WWA	3.28	0.11	0.64	67.17	15.90	1.96	0.05	9.45	1.97	7.47	230	0.10	0.48	0.43
PS68/263-1	spring 2006	FEVI 10	179	2582	2006-04-29 / 2006-05-14	4.34	79.02	WWA	1.44	0.12	1.66	55.35	13.48	1.77	0.04	8.88	1.38	4.85	38	0.07	0.61	0.32
PS68/263-1	summer 2006a	FEVI 10	179	2582	2006-06-13 / 2006-06-28	4.34	79.02	WWA	1.76	0.10	0.04	83.18	23.95	3.00	0.02	9.31	1.27	7.25	4	0.00	0.41	0.59
MSM2/787-1	summer 2006b	FEVI 13	230	2379	2006-09-15 / 2006-09-22	4.34	79.02	WWA	3.43	0.08	0.00	81.97	4.75	0.54	0.05	10.32	0.57	4.96	188	0.00	0.28	0.72
PS70/218-1	summer 2007	FEVI 16	190	2598	2007-08-15 / 2007-08-31	4.35	79.02	WWA	3.54	0.08	3.00	25.01	15.59	2.31	0.23	8.88	8.51	10.32	89	0.00	0.09	0.91
PS70/218-1	spring 2008	FEVI 16	190	2598	2008-03-31 / 2008-04-15	4.35	79.02	Post-WWA	1.27	0.02	0.59	35.09	23.49	3.77	0.01	7.86	0.48	8.39	36	0.75	0.16	0.09

PS72/155-1	summer 2008	FEVI 18	196	2343	2008-08-20 / 2008-08-31	4.33	79.01	Post-WWA	3.15	0.04	7.15	19.49	29.97	4.88	0.15	7.28	10.49	23.20	405	0.00	0.06	0.94
PS72/155-1	spring 2009a	FEVI 18	196	2343	2009-03-31 / 2009-04-15	4.33	79.01	Post-WWA	0.70	0.01	1.86	30.51	22.68	2.66	0.01	7.17	0.45	12.61	25	0.54	0.17	0.29
PS72/155-1	spring 2009b	FEVI 18	196	2343	2009-04-15 / 2009-04-30	4.33	79.01	Post-WWA	0.63	0.01	17.23	3.82	20.26	1.80	0.02	9.94	0.83	16.73	59	0.14	0.03	0.83
PS74/125-2	summer 2009a	FEVI 20	80	2605	2009-07-31 / 2009-08-10	4.33	79.01	Post-WWA	3.99	0.09	0.32	40.54	42.15	5.31	0.01	13.10	1.02	14.11	0	0.00	0.51	0.49
PS74/125-2	summer 2009b	FEVI 20	80	2605	2009-08-10 / 2009-08-20	4.33	79.01	Post-WWA	3.95	0.01	0.48	33.59	46.73	6.44	0.05	9.26	5.00	46.85	22	0.00	0.45	0.55
PS74/125-2	summer 2010	FEVI 20	80	2605	2010-06-15 / 2010-06-30	4.33	79.01	Post-WWA	2.45	0.56	2.25	41.42	29.26	3.43	0.01	8.47	0.52	9.06	88	0.00	0.43	0.57
PS76/147-1	spring 2011	FEVI 22	200	2603	2011-04-30 / 2011-05-10	4.33	79.01	Post-WWA	1.15	0.25	0.30	50.67	10.02	1.13	0.05	9.95	1.14	7.87	76	0.08	0.25	0.67
PS78/177-1	summer 2011	FEVI 24	200	2605	2011-08-31 / 2011-09-10	4.33	79.01	Post-WWA	4.84	0.04	0.00	115.52	17.38	3.13	0.08	10.38	3.37	95.26	569	0.00	0.45	0.55
PS78/177-1	spring 2012	FEVI 24	200	2605	2012-04-30 / 2012-05-10	4.33	79.01	Post-WWA	1.29	0.01	0.39	39.01	24.19	2.23	0.01	6.47	0.36	15.42	48	0.56	0.33	0.12

Export fluxes during HPF events

Usually two HPF events were observed per year, in spring and summer (Figure 2). Throughout the time-series, HPF events corresponded between 2.6% and 41.9% (average 25.5%) of the total POC flux per sampling period, defined as the total number of days the collecting cups were open of each deployed sediment trap (Table 2). HPF summer events were on average higher (average 26.57 mg m^{-2} d^{-1}, 4.75 – 49.37) than HPF spring events (average 16.36 mg m^{-2} d^{-1}, 7.61 – 24.19), but differences were not significant (ANOVA $p > 0.05$). HPF events did not show significant differences between the WWA categories (pre-WWA, WWA and post-WWA; ANOVA $p > 0.05$), due to the high interannual variation, and the few time points available for the WWA. However, during the WWA the HPF was substantially lower (average 13.55 mg m^{-2} d^{-1}, range 4.75 – 23.95) compared to pre-WWA (average 25.56 mg m^{-2} d^{-1}, range 9.13 – 49.37) and post-WWA values (average 26.61 mg m^{-2} d^{-1}, range 10.02 – 46.73).

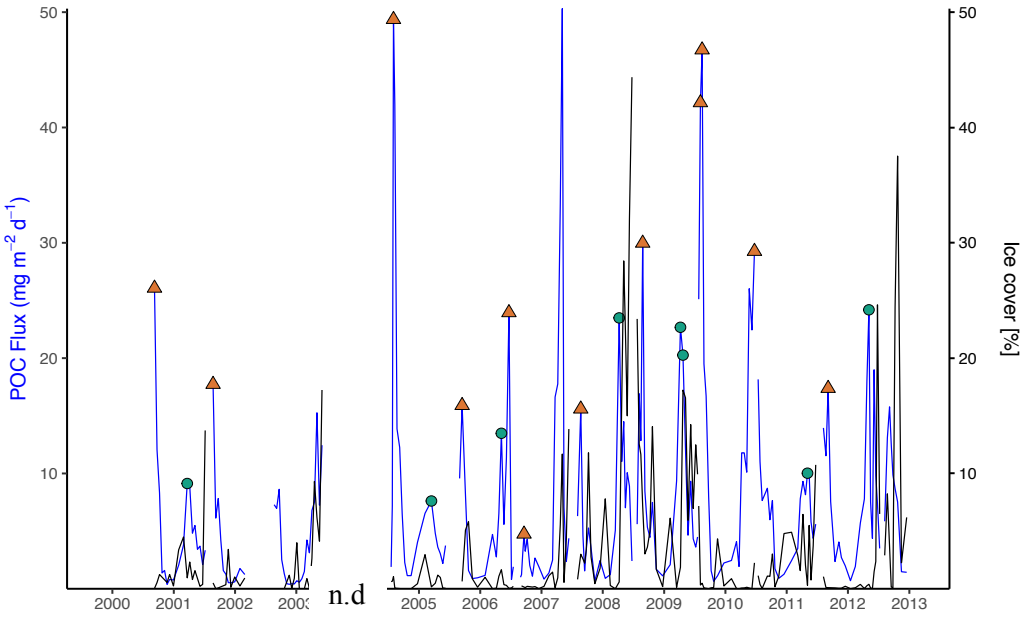

Figure 2. POC flux (mg m^{-2} d^{-1}) (blue), and ice cover (%) (black) in the catchment area of the sediment trap at the mooring location of the central station (HGIV) for the period from 2000 to 2012. The peak POC values selected for this study are noted by green circles for spring HPF events and orange triangles for summer HPF events. n.d; Data not available.

Trends in PON flux generally agreed with POC during the HPF (Figure S4). The summer-PON fluxes were higher (average 3.56 mg m^{-2} d^{-1}, 0.54 – 7.10) compared to spring-PON fluxes (average 1.90 mg m^{-2} d^{-1}, 0.70 – 3.77), but without significant differences (ANOVA $p > 0.05$). Like POC fluxes, PON fluxes did not show significant differences between the WWA

categories (ANOVA $p > 0.05$). During HPF events, C:N ratios were mostly similar throughout the time series, and close to Redfield with on average 8.8 in spring and 10.1 in summer (Table 1). The highest ratios (> 12) were observed in samples from August 2001, August 2009, and from March 2005; lowest ratios occurred in May 2012, April 2008, August 2008 and in April 2009.

Table 2. Total POC flux per sampling period and the contribution of the HPF to total POC. Total values were calculated based on the number of days the cups were open during deployment and therefore some values are higher than 365. SP: Sampling period. Note that the sampling period for 2000 started in 2000-08-31.

Sampling period	Total sampling days (n)	POC flux (g SP^{-1})	% of HPF to sampling period
2000/2001	317	1.73	30.56
2001/2002	212	0.84	36.02
2002/2003	300	1.08	-
2004/2005	335	2.59	41.87
2005/2006	330	2.25	39.43
2006/2007	298	1.29	2.57
2007/2008	344	2.32	26.97
2008/2009	370	3.46	28.8
2009/2010	345	5.15	26.76
2010/2011	355	2.45	4.09
2011/2012	349	2.99	17.90

PbSi and $CaCO_3$ fluxes displayed high interannual variability. Peaks in PbSi fluxes are mostly observed in late summer and in autumn, and $CaCO_3$ fluxes are higher in winter and autumn, thus the spring and summer HPF usually did not match with highest PbSi and $CaCO_3$ flux events (Bauerfeind et al., 2014) (Figure S4). PbSi:C ratios were on average 0.02 in spring, and 0.13 in summer (Table 1). Like POC fluxes, PbSi fluxes were significantly lower during the WWA (Post-hoc Wilcoxon, p-adjust < 0.01). PbSi fluxes were much higher in earlier years (average 18.35 mg $m^{-2}d^{-1}$, 0.32 – 37.30), compared to the period of the WWA (2.33 mg m^{-2} d^{-1}, 0.29 – 8.51); PbSi fluxes slightly increased again after that, but remained low for the post-WWA period (2.37 mg m^{-2} d^{-1}, 0.36 –10.49). PbSi fluxes measured during HPF events corresponded in summer to 21% of the annual PbSi fluxes, and in spring 3.6% of the annual PbSi fluxes. $CaCO_3$ fluxes measured during summer HPF events corresponded to 13% of the

annual $CaCO_3$ fluxes compared to 6% in spring. $CaCO_3$ fluxes were significantly higher in the post-WWA period (Post-hoc Wilcoxon, *p*-adjust < 0.01).

Microbial composition of sinking particles during HPF events

Eukaryotic community

The eukaryotic microbiome of sinking particles during HPF events was dominated by diatoms (*Bacillariophyta*), dinoflagellates (*Syndiniales*), and radiolarians (*Acantharea)*, together they comprised 59% of the eukaryotic sequences. *Bacillariophyta* were mainly comprised of the common Arctic diatom genera *Chaetoceros*, *Thalassiosira* and *Melosira. Syndiniales* were dominated by members of the orders *Dino-Group-I*, and *Dino-Group-II* that represented 20% of the eukaryotic ASVs. *Acantharea* were strongly dominated by ASVs of the order *Chaunacanthida*. Metazoans comprised 5% of the total ASVs. The division *Metazoa* was strongly dominated by sequences of copepod taxa, mainly *Calanus, Neocalanus* and *Metridia*.

In a hierarchical clustering based on Bray-Curtis dissimilarity (Figure 3A), the eukaryotic community clustered into 3 main groups. The first cluster grouped samples from the summer events and contained a high proportion of heterotrophic and mixotrophic eukaryotes of the classes *Acantharea, Dinophyceae* and *Syndiniales* dominating during this time (Figure 3B). The second cluster comprised mainly samples from the WWA period (Table 1), and was characterized by an increased proportion of heterotrophic pico- and nano-plankton taxa such as MAST-9, MAST-1, and other protists like the heterotrophic *Filosa-Thecofilosea* and *Telonemia*. ASVs affiliated with diatoms decreased and the dominant *Chaetoceros* was absent in the second cluster (0 clr-transformed ASVs in WWA samples, compared to 14 – 21 in pre-WWA and 10 – 20 post-WWA samples). Moreover, the second cluster was also characterized by an increase of the coccolithophore *Gephyrocapsa* and the increase of flagellate ASVs assigned to *Phaeocystis* and *Prymnesium* towards the end of the WWA period (Figure 4). The third cluster corresponded to samples from spring events, all from the post-WWA period, except for one sample (September 2000) (Figure 3A). Samples from the third cluster showed a higher representation of autotrophic groups such as *Prymnesiophyceae* (*Haptophyta*) including the flagellates *Phaeocystis, Chrysochromulina* and *Prymnesium* and a

few members of the *Chlorophyta*, mainly *Mamiellophyceae.* These samples were also marked by an increase of zooplankton taxa, especially copepods (*Calanus*) which comprised a significant proportion of the community, as well as fungi sequences affiliated with *Ascomycota*. Diatom sequences in the third cluster were mainly represented by *Chaetoceros* (Figure 4).

A transition in the dominance of diatom ASVs was linked to the WWA. From 2004 to 2006 *Thalassiosira* clr-transformed ASV counts increased from 3 to 11 (peaked in 2005) and dominated diatom sequences only during this period. *Thalassiosira* was also the most dominant diatom in early samples with low light (8 – 11 h) in March 2001 and 2005 (0.6 and 11 clr-transformed ASV counts respectively) (Figure 4). Towards the peak of the WWA in 2006 all diatoms sequences were substantially decreased and only *Melosira* showed a peak in September 2006 with 17 clr-transformed ASVs (compared to the average 15 counts of *Chaetoceros* in the data set). Moreover, in 2006 the fungi classes *Basidiomycota* and *Chytridiomycota* significantly increased, concomitant with the sharp decrease of diatom sequences (Figure S9).

Bacterial community

The bacterial communities were strongly dominated by typical phytoplankton-associated bacteria, mainly the classes *Gammaproteobacteria*, *Bacteroidia*, *Alphaproteobacteria* and *Verrucomicrobiae* (Figure 3B). Thirty percent of the bacterial ASVs were classified as *Gammaproteobacteria* mainly of the orders *Cellvibrionales* and *Alteromonadales*. *Bacteroidales* was dominated by the diatom-associated order *Flavobacteriales*, which represented 13% of the bacterial ASVs. Zooplankton-associated taxa of the order *Entomoplasmatales* (class *Bacilli*), the majority assigned to *Candidatus* Hepatoplasma, comprised 14% of the total community and strongly dominated samples of the spring events and only after the WWA period.

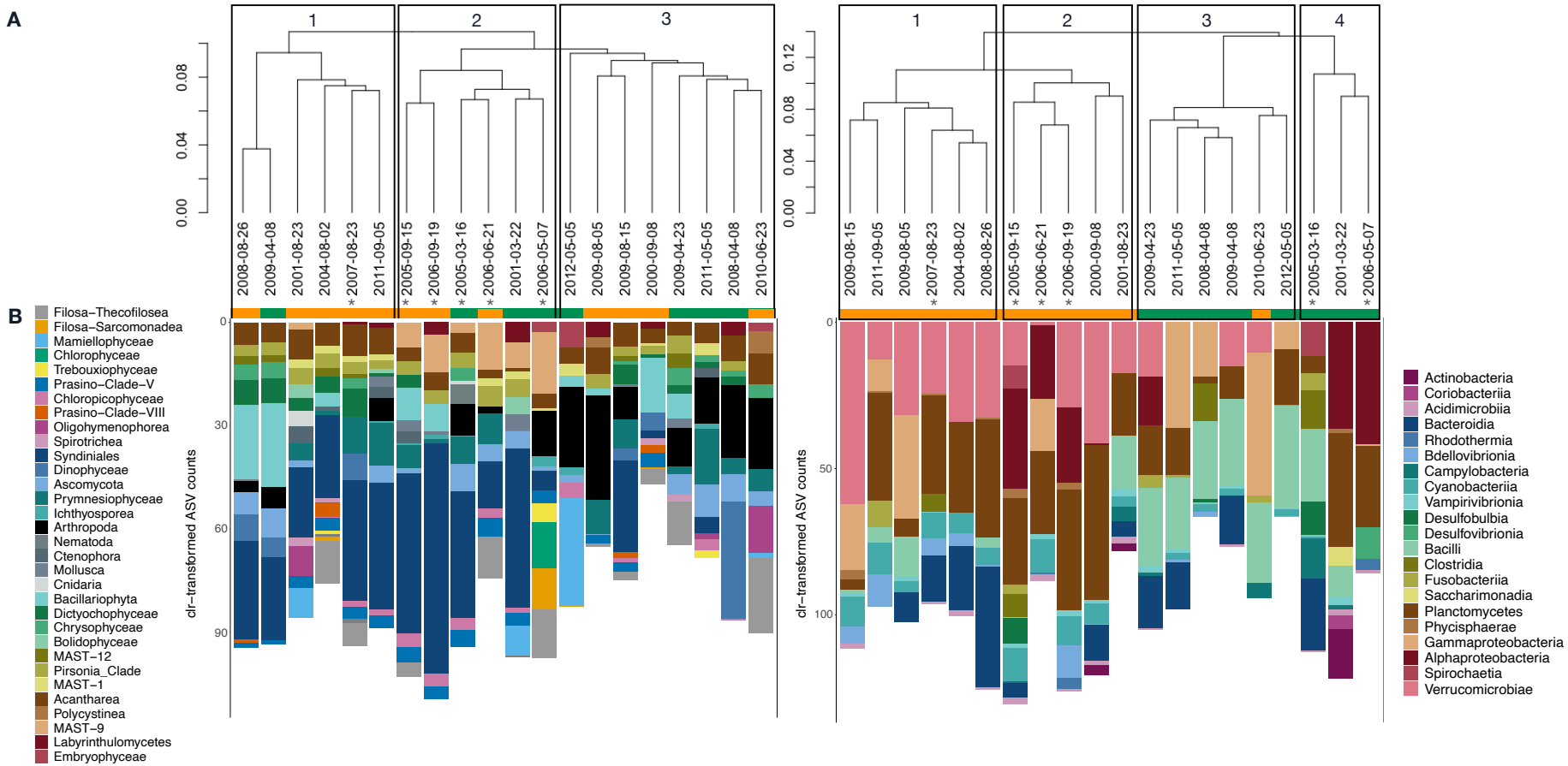

Figure 3. A) Beta diversity of eukaryotic (left) and bacterial (right) communities based on hierarchical clustering using Bray-Curtis dissimilarity and B) community composition on class level based on clr-transformed ASV sequence counts. The displayed positive clr values indicate the enrichment of the corresponding class. The asterisk (*) indicates samples corresponding to the warm water anomaly (WWA) 2005-2007. The color bars below the hierarchical clusters indicate the sampling period: spring (March to May) in green color and summer (June to September) in orange.

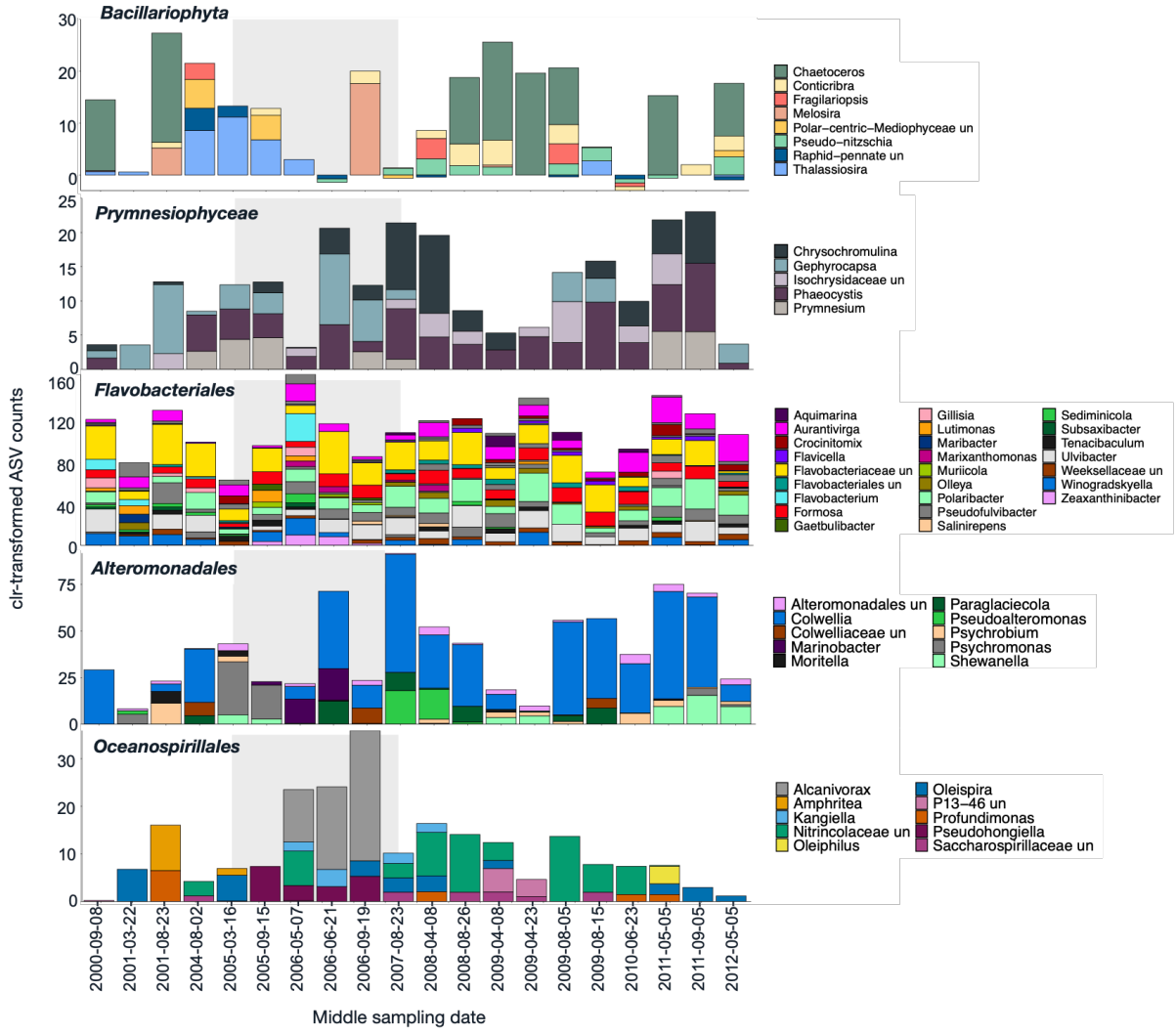

Figure 4. Main changes in selected groups of eukaryotes (diatoms and flagellates) and main bacterial orders based on clr-transformed ASV counts. Dates correspond to the middle date of the sampling period. The light gray area in the background panels behind the bars indicates the WWA period from 2005 to 2007.

The bacterial community clustered into 4 groups based on beta diversity assessment (Figure 3A). In the first and second cluster, the majority of the samples consisted of summer events and contained a higher representation of *Verrucomicrobiae* and *Planctomycetes*, whereas the third and fourth cluster grouped samples of the spring events. The third cluster was characterized by a strong presence of *Gammaproteobacteria* and *Bacilli* (Figure 3B). Bacterial communities of the WWA clustered in two branches, unlike the eukaryotic community, i.e. the second and fourth cluster, except for one sample from August 2007. The fourth cluster did not contain *Verrucomicrobiae* sequences, and unlike other spring samples cluster 4 was also characterized by a notable decrease in the number of *Bacilli* sequences (Figure 3B).

Seasonality (early vs. late export events)

Microbial communities showed a strong seasonal separation of samples particularly in the bacterial cluster (Figure 3A). To further explore the seasonality of the microbial composition of the sinking particles, we grouped samples by spring and summer and identified the respective core communities. We defined core taxonomic groups as those present in all samples of one season, and with sequence abundances >0.5% of the eukaryotic seasonal data set, and >1.5% for the bacterial data (Table 3 & S2). The great majority of the core ASVs belonged to the most abundant orders in the dataset. In total, 7 eukaryotic and 14 bacterial core ASVs were found to be present across the datasets.

Seasonality of eukaryotic communities

In spring events, the core eukaryotic ASVs comprised 44% of the total eukaryotic community, and in the summer events the core ASVs were 42% of the total community (Table 3). The spring core community was dominated by an ASV of the order *Dino-Group-I* (8.5%) with a similar sequence abundance in the summer (7.8%), followed by the copepod *Calanus* (6%) and an unclassified ASV of the radiolarian class *Chaunacanthida* (4%) consistent with the early stages of the phytoplankton bloom. The stronger presence of *Chaunacanthida* and *Chaetoceros* was observed in summer events. *Chaunacanthida* dominated 27% of the summer sequences. *Chaetoceros* made up 4% of the community in spring, and 13% in the summer. The flagellate *Phaeocystis* and the chlorophyte *Micromonas* were also part of the summer core community.

Seasonality of bacterial communities

Based on beta diversity assessments discussed in section 3.3.2, bacterial communities showed a stronger separation between spring and summer events compared to eukaryotic communities. The proportion of the bacterial microbiome represented by the core bacterial ASVs was substantially higher in the summer events (40%) than in the spring events (25%). The spring events were dominated by two *Candidatus* Hepatoplasma ASVs and one *Mycoplasma*. ASV and together made up 38% of the spring community (Table 3). *Candidatus* Hepatoplasma ASVs were also part of the core community in summer events (7%), highlighting the prominence of this taxonomic group in the sinking particles.

Overall, the proportions of *Flavobacteriales*, *Gammaproteobacteria* and *Verrucomicrobiales* core ASVs were higher in summer (Table 3 & S2). *Flavobacteriales* core ASVs comprised 11% of spring communities and 21% of summer communities. *Flavobacteriales* summer core ASVs were dominated by *Formosa* (6.3%). *Luteolibacter* ASVs (*Verrucomicrobiales*) and ASVs of the *Gammaproteobacteria* clade *OM60(NOR5)*, together comprised 13% of the sequences. Core ASVs of *Formosa, Luteolibacter* and an ASV of the *OM60(NOR5)* clade showed a twofold increase in summer events (Figure S5). Moreover, summer events had a higher number of ASVs associated with phytoplankton, which included *Flavobacteriales* ASVs, *Verrucomicrobiales* ASVs and *Cellvibrionales* (Figure 3, Table 3).

Microbial connectivity in sinking particles

Overall changes in bacterial community structure were significantly correlated with changes in the eukaryotic community (Mantel test r=0.38, p=0.001). However, bacterial communities showed also additional beta diversity clustering patterns, and a high sensitivity for seasonal change (Figure 3). To address potential associations between bacteria and eukaryotes in the sinking particles, co-occurrence networks were constructed from families of the three identified eukaryotic clusters based on the assumption that the eukaryotes are the main particle formers. In all three networks, the proportion of positive associations was higher (56% – 58%) than negative associations (42% – 44%), both positive and negative proportions varied little between the three networks. Overall, the networks of the first, second and third cluster consisted of 531, 487, and 420 nodes of bacterial and eukaryotic ASVs, respectively.

Table 3. Most abundant core sequences in the 16S and 18S assemblages in sinking particles in spring (March to May) and summer (June to September) from 2000 to 2012. Core community is defined as those present in all samples for each corresponding event. Total number of bacterial sequences in the spring = 587590 and in the summer = 809338. Total number of eukaryotic sequences in the spring = 165648 and in the summer = 507344. Only ASVs with more than 0.5% sequence abundance in the eukaryotic data set and more than 2.5% in the bacterial data set were included in this table.

ASV	Absolute sequence abundance in the season	% sequence abundance in the season	Absolute sequence abundance in data set	% sequence abundance in data set	Eukaryotic taxonomic classification				
					Supergroup & Division	Class	Order	Family	Genus
Spring events									
sq4	14063	8.5	53457	7.9	*Alveolata; Dinoflagellata*	*Syndiniales*	*Dino-Group-I*	*Dino-Group-I-Clade-1*	*Dino-Group-I-Clade-1 un*
sq8	9932	6	12983	1.9	*Opisthokonta; Metazoa*	*Arthropoda*	*Crustacea*	*Maxillopoda*	*Calanus*
sq1	6854	4.1	144013	21.4	*Rhizaria; Radiolaria*	*Acantharea*	*Chaunacanthida*	*Chaunacanthida un*	*Chaunacanthida un*
sq2	6076	3.7	72884	10.8	*Stramenopiles; Ochrophyta*	*Bacillariophyta*	*Bacillariophyta un*	*Polar-centric-Mediophyceae*	*Chaetoceros*
sq9	5579	3.4	10333	1.5	*Archaeplastida; Chlorophyta*	*Mamiellophyceae*	*Mamiellales*	*Mamiellaceae*	*Micromonas*
sq21	2645	1.6	3791	0.6	*Opisthokonta; Fungi*	*Ascomycota*	*Pezizomycotina*	*Sordariomycetes*	*Simplicillium*
Summer events									
sq1	137159	27	144013	21.4	*Rhizaria; Radiolaria*	*Acantharea*	*Chaunacanthida*	*Chaunacanthida un*	*Chaunacanthida un*
sq2	66808	13.2	72884	10.8	*Stramenopiles; Ochrophyta*	*Bacillariophyta*	*Bacillariophyta un*	*Polar-centric-Mediophyceae*	*Chaetoceros*
sq4	39394	7.8	53457	7.9	*Alveolata; Dinoflagellata*	*Syndiniales*	*Dino-Group-I*	*Dino-Group-I-Clade-1*	*Dino-Group-I-Clade-1 un*
sq9	4754	0.9	10333	1.5	*Archaeplastida; Chlorophyta*	*Mamiellophyceae*	*Mamiellales*	*Mamiellaceae*	*Micromonas*
sq28	2402	0.5	3442	0.5	*Hacrobia; Haptophyta*	*Prymnesiophyceae*	*Phaeocystales*	*Phaeocystaceae*	*Phaeocystis*
ASV	Absolute sequence abundance in the season	% sequence abundance in the season	Absolute sequence abundance in data set	% sequence abundance in data set	Bacterial taxonomic classification				
					Phylum	Class	Order	Family	Genus
Spring events									

sq1	126890	21.6	151327	10.8	*Firmicutes*	*Bacilli*	*Entomoplasmatales*	*Entomoplasmatales Incertae Sedis*	*Candidatus Hepatoplasma*
sq2	70607	12	105311	7.5	*Firmicutes*	*Bacilli*	*Entomoplasmatales*	*Entomoplasmatales Incertae Sedis*	*Candidatus Hepatoplasma*
sq9	26406	4.5	28445	2	*Firmicutes*	*Bacilli*	*Mycoplasmatales*	*Mycoplasmataceae*	*Mycoplasma*
sq8	16901	2.9	30471	2.2	*Bacteroidota*	*Bacteroidia*	*Flavobacteriales*	*Flavobacteriaceae*	*Polaribacter*
sq14	14909	2.5	21483	1.5	*Bacteroidota*	*Bacteroidia*	*Flavobacteriales*	*Flavobacteriaceae*	*Aurantivirga*
Summer events									
sq4	50727	6.3	52368	3.8	*Bacteroidota*	*Bacteroidia*	*Flavobacteriales*	*Flavobacteriaceae*	*Formosa*
sq3	48319	6	55070	3.9	*Verrucomicrobiota*	*Verrucomicrobiae*	*Verrucomicrobiales*	*Rubritaleaceae*	*Luteolibacter*
sq2	34704	4.3	105311	7.5	*Firmicutes*	*Bacilli*	*Entomoplasmatales*	*Entomoplasmatales Incertae Sedis*	*Candidatus Hepatoplasma*
sq5	32526	4	34463	2.5	*Proteobacteria*	*Gammaproteobacteria*	*Cellvibrionales*	*Halieaceae*	*OM60(NOR5) clade*
sq1	24437	3	151327	10.8	*Firmicutes*	*Bacilli*	*Entomoplasmatales*	*Entomoplasmatales Incertae Sedis*	*Candidatus Hepatoplasma*
sq6	23202	2.9	31638	2.3	*Bacteroidota*	*Bacteroidia*	*Flavobacteriales*	*Flavobacteriaceae*	*Polaribacter*
sq13	20799	2.6	22131	1.6	*Verrucomicrobiota*	*Verrucomicrobiae*	*Verrucomicrobiales*	*Rubritaleaceae*	*Luteolibacter*

Based on co-occurrence, the highest number of potential associations between bacteria and eukaryotes in all three networks involved families of the bacterial orders *Alphaproteobacteria* and *Gammaproteobacteria* with alveolate families of the *Syndiniales* and *Dinophyceae*, and pico- and nano-plankton affiliated with marine stramenopiles (MAST) (Figure 3).

In the network of the first cluster, co-occurrences between *Syndiniales* and other eukaryotes like *Haptophyta* and *Stramenopiles* were substantial compared with the second and third cluster networks. After diatoms, *Syndiniales* were the second most dominant taxa comprising 14% of the eukaryotic sequences in the network. Of the *Syndiniales*, families of *Dino-Group-II* showed the highest number of potential associations with bacterial families, of *Gammaproteobacteria* and *Alphaproteobacteria* (Figure S6). MAST families co-occurred with other *Syndiniales*, and *Haptophyta*. Families of diatoms which made up 18% of the eukaryotic community of the first network, co-occurred diversely with *Fungi*, *Syndiniales*, *Chlorophyta* and few bacterial families including *Flavobacteriales,* which however contributed 25% of the sequences of bacterial sequences in the first network.

In the second cluster we identified co-occurrences between eukaryotic families and proteobacterial families. These were numerous, mainly between families of taxa that increased during the WWA (Figure S7), even though families of the *Flavobacteriales* comprised the majority of bacterial sequences in the second network (25% of the network community). For instance, a *Telonemia-Group-2* family co-occurred with 4 *Gammaproteobacteria* and *Alphaproteobacteria* families. Similarly, *Sandonidae* a family of the *Filosa-Sarcomonadea* co-occurred with 4 families of the *Gammaproteobacteria* and *Saccharimonadales.* Families of the orders MAST-9, MAST-1, and MAST-12 were not dominant members of the eukaryotic community of the network (< 5%), however they co-occurred with 22 *Proteobacteria* families of the *Gammaproteobacteria* and *Alphaproteobacteria* which increased during the WWA and included families of the *Oceanospirillales* (7% of the network community), *Alteromonadales* (9% of the network community) (e.g *Marinobacteraceae*), and *Micavibrionales*. The coccolithophore family *Noelaerhabdaceae* that includes *Gephyrocapsa* co-occurred with 5 bacterial families, and the flagellate families *Phaeocystaceae, Prymnesiaceae* and *Chrysochromulinaceae* showed co-occurrence with 15 bacterial families. The diatom families *Polar-centric-Mediophyceae* and

Radial-centric-basal-Coscinodiscophyceae were potentially associated with 8 bacterial families of the *Flavobacteriaceae, Oceanospirillales, Desulfocapsaceae, NB1-j* and *Micavibrionales.* Co-occurrence between *Proteobacteria* families were stronger and more numerous in the second cluster.

In the third cluster, only 4 potential associations between families of flagellates and bacteria families of *Gammaproteobacteria* and *Alphaproteobacteria* were observed (Figure S8). Families of the orders MAST-9, MAST-1 were associated with 13 bacterial families. Families of MAST affiliation co-occurred with other numerous eukaryotes, a feature observed in the constructed network of the first cluster, but not observed in the network of the second cluster. Notably, 40% of the eukaryotic sequences were assigned to metazoans. Six bacterial families of the *Gammaproteobacteria* (17% of the bacterial network community), including *Porticoccaceae* and *Burkholderiaceae* were associated with the copepod family *Maxillopoda* and a *Metazoan* family. Moreover, in the third cluster the *Chaetoceros* family *Polar-centric-Mediophyceae* which also comprised 23% of the eukaryotic community in the third network, potentially associated with the bacterial families *Pirellulaceae, Burkholderiaceae, Nitrincolaceae* and *Caulobacteraceae*.

Relationship between environmental parameters and microbial composition of sinking particles

The changes observed in the microbial composition of sinking particles suggest that the community reflected oceanographic variations in the eastern Fram Strait (Figure 3 & 4). To investigate decadal changes in the particle-associated microbial community associated with changing environmental conditions marked by the WWA, we performed a WGCNA, a method applied to study microbial communities and correlations with environmental traits e.g (Duran-Pinedo et al., 2011; Guidi et al., 2016; Wilson et al., 2018). In addition, we identified the main ASVs in each ME as candidate microbial indicators (Figures 5 & 6).

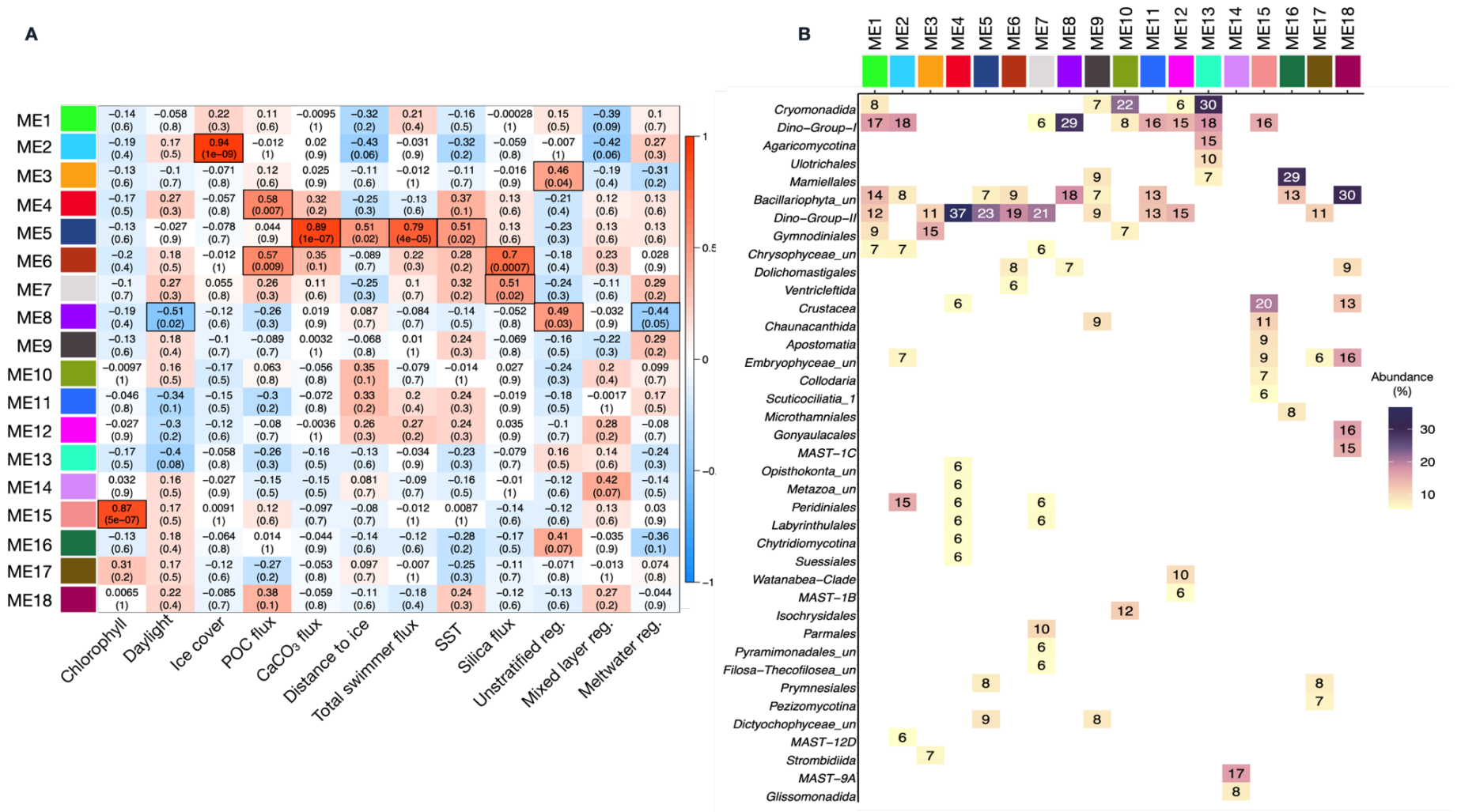

Figure 5. Weighted gene correlation network analysis WGCNA on eukaryotic communities (A) heatmap of Pearson's correlation between environmental parameters and eukaryotic module Eigengenes (ME), significant correlations are outlined with black boxes. (B) phylogenetic affiliation and relative abundance of different ASVs in each ME grouped at order level. Only ASVs with abundances higher than 5% were included in the plot.

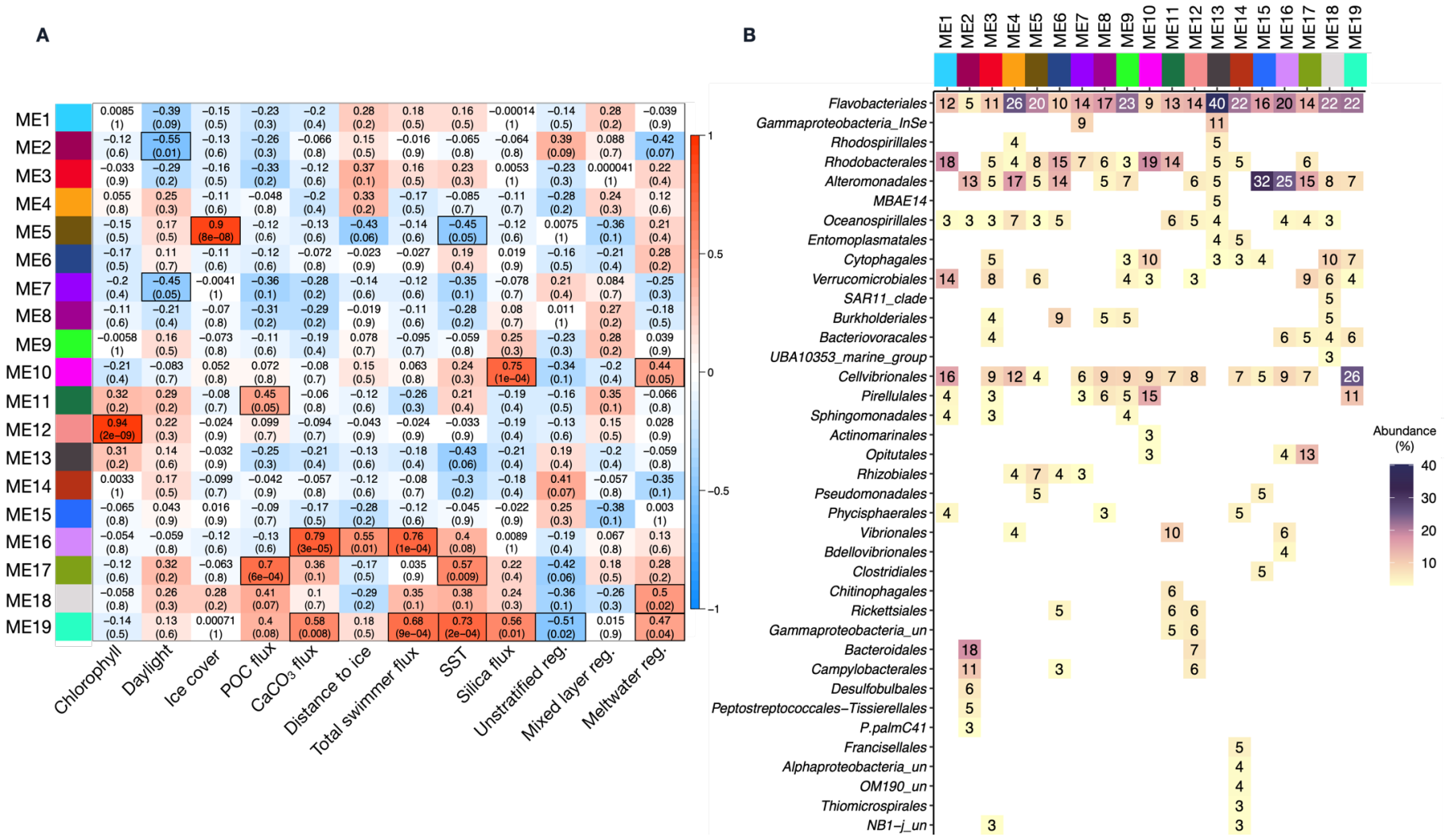

Figure 6. Weighted gene correlation network analysis WGCNA on bacterial communities (A) heatmap of Pearson's correlation between environmental parameters and bacterial module Eigengenes (ME), significant correlations are outlined with black boxes. (B) phylogenetic affiliation and abundance of different ASVs in each ME grouped at order level. Only ASVs which abundances higher than 3% were included in the plot.

Eukaryotic community

Eight eukaryotic MEs correlated with environmental variables (Figure 5, Table 1). Two modules ME2 and ME5 correlated with the changing ice cover and distance to the ice edge. ME2 displayed a strong positive correlation with ice cover (Pearson's correlation; r=0.94, p-value<0.01). ME2 was comprised mostly of ASVs of *Dino-Group-I* (18%), the dinoflagellate *Heterocapsa* (15%), and ASVs of diatoms mainly *Chaetoceros* (8%) coinciding with the strong presence of ice cover before and after the WWA (Figure 5). ME5 correlated positively with distance to the sea ice, SST, $CaCO_3$ flux and swimmer flux (Pearson's correlation; r>0.51, p-value<0.02). ME5 was dominated mainly by summer taxa (Table 3), ASVs of the order *Dino-Group-II* (23%), and small flagellates including *Dictyochophyceae* (9%) and *Prymnesiales* assigned to *Chrysochromulina* (8%).

ME3 and ME8 correlated positively with the unstratified water regime characteristic of the spring (Pearson's correlation; r>0.4, p-value<0.05) (Figure S3A). ME3 had the largest proportion of mixotrophs and heterotrophs, particularly dinoflagellate ASVs affiliated with *Gymnodinium* (15%), and the orders *Dino-Group-II* (11%), and *Strombidiida* (7%). ME8 correlated negatively with daylight and the MW regime. ME8 was comprised mostly of ASVs of *Dino-Group-I* (29%) and *Thalassiosira* (18%). With the exception of one sample in summer 2009, sequences of *Thalassiosira* were only detected in 2004, 2005 and 2006 towards the WWA, which was also characterized by a smaller proportion of the MW regime (Figure S3B).

Bacterial community

Ten bacterial MEs correlated strongly with environmental variables (Figure 6, Table 1). The order *Flavobacteriales* dominated in the majority of the modules, followed by *Alteromonadales* and *Rhodobacterales*.

ME5 was the only module that correlated strongly and positively with ice cover (Pearson's correlation; r=0.9, p-value<0.01), and negatively with SST (Pearson's correlation; r=-0.45, p-value=0.05). *Flavobacteriales* dominated 20% of the ME5 including *Ulvibacter*, *Polaribacter*, *Winogradskyella* and *Maribacter* followed by unassigned ASVs of the *Rhodobacteraceae*

family that increased only in pre-WWA (8%), and *Methylobacterium-Methylorubrum* (*Rhizobiales*) a species only detected in post-WWA samples.

ME2 and ME7 showed negative correlations with daylight (Pearson's correlation; $r<-0.45$, p-value<0.01). ME2 was the only module with a high proportion of members of the *Marinifilaceae* family (18%) (*Bacteroidales*) which were only present in samples with less than 11 h of daylight in March of 2005 and 2001, followed by *Psychromonas* and *Moritella* (*Alteromonadales*) also identified in 2001 and 2005 (Figure 4). The main ASVs of ME2 coincided with the presence of diatoms *Thalassiosira* and the absence of *Chaetoceros* in March 2001 and 2005. ME7 contained a large number of *Flavobacteriaceae* (14%) which also showed potential associations with *Thalassiosira* and *Melosira* genera based on co-occurrence network analysis (Figure S7).

ME19 correlated positively with the MW regime (Pearson's correlation; $r>0.4$, p-value<0.05). ME19 was strongly dominated by ASVs enriched in summer events (Figure S5), and included *Cellvibrionales* (26%), and the clades *OM60(NOR5)* and *BD1-7*. In addition to the proportion of MW regime, ME19 correlated positively with $CaCO_3$ flux, swimmer flux, SST and PbSi flux and negatively with unstratified water. Similarly, ME16, mainly composed of *Alteromonadales* (25%) and *Flavobacteriales* (20%), correlated positively with $CaCO_3$ flux, swimmer flux and distance to the sea ice (Pearson's correlation; $r>0.55$, p-value<0.01), variables that followed a substantial increase in summer after the WWA (Table 1; Figures S1 S4).

Discussion

The composition, quantity and interannual variation of sinking particulate matter has been studied at the central HAUSGARTEN station (HGIV) in Fram Strait since 2000 (Soltwedel et al., 2016). The temporal variability of export fluxes has been characterized for the majority of the sampling period, providing a long-term record of biogenic material export and its causes and consequences as well as its key agents (Bauerfeind et al., 2009; Lalande et al., 2011, 2013, 2016; Nöthig et al., 2020). In this study, we tested the hypothesis, that the microbial

community of primary producers and heterotrophs are sensitive to interannual changes in the ecosystem state. To investigate this, we studied the seasonality and interannual variation of microbial communities and their associations at times of highest organic carbon export (i.e. spring and summer) in the eastern Fram Strait from 2000 to 2012.

Early and late POC flux events reflect seasonal changes

Sea ice coverage reached its maximum in the sediment trap catchment area usually towards the end of the summer, matching the higher contribution of MW regime originating from sea ice melt in summer events. Strong stratification during ice melting has been observed during summer conditions in the central Arctic Ocean and the Fram Strait (Peralta-Ferriz and Woodgate, 2015; von Appen et al., 2021), whereas spring events were mainly characterized by first light meeting a ML regime or weakly stratified water column. Although the meltwater-induced stratification could trigger primary production already in spring (Figure S3), higher sea ice coverage and the resulting MW regime that dominated in summer aided the development and export of diatom blooms over the catchment area of the sediment traps characteristic of the pre- and post-WWA years (Lalande et al., 2007, 2013). Thus, PbSi fluxes were higher during summer, indicating the important role of diatoms in the peak POC fluxes.

The eukaryotic spring core community saw a strong dominance of heterotrophic representatives (ASVs of *Dino-Group-I* and *Calanus*) highlighting the relevance of heterotrophic protists in the contribution to POC export (Fontanez et al., 2015; Guidi et al., 2016; Boeuf et al., 2019). Moreover, putative parasite-host relationships between *Chaetoceros* and *Syndiniales* have been previously observed in polar regions (Cleary and Durbin, 2016; Clarke et al., 2019), and indicate an indirect contribution of *Syndiniales* (e.g. *Dino-Group-II*) to POC flux through parasitism and the constitution and transformation of the sinking particles. Core ASV of the copepod *Calanus* also dominated in spring and comprised a considerable fraction of the eukaryotic sequences in sinking particles. Zooplankton in Fram Strait is expected to profit from the onset of the phytoplankton bloom already in spring (Falk-Petersen et al., 2002; Cleary et al., 2017). In addition to copepods, amphipods and chaetognaths were expected to increase in abundance in spring (Ramondenc et al., 2022).

However, amphipods and chaetognaths were absent in our dataset. It is likely that the primer set used in this study does not resolve metazoan 18S rRNA gene sequences well.

An ASV assigned to *Micromonas* comprised 3.4% of the spring core community, 4-fold higher than in the core summer community. Previous studies showed that the picoeukaryote *Micromonas* can be exported to deeper water via sinking particles although the explicit mechanisms of export remain unclear (Bachy et al., 2022). *Micromonas* did not exhibit significant interannual variability and was not particularly abundant in our dataset, however we detected sequences of *Micromonas* in all samples likely packed into fecal pellets. Our findings support previous statements on the relevance of small-cell phytoplankton to carbon flux in Fram Strait waters (Metfies et al., 2017; Bachy et al., 2022), future studies should address further mechanisms of export of these chlorophytes as they gain attention as sentinels of ocean warming due to the species-specific responses to water temperature (Li et al., 2009; Demory et al., 2019; Bachy et al., 2022).

Representatives ASVs of the radiolarian order *Chaunacanthida* and the pelagic diatom *Chaetoceros* were part of the spring and summer eukaryotic core community but comprised a significant fraction of the summer core community (40.2%). Both correlated positively with POC flux quantities (Figure 5). The correlation of diatoms to carbon export has been previously observed during summer in the North Pacific Ocean with high export pulses at abyssal depths even in silicate-depleted regions (Poff et al., 2021). Diatoms, especially *Chaetoceros* have also been found to be major contributors to the seasonal export of POC that reaches abyssal depths in the North Pacific (Preston et al., 2020). In general, radiolarians were the most abundant group present in our samples, as previously detected by microscopy in sediment trap samples from 2000-2005 at the same site (Bauerfeind et al., 2009). Radiolarians have frequently been recovered from Arctic 18S rRNA gene libraries from surface to the deep ocean (Lovejoy and Potvin, 2011). *Chaunacanthida* have also been associated with diatom aggregates of *Chaetoceros* in the Artic water column (~ 200 m) of Baffin Bay (west coast of Greenland) (Greco et al., 2021), matching our observations of summer assemblages. Moreover, radiolarians are known to contribute to the downward POC flux in summer subsurface waters (Decelle et al., 2013; Fontanez et al., 2015; Guidi et al.,

2016; Poff et al., 2021). In addition to foraminifera and pteropods (Ramondenc et al., 2022), radiolarians may also be a significant group of sinkers when exported as cysts (Martin et al., 2010). Hence, *Chaunacanthida* might be key contributors to carbon remineralization due to their heterotrophic lifestyle (Lovejoy, 2014), and to carbon export via their association with sinking particles. However, we cannot rule out that the multiple nuclei found in *Chaunacanthida* might amplify their relative contribution in the microbial community of sinking particles in our samples (Decelle and Not, 2015).

Bacterial communities indicated even stronger seasonal differences between spring and summer compared to eukaryotic communities. *Bacilli*, *Bacteroidia*, *Verrucomicrobiae* and *Gammaproteobacteria* were the classes that shifted the most between seasons. The spring events were strongly dominated by *Bacilli* taxa known for the absence of a cell wall and being associated with zooplankton i.e. ASVs of *Candidatus* Hepatoplasma and *Mycoplasma* of the class *Entomoplasmatales* (Gallet et al., 2019; Jaspers et al., 2020). The strong presence of *Candidatus* Hepatoplasma ASVs as part of the core community in both seasons highlights the relevance of zooplankton-associated taxa in sinking particles.

Marinifilaceae (*Bacteroidales*), *Psychromonas* and *Moritella* (*Alteromonadales*), and the diatom *Thalassiosira* were identified to peak in the earliest HPF with only 8 to 11 h of daylight in March 2001 and 2005. The low availability of sunlight likely prevented the occurrence of an early diatom bloom in March 2001 and 2005, reflected by the low PbSi flux and POC compared with other spring events. Resting spores of *Thalassiosira* that became trapped during sea ice formation could have contributed to the export of carbon (Rembauville et al., 2016), but the low PbSi:C ratios in both periods were similar to that of winter samples (Table 1; Data not shown). During the transition from winter to spring, *Thalassiosira* dominated the water column as well as the sea ice diatom communities at the marginal ice zone (Bauerfeind et al., 2009; Kauko et al., 2018). Thus, the particle-associated microbial communities in these early events were likely remnants of winter communities.

Bacterial ASVs that increased almost exclusively in summer included *Cyclobacteriaceae*, *Flavobacteriaceae*, *Ulvibacter*, *Vicingus*, *Colwellia*, *Rhodobacteraceae*, *Pirellulaceae* and

Blastopirellula, *OM60(NOR5)* and *BD1-7*, and they correlated positively with hydrography variables that represented summer conditions including the MW regime, SST and fluxes. These results further support the hypothesis that the seasonal succession in particle-associated bacteria might be constrained not only by specific interactions with eukaryotes forming the particles, or the presence of zooplankton but also by abiotic factors including physicochemical characteristics of the water column.

Microbial composition of sinking particles reflects changes in oceanographic conditions marked by a warm water anomaly

The eukaryotic community showed a clear trend in the interannual variability related to a known warm water event in the Arctic (Beszczynska-Möller et al., 2012). They clustered into pre-, WWA and post-WWA communities, and particularly the WWA communities were characterized by an overall decrease of diatom sequences (Figure 4). Already with the onset of the increase in temperature at the core of the WSC in 2004 (Beszczynska-Möller et al., 2012) diatom sequences of the dominant taxa of *Chaetoceros* were absent (<1 clr-transformed counts) until 2007 at the end of the WWA period. The diatoms present with the onset of the WWA were mainly assigned to *Thalassiosira* (from August 2004 to May 2006). The peak of the WWA between March 2005 and September 2006 was characterized by a sharp decrease in diatom sequences. These findings concur with an expected reduction of the overall export of diatom production in the warmer waters of the WWA (Lalande et al., 2013). At the time of the WWA, the catchment area was mostly characterized by the ML regime, whereas before and after the WWA stronger sea ice presence created a MW regime with stronger stratification (Figure S7). Our data further imply that the WWA/ML regime favoured a change in the composition of the particles that weakened the export of POC. Furthermore, previous studies indicated that a ML regime could benefit export as long as diatoms are winners in the system (von Appen et al., 2021). Because diatoms did not dominate during the WWA/ML regime this could signify in less export flux.

Despite the absence of diatoms during the WWA, we identified a large peak of *Melosira* in September 2006. *Melosira arctica* is a mat-forming diatom attached to sea ice common in Arctic bottom ice and sub-ice communities (Boetius et al., 2013; Hop et al., 2020). Although

biomass falls of *Melosira* are rare (Boetius et al., 2013; Wiedmann et al., 2020), the presence of this taxa in our samples could be explained from an ice floe in the proximity of the catchment area but that was not identified in the sea ice data. Moreover, 2006 was mostly characterized by a ML regime between June and August whereas the proportion of MW regime extended over the summer and peaked in October, a pattern that was substantially different than in previous years (Figure S3 & S11). In addition, we detected a substantially larger number of fungi sequences in May 2006, specifically of the heterotrophic fungi *Chytridiomycota*. In the Arctic Ocean, *Chytridiomycota* have been shown to associate with diatoms during sea ice melt (Kilias et al., 2020). The parasitic and saprotrophic nature of *Chytridiomycota* in aquatic systems (Ibelings et al., 2004; Gutiérrez et al., 2016) could further explain the sharp decline of diatoms in the spring of May 2006 and highlights potential ecological implications of chytrids for the biological carbon pump. Further examinations of diatoms in sinking particles in 2006 should include a higher temporal resolution to understand the role of sea ice dynamics and melt water regimes in diatom export at the peak of the WWA in 2006.

Previous studies revealed a shift in summer phytoplankton from mainly diatom-dominated to more flagellate-dominated communities in the water column of Fram Strait after the WWA (Bauerfeind et al., 2009; Nöthig et al., 2015). Our results extent these observations to the molecular level based on amplicon sequencing. Both microscopy and amplicon sequencing methods have their limitations in the quantification of phytoplankton cells (Eiler et al., 2013; Decelle and Not, 2015; Bradley et al., 2016; Onda et al., 2020; Fadeev et al., 2021a), however, we find that the observed shifts as a result of the WWA generally agree between methods and with previous observations in the water column. However, our data suggest that the transition in the dominance of the phytoplankton composition might have started earlier than previously reported. For instance, cell counts of the coccolithophore *Emiliania huxleyi* increased already in numbers from 2000 until 2004, and then these were no longer detectable (Nöthig et al., 2015). We did not identify ASVs assigned to *E. huxleyi* in HPF samples, likely due to the reported lower coverage of *Isochrydales* by the primer pair applied in our study (Onda et al., 2020). Other coccolithophores such as *Gephyrocapsa* were identified in the sinking particles in higher proportions until 2006, and afterwards unassigned

members of the *Isochrysidaceae* family remained present in low numbers. Another documented shift in the phytoplankton community concerns *Phaeocystis pouchetii*, which profited from the WWA (Nöthig et al., 2015; Metfies et al., 2016), beyond the known increase in abundance during summer (Fadeev et al., 2018). We observed an increase of the flagellate taxa *Phaeocystis, Prymnesium* and *Chrysochromulina* already in summer of 2004. Additionally, flagellate ASVs significantly decreased between 2005 and 2006, and less than 5 clr-transformed counts were detected by spring 2006. *Phaeocystis*, *Chrysochromulina* and *Chaetoceros* were consistently dominant again in post-WWA samples. Furthermore, the correlation of flagellates with $CaCO_3$, SST and swimmer flux suggest that flagellates were exported as a result of grazing from swimmers. This supports the hypothesis of an overall change of the summer phytoplankton community in sinking particles with ocean warming, and especially the occurrence of the WWA event. We also conclude that in addition to *Chaetoceros* flagellates are and will be important contributors to POC flux in the future.

WWA and hydrography-driven shifts in phytoplankton and bacterial communities are reflected in export fluxes

The studied period was marked by substantial interannual variability of the sea ice coverage in the sediment trap catchment area that significantly decreased during the WWA (Lalande et al., 2013; Wekerle et al., 2018). Warming of the Arctic Ocean has also increased the sea ice export out of Fram Strait (Krumpen et al., 2019; von Appen et al., 2021). The coupling between ice export and measured stratification regimes at the HGIV station has been previously identified for 2017 and 2018, also highlighting the interannual variability of sea ice export through Fram Strait (von Appen et al., 2021). Here, we further applied assessments of sea ice coverage and stratification regimes obtained from modelled data between 2000 and 2012 and explored their impact on the eukaryotic and bacterial community structure of sinking particles during high carbon export events marked by the WWA of 2005-2007.

Sea ice retreat is known to impact carbon flux at station HGIV in Fram Strait (Fadeev et al., 2021b; von Appen et al., 2021). Indeed, the WWA and the reduced ice export had an effect on the phytoplankton composition between 2000-2012, leading to a significant reduction of annual particle flux, POC and PbSi during the WWA (Bauerfeind et al., 2009; Lalande et al.,

2013). Diatoms are important contributors to total POC and PbSi flux through the export of resting spores (Salter et al., 2012; Rynearson et al., 2013; Rembauville et al., 2016), empty diatom frustules or packed into fecal pellets, as seen in Fram Strait and the Antarctic Polar Front region (Dagg et al., 2003; Lalande et al., 2011). From microscope observations we know that diatom aggregates in ice-covered regions in the Arctic Ocean led to higher carbon export efficiency near the sea ice edge North of Svalbard (Dybwad et al., 2021), as well as stronger vertical microbial connectivity in Fram Strait (Fadeev et al., 2021b), and the Barents Sea (Olli et al., 2019), playing an important role in export of nutrients to the deep-sea. This study and others indicate that diatoms are negatively affected by ocean warming and sea-ice loss in the Arctic.

Additionally, we identified a bacterial cluster based on Bray-Curtis dissimilarity that grouped post-WWA samples of spring events with a strong fraction of zooplankton-associated bacterial ASVs assigned to *Ca.* Hepatoplasma (order *Entomoplasmatales*) (Figure 3). *Entomoplasmatales* have been identified as symbionts in meso- and macro-zooplankton (Zbinden and Cambon-Bonavita, 2003; Gallet et al., 2019; Jaspers et al., 2020). Moreover, *Ca.* Hepatoplasma is a genus associated with midgut (hepatopancreas) communities of hadal amphipods (Cheng et al., 2019), and Antarctic krill (Clarke et al., 2019). Neither of these bacterial taxonomic groups were previously identified in such abundance in particle-associated communities in the Fram Strait (Fadeev et al., 2021b), or in sinking particles in other oceanographic regions (Fontanez et al., 2015; Boeuf et al., 2019; Preston et al., 2020; Poff et al., 2021). We find that for the time period 2000-2012, both *Calanus* and *Ca.* Hepatoplasma sequences increased substantially after the WWA. The increase in $CaCO_3$ flux, as an indicator of pteropod occurrence (Bauerfeind et al., 1997, 2009), swimmer flux and the correlation of *Metridia* and *Calanus*. ASVs with POC flux show that the input of POC from fecal pellets might have been significant in the post-WWA period, as previously suggested (Lalande et al., 2013). A recent study of 16 years of zooplankton dynamics in Fram Strait observed that sea ice dynamics influence the migration patterns of different swimmers in surface waters (Ramondenc et al., 2022). For instance, an increase of chaetognatha was observed post-WWA and was correlated with temperature changes (Ramondenc et al., 2022). Despite the apparent lack of primer coverage of zooplankton, our observations

corroborate the findings by (Ramondenc et al., 2022) that overall zooplankton abundances changed considerably in response to temperature changes associated with the WWA and changes in sea ice coverage, and also agree with an increase in zooplankton abundances reported from the Fram Strait in the years following the WWA (Bauerfeind et al., 2014; Busch et al., 2015; Soltwedel et al., 2016). *Entomoplasmatales* sequences may thus serve as bacterial indicators of the occurrence of zooplankton in surface waters and as an important part of the bacterial community in the particles.

Oceanographic conditions during the WWA induce community shifts leading to decreased carbon export

Co-occurrence network analyses revealed potential associations mostly between diverse families of eukaryotes of the divisions *Alveolata, Hacrobia* and *Stramenopiles*, and bacterial families of the classes *Gammaproteobacteria*, *Alphaproteobacteria*, *Verrucomicrobiae* and *Bacteroidia*, the latter a diverse group known to be functionally associated with phytoplankton blooms in the region and to respond to nutrient pulses (Buchan et al., 2014; Wilson et al., 2017; Fadeev et al., 2018; Cardozo-Mino et al., 2021). The relatively increased organic matter content of the particles during the HPF events explains the large number of associations that involved copiotrophic taxa of *Gammaproteobacteria*, *Alphaproteobacteria* and *Verrucomicrobia* seen in all three networks.

We expected the putative associations between bacteria and eukaryotes to change qualitatively before, during and after the WWA, because different phytoplankton communities composed the particles. In addition, more bacteria-to-bacteria associations (e.g. *Gammaproteobacteria* and *Alphaproteobacteria*) were observed in the WWA, as well as associations between eukaryotes in the post-WWA were detected. Altogether, the changes described here indicate a perturbation of the microbial network structure and a substantial change of particle composition, colonization and degradation of the particles at the time of the WWA.

The shift initiated in 2004 from a dominance of large diatom cells to smaller cells like coccolithophores and flagellates observed during the WWA, and matched the lowest peak POC and PON fluxes in HPF events, indicating a change in the size of the particles (Henson

et al., 2019). The likely higher retention of small buoyant particles of flagellates at the surface may have allowed for a different set of bacterial taxa to colonize the particles and allowed for more retention of carbon at the surface (Vernet et al., 2017). The presence of bacteria not usually associated with phytoplankton blooms such as *Alcanivorax*, *Psychromonas* and the numerous associations of diatoms of the WWA i.e. *Thalassiosira* and *Melosira*, *Gephyrocapsa* and the flagellates with bacterial families which were unique to the WWA period further supports an altered, potentially more active microbial loop that might resulted in lower carbon export reflected in our samples during this time. This also matches a decrease in fecal pellet production and volume during the WWA (Lalande et al., 2013), and lower organic matter concentrations observed at the deep seafloor during this period (Jacob, 2014).

In order to investigate in more detail changes in the composition of the particles that affect POC export, we identified putative associations between bacterial and eukaryotic families specific to the WWA. For instance, associations between heterotrophic pico- and nano-plankton families of MAST-1, MAST-9 and MAST-12 affiliation, and other heterotrophs including the divisions *Filosa-Sarcomonadea* and *Telonemia* with bacterial taxa assigned to the orders *Oceanospirillales, Alteromonadales* and *Rhodobacterales* that increased during the WWA. Approaching the peak

of the WWA in 2005 and 2006, we observed a notable increase in the sequence abundance of groups not detected as dominant taxa in surveys of free-living and particle-associated bacteria in Fram Strait before (Wilson et al., 2017; Fadeev et al., 2018, 2021b), namely ASVs of copiotrophic genera like *Marinobacter* and *Sulfitobacter.* Species within these genera are known to associate with eukaryotes (Chernikova et al., 2020) and to be enriched in DOM of unfixed sediment trap samples (Fontanez et al., 2015). For instance, *Marinobacter* has shown specific attachment to diatom cells of *Thalassiosira weissflogii* (Gärdes et al., 2010), and coccolithophorids including *Emiliania huxleyi* (Green et al., 2015). However, here *Marinobacter* showed possible associations with ASVs assigned to MAST-9C, *Protaspa-lineage* and *Chaunacanthida* during the WWA. Although, coccolithophorids, *Thalassiosira* and *Marinobacter* increased during the WWA, their lack of association in the network analysis might indicate a stronger effect of heterotrophic protists like MAST in the construction of the network and thus highlights their significance during the WWA. *Alcanivorax* may be involved

in the degradation of hydrocarbons in marine POM, such as *n*-alkanes potentially produced by dinoflagellates of the WWA, e.g. *Gymnodinium catenatumco*, which has been isolated from drifting sea ice north of Svalbard (Green et al., 2004; de Sousa et al., 2019), or oils derived from zooplankton (Yoshimura and Hama, 2012) (Daase et al., 2014).

Conclusions

We integrated 12-years of observations of sinking particle fluxes with molecular analyses of archived sediment trap samples, and with remote sensing and modelled data from a high-resolution Lagrangian back-tracking model, and identified significant changes in the microbial composition of sinking particles over this time period. These were mainly driven by surface oceanographic conditions in the area, most importantly by the presence/absence of sea ice, and by marked changes during a WWA episode between 2005 and 2007. The WWA period was characterized by low ice cover, higher temperatures, and unstratified waters, favouring the development of microbial communities and specific networks indicative of a retention system, which can explain reduced POC fluxes during this period. Despite some differences, the agreement of our results with previous microscopic observations suggest that mercury-chloride preserved sediment trap samples are a valid approach to address changes in the microbial composition of sinking particles over long time scales. This offers high-throughput and high-resolution insights into community dynamics. At the same time, the heterogeneous composition of the sinking organic matter (and resulting molecular signal), including phytoplankton, zooplankton and their associated bacterial microbiomes, may mask more subtle patterns and specific associations between taxonomic groups. The future Arctic Ocean will become warmer and sea ice cover will continue to decline. Our observations expand previous reports, indicating that changes in sea ice cover and hydrography will have major impacts on the efficiency of POC export, by altering phytoplankton composition and associated microbial networks. To better predict consequences of these changes for the biological carbon pump, future studies should address Arctic microbial community dynamics at high temporal resolution and from surface to seafloor.

Author contributions

IS, CB and AB conceived and designed the study. KM and IS conducted Illumina sequencing of the samples. EMN provided background and data for the sediment trap time series. SR determined the distance to the sea ice edge from remote sensing data products. CW obtained the catchment area from a backward Lagrangian model. IS, TK and CW provided weighted means of sea ice coverage, SST and chlorophyll. MC-M analyzed the data and wrote the manuscript with guidance from CB, IS, EMN and AB. All authors critically revised the manuscript and gave their approval of the submitted version.

Acknowledgements

We thank the captains and crew of RV Polarstern and RV Maria S. Merian expeditions to Fram Strait from 2000 to 2013, as well as the chief scientists and scientific crews. We thank Eduard Bauerfeind for the design, and deployment and recovery of sediment traps in Fram Strait. Nadine Knüppel, Christiane Lorenzen, Sandra Murawski, Liz Bonk and many student helpers and apprentices greatly acknowledged for their support on board and in the laboratory. We thank Theresa Hargesheimer for processing samples for molecular analyses. Halina Tegetmeyer performed sequencing of the bacterial samples and Swantje Rogge of eukaryotic samples. This work was conducted in the framework of the HGF Infrastructure Program FRAM of the Alfred-Wegener-Institute Helmholtz Center for Polar and Marine Research. Funding was provided by the Alfred Wegener Institute Helmholtz Center for Polar and Marine Research, the Max Planck Society and the Hector Fellow Academy, as well as the European Research Council (ERC) Advanced Grant ABYSS (no. 294757) to AB.

Conflict of Interest

The authors declare that the research was conducted in the absence of any commercial or financial relationships that could be construed as a potential conflict of interest.

References

Alldredge, A. L., and Silver, M. W. (1988). Characteristics, dynamics and significance of marine snow. *Prog. Oceanogr.* 20, 41–82. doi:10.1016/0079-6611(88)90053-5.

Arrigo, K. R., Perovich, D. K., Pickart, R. S., Brown, Z. W., Van Dijken, G. L., Lowry, K. E., et al. (2012). Massive phytoplankton blooms under arctic sea ice. *Science (80-.).* 336, 1408. doi:10.1126/science.1215065.

Azam, F., and Malfatti, F. (2007). Microbial structuring of marine ecosystems. *Nat. Rev. Microbiol.* 5, 782–791. doi:10.1038/nrmicro1747.

Bach, L. T., Boxhammer, T., Larsen, A., Hildebrandt, N., Schulz, K. G., and Riebesell, U. (2016). Influence of plankton community structure on the sinking velocity of marine aggregates. *Global Biogeochem. Cycles* 30, 1145–1165.

Bachy, C., Sudek, L., Choi, C. J., Eckmann, C. A., Nöthig, E.-M., Metfies, K., et al. (2022). Phytoplankton Surveys in the Arctic Fram Strait Demonstrate the Tiny Eukaryotic Alga Micromonas and Other Picoprasinophytes Contribute to Deep Sea Export. *Microorg.* 10. doi:10.3390/microorganisms10050961.

Bauerfeind, E., Garrity, C., Krumbholz, M., Ramseier, R. O., and Voβ, M. (1997). Seasonal variability of sediment trap collections in the Northeast Water Polynya. Part 2. Biochemical and microscopic composition of sedimenting matter. *J. Mar. Syst.* 10, 371–389.

Bauerfeind, E., Nöthig, E.-M., Lorenzen, C., Knüppel, N., and Soltwedel, T. (2015a). Biogenic particle flux at AWI HAUSGARTEN central station HGIV from mooring FEVI1. *Alfred Wegener Institute, Helmholtz Centre for Polar and Marine Research, Bremerhaven.* doi:10.1594/PANGAEA.855463.

Bauerfeind, E., Nöthig, E.-M., Lorenzen, C., Knüppel, N., and Soltwedel, T. (2015b). Biogenic particle flux at AWI HAUSGARTEN central station HGIV from mooring FEVI10. *Alfred Wegener Institute, Helmholtz Centre for Polar and Marine Research, Bremerhaven.* doi:10.1594/PANGAEA.855467.

Bauerfeind, E., Nöthig, E.-M., Lorenzen, C., Knüppel, N., and Soltwedel, T. (2015c). Biogenic particle flux at AWI HAUSGARTEN central station HGIV from mooring FEVI13. *Alfred Wegener Institute, Helmholtz Centre for Polar and Marine Research, Bremerhaven*. doi:10.1594/PANGAEA.855468.

Bauerfeind, E., Nöthig, E.-M., Lorenzen, C., Knüppel, N., and Soltwedel, T. (2015d). Biogenic particle flux at AWI HAUSGARTEN central station HGIV from mooring FEVI18. *Alfred Wegener Institute, Helmholtz Centre for Polar and Marine Research, Bremerhaven*. doi:10.1594/PANGAEA.855470.

Bauerfeind, E., Nöthig, E.-M., Lorenzen, C., Knüppel, N., and Soltwedel, T. (2015e). Biogenic particle flux at AWI HAUSGARTEN central station HGIV from mooring FEVI2. *Alfred Wegener Institute, Helmholtz Centre for Polar and Marine Research, Bremerhaven*. doi:10.1594/PANGAEA.855464.

Bauerfeind, E., Nöthig, E.-M., Lorenzen, C., Knüppel, N., and Soltwedel, T. (2015f). Biogenic particle flux at AWI HAUSGARTEN central station HGIV from mooring FEVI20. *Alfred Wegener Institute, Helmholtz Centre for Polar and Marine Research, Bremerhaven*. doi:10.1594/PANGAEA.855471.

Bauerfeind, E., Nöthig, E.-M., Lorenzen, C., Knüppel, N., and Soltwedel, T. (2015g). Biogenic particle flux at AWI HAUSGARTEN central station HGIV from mooring FEVI22. *Alfred Wegener Institute, Helmholtz Centre for Polar and Marine Research, Bremerhaven* doi:10.1594/PANGAEA.855472.

Bauerfeind, E., Nöthig, E.-M., Lorenzen, C., Knüppel, N., and Soltwedel, T. (2015h). Biogenic particle flux at AWI HAUSGARTEN central station HGIV from mooring FEVI24. *Alfred Wegener Institute, Helmholtz Centre for Polar and Marine Research, Bremerhaven*. doi:10.1594/PANGAEA.855473.

Bauerfeind, E., Nöthig, E.-M., Lorenzen, C., Knüppel, N., and Soltwedel, T. (2015i). Biogenic particle flux at AWI HAUSGARTEN central station HGIV from mooring FEVI3. *Alfred Wegener Institute, Helmholtz Centre for Polar and Marine Research, Bremerhaven*. doi:10.1594/PANGAEA.855465.

Bauerfeind, E., Nöthig, E.-M., Lorenzen, C., Knüppel, N., and Soltwedel, T. (2015j). Biogenic particle flux at AWI HAUSGARTEN central station HGIV from mooring FEVI7. *Alfred Wegener Institute, Helmholtz Centre for Polar and Marine Research, Bremerhaven*. doi:10.1594/PANGAEA.855466.

Bauerfeind, E., Nöthig, E.-M., Lorenzen, C., Knüppel, N., and Soltwedel, T. (2017). Biogenic particle flux at AWI HAUSGARTEN central station HGIV from mooring FEVI16. *Alfred Wegener Institute, Helmholtz Centre for Polar and Marine Research, Bremerhaven*. doi:10.1594/PANGAEA.879532.

Bauerfeind, E., Nöthig, E.-M., Pauls, B., Kraft, A., and Beszczynska-Möller, A. (2014). Variability in pteropod sedimentation and corresponding aragonite flux at the Arctic deep-sea long-term observatory HAUSGARTEN in the eastern Fram Strait from 2000 to 2009. *J. Mar. Syst.* 132, 95–105. doi:https://doi.org/10.1016/j.jmarsys.2013.12.006.

Bauerfeind, E., Nöthig, E. M., Beszczynska, A., Fahl, K., Kaleschke, L., Kreker, K., et al. (2009). Particle sedimentation patterns in the eastern Fram Strait during 2000-2005: Results from the Arctic long-term observatory HAUSGARTEN. *Deep. Res. Part I Oceanogr. Res. Pap.* 56, 1471–1487. doi:10.1016/j.dsr.2009.04.011.

Beszczynska-Moeller, A., Woodgate, R. A., Lee, C., Melling, H., and Karcher, M. (2011). A synthesis of exchanges through the main oceanic gateways to the Arctic Ocean. *Oceanography* 24, 82–99.

Beszczynska-Möller, A., Fahrbach, E., Schauer, U., and Hansen, E. (2012). Variability in Atlantic water temperature and transport at the entrance to the Arctic Ocean, 19972010. *ICES J. Mar. Sci.* 69, 852–863. doi:10.1093/icesjms/fss056.

Bodungen, B. V, Wunsch, M., and Fürderer, H. (1991). Sampling and analysis of suspended and sinking particles in the northern North Atlantic. *Washingt. DC Am. Geophys. Union Geophys. Monogr. Ser.* 63, 47–56.

Boetius, A., Albrecht, S., Bakker, K., Bienhold, C., Felden, J., Fernández-Méndez, M., et al. (2013). Export of algal biomass from the melting arctic sea ice. *Science (80-.).* 339, 1430–1432. doi:10.1126/science.1231346.

Boeuf, D., Edwards, B. R., Eppley, J. M., Hu, S. K., Poff, K. E., Romano, A. E., et al. (2019). Biological composition and microbial dynamics of sinking particulate organic matter at abyssal depths in the oligotrophic open ocean. *Proc. Natl. Acad. Sci. U. S. A.* 116, 11824–

11832. doi:10.1073/pnas.1903080116.

Bradley, I. M., Pinto, A. J., and Guest, J. S. (2016). Design and evaluation of Illumina MiSeq-compatible, 18S rRNA gene-specific primers for improved characterization of mixed phototrophic communities. *Appl. Environ. Microbiol.* 82, 5878–5891.

Buchan, A., LeCleir, G. R., Gulvik, C. A., and González, J. M. (2014). Master recyclers: features and functions of bacteria associated with phytoplankton blooms. *Nat. Rev. Microbiol.* 12, 686–698. doi:10.1038/nrmicro3326.

Buesseler, K. O., and Boyd, P. W. (2009). Shedding light on processes that control particle export and flux attenuation in the twilight zone of the open ocean. *Limnol. Oceanogr.* 54, 1210–1232. doi:10.4319/lo.2009.54.4.1210.

Busch, K., Bauerfeind, E., and Nöthig, E. M. (2015). Pteropod sedimentation patterns in different water depths observed with moored sediment traps over a 4-year period at the LTER station HAUSGARTEN in eastern Fram Strait. *Polar Biol.* 38, 845–859. doi:10.1007/s00300-015-1644-9.

Callahan, B. J., McMurdie, P. J., Rosen, M. J., Han, A. W., Johnson, A. J. A., and Holmes, S. P. (2016). DADA2: High-resolution sample inference from Illumina amplicon data. *Nat. Methods* 13, 581–583. doi:10.1038/nmeth.3869.

Cardozo-Mino, M. G., Fadeev, E., Salman-Carvalho, V., and Boetius, A. (2021). Spatial Distribution of Arctic Bacterioplankton Abundance Is Linked to Distinct Water Masses and Summertime Phytoplankton Bloom Dynamics (Fram Strait, 79°N). *Front. Microbiol.* 12, 1067. doi:10.3389/fmicb.2021.658803.

Cavalieri, D. J. (2003). Sea ice concentrations from Nimbus-7 SMMR and DMSP SSM/I passive microwave data. *Boulder, Color. USA, NASA Natl. Snow Ice Data Cent. Distrib. Act. Arch. Center, doi* 10. Available at: http://home.earthlink.net/~tech_comm/SupportFiles/Portfolio/NSIDC/nsidc0051_gsfc_seaice.gd.pdf.

Cheng, X., Wang, Y., Li, J., Yan, G., and He, L. (2019). Comparative analysis of the gut microbial communities between two dominant amphipods from the Challenger Deep, Mariana Trench. *Deep Sea Res. Part I Oceanogr. Res. Pap.* 151, 103081.

Chernikova, T. N., Bargiela, R., Toshchakov, S. V, Shivaraman, V., Lunev, E. A., Yakimov, M. M., et al. (2020). Hydrocarbon-Degrading Bacteria Alcanivorax and Marinobacter Associated with Microalgae Pavlova lutheri and Nannochloropsis oculata. *Front. Microbiol.* 11. Available at: https://www.frontiersin.org/article/10.3389/fmicb.2020.572931.

Clarke, L. J., Bestley, S., Bissett, A., and Deagle, B. E. (2019). A globally distributed Syndiniales parasite dominates the Southern Ocean micro-eukaryote community near the sea-ice edge. *ISME J.* 13, 734–737.

Cleary, A. C., and Durbin, E. G. (2016). Unexpected prevalence of parasite 18S rDNA sequences in winter among Antarctic marine protists. *J. Plankton Res.* 38, 401–417. doi:10.1093/plankt/fbw005.

Cleary, A. C., Søreide, J. E., Freese, D., Niehoff, B., and Gabrielsen, T. M. (2017). Feeding by Calanus glacialis in a high arctic fjord: potential seasonal importance of alternative prey. *ICES J. Mar. Sci.* 74, 1937–1946.

Cram, J. A., Xia, L. C., Needham, D. M., Sachdeva, R., Sun, F., and Fuhrman, J. A. (2015). Cross-depth analysis of marine bacterial networks suggests downward propagation of temporal changes. *ISME J.* 9, 2573–2586. doi:10.1038/ismej.2015.76.

Daase, M., Varpe, Ø., and Falk-Petersen, S. (2014). Non-consumptive mortality in copepods:

occurrence of Calanus spp. carcasses in the Arctic Ocean during winter. *J. Plankton Res.* 36, 129–144.

Dagg, M. J., Urban-Rich, J., and Peterson, J. O. (2003). The potential contribution of fecal pellets from large copepods to the flux of biogenic silica and particulate organic carbon in the Antarctic Polar Front region near 170°W. *Deep Sea Res. Part II Top. Stud. Oceanogr.* 50, 675–691. doi:https://doi.org/10.1016/S0967-0645(02)00590-8.

Dai, A., Luo, D., Song, M., and Liu, J. (2019). Arctic amplification is caused by sea-ice loss under increasing CO 2. *Nat. Commun.* 10, 121. doi:10.1038/s41467-018-07954-9.

Datta, M. S., Sliwerska, E., Gore, J., Polz, M. F., and Cordero, O. X. (2016). Microbial interactions lead to rapid micro-scale successions on model marine particles. *Nat. Commun.* 7, 1–7.

De La Rocha, C. L., and Passow, U. (2007). Factors influencing the sinking of POC and the efficiency of the biological carbon pump. *Deep. Res. Part II Top. Stud. Oceanogr.* 54, 639–658. doi:10.1016/j.dsr2.2007.01.004.

de Sousa, A. G. G., Tomasino, M. P., Duarte, P., Fernández-Méndez, M., Assmy, P., Ribeiro, H., et al. (2019). Diversity and composition of pelagic prokaryotic and protist communities in a thin Arctic sea-ice regime. *Microb. Ecol.* 78, 388–408.

Decelle, J., Martin, P., Paborstava, K., Pond, D. W., Tarling, G., Mahé, F., et al. (2013). Diversity, Ecology and Biogeochemistry of Cyst-Forming Acantharia (Radiolaria) in the Oceans. *PLoS One* 8, e53598. doi:10.1371/journal.pone.0053598.

Decelle, J., and Not, F. (2015). Acantharia. *eLS*, 1–10.

Demory, D., Baudoux, A.-C., Monier, A., Simon, N., Six, C., Ge, P., et al. (2019). Picoeukaryotes of the Micromonas genus: sentinels of a warming ocean. *ISME J.* 13, 132–146. doi:10.1038/s41396-018-0248-0.

Diepenbroek, M., Glöckner, F. O., Grobe, P., Güntsch, A., Huber, R., König-Ries, B., et al. (2014). "Towards an integrated biodiversity and ecological research data management and archiving platform: the German federation for the curation of biological data (GFBio)," in *Informatik 2014*, eds. E. Plödereder, L. Grunske, E. Schneider, and D. Ull (Bonn: Gesellschaft für Informatik e.V.), 1711–1721.

Ducklow, H. W., Steinberg, D. K., and Buesseler, K. O. (2001). Upper ocean carbon export and the biological pump. *Oceanography* 14, 50–58. doi:10.5670/oceanog.2001.06.

Duran-Pinedo, A. E., Paster, B., Teles, R., and Frias-Lopez, J. (2011). Correlation Network Analysis Applied to Complex Biofilm Communities. *PLoS One* 6, e28438. doi:10.1371/journal.pone.0028438.

Dybwad, C., Assmy, P., Olsen, L. M., Peeken, I., Nikolopoulos, A., Krumpen, T., et al. (2021). Carbon Export in the Seasonal Sea Ice Zone North of Svalbard From Winter to Late Summer. *Front. Mar. Sci.* 7. Available at: https://www.frontiersin.org/article/10.3389/fmars.2020.525800.

Eiler, A., Drakare, S., Bertilsson, S., Pernthaler, J., Peura, S., Rofner, C., et al. (2013). Unveiling Distribution Patterns of Freshwater Phytoplankton by a Next Generation Sequencing Based Approach. *PLoS One* 8, e53516. Available at: https://doi.org/10.1371/journal.pone.0053516.

Elwood, H. J., Olsen, G. J., and Sogin, M. L. (1985). The small-subunit ribosomal RNA gene sequences from the hypotrichous ciliates Oxytricha nova and Stylonychia pustulata. *Mol. Biol. Evol.* 2, 399–410. doi:10.1093/oxfordjournals.molbev.a040362.

Fadeev, E., Cardozo-Mino, M. G., Rapp, J. Z., Bienhold, C., Salter, I., Salman-Carvalho, V., et al. (2021a). Comparison of Two 16S rRNA Primers (V3–V4 and V4–V5) for Studies of

Arctic Microbial Communities. *Front. Microbiol.* 12, 283. Available at: https://www.frontiersin.org/articles/10.3389/fmicb.2021.637526/full.

Fadeev, E., Rogge, A., Ramondenc, S., Nöthig, E.-M., Wekerle, C., Bienhold, C., et al. (2021b). Sea ice presence is linked to higher carbon export and vertical microbial connectivity in the Eurasian Arctic Ocean. *Commun. Biol.* 4, 1255. doi:10.1038/s42003-021-02776-w.

Fadeev, E., Salter, I., Schourup-Kristensen, V., Nöthig, E. M., Metfies, K., Engel, A., et al. (2018). Microbial communities in the east and west fram strait during sea ice melting season. *Front. Mar. Sci.* 5, 429. doi:10.3389/fmars.2018.00429.

Falk-Petersen, S., Dahl, T. M., Scott, C. L., Sargent, J. R., Gulliksen, B., Kwasniewski, S., et al. (2002). Lipid biomarkers and trophic linkages between ctenophores and copepods in Svalbard waters. *Mar. Ecol. Prog. Ser.* 227, 187–194.

Fontanez, K. M., Eppley, J. M., Samo, T. J., Karl, D. M., and DeLong, E. F. (2015). Microbial community structure and function on sinking particles in the North Pacific Subtropical Gyre. *Front. Microbiol.* 6, 469. doi:10.3389/fmicb.2015.00469.

Gallet, A., Koubbi, P., Léger, N., Scheifler, M., Ruiz-Rodriguez, M., Suzuki, M. T., et al. (2019). Low-diversity bacterial microbiota in Southern Ocean representatives of lanternfish genera Electrona, Protomyctophum and Gymnoscopelus (family Myctophidae). *PLoS One* 14, e0226159.

Gärdes, A., Kaeppel, E., Shehzad, A., Seebah, S., Teeling, H., Yarza, P., et al. (2010). Complete genome sequence of Marinobacter adhaerens type strain (HP15), a diatom-interacting marine microorganism. *Stand. Genomic Sci.* 3, 97–107. doi:10.4056/sigs.922139.

Gibbons, S. M., Caporaso, J. G., Pirrung, M., Field, D., Knight, R., and Gilbert, J. A. (2013). Evidence for a persistent microbial seed bank throughout the global ocean. *Proc. Natl. Acad. Sci. U. S. A.* 110, 4651–4655. doi:10.1073/pnas.1217767110.

Grabowski, E., Letelier, R. M., Laws, E. A., and Karl, D. M. (2019). Coupling carbon and energy fluxes in the North Pacific Subtropical Gyre. *Nat. Commun.* 10, 1–9. doi:10.1038/s41467-019-09772-z.

Greco, M., Morard, R., and Kucera, M. (2021). Single-cell metabarcoding reveals biotic interactions of the Arctic calcifier Neogloboquadrina pachyderma with the eukaryotic pelagic community. *J. Plankton Res.* doi:10.1093/plankt/fbab015.

Green, D. H., Echavarri-Bravo, V., Brennan, D., and Hart, M. C. (2015). Bacterial Diversity Associated with the Coccolithophorid Algae *Emiliania huxleyi* and *Coccolithus pelagicus* f. *braarudii*. *Biomed Res. Int.* 2015, 194540. doi:10.1155/2015/194540.

Green, D. H., Llewellyn, L. E., Negri, A. P., Blackburn, S. I., and Bolch, C. J. S. (2004). Phylogenetic and functional diversity of the cultivable bacterial community associated with the paralytic shellfish poisoning dinoflagellate Gymnodinium catenatum. *FEMS Microbiol. Ecol.* 47, 345–357.

Grosfeld, K., Treffeisen, R., Asseng, J., Bartsch, A., Bräuer, B., Fritzsch, B., et al. (2016). Online sea-ice knowledge and data platform. *Polarforschung* 85, 143–155.

Grossart, H.-P., Kiørboe, T., Tang, K., and Ploug, H. (2003). Bacterial colonization of particles: growth and interactions. *Appl. Environ. Microbiol.* 69, 3500–3509. doi:10.1128/aem.69.6.3500-3509.2003.

Guidi, L., Chaffron, S., Bittner, L., Eveillard, D., Larhlimi, A., Roux, S., et al. (2016). Plankton networks driving carbon export in the oligotrophic ocean. *Nature* 532, 465–470. doi:10.1038/nature16942.

Guidi, L., Stemmann, L., Jackson, G. A., Ibanez, F., Claustre, H., Legendre, L., et al. (2009). Effects of phytoplankton community on production, size and export of large aggregates: A world-ocean analysis. *Limnol. Oceanogr.* 54, 1951–1963. doi:10.4319/lo.2009.54.6.1951.

Guillou, L., Bachar, D., Audic, S., Bass, D., Berney, C., Bittner, L., et al. (2013). The Protist Ribosomal Reference database (PR2): A catalog of unicellular eukaryote Small Sub-Unit rRNA sequences with curated taxonomy. *Nucleic Acids Res.* 41, D597–D604. doi:10.1093/nar/gks1160.

Gutiérrez, M. H., Jara, A. M., and Pantoja, S. (2016). Fungal parasites infect marine diatoms in the upwelling ecosystem of the Humboldt current system off central Chile. *Environ. Microbiol.* 18, 1646–1653.

Harrison, P. W., Ahamed, A., Aslam, R., Alako, B. T. F., Burgin, J., Buso, N., et al. (2021). The European Nucleotide Archive in 2020. *Nucleic Acids Res.* 49, D82–D85. doi:10.1093/nar/gkaa1028.

Henson, S., Le Moigne, F., and Giering, S. (2019). Drivers of carbon export efficiency in the global ocean. *Global Biogeochem. Cycles* 33, 891–903.

Hop, H., Assmy, P., Wold, A., Sundfjord, A., Daase, M., Duarte, P., et al. (2019). Pelagic ecosystem characteristics across the Atlantic water boundary current from Rijpfjorden, Svalbard, to the Arctic Ocean during summer (2010–2014). *Front. Mar. Sci.* 6, 181.

Hop, H., Vihtakari, M., Bluhm, B. A., Assmy, P., Poulin, M., Gradinger, R., et al. (2020). Changes in Sea-Ice Protist Diversity With Declining Sea Ice in the Arctic Ocean From the 1980s to 2010s. *Front. Mar. Sci.* 7. doi:10.3389/fmars.2020.00243.

Hsieh, T. C., Ma, K. H., and Chao, A. (2016). iNEXT: an R package for rarefaction and extrapolation of species diversity (H ill numbers). *Methods Ecol. Evol.* 7, 1451–1456.

Ibelings, B. W., De Bruin, A., Kagami, M., Rijkeboer, M., Brehm, M., and Donk, E. Van (2004). Host parasite interactions between freshwater phytoplankton and chytrid fungi (chytridiomycota) 1. *J. Phycol.* 40, 437–453.

Iversen, M. H., and Ploug, H. (2010). Ballast minerals and the sinking carbon flux in the ocean: Carbon-specific respiration rates and sinking velocity of marine snow aggregates. *Biogeosciences* 7, 2613–2624. doi:10.5194/bg-7-2613-2010.

Jacob, M. (2014). Influence of Global Change on microbial communities in Arctic sediments.

Jaspers, C., Weiland-Bräuer, N., Rühlemann, M. C., Baines, J. F., Schmitz, R. A., and Reusch, T. B. H. (2020). Differences in the microbiota of native and non-indigenous gelatinous zooplankton organisms in a low saline environment. *Sci. Total Environ.* 734, 139471.

Jiao, N., Herndl, G. J., Hansell, D. A., Benner, R., Kattner, G., Wilhelm, S. W., et al. (2010). Microbial production of recalcitrant dissolved organic matter: long-term carbon storage in the global ocean. *Nat. Rev. Microbiol.* 8, 593–599. doi:10.1038/nrmicro2386.

Kauko, H. M., Olsen, L. M., Duarte, P., Peeken, I., Granskog, M. A., Johnsen, G., et al. (2018). Algal Colonization of Young Arctic Sea Ice in Spring. *Front. Mar. Sci.* 5. Available at: https://www.frontiersin.org/article/10.3389/fmars.2018.00199.

Kilias, E. S., Junges, L., Šupraha, L., Leonard, G., Metfies, K., and Richards, T. A. (2020). Chytrid fungi distribution and co-occurrence with diatoms correlate with sea ice melt in the Arctic Ocean. *Commun. Biol.* 3, 183. doi:10.1038/s42003-020-0891-7.

Klindworth, A., Pruesse, E., Schweer, T., Peplies, J., Quast, C., Horn, M., et al. (2013). Evaluation of general 16S ribosomal RNA gene PCR primers for classical and next-generation sequencing-based diversity studies. *Nucleic Acids Res.* 41, e1–e1. doi:10.1093/nar/gks808.

Kremling, K., Lentz, U., Zeitzschel, B., Schulz-Bull, D. E., and Duinker, J. C. (1996). New type of time-series sediment trap for the reliable collection of inorganic and organic trace chemical substances. *Rev. Sci. Instrum.* 67, 4360–4363. doi:10.1063/1.1147582.

Krumpen, T., Belter, H. J., Boetius, A., Damm, E., Haas, C., Hendricks, S., et al. (2019). Arctic warming interrupts the Transpolar Drift and affects long-range transport of sea ice and ice-rafted matter. *Sci. Rep.* 9, 1–9.

Kwok, R., and Rothrock, D. A. (2009). Decline in Arctic sea ice thickness from submarine and ICESat records: 1958–2008. *Geophys. Res. Lett.* 36.

Lalande, C., Bauerfeind, E., and Nöthig, E. M. (2011). Downward particulate organic carbon export at high temporal resolution in the eastern Fram Strait: Influence of Atlantic Water on flux composition. *Mar. Ecol. Prog. Ser.* 440, 127–136. doi:10.3354/meps09385.

Lalande, C., Bauerfeind, E., Nöthig, E. M., and Beszczynska-Möller, A. (2013). Impact of a warm anomaly on export fluxes of biogenic matter in the eastern Fram Strait. *Prog. Oceanogr.* 109, 70–77. doi:10.1016/j.pocean.2012.09.006.

Lalande, C., Grebmeier, J. M., Wassmann, P., Cooper, L. W., Flint, M. V, and Sergeeva, V. M. (2007). Export fluxes of biogenic matter in the presence and absence of seasonal sea ice cover in the Chukchi Sea. *Cont. Shelf Res.* 27, 2051–2065.

Lalande, C., Nöthig, E.-M., Bauerfeind, E., Hardge, K., Beszczynska-Möller, A., and Fahl, K. (2016). Lateral supply and downward export of particulate matter from upper waters to the seafloor in the deep eastern Fram Strait. *Deep Sea Res. Part I Oceanogr. Res. Pap.* 114, 78–89. doi:https://doi.org/10.1016/j.dsr.2016.04.014.

Lalande, C., Nöthig, E. M., Somavilla, R., Bauerfeind, E., Shevchenko, V., and Okolodkov, Y. (2014). Variability in under-ice export fluxes of biogenic matter in the Arctic Ocean. *Global Biogeochem. Cycles* 28, 571–583. doi:10.1002/2013GB004735.

Langfelder, P., and Horvath, S. (2008). WGCNA: an R package for weighted correlation network analysis. *BMC Bioinformatics* 9, 1–13.

Lannuzel, D., Tedesco, L., van Leeuwe, M., Campbell, K., Flores, H., Delille, B., et al. (2020). The future of Arctic sea-ice biogeochemistry and ice-associated ecosystems. *Nat. Clim. Chang.* 10, 983–992. doi:10.1038/s41558-020-00940-4.

Leu, E., Søreide, J. E., Hessen, D. O., Falk-Petersen, S., and Berge, J. (2011). Consequences of changing sea-ice cover for primary and secondary producers in the European Arctic shelf seas: Timing, quantity, and quality. *Prog. Oceanogr.* 90, 18–32. doi:10.1016/j.pocean.2011.02.004.

Lewis, K. M., Van Dijken, G. L., and Arrigo, K. R. (2020). Changes in phytoplankton concentration now drive increased Arctic Ocean primary production. *Science (80-.).* 369, 198–202. doi:10.1126/science.aay8380.

Li, W. K. W., McLaughlin, F. A., Lovejoy, C., and Carmack, E. C. (2009). Smallest algae thrive as the arctic ocean freshens. *Science (80-.).* 326, 539. doi:10.1126/science.1179798.

Liu, Y., Blain, S., Crispi, O., Rembauville, M., and Obernosterer, I. (2020). Seasonal dynamics of prokaryotes and their associations with diatoms in the Southern Ocean as revealed by an autonomous sampler. *Environ. Microbiol.* 22, 3968–3984. doi:10.1111/1462-2920.15184.

Love, M. I., Huber, W., and Anders, S. (2014). Moderated estimation of fold change and dispersion for RNA-seq data with DESeq2. *Genome Biol.* 15, 1–21.

Lovejoy, C. (2014). Changing views of Arctic protists (marine microbial eukaryotes) in a changing Arctic. *Acta Protozool.* 53.

Lovejoy, C., and Potvin, M. (2011). Microbial eukaryotic distribution in a dynamic Beaufort

Sea and the Arctic Ocean. *J. Plankton Res.* 33, 431–444.
Martin, M. (2011). Cutadapt removes adapter sequences from high-throughput sequencing reads. *EMBnet.journal* 17, 10. doi:10.14806/ej.17.1.200.
Martin, P., Allen, J. T., Cooper, M. J., Johns, D. G., Lampitt, R. S., Sanders, R., et al. (2010). Sedimentation of acantharian cysts in the Iceland Basin: Strontium as a ballast for deep ocean particle flux, and implications for acantharian reproductive strategies. *Limnol. Oceanogr.* 55, 604–614. doi:10.4319/lo.2010.55.2.0604.
McMurdie, P. J., and Holmes, S. (2013). Phyloseq: An R Package for Reproducible Interactive Analysis and Graphics of Microbiome Census Data. *PLoS One* 8, e61217. doi:10.1371/journal.pone.0061217.
Mestre, M., Ruiz-González, C., Logares, R., Duarte, C. M., Gasol, J. M., and Sala, M. M. (2018). Sinking particles promote vertical connectivity in the ocean microbiome. *Proc. Natl. Acad. Sci. U. S. A.* 115, E6799–E6807. doi:10.1073/pnas.1802470115.
Metfies, K., Bauerfeind, E., Wolf, C., Sprong, P., Frickenhaus, S., Kaleschke, L., et al. (2017). Protist communities in moored long-term sediment traps (Fram Strait, Arctic)-preservation with mercury chloride allows for PCR-based molecular genetic analyses. *Front. Mar. Sci.* 4, 301. doi:10.3389/fmars.2017.00301.
Metfies, K., von Appen, W.-J., Kilias, E., Nicolaus, A., and Nöthig, E.-M. (2016). Biogeography and photosynthetic biomass of arctic marine pico-eukaroytes during summer of the record sea ice minimum 2012. *PLoS One* 11, e0148512.
Nöthig, E. M., Bracher, A., Engel, A., Metfies, K., Niehoff, B., Peeken, I., et al. (2015). Summertime plankton ecology in fram strait-a compilation of long-and short-term observations. *Polar Res.* 34, 23349. doi:10.3402/polar.v34.23349.
Nöthig, E. M., Ramondenc, S., Haas, A., Hehemann, L., Walter, A., Bracher, A., et al. (2020). Summertime Chlorophyll a and Particulate Organic Carbon Standing Stocks in Surface Waters of the Fram Strait and the Arctic Ocean (1991–2015). *Front. Mar. Sci.* 7. doi:10.3389/fmars.2020.00350.
Oksanen, J., Blanchet, F. G., Kindt, R., Legendre, P., Minchin, P. R., O'hara, R. B., et al. (2013). Community ecology package. *R Packag. version* 2.
Olli, K., Halvorsen, E., Vernet, M., Lavrentyev, P. J., Franzè, G., Sanz-Martin, M., et al. (2019). Food Web Functions and Interactions During Spring and Summer in the Arctic Water Inflow Region: Investigated Through Inverse Modeling . *Front. Mar. Sci.* 6. Available at: https://www.frontiersin.org/article/10.3389/fmars.2019.00244.
Onda, D. F., Wolf, C., Metfies, K., Salter, I., and Noethig, E. (2020). Changes in exported key phytoplankton taxa related to a warm anomaly in the Fram Strait inferred from three complementary 18S rRNA gene meta-barcoding primer sets. *Authorea Prepr.*, 1–21.
Peng, G., and Meier, W. N. (2018). Temporal and regional variability of Arctic sea-ice coverage from satellite data. *Ann. Glaciol.* 59, 191–200. doi:10.1017/aog.2017.32.
Peralta-Ferriz, C., and Woodgate, R. A. (2015). Seasonal and interannual variability of pan-Arctic surface mixed layer properties from 1979 to 2012 from hydrographic data, and the dominance of stratification for multiyear mixed layer depth shoaling. *Prog. Oceanogr.* 134, 19–53.
Perovich, D. K. (2011). The changing Arctic sea ice cover. *Oceanography* 24, 162–173.
Poff, K. E., Leu, A. O., Eppley, J. M., Karl, D. M., and DeLong, E. F. (2021). Microbial dynamics of elevated carbon flux in the open ocean's abyss. *Proc. Natl. Acad. Sci. U. S. A.* 118. doi:10.1073/pnas.2018269118.
Preston, C. M., Durkin, C. A., and Yamahara, K. M. (2020). DNA metabarcoding reveals

organisms contributing to particulate matter flux to abyssal depths in the North East Pacific Ocean. *Deep. Res. Part II Top. Stud. Oceanogr.* 173, 104708. doi:10.1016/j.dsr2.2019.104708.

Quast, C., Pruesse, E., Yilmaz, P., Gerken, J., Schweer, T., Yarza, P., et al. (2013). The SILVA ribosomal RNA gene database project: Improved data processing and web-based tools. *Nucleic Acids Res.* 41, D590–D596. doi:10.1093/nar/gks1219.

Ramondenc, S., Nöthig, E.-M., Hufnagel, L., Bauerfeind, E., Busch, K., Knüppel, N., et al. (2022). Effects of Atlantification and changing sea-ice dynamics on zooplankton community structure and carbon flux between 2000 and 2016 in the eastern Fram Strait. *Limnol. Oceanogr.* n/a. doi:10.1002/lno.12192.

Rapp, J. Z., Fernández-Méndez, M., Bienhold, C., and Boetius, A. (2018). Effects of ice-algal aggregate export on the connectivity of bacterial communities in the central Arctic Ocean. *Front. Microbiol.* 9, 1035. doi:10.3389/fmicb.2018.01035.

Rembauville, M., Manno, C., Tarling, G. A., Blain, S., and Salter, I. (2016). Strong contribution of diatom resting spores to deep-sea carbon transfer in naturally iron-fertilized waters downstream of South Georgia. *Deep. Res. Part I Oceanogr. Res. Pap.* 115, 22–35. doi:10.1016/j.dsr.2016.05.002.

Ruiz-González, C., Mestre, M., Estrada, M., Sebastián, M., Salazar, G., Agustí, S., et al. (2020). Major imprint of surface plankton on deep ocean prokaryotic structure and activity. *Mol. Ecol.* 29, 1820–1838.

Rynearson, T. A., Richardson, K., Lampitt, R. S., Sieracki, M. E., Poulton, A. J., Lyngsgaard, M. M., et al. (2013). Major contribution of diatom resting spores to vertical flux in the sub-polar North Atlantic. *Deep. Res. Part I Oceanogr. Res. Pap.* 82, 60–71. doi:10.1016/j.dsr.2013.07.013.

Salter, I., Kemp, A. E. S., Moore, C. M., Lampitt, R. S., Wolff, G. A., and Holtvoeth, J. (2012). Diatom resting spore ecology drives enhanced carbon export from a naturally iron-fertilized bloom in the Southern Ocean. *Global Biogeochem. Cycles* 26. doi:10.1029/2010GB003977.

Schröter, F., Havermans, C., Kraft, A., Knüppel, N., Beszczynska-Möller, A., Bauerfeind, E., et al. (2019). Pelagic amphipods in the eastern fram strait with continuing presence of Themisto compressa based on sediment trap time series. *Front. Mar. Sci.* 6, 311. doi:10.3389/fmars.2019.00311.

Simon, M., Grossart, H. P., Schweitzer, B., and Ploug, H. (2002). Microbial ecology of organic aggregates in aquatic ecosystems. *Aquat. Microb. Ecol.* 28, 175–211. doi:10.3354/ame028175.

Soltwedel, T., Bauerfeind, E., Bergmann, M., Bracher, A., Budaeva, N., Busch, K., et al. (2016). Natural variability or anthropogenically-induced variation? Insights from 15 years of multidisciplinary observations at the arctic marine LTER site HAUSGARTEN. *Ecol. Indic.* 65, 89–102. doi:10.1016/j.ecolind.2015.10.001.

Thiele, S., Fuchs, B. M., Amann, R., and Iversen, M. H. (2015). Colonization in the photic zone and subsequent changes during sinking determine bacterial community composition in marine snow. *Appl. Environ. Microbiol.* 81, 1463–1471. doi:10.1128/AEM.02570-14.

Turner, J. T. (2015). Zooplankton fecal pellets, marine snow, phytodetritus and the ocean's biological pump. *Prog. Oceanogr.* 130, 205–248. doi:10.1016/j.pocean.2014.08.005.

Vernet, M., Richardson, T. L., Metfies, K., Eva-Maria Nöthig, and Peeken, I. (2017). Models of plankton community changes during a warm water anomaly in Arctic waters show altered trophic pathways with minimal changes in carbon export. *Front. Mar. Sci.* 4, 160.

doi:10.3389/fmars.2017.00160.
von Appen, W.-J., Waite, A. M., Bergmann, M., Bienhold, C., Boebel, O., Bracher, A., et al. (2021). Sea-ice derived meltwater stratification slows the biological carbon pump: results from continuous observations. *Nat. Commun.* 12, 1–16.
Walczowski, W., Beszczynska-Möller, A., Wieczorek, P., Merchel, M., and Grynczel, A. (2017). Oceanographic observations in the Nordic Sea and Fram Strait in 2016 under the IO PAN long-term monitoring program AREX. *Oceanologia* 59, 187–194. doi:10.1016/j.oceano.2016.12.003.
Wassmann, P., and Reigstad, M. (2011). Future Arctic Ocean seasonal ice zones and implications for pelagic-benthic coupling. *Oceanography* 24, 220–231. doi:10.5670/oceanog.2011.74.
Wekerle, C., Krumpen, T., Dinter, T., von Appen, W. J., Iversen, M. H., and Salter, I. (2018). Properties of sediment trap catchment areas in fram strait: Results from Lagrangian modeling and remote sensing. *Front. Mar. Sci.* 9, 407. doi:10.3389/fmars.2018.00407.
Weydmann, A., Carstensen, J., Goszczko, I., Dmoch, K., Olszewska, A., and Kwasniewski, S. (2014). Shift towards the dominance of boreal species in the Arctic: Inter-annual and spatial zooplankton variability in the West Spitsbergen Current. *Mar. Ecol. Prog. Ser.* 501, 41–52. doi:10.3354/meps10694.
Wickham, H., Averick, M., Bryan, J., Chang, W., McGowan, L., François, R., et al. (2019). Welcome to the Tidyverse. *J. Open Source Softw.* 4, 1686. doi:10.21105/joss.01686.
Wiedmann, I., Ershova, E., Bluhm, B. A., Nöthig, E.-M., Gradinger, R. R., Kosobokova, K., et al. (2020). What Feeds the Benthos in the Arctic Basins? Assembling a Carbon Budget for the Deep Arctic Ocean. *Front. Mar. Sci.* 7. doi:10.3389/fmars.2020.00224.
Wietz, M., Metfies, K., Bienhold, C., Wolf, C., Janssen, F., Salter, I., et al. (2022). Impact of preservation method and storage period on ribosomal metabarcoding of marine microbes: Implications for remote automated samplings. *Front. Microbiol.* 13. doi:10.3389/fmicb.2022.999925.
Wilson, B., Müller, O., Nordmann, E. L., Seuthe, L., Bratbak, G., and Øvreås, L. (2017). Changes in marine prokaryote composition with season and depth over an Arctic polar year. *Front. Mar. Sci.* 4, 95. doi:10.3389/fmars.2017.00095.
Wilson, J. M., Litvin, S. Y., and Beman, J. M. (2018). Microbial community networks associated with variations in community respiration rates during upwelling in nearshore Monterey Bay, California. *Environ. Microbiol. Rep.* 10, 272–282. doi:10.1111/1758-2229.12635.
Yilmaz, P., Kottmann, R., Field, D., Knight, R., Cole, J. R., Amaral-Zettler, L., et al. (2011). Minimum information about a marker gene sequence (MIMARKS) and minimum information about any (x) sequence (MIxS) specifications. *Nat. Biotechnol.* 29, 415–420.
Yoshimura, K., and Hama, T. (2012). Degradation and dissolution of zooplanktonic organic matter and lipids in early diagenesis. *J. Oceanogr.* 68, 205–214.
Zbinden, M., and Cambon-Bonavita, M.-A. (2003). Occurrence of Deferribacterales and Entomoplasmatales in the deep-sea Alvinocarid shrimp Rimicaris exoculata gut. *FEMS Microbiol. Ecol.* 46, 23–30.

Supplementary Material

Table S1. Data sets from sediment traps included in this study.

PANGAEA Station ID	Sed. trap ID	Sample depth (m)	Raw data PANGAEA DOI	Reference
PS57/273-1	FEVI1	280	https://doi.org/10.1594/PANGAEA.855463	(Bauerfeind et al., 2015a)
PS59/101-1	FEVI2	260	https://doi.org/10.1594/PANGAEA.855464	(Bauerfeind et al., 2015e)
PS62/179-2	FEVI3	280	https://doi.org/10.1594/PANGAEA.855465	(Bauerfeind et al., 2015i)
PS66/129-1	FEVI7	280	https://doi.org/10.1594/PANGAEA.855466	(Bauerfeind et al., 2015j)
PS68/263-1	FEVI10	179	https://doi.org/10.1594/PANGAEA.855467	(Bauerfeind et al., 2015b)
MSM2/787-1	FEVI13	230	https://doi.org/10.1594/PANGAEA.855468	(Bauerfeind et al., 2015c)
PS70/218-1	FEVI16	190	https://doi.org/10.1594/PANGAEA.879532	(Bauerfeind et al., 2017)
PS72/155-1	FEVI18	196	https://doi.org/10.1594/PANGAEA.855470	(Bauerfeind et al., 2015d)
PS74/125-2	FEVI20	80	https://doi.org/10.1594/PANGAEA.855471	(Bauerfeind et al., 2015f)
PS76/147-1	FEVI22	200	https://doi.org/10.1594/PANGAEA.855472	(Bauerfeind et al., 2015g)
PS78/177-1	FEVI24	200	https://doi.org/10.1594/PANGAEA.855473	(Bauerfeind et al., 2015h)

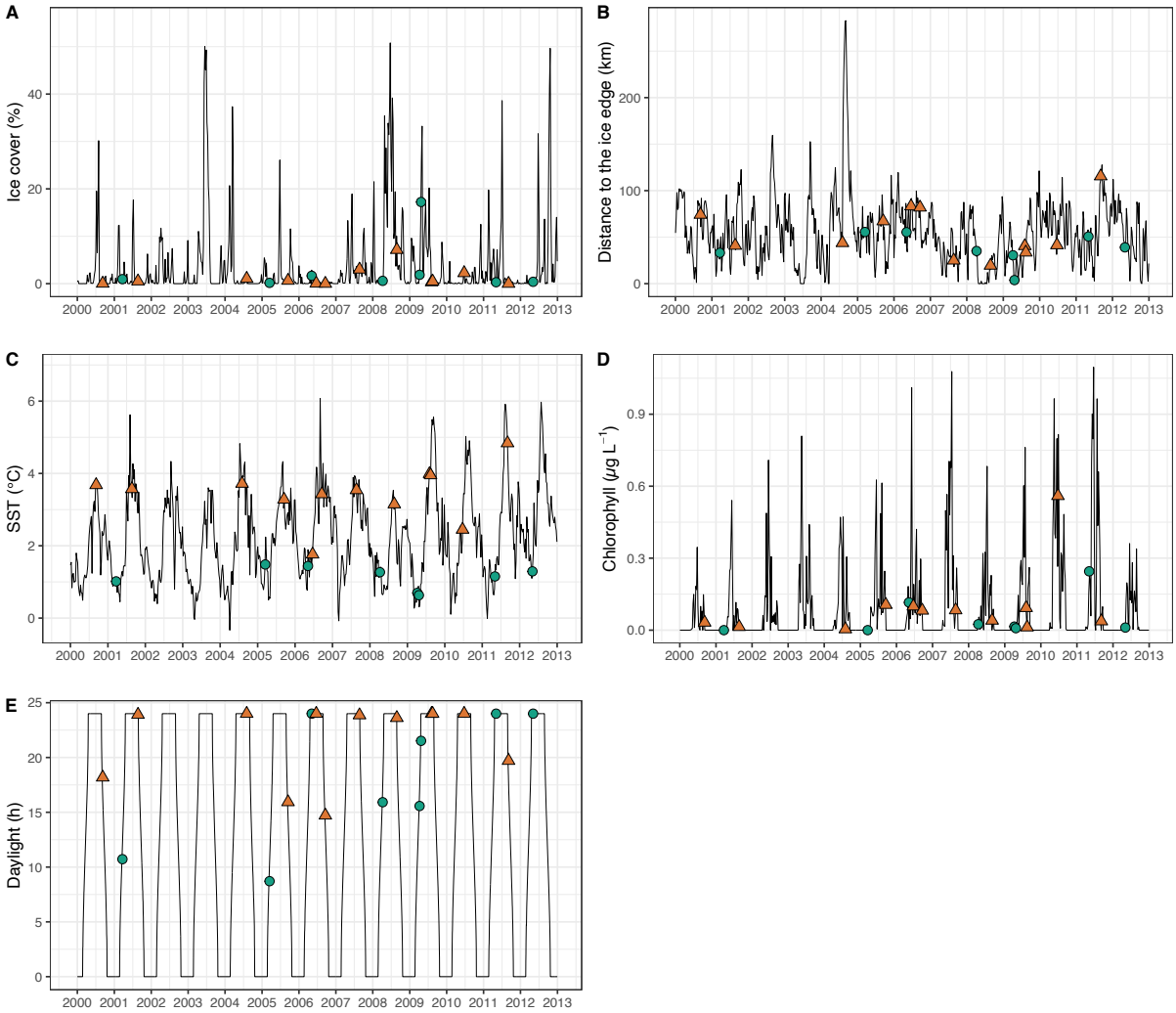

Figure S1. Time series of satellite-derived sea ice, temperature and chlorophyll measurements and daylight. (A) Ice cover (%). (B) Distance to the sea ice edge from the mooring position at the central HAUSGARTEN station (HGIV). The ice edge was defined as sea ice concentrations of at least 15%. (C) Sea surface temperature SST (°C). (D) Chlorophyll concentration (μgL^{-1}). Ice cover, SST and Chlorophyll values were obtained from remote sensing products and integrated over the sediment trap catchment area defined in a particle backtracking model from 200 m depth and with a sinking velocity of 60 m d^{-1} (Wekerle et al., 2018). (E) Daylight (h). Values are represented as 8-day means. The HPF corresponding values are noted by green circles for spring events and orange triangles for summer events. All HPF values were averaged across the opening times of the cups with a 4-day lag and plotted with to the middle sampling date.

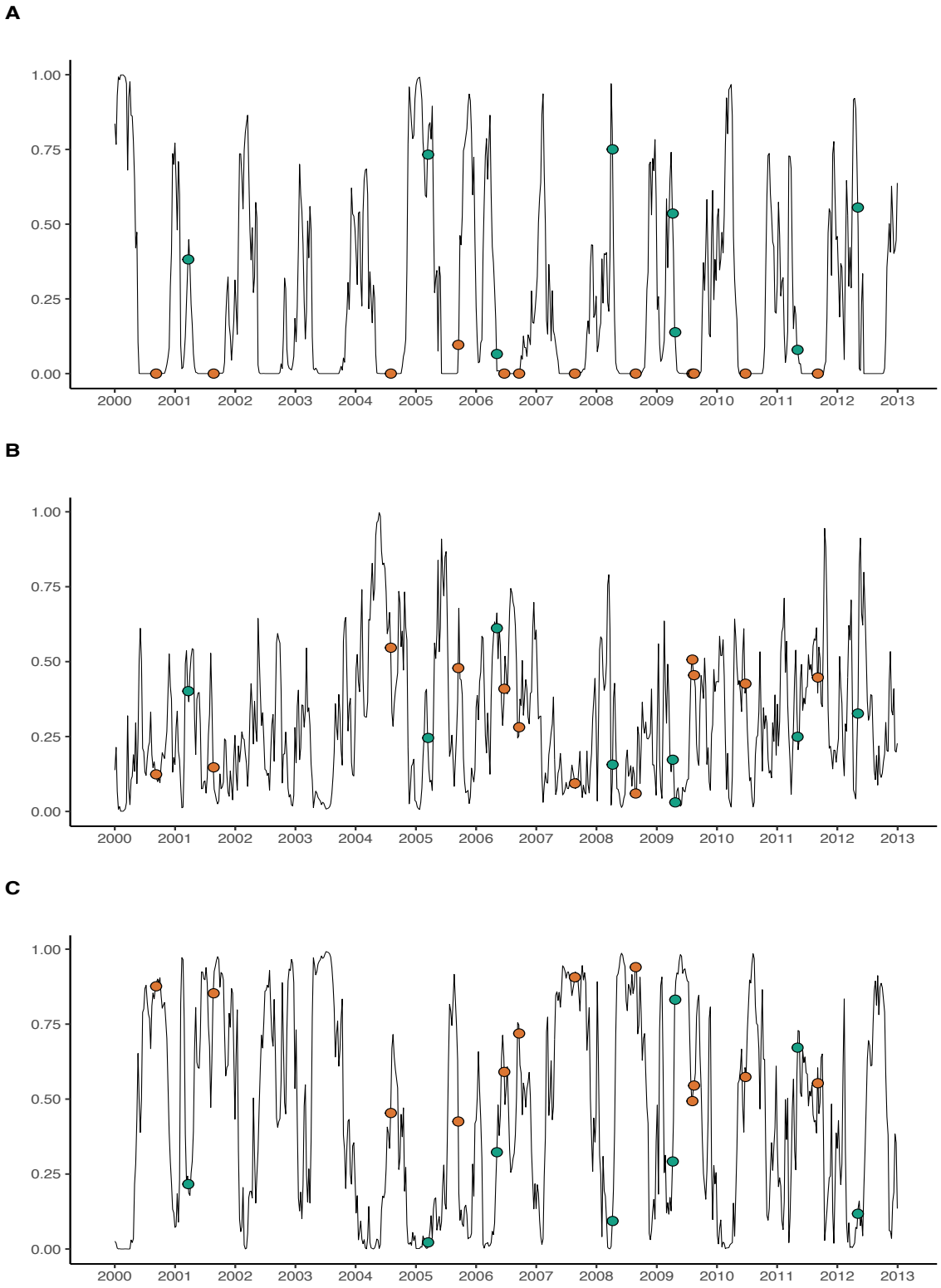

Figure S2. Water stratification regimes represented as proportions (y-axis) and calculated as 8-day means. The three regimes were computed from daily means and weighted with the particle distribution in the catchment area of the sediment traps. (A) Unstratified water described with a mixed layer >50 m. (B) Mixed layer (ML) regime with a mixed layer depth < 50 m and a salinity difference <1 between 100 m and the surface. (C) Meltwater regime (MW), with a mixed layer depth < 50 m and a strong salinity stratification between 100 m and the surface (salinity difference >1). The HPF are noted by green circles for spring events and orange triangles for summer events, and calculated as averages across the opening times of the cups with a 4-day lag.

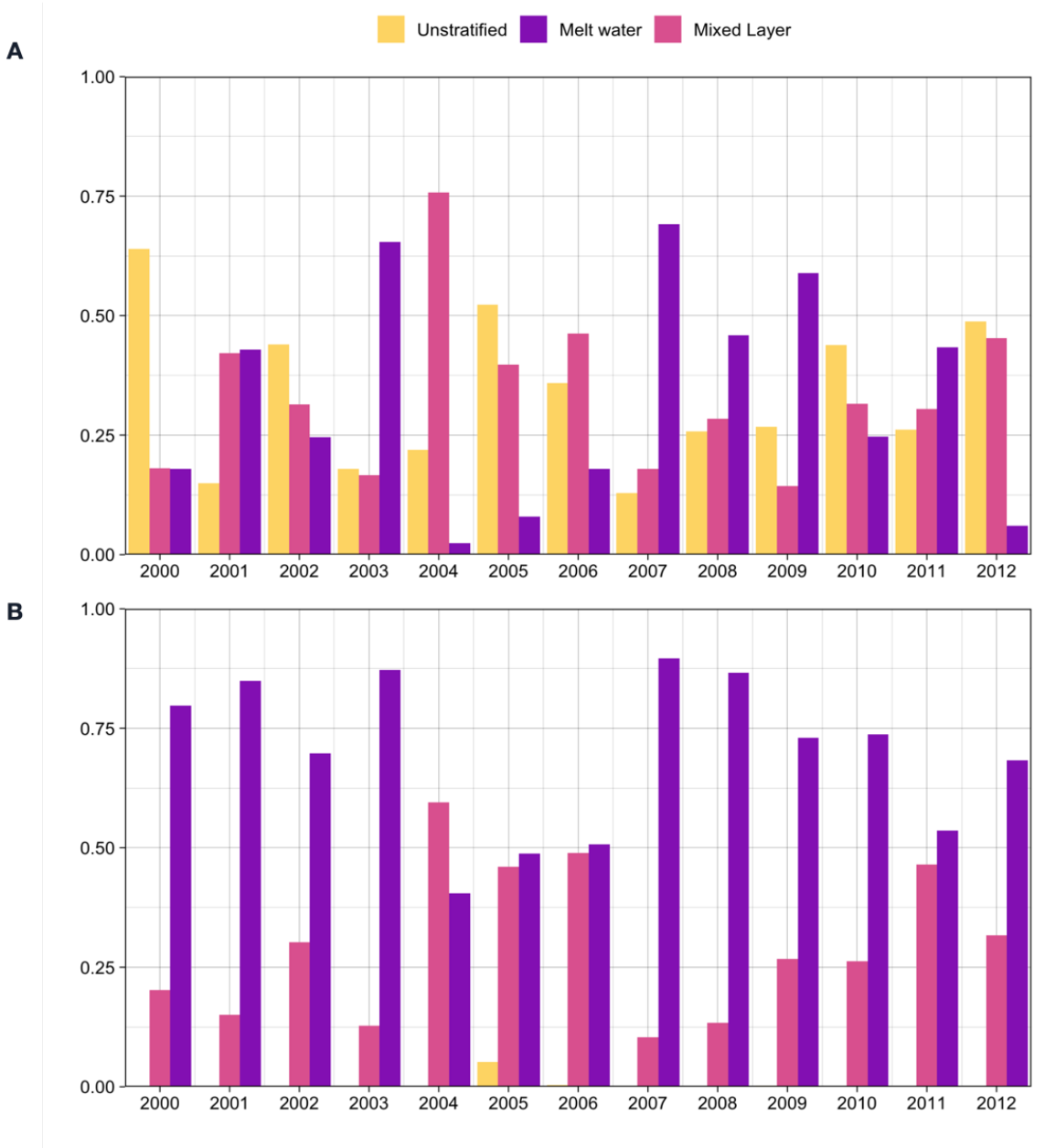

Figure S3. Proportional representation of stratification regimes (%) in (A) spring (March to May) and (B) summer (June to September).

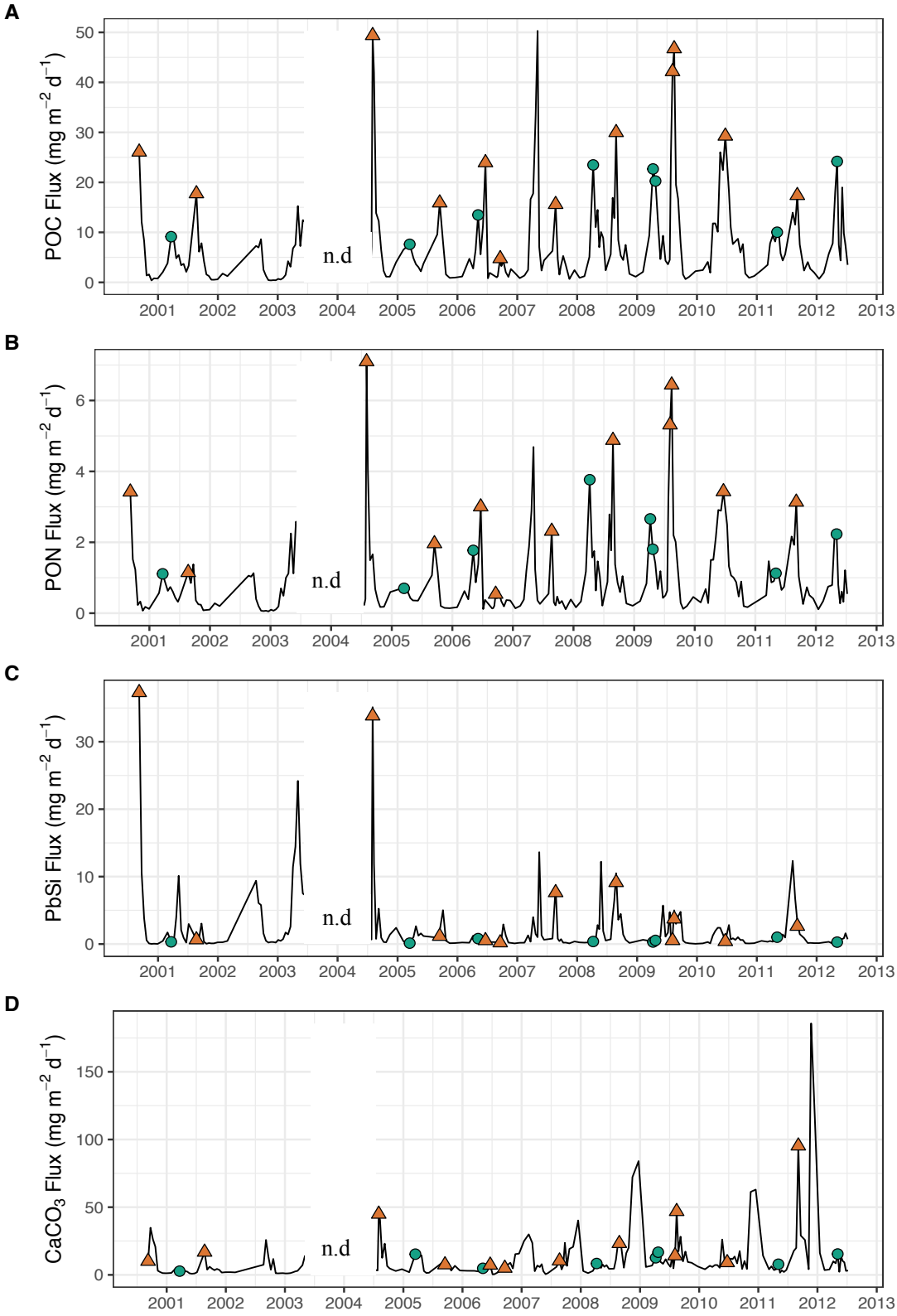

Figure S4. Time-series of export fluxes. (A) POC flux. (B) PON flux (C) PbSi flux. (D) $CaCO_3$ flux obtained from sediment traps deployed from 2000 to 2012. Empty spaces indicate mooring turnover periods. The peak POC values selected for this study are noted by green circles for spring and orange triangles for sumer events. n.d; Data not available.

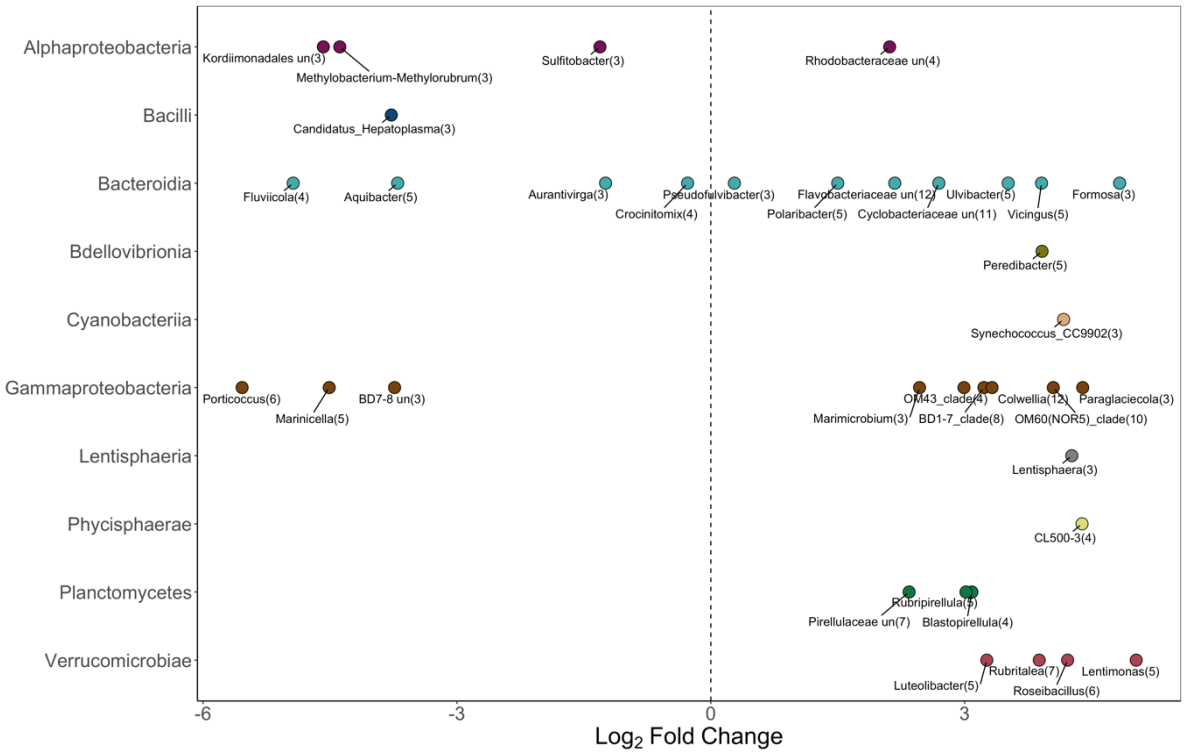

Figure S5. Differences in bacterial community composition between seasons as defined by stratification regimes in spring (March to May) and summer (June to September). The x-axis represents the mean log2 fold change for microbial genera with absolute log2 fold change values higher than 1. Positive values represent enrichment in summer events and negative value represents enrichment in spring events. Numbers indicate the number of enriched ASVs within the genera. The y-axis is labeled and ordered alphabetically by taxonomic classes.

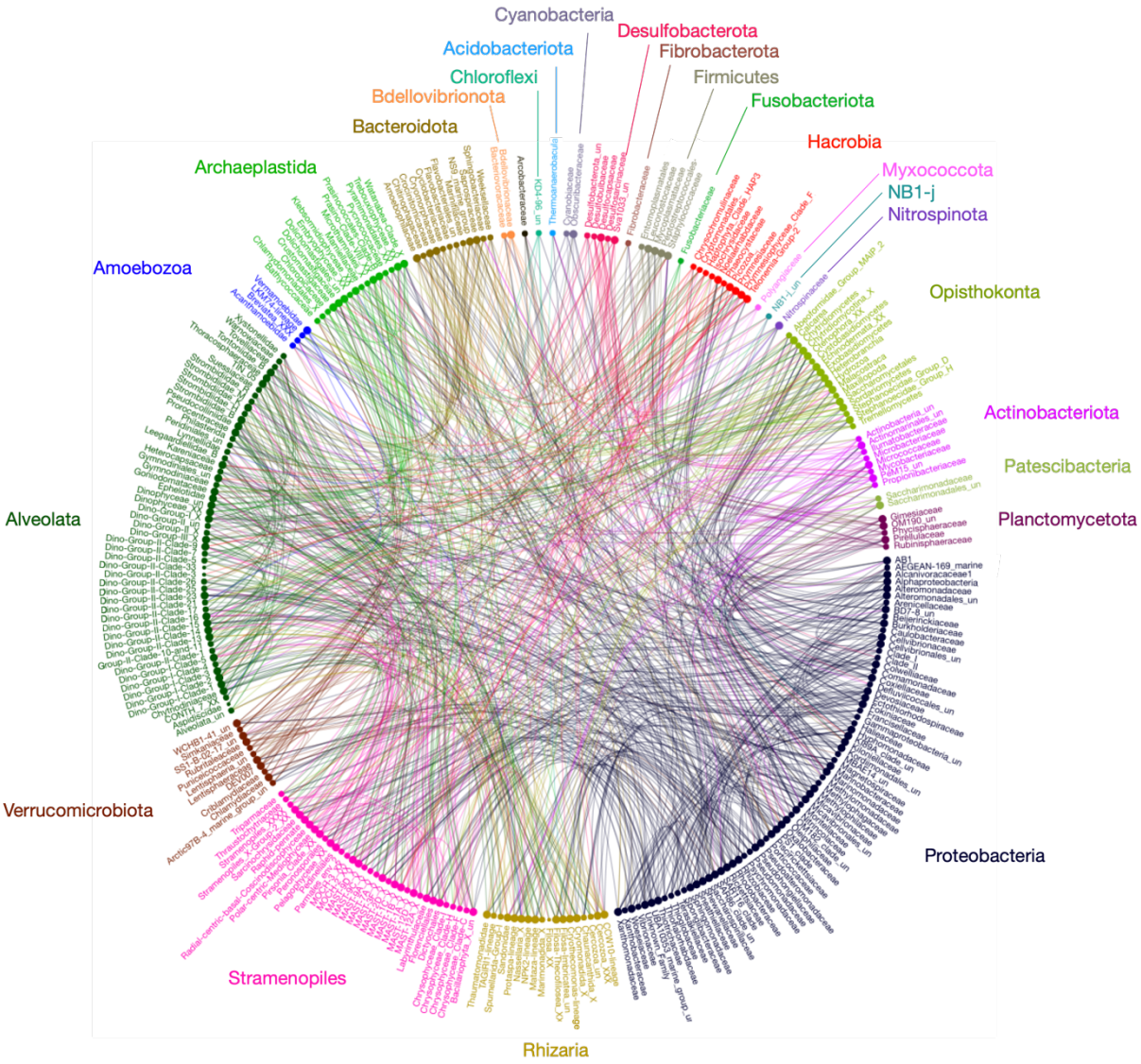

Figure S6. Microbial network showing associations between families reconstructed from samples of the first eukaryotic cluster (defined in Figure 3). The lines are edges representing associations between eukaryotic and bacterial families. Colors indicate nodes of bacteria phyla and eukaryotic supergroups.

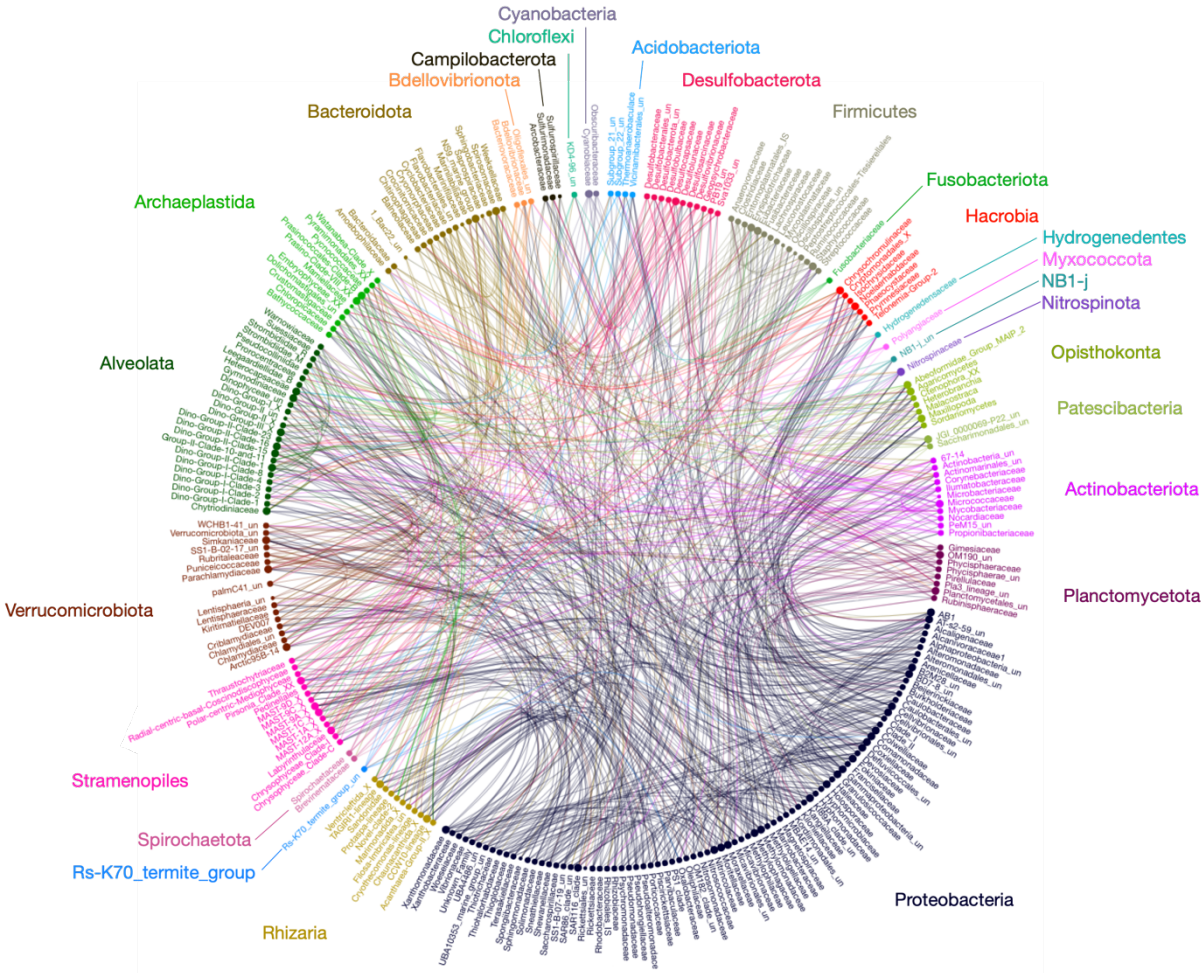

Figure S7. Microbial network showing associations between families reconstructed from samples of the second WWA eukaryotic cluster (defined in Figure 3). The lines are edges representing associations between eukaryotic and bacterial families. Colors indicate nodes of bacteria phyla and eukaryotic supergroups.

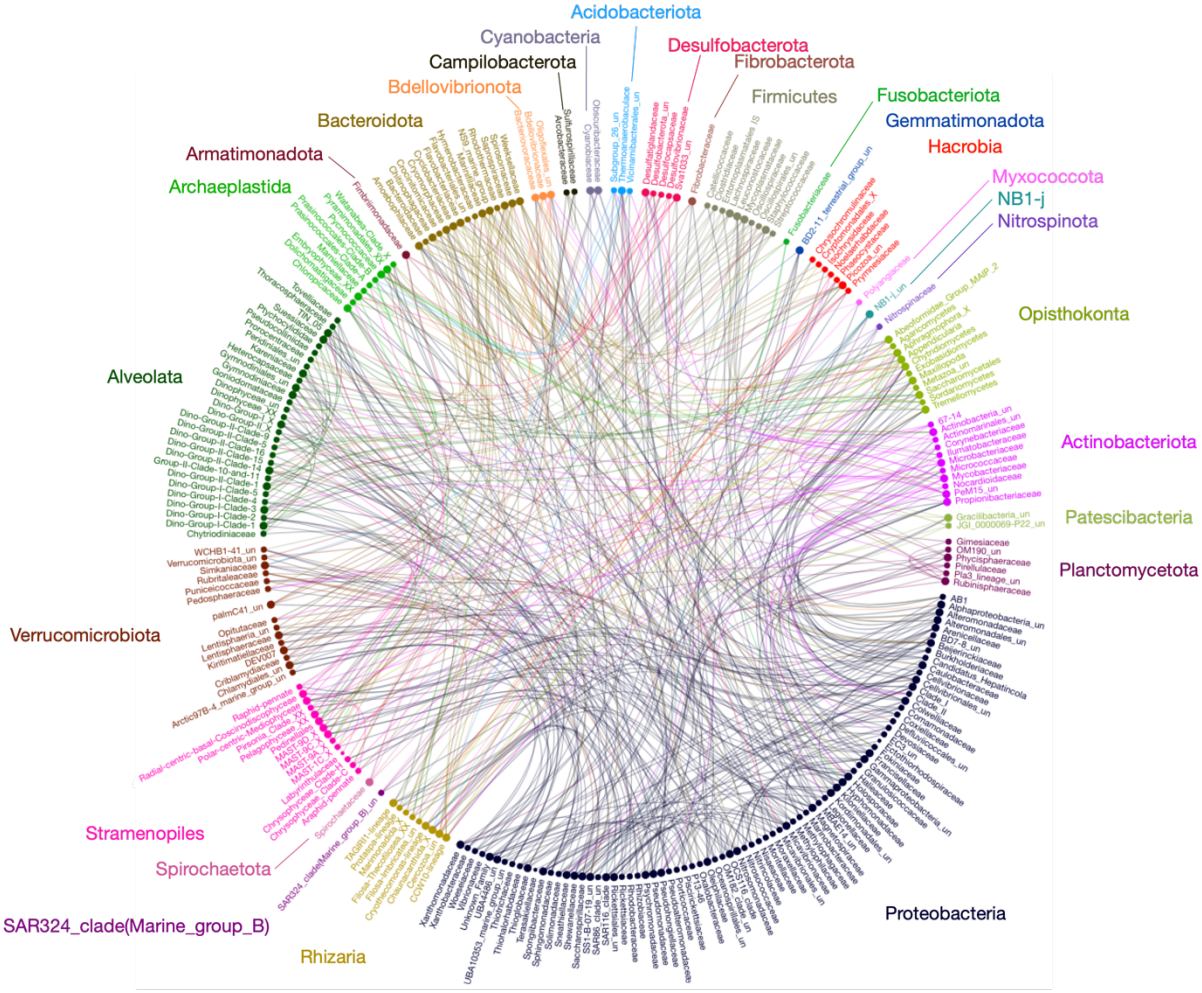

Figure S8. Microbial network showing associations between families reconstructed from samples of the third eukaryotic cluster (defined in Figure 3). The lines are edges representing associations between eukaryotic and bacterial families. Colors indicate nodes of bacteria phyla and eukaryotic supergroups.

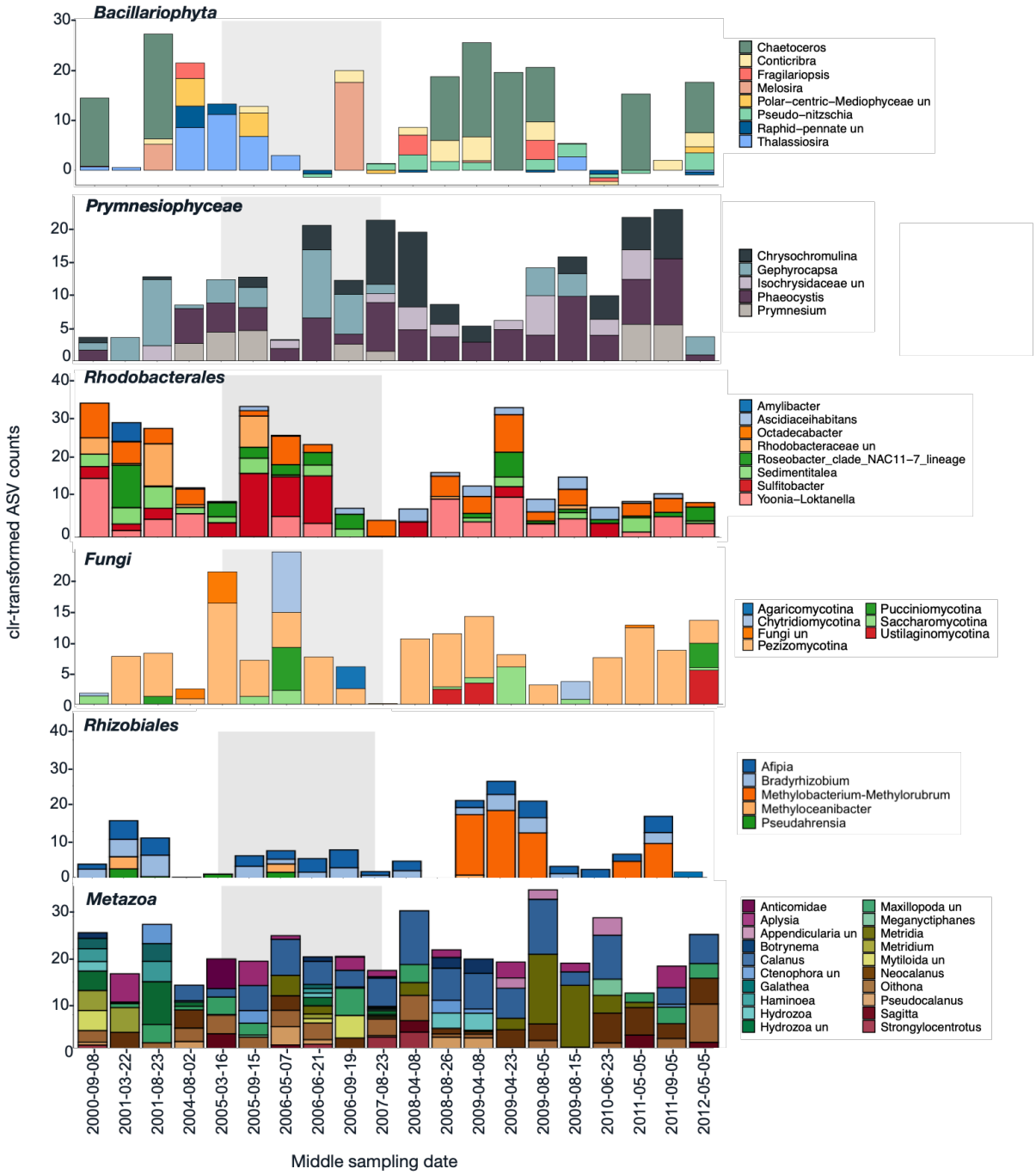

Figure S9. Changes in selected groups of eukaryotes and bacterial orders based on clr-transformed ASVs counts. Dates correspond to the middle sampling date. The light gray area indicates the WWA period from 2005 to 2007.

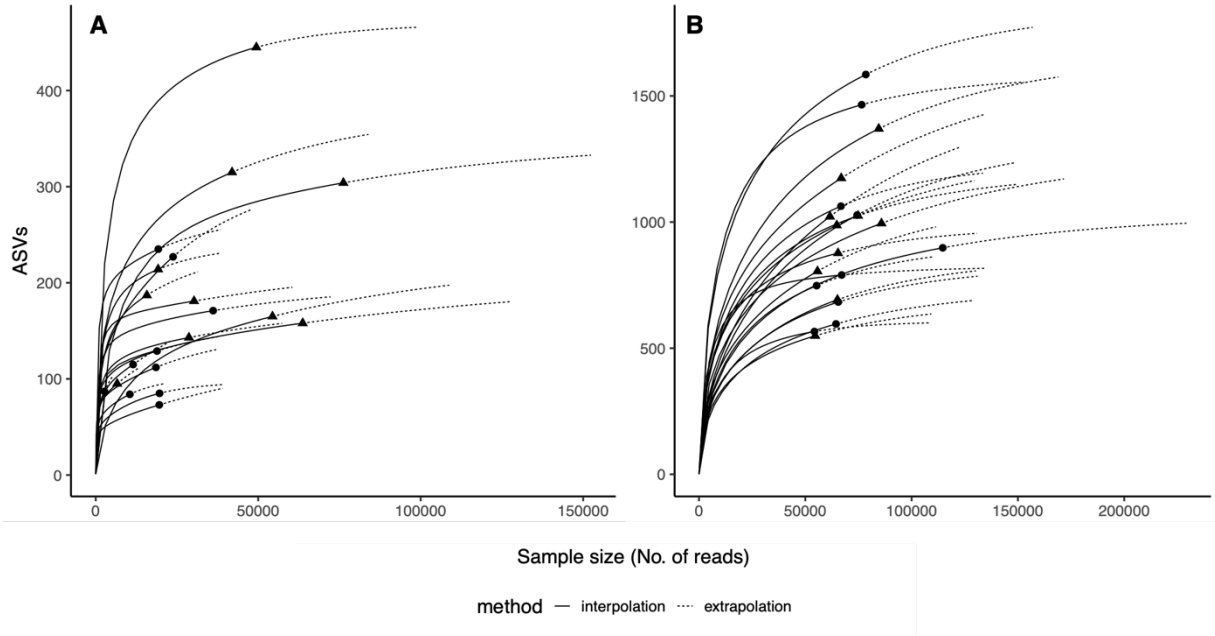

Figure S10. Rarefaction curves displaying the effect of sequencing depth on the recovery of ASVs for (A) eukaryotic and (B) bacterial communities. Solid lines indicate the observed interpolation of the number of reads sampled and dashed lines indicate the extrapolated accumulation up to the double amount of reads. The curves were calculated based on the Hill number of order q = 0 and with 100 iterations with the R-package "iNEXT" (Hsieh et al., 2016). The observed values are noted by solid shapes for spring (circles) and summer (triangles).

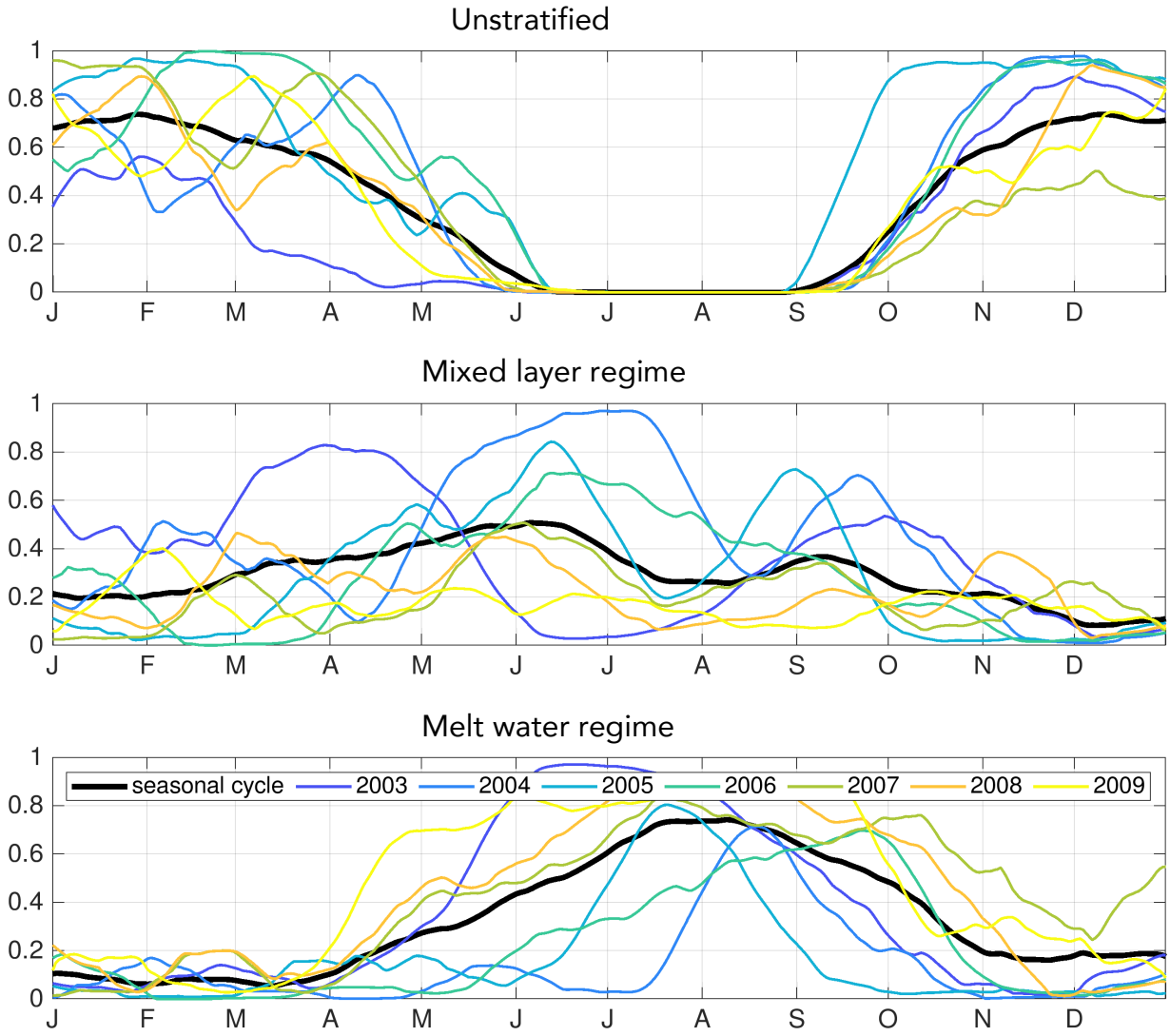

Figure S11. Year progression of water regimes from 2003 to 2009.

Chapter IV

Ice-seawater connectivity of eukaryotes, bacteria and metabolites

Magda G. Cardozo-Miño [1,2,3] *Julian Merder*[4], *Silvia Vidal-Melgosa*[1,5], *Katja Metfies*[2], *Thorsten Dittmar*[6,7], *Jan-Hendrik Hehemann*[1,5], *Antje Boetius*[1,2,5], *Matthias Wietz*[1,2]

[1]Max Planck Institute for Marine Microbiology, Bremen, Germany
[2]Alfred Wegener Institute, Helmholtz Center for Polar and Marine Research, Bremerhaven, Germany
[3]Faculty of Geosciences, University of Bremen, Bremen, Germany
[4]Department of Global Ecology, Carnegie Institution for Science, Stanford, CA, United States of America
[5]MARUM, University of Bremen, Bremen, Germany
[6]Marine Geochemistry (MPI-ICBM Bridging Group), Institute for Chemistry and Biology of the Marine Environment, University of Oldenburg, Oldenburg, Germany
[7]Helmholtz Institute for Functional Marine Biodiversity at the University of Oldenburg, Oldenburg, Germany

Keywords: Arctic Ocean, Fram Strait, Sea ice, Seawater, Microcosm, DOM, Amplicon sequencing, FT-ICR-MS

Publication in preparation.

Abstract

The changing Arctic sea ice following climate change affects the microbial communities inside sea ice and in the underlying seawater. Here, we performed a microcosm experiment in Fram Strait to track microbial and chemical patterns during ice melt. Amplicon sequencing of 18S and 16S rRNA genes elucidated eukaryotic and bacterial communities in different size fractions, and how these communities changed as sea ice melted in seawater. *Chloropicales*, *Mamiellales*, unclassified *Bacillariophyta* and *Dictyochophyceae* were the most abundant eukaryotic orders in seawater (SW) and seawater control (SW-ref). Bacterial communities were dominated by the orders *Flavobacteriales* (class *Bacteroidia*), *Rhodobacterales* (class *Alphaproteobacteria*). Our results indicated the potential seeding of diatoms and connecting taxa between seawater and ice, mainly *Attheya*, *Chaetoceros*, *Naviculales* and *Cylindrotheca* and identified members of the *Flavobacteriales* appear to follow the seeding of diatoms. We identified bacterial taxa known for their ability to degrade of complex compounds of the *Rhodobacterales* and *Verrucomicrobiales* to be abundant in ICE-ref and ICE samples compared to SW samples. Mainly *Octadecabacter, Yoonia-Loktanella* and *Rubritalea*. Furthermore, the prevalence of molecular formulae of aliphatic compounds in the ICE-ref coincided with the enrichment of hydrocarbon-degrading bacteria mainly *Glaciecola* (*Alteromonadales*), *Oleispira* and *Oleiphilus* (*Oceanospirillales*) suggesting a linkage to substrate provision from the ice reflected by DOM signatures. Overall, our study shows that an "ice signature" can be found in the surrounding seawater during melt, indicating a distinct microbial and chemical connectivity with potential implications for the biological carbon pump. These processes might amplify in the warming Arctic, with yet unknown consequences for local and regional ecosystem functioning.

Introduction

The Arctic Ocean is undergoing rapid changes in water temperature and in the extent, concentration and thickness of sea ice (Polyakov et al., 2017; Peng and Meier, 2018; Dai et

al., 2019; Lannuzel et al., 2020; Lin et al., 2022). Overall, sea ice regimes increasingly shift from thick multi-year ice (MYI) to thinner first-year ice (FYI) (Stroeve and Notz, 2018; Lin et al., 2022). This shift from MYI to FYI will likely amplify in the coming years (AMAP, 2017), with ice-free summers predicted to occur within the next decades (Wang and Overland, 2012; Notz and Community, 2020; Docquier and Koenigk, 2021). These changes have profound implications for biological, chemical and physical processes across regions and ecosystem compartments (Arrigo et al., 2012; Nöthig et al., 2015; Lewis et al., 2020). Sea ice provides a habitat for sympagic communities, including algae (diatoms), bacteria, archaea and viruses (Deming and Eric Collins, 2017), heterotrophic protists, and meiofauna including copepods and ciliophores and nematods (Arrigo, 2014; Thomas, 2017; Bluhm et al., 2018). Thickness and physical changes of the sea ice will affect light availability and primary production in the sea ice and underlying seawater (Nicolaus et al., 2012), with consequences for trophic interactions, bloom dynamics and zooplankton migration (Richardson, 2008; Castellani et al., 2022; Ramondenc et al., 2022). Several studies have addressed the microbial composition of sea ice (Boetius et al., 2015; Fernández-Méndez et al., 2016; Metfies et al., 2016; Rapp et al., 2018) and seawater in the Arctic Ocean (Sherr et al., 2003; Pedrós-Alió et al., 2015; Wilson et al., 2017; Fadeev et al., 2018; Wietz et al., 2021), but how changes in sea ice cover and hydrography will affect microbiome dynamics at the sea ice-seawater interphase remains to be explored. Likewise, substrate regimes will presumably be affected. Organic matter in sea ice originates from autochthonous algal and bacterial production, as well as from allochthonous origin during ice formation (Stedmon et al., 2007; Underwood et al., 2010; Aslam et al., 2012; Müller et al., 2013). Sea ice can contain elevated organic carbon concentrations in the form of EPS and dissolved carbohydrates (dCHO), amino acids, proteins and humic substances (Thomas et al., 2010).

An important aspect is the biological and chemical connectivity of sea ice and the underlying seawater, and how these dynamics change during melt. Melting ice can result in the release of large algal aggregates and particulate organic matter and small metabolites (Underwood et al., 2010; Boetius et al., 2013; Lalande et al., 2019), mediating organic matter export from the sea ice-water interface to the deep sea (Palmisano and Garrison, 1993; Lizotte, 2003; Bowman, 2013). Sea ice cover and primary productivity can modulate the composition of DOM of porewater in central Arctic sediments (Rossel et al., 2016) and in Fram Strait

sediment (Rossel et al., 2020), influencing the activity and structure of benthic communities (Bienhold et al., 2012; Jacob et al., 2013). These processes are shaped via microbial metabolic activities, e.g. bacterial transformations of carbon synthesized by sympagic sea ice algae and subsequent effects on higher trophic levels (Azam and Malfatti, 2007).

Bacteria utilize and convert dissolved organic matter (DOM) derived from photosynthesis, extracellular polymeric substances (EPS), or from grazing and lysis. In turn, bacteria can support primary producers by the provision of nutrients (Simon et al., 2002; Azam and Malfatti, 2007; Grossart and Simon, 2007). Microcosm experiments demonstrated close coupling between sea-ice bacteria and algae (Martin et al., 2012). Moreover, Arctic sea-ice DOM stimulates under-ice microbial activity (Niemi et al., 2014), creating distinct ecological niches for bacterial taxa relating to specific DOM fractions (Underwood et al., 2019). However, it remains unknown to what extent sea-ice associated organisms "inoculate" the underlying water during ice melt, and how the ambient seawater community responds to such events.

The continuing decline in sea ice and the inflow of warmer Atlantic water will have a strong impact on the composition, diversity and abundance of the sympagic eukaryotic and bacterial communities, with consequences for the composition and quantity of organic matter exported to the deep sea. Therefore, monitoring microbial responses is crucial to understanding the ecological effects of changing ice regimes.

The East Greenland Current (EGC) in the western part of Fram Strait carries sea-ice and cold Polar Water out of the central Arctic, meeting the warmer Atlantic Water from the West Spitsbergen Current (WSC) in the marginal ice zone (MIZ). The MIZ is characterized by variable sea ice conditions that influence the timing and composition of phytoplankton blooms (Soltwedel et al., 2016), and associated bacterial communities (Fadeev et al., 2018; von Appen et al., 2021). Shifting sea-ice conditions amplified by increasing Atlantic water inflow, termed Atlantification (Polyakov et al., 2017), are expected to lead to changes in species composition (Nöthig et al., 2015; Ramondenc et al., 2022) and deep-sea carbon export (Lalande et al., 2013; Fadeev et al., 2021).

The present study addressed the connectivity between microbial communities in sea ice and surrounding water at the end of the ice life cycle, when exiting Fram Strait after its pan-Arctic transport. We sampled bottom sea ice and surface seawater at the MIZ of Fram Strait at the Long-Term Ecological Research site HAUSGARTEN, and monitored microbial and chemical signatures during ice melt in a microcosm experiment on-board R/V Polarstern. Through amplicon sequencing, high-performance liquid chromatography of carbohydrates and ultrahigh resolution screening of dissolved organic matter, we elucidated how seawater microbiomes change upon ice melt, and how sea ice microbiomes react when suddenly exposed to water through ice melt. We hypothesized 1) a significant separation of microbial communities by size class, 2) that sea ice melt coincides with specific bacterial community signatures - either "inoculated" from the ice core, or "water bacteria" that respond to ice substrates, and 3) that bacterial dynamics might be a response to ice-derived metabolites or substrates.

Materials and Methods

Site description and sample collection

As part of the HAUSGARTEN / FRAM (Frontiers in Arctic Marine Monitoring) Molecular Observatory framework, sea ice cores were obtained during RV Polarstern expedition PS121 (10th August – 13th September 2019) from the marginal ice zone (MIZ) in Fram Strait (80°19.15' N, 001°19.85' E) (Figure 1A). Cores were obtained from a snow-covered floe with visible formations of refrozen water, likely related to summer melt ponds which were also observed in the sea ice cores (Figure 1B). Using a 9 cm diameter ice corer (Kovacs, Roseburg, OR, USA) and an electric hand drill (Makita, Japan), 18 ice cores were extracted and placed on a barrel rinsed with 70% ethanol. The cores were immediately sectioned with a hand saw previously cleaned with 70% ethanol, and the lower 20 cm section stored in Nasco Whirl-Pak sterile sampling bags with puncture proof tabs (Nasco, Fort Atkinson, WI, USA). Ice cores were transported to the shipboard lab in cooling boxes. Seawater was sampled from 10 m depth at a nearby station (about 189 nautical miles) a day before (79°43.98' N, 004°28.29' E) using 12 L Niskin bottles mounted on a CTD rosette (Sea-Bird Electronics Inc. SBE 911 plus probe).

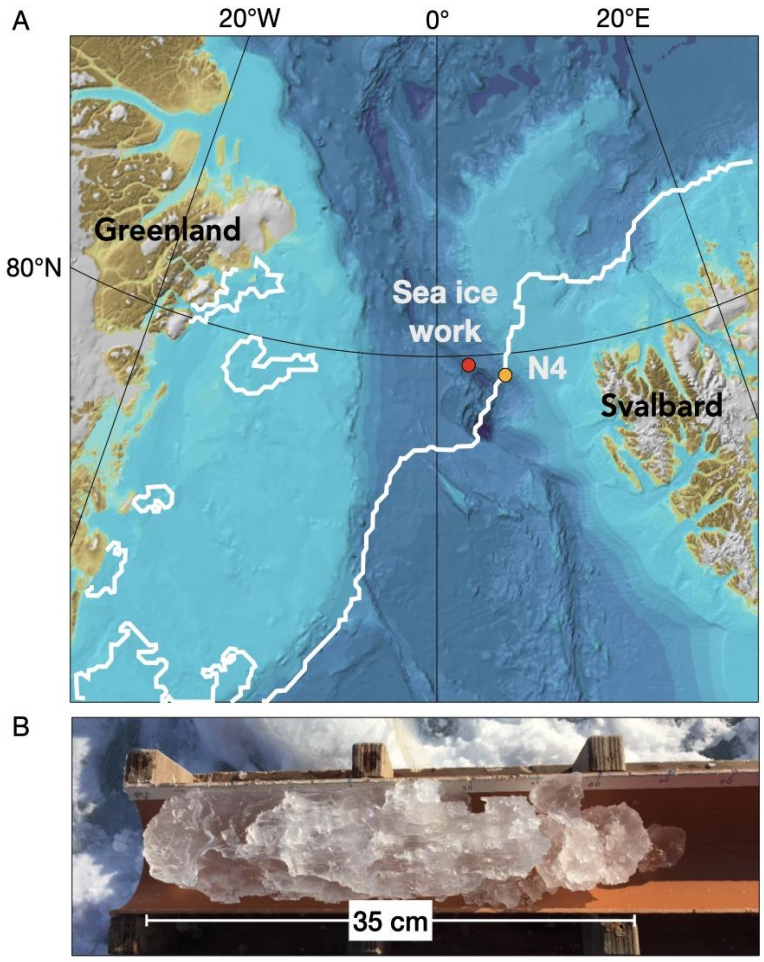

Figure 1. (A) Map of the Fram Strait area depicting the sampling locations of sea ice (80°19.15′ N, 001°19.85′ E) and seawater (station N4; 79°43.98′ N, 004°28.29′ E). The median ice edge in August 2019 is depicted by the white line. The map was created using ArcGIS based on the International Bathymetric Chart of the Arctic Ocean (IBCAO) Version 3.0 (Jakobsson et al., 2012). Sea ice data was exported from maps produced by AWI: https://maps.awi.de (Grosfeld et al., 2016). (B) Appearance of the lower section of a representative sea ice core.

Experimental set-up

On board the research vessel, sea ice sections were immersed in 20 L plastic canisters (Nalgene, Rochester, NY, USA) previously rinsed with filtered seawater, and filled with 20 L of reference seawater (Figure S1). Seawater controls without sea ice (SW) and ice-melt set ups (ICE) were kept in a dark cold container at 1 – 2 °C as close as possible to the in-situ temperature (Metfies et al., 2021). Incubation was conducted in a dark container to simulate the early low light conditions in autumn at the beginning of the Polar night characterized by shorter daylight hours (< 20 h) and when the sea ice experiences melting periods and re-forms later in autumn (Stroeve and Notz, 2018). The experimental regimes were compared to seawater and ice reference samples. Sea ice core sections were used as reference (ICE-

ref), and kept at 4 °C until melted (4 days), then filtered onto through 3 µm and 0.2 µm 47 mm Nucleopore polycarbonate Track-Etch filters (Whatman, Buckinghamshire, UK). 2 L of the original seawater (see above) was directly filtered onto 0.22 µm Sterivex membranes (SW-ref), and stored at -80 °C until further processing.

DNA extraction and Illumina amplicon sequencing

Per sampling event, 2 L were withdrawn taken from the canisters after vigorous shaking, then sequentially filtered through 3 µm and 0.2 µm 47 mm Nucleopore polycarbonate Track-Etch filters (Whatman, Buckinghamshire, UK). Filters were placed in sterile 2 mL microcentrifuge cups (Eppendorf, Hamburg, Germany), flash-frozen in liquid nitrogen and stored at -80 °C until DNA extraction in the home lab. DNA was isolated using the DNeasy PowerWater kit (QIAGEN, Hilden, Germany) following the manufacturer's protocol. For this, filters were cut into smaller pieces with a sterile scalpel and placed into the PowerWater Bead Tubes. Sterivex cartridges (SW-ref) were cracked open in order to place the filters into the kit-supplied tubes. DNA was quantified using a Quantus Fluorometer (Promega, Madison, WI, USA) and stored at -20 °C.

Library preparation was performed according to the 16S Metagenomic Sequencing Library Preparation protocols (Illumina, San Diego, CA, USA). The hypervariable V4 – V5 region of bacterial 16S rRNA genes was amplified using the 515F-Y (5'-GTGYCAGCMGCCGCGGTAA-3') and 926R (5'-CCGYCAATTYMTTTRAGTTT-3') primer pair (Parada et al., 2016). For 18S rRNA amplicon sequencing, the V4 region of the 18S rDNA gene was amplified with the 528iF (5'-GCGGTAATTCCAGCTCC-3') (Elwood et al., 1985) and 964iR (5'-AC TTTCGTTCTTGATYRR-3') primer pair (Onda et al., 2020). Amplicons were sequenced at AWI using the Illumina MiSeq platform to obtain 2 × 300 bp paired-end reads.

Bioinformatic analysis

Primers from paired-end reads were removed with Cutadapt (Martin, 2011). Subsequently, DADA2 v. 1.164.1 (Callahan et al., 2016) was used in R v. 4.2.1 (www.r-project.org) in RStudio v. 2022.07.1 following the suggested workflow (https://benjjneb.github.io/dada2/tutorial.html) to generate amplicon sequence variants

(ASVs). Briefly, after quality trimming and filtering of reads, dereplication was used to identify unique sequences and determine their abundance. The output of the dereplication and the error model were fed into the subsequent denoising step to resolve ASVs of up to one nucleotide difference using the quality score distribution in a probability model. Chimeras and singletons were filtered out. 16S and 18S rRNA taxonomies were assigned using the Silva v 138 (Quast et al., 2013), and PR2 v. 4.12.0 (Guillou et al., 2013) databases respectively. ASVs unclassified at the kingdom level were removed. ASVs classified as *Mitochondria*, *Chloroplast*, and *Metazoa* were removed. ASVs affiliated with, *Propionibacteriales*, *Corynebacteriales*, *Anaerobacillus*, *Staphylococcales*, *Clostridiales*, and *Enterobacterales* were considered as human contaminants, and were removed from the dataset.

Sample data matrices were handled with the R-package "phyloseq" v. 1.41.0 (McMurdie and Holmes, 2013). Alpha-diversity was analyzed using the R-packages "phyloseq" and "iNEXT" v. 2.0.20 (Hsieh et al., 2016). Beta-diversity analyses were performed after removing ASVs appearing in < 1% of samples. Community composition was visualized using the R-package "ampvis2" v. 2.7.24 (Andersen et al., 2018).

Catalyzed reported deposition-fluorescence in situ hybridization (CARD-FISH) and cell counting

50 ml samples were withdrawn from ICE and SW and at the first sampling point (15 h) and after melting (48 h), and from ICE-ref after melting of the and immediately fixed with formalin in a final concentration of 2% for 10 – 12 hours, then filtered onto 0.2 µm Nucleopore polycarbonate Track-Etch filters (Whatman, Buckinghamshire, UK) and stored at -20 °C until cell staining and enumeration at the home lab.

CARD-FISH was applied based on the protocol established by (Pernthaler et al., 2002) and described for Arctic communities described in (Cardozo-Mino et al., 2021), using horseradish-peroxidase (HRP)–labelled oligonucleotide probes for *Bacteria* (EUB338 I, EUB338 II, EUB338 III described in (Cardozo-Mino et al., 2021)) (Biomers.net, Ulm, Germany). All filters were embedded in 0.2% low-gelling-point agarose, and treated with 10 mg mL^{-1} lysozyme solution (Sigma-Aldrich Chemie, Hamburg, Germany) for 1 h at 37 °C. Endogenous peroxidases were

inactivated by submerging the filter pieces in 0.15% H_2O_2 in methanol for 30 min before rinsing in Milli-Q water and dehydration in 96% ethanol. Then, the filters were covered in hybridization buffer and the probes for enumerating *Bacteria* in a concentration of 0.2 ng μL^{-1}. Hybridization was performed at 46 °C for 2.5 h, followed by washing in pre-warmed washing buffer at 48 °C for 10 min, and 15 min in 1x PBS. Signal amplification was carried out for 45 min at 46 °C with amplification buffer containing either tyramide-bound Alexa 488 (1 µg mL^{-1}). Cells were counterstained in 1 µg mL^{-1} DAPI (4',6-diamidino-2-phenylindole; Thermo Fisher Scientific, Germany) for 10 min at 46 °C. After rinsing with Milli-Q water and 96% ethanol, the filter pieces were embedded in a 4:1 mix of Citifluor (Citifluor Ltd, United Kingdom) and Vectashield (Vector Laboratories, Burlingame, CA, United States), and stored overnight at -20 °C. The filters were evaluated microscopically and cell counting was performed under a Zeiss Axio Imager.Z2 stand (Carl Zeiss MicroImaging, Jena, Germany). Total bacterioplankton cells were determined as the total amount of DAPI-stained cells. Counts for *Bacteria* included only cells that were simultaneously stained by DAPI and the taxa-specific FISH probe.

Molecular analysis of DOM via FT-ICR-MS

Per sampling event, duplicates of 50 mL were withdrawn from ICE and SW, SW-ref and after melting of ICE-ref and filtered using a GFF filter (Sigma-Aldrich, Hamburg, Germany) previously rinsed with ultrapure C-clean water. Two subsamples were filtered per replicate. Samples were acidified to pH 2 with 130 µl HCl (25 %) and kept at 4 °C in the dark until further processing at the home lab. Prior to FT-ICR MS analysis, samples were mixed in a solution of methanol and ultrapure water (50:50 v/v). Samples were adjusted to a final concentration of 2.5 ppm of DOC. Mass spectrometric analysis of DOM extracts was performed via FT-ICR MS on a 15 T solariX XR Fourier-transform ion cyclotron resonance mass spectrometer (Bruker Daltonik, Bremen, Germany) and equipped with an electrospray ionization source (ESI, Bruker Apollo II) applied in negative ionization mode. Once spectrum consisted of 200 scans with an accumulation time of 0.1 s recorded with a mass range of m/z 92-2000 Da. Data was processed using the software ICBM-OCEAN to assign molecular formulas and remove contaminants (Merder et al., 2020).

Quantification of monosaccharides with HPAEC-PAD

Only the ICE-ref samples and ICE samples at 15 h were successfully measured and used to set a baseline for sea ice sugar content. Duplicates of 50 mL samples were taken and kept at -20 °C. Prior to performance anion exchange chromatography (HPAEC), samples were thawed at room temperature and each 150 µL acid-hydrolyzed at 100 °C for 24 h with 150 µL of 2 M HCl (7647-01-0, Analar Normapur) in pre-combusted glass vials (400 °C, 4 h). Monosaccharides were quantified based on the protocol from (Vidal-Melgosa et al., 2021). Monosaccharide standards were used to identify peaks by retention time. A standard mix (1–10 to 1000 µg L^{-1}) was used to quantify the amount of monosaccharide (x axis amount and y axis peak area).

Statistical analyses

All statistical analyses and calculations were performed using R v. 4.2.1 in RStudio v. 2022.07.1. Statistical tests for normality and significance were performed with the R-package vegan v. 2.6-2 (Oksanen et al., 2013). Plots were generated using the R-package ggplot2 v3.3.2 (Wickham, 2016) and tidyverse v1.3.2 (Wickham et al., 2019).

Results and Discussion

Environmental conditions of the ice core, salinity and cell counts

Extracted ice cores had a length > 2 m, i.e. constituted MYI (Eicken et al., 1995). Larger brine channels and clear crystals, including some slushy layers, indicated meltwater infiltration and refreezing since we sampled in September during the minimum sea ice extent. The bottom 20 cm of the cores also lacked visible presence of sea ice algae (Figure 1B).

Total cell abundance (i.e. all DAPI-stained cells) in the original sea ice (ICE-ref) were 5.9×10^5 cells mL^{-1}, lower than reported for algal-band ice samples (Junge et al., 2002) but within range of MYI and FYI samples (Hatam et al., 2014) (Table 1). *Bacteria* cell abundance in ICE-ref was 3.6×10^5 cells mL^{-1}. In ICE samples, total cell abundance remained constant at 15 h and at 48 h, as well as in SW samples (range: 1×10^6 cells mL^{-1}). Similarly, *Bacteria* cell abundance

varied little throughout the incubation time (range: 1 – 6 $\times 10^6$ cells mL^{-1}) in ICE and SW. However, the contribution of *Bacteria* to total cells was higher in SW samples (71 – 77 %) than in ICE 15 h and ICE-ref samples (62 – 73 %) likely due to the higher presence of eukaryotic cells in bottom sea ice compared to the surface water (Bowman, 2013).

Table 1. Average cell abundances in the sea ice and water samples obtained at the first sampling point (15 h) and at the end (48 h) of the experiment. The DAPI counts represent total cell abundance (all DAPI-stained cells). The proportions (%) *Bacteria* (EUB) were calculated based on the total cell abundances (DAPI stained cells).

Sample	Sampling time (h)	DAPI	Bacteria	%
ICE	15	9.8×10^6 cells mL^{-1}	6.3×10^5 cells mL^{-1}	62.5
ICE	48	1.2×10^6 cells mL^{-1}	8.9×10^5 cells mL^{-1}	72.8
SW	15	1.1×10^6 cells mL^{-1}	8.1×10^5 cells mL^{-1}	71.1
SW	48	1.1×10^6 cells mL^{-1}	8.2×10^5 cells mL^{-1}	76.6
ICE-ref	-	6×10^5 cells mL^{-1}	3.6×10^5 cells mL^{-1}	60.2

The salinity of the original seawater (SW-ref) was on average 33.53 PSU, corresponding to summer Polar Surface Water (PSW) and warm Polar Surface Water (PSWw) (Laukert et al., 2017), PSW is carried by the EGC whereas PSWw forms when PSW is freshened when sea ice melts in warmer Atlantic water (Rudels et al., 2002). At the end of the incubation period, the salinity values of ICE samples were on average ~29 PSU compared to 33.4 PSU in SW samples.

Microbial richness and diversity

Amplicon sequencing of 16S and 18S rRNA genes illuminated the diversity of sea ice and seawater microbial communities. The final data set consisted of 2,947,343 16S and 3,841,108 18S rRNA sequences respectively (Table S1, Table S2), from which 9,736 bacterial ASVs and 8,742 eukaryotic ASVs were identified. Rarefaction curves showed that, despite lower ASV numbers for samples in 2 samples in seawater; most of the bacterial and eukaryotic diversity was sufficiently covered (Figure S2). Eukaryotic ASV richness varied greatly among samples (80 to 1148, average: 624), with <90 ASVs in two outliers. On the other hand, bacterial richness varied less, ranging from 242 to 905 (average 695). Eukaryotic richness varied significantly between size fractions in ICE and SW based on the Shannon and Simpson

diversity indices (ANOVA, $p < 0.05$), although this was not observed in the bacterial data. Bacterial richness significantly differed only between SW-ref and SW (Shannon index; post-hoc TukeyHSD Test; *p*-adjusted = 0.04), and between ICE-ref and ICE samples (Shannon index; post-hoc TukeyHSD Test; *p*-adjusted = 0.01).

Eukaryotic community composition

The eukaryotic community varied significantly between ICE and SW (PERMANOVA test; $F_{3,10}$ = 1.74, R^2 = 0.34, p = 0.04) across all size fraction (Figure 2). Nonetheless, communities were overall dominated by taxa prevalent during summer in Fram Strait (Nöthig et al., 2015; Metfies et al., 2016, 2017) and around Svalbard (Zhang et al., 2019) and the Nordic Seas (Dąbrowska et al., 2020). These included small chlorophytes from the *Chloropicales* (0 – 86%) and *Mamiellales* (0 – 9%) orders, unclassified *Bacillariophyta* (0 – 22%), followed by *Phaeocystales* (0 – 16%) and dinoflagellates assigned to the *Syndiniales* order *Dino-Group-I* (0 – 11%) (Figure 3A).

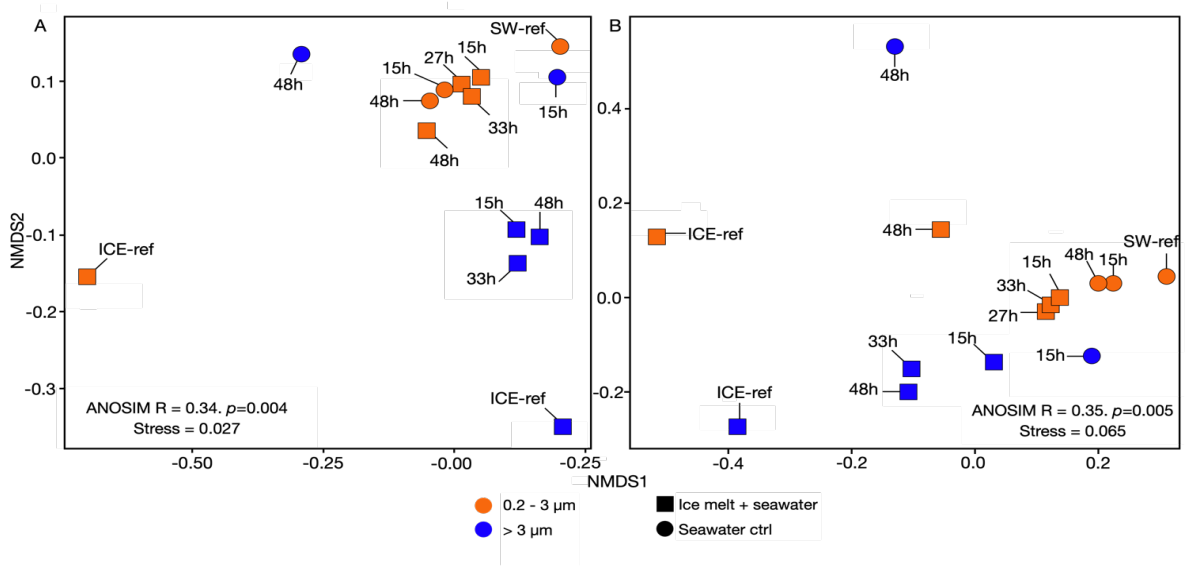

Figure 2. Nonmetric multidimensional scaling of Bray-Curtis community dissimilarities for (A); eukaryotes and (B); bacteria and archaea. Dissimilarity matrices and ANOSIM tests for experimental set up (ICE and SW) in each size fraction were calculated based on the Bray-Curtis dissimilarity measure on Hellinger-transformed ASV abundances.

Moreover, significant differences between the references (ICE-ref and SW-ref) and the microcosms (ICE and SW) were observed in both size fractions (PERMANOVA test; $F_{1,12}$ = 3.3, R^2 =0.215, p = 0.002). The SW-ref showed higher representation (2 – 13%) of small mixo-

and heterotrophic taxa compared to SW, and included protists members of *Telonemia* and *Picozoa*, cryptomonads of the class *Cryptophyceae*, as well as members of the *Gymnodiniales*, flagellates of the *Dictyochophyceae* and dinoflagellates of *Dinophyceae*. The prevalence of *Dinophyceae* is consistent with under-ice surveys at the central Arctic (Hardge et al., 2017b). At the end of the experiment the >3 µm SW samples were dominated by heterotrophs and mixotrophs of the class *Dictyochophyceae* (27%) mainly of the family *Pedinellales* known to feed on bacteria (Piwosz et al., 2010), followed by members of the chlorophyte order *Chloropicales* (21%) and *Dinophyceae* (17%) consistent with a heterotrophic system present in SW-ref with low chlorophyll a concentrations (0.91 µg L^{-1}) measured at station N4 compared to the other stations (Figure S3). The high abundance of heterotrophic protist in the seawater is consistent with previous observations in the Arctic Ocean at the end of summer, when the abundance of autotrophic taxa has declined (Sherr et al., 2003) and nutrients become depleted (Figure S3).

ICE-ref samples contained taxa that was exclusive found in the ICE-ref (i.e. with less than 1.5% of abundance in the ICE or SW (Figure 3A)), dominated by nanoflagellates in the > 3 µm fraction, followed by *Pelagophyceae*, mainly order *Sarcinochrysidales*, and the *choanoflagellida* order *Acanthoecida* in the 0.2 – 3µm fraction (comprising between 16% to 34% of the total community in the 0.2 – 3µm sample). *Pelagophyceae* can dominate surface waters during the Arctic summer (Balzano et al., 2012). Choanoflagellates sequences have been primarily found throughout the Arctic water column (Thaler et al., 2015), but are also abundant in brackish and freshwater systems (del Campo and Massana, 2011), thus suggesting that these groups were trapped in the sea ice during freezing but sourced from pelagic waters. The > 3 µm ICE-ref sample contained a larger representation of *Chlamydomonadales, Pyramimonadales, Pelagophyceae* and unidentified members of the *Chrysophyceae*. *Chlamydomonadales* and *Chrysophytes* were comparable to protist communities in Arctic melt ponds (Kilias et al., 2014; Hardge et al., 2017b; Xu et al., 2020), whereas being considered minor contributors to sea ice communities (Hop et al., 2020). Presumably, the sea ice might have partially melted thus allowing for seawater to infiltrate through larger channels before refreezing, which is common when the ice experience an extended summer period (Stroeve et al., 2014; Stroeve and Notz, 2018). Hence, these

taxonomic groups possibly originate from later introduction into the sea from water, consistent with a degraded/refrozen appearance of the lower ice core (Figure 1B).

The 3 µm ICE-ref fraction comprised unclassified *Bacillariophyta* (27%) and 26% dinoflagellates from orders *Suessiales*, *Gymnodiniales* and *Peridiniales*. Other heterotrophic protists of the *Filosa-Thecofilosea* including *Cryomonadida* and *Ebriida* contributed in total 15%. The majority of these groups were also identified in the ICE samples, while constituting < 1% in SW.

To investigate community dynamics during melt in greater detail, we tracked changes in the most abundant genera. The diatom community (class *Bacillariophyta*) comprised equal fractions of pennate and centric diatoms (Table S3), with overall higher abundances in the >3 µm fraction. ICE and SW samples were dominated by the pennate diatom *Fragilariopsis* and the small diatom *Minutocellus* (7 – 71%) except for the 3 µm ICE-ref. These species are predominately found in sea ice and under-ice seawater in the Arctic and subarctic seas (Mundy et al., 2011; Belevich et al., 2020). *Minutocellus* is a dominant member of small-size diatom communities in other oceanographic regions (Vaulot et al., 2008). *Fragilariopsis* are among the most abundant Arctic sea ice algae (van Leeuwe et al., 2018), dominating spring sea ice communities as well as in under-ice blooms (Laney and Sosik, 2014; Hardge et al., 2017b; Ardyna et al., 2020).

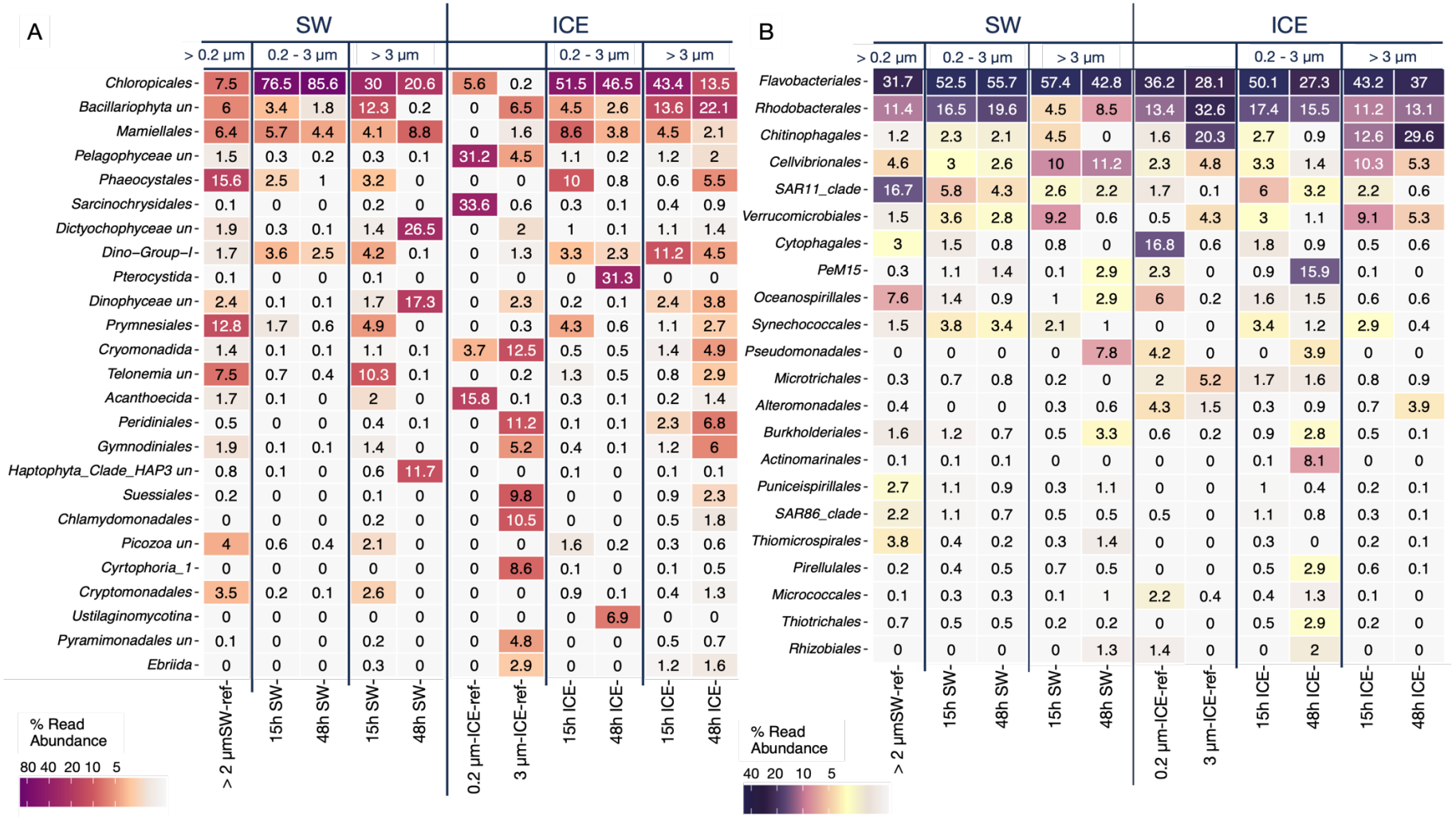

Figure 3. Relative abundance heatmap of main (A) eukaryotic and (B) bacterial orders identified in the seawater control (SW) and seawater + melting ice (ICE) compared to the original seawater (SW-ref) and the original ice core (ICE-ref) by size fractions. Includes only the most abundant taxa with at least > 1% abundance in all samples

The genera *Navicula, Chaetoceros, Cylindrotheca* and *Bacillaria* constituted 66% of the diatom community in ICE-ref but only 2 – 4% in ICE, and with the exception of *Chaetoceros*, completely absent (less than 1% abundance) in the seawater SW samples (Table S3). Diatoms that were substantially more abundant in the sea ice (ICE) were the pennate diatoms *Navicula*, *Cylindrotheca* and *Bacillaria* that dominated the 3 µm-ICE-ref sample, absent in all SW samples. Their abundance increased overtime as sea ice melted but were overall low (0 – 5%) in ICE samples likely due to dilution. *Cylindrotheca* have a strong preference for sea ice (Hardge et al., 2017b). In general, high abundances of pennate diatoms are representative of autumn/winter communities (Niemi et al., 2011), representing the dominant taxa from Arctic sea ice communities (Kauko et al., 2018; van Leeuwe et al., 2018; Hop et al., 2020).

Attheya, *Chaetoceros* and *Naviculales* were also presents mostly in sea ice and constituted a significant fraction of the diatom population (2 – 21%) in ICE and ICE-ref compared to 0.1 – 14% in SW samples (Table S3). *Chaetoceros* is a pelagic diatom abundant during the summer in Fram Strait, especially in meltwater regimes (von Appen et al., 2021), but also occurs in sea ice (Mikkelsen et al., 2008; van Leeuwe et al., 2022). The finding of *Chaetoceros* in the ice and the underlying seawater has been previously identified (Hardge et al., 2017b), along with *Gymnodinium* (*Dinophyceae*). Their increasing abundance in sea ice towards autumn has been attributed to entrapment during sea ice melting and refreezing periods that occur in the sea ice during autumn (Niemi et al., 2011) which in a foreseen extended Arctic ice-melt season could have implications for sea ice algae abundance in newly formed ice (Niemi et al., 2011; Hardge et al., 2017b).

Of the pico-eukaryotic community, chlorophytes strongly dominated in our samples except for the > 3 ICE-ref sample and mainly represented by *Chloroparvula*, *Micromonas* (Figure 3). Within the *Chlorophyta* division, the genus *Chloroparvula* constituted more than half of the chlorophyte community in all ICE and SW samples, followed by *Micromonas* (4 – 35%) abundance (Table S3). *Micromonas*, was absent (< 1%) in ICE-ref samples matching previous observations of its prevalence in Arctic surface waters rather than sea ice (Hardge et al., 2017a). In contrast, *Carteria*, *Mantoniella*, and *Pyramimonadales* represented larger proportions (8 – 60%) of the chlorophytes in the 3 µm-ICE-ref mainly (Table S3). Chlorophytes

are a relevant part of the pelagic ecosystem as they can also be exported to the deep sea via sinking particles (Metfies et al., 2017; Bachy et al., 2022) and it has been shown that species of chlorophytes were favoured by meltwater (Kilias et al., 2014) overall indicating that they might have been sourced from previous melted ponds in the ice floe.

Flagellates of the *Haptophyta* were dominated by the *Prymnesiophyceae* genera *Phaeocystis* and *Chrysochromulina* (4 – 80%) present in all samples (Table S3). Coccolithophores prevailed in the 3 µm larger fraction, mainly represented by the *Isochrysidaceae* family (24% in ICE-ref and 6% in ICE) as well as *Coccolithus* that comprised 4% of the ICE samples. The dominant species are common taxa of pelagic summer phytoplankton communities in the upper water column of Fram Strait during inflow of warmer water from the Atlantic (Nöthig et al., 2015; Fadeev et al., 2018) and the Barents Sea (Olli et al., 2002). ASVs assigned to the family *Isochrysidaceae* and *Pseudohaptolina* were the only *Haptophyta* species with higher abundance in sea ice. Due to the occurrence of *Phaeocystis* in warmer Atlantic waters (Nöthig et al., 2015) and the ability to grow under Arctic sea ice (Ardyna et al., 2020) and the relevance of coccolithophores for carbon export flagellates and coccolithophores might contribute in the sympagic-pelagic connectivity with potential repercussions for productivity and carbon export.

Bacterial community composition

Bacterial communities were overall dominated by the orders *Flavobacteriales* (class *Bacteroidia*) and *Rhodobacterales* (class *Alphaproteobacteria*) and comprised 48% and 15% of the bacterial community, respectively. Bacterial communities showed differences by between size fractions (PERMANOVA test; $F_{1,12}$ = 3.46, R^2 =0.22, p = 0.01) (Figure 2). Members of *Alphaproteobacteria* constituted 25% of all 0.2 – 3 µm samples, particularly the pelagic SAR11 clade that constituted ~ 9% in SW and ICE samples. In contrast, the orders *Chitinophagales*, *Cellvibrionales* and *Verrucomicrobiales* were enriched in the > 3 µm fraction (5 – 28%) compared to 0.2 – 3 µm (1 – 5%). SW-ref was dominated by SAR11 (17%), abundant in the global oceans (Giovannoni, 2017) including the Arctic Ocean (Wilson et al., 2017; Balmonte et al., 2018; Kraemer et al., 2020). Additionally, higher representation of *Gammaproteobacteria* and *Alphaproteobacteria* orders were also observed in the SW-ref

compared to SW samples (16% and 9%, respectively) including *Burkholderiales*, SAR86, *Puniceispirillales*, *Oceanospirillales* and *Thiomicrospirales* matching with previous pelagic surveys in the Fram Strait water column (Wilson et al., 2017; Fadeev et al., 2018).

Bacterial communities also varied significantly in composition in ICE and SW samples (PERMANOVA test; $F_{3,10} = 2.1$, $R^2 = 0.38$, $p = 0.013$). Particularly in the 0.2 – 3 µm fraction, the *Actinobacteria* orders PeM15, *Microtrichales* and *Micrococcales* were more abundant in ICE and comprising on average 6% of the 0.2 µm-ICE-ref community. *Actinobacteria* are not commonly dominant taxa (Deming and Eric Collins, 2017), but can be found in sea ice (Boetius et al., 2015). Members of *Actinobacteria* have been reported mainly as freshwater taxa (Herlemann et al., 2011) at the surface of the in the MIZ and meltwater (Hatam et al., 2014, 2016). *Actinobacteria* has been attributed as an indicator of melting ice and the presence of melt ponds (Fernández-Gómez et al., 2019) further supporting the hypothesis that specific bacteria and eukaryotic taxa that originated in seawater were trapped into the sea ice during its formation.

Species-specific response to potential seeding of diatoms

Overall, the bacteria community was represented by *Flavobacteria* and *Rhodobacterales*, which are often associated with algae and organic matter content (Teeling et al., 2012; Xing et al., 2015; Unfried et al., 2018; Tisserand et al., 2020; Piontek et al., 2022). We analysed the most abundant genera within these orders (Table S4). *Flavobacteria* showed a higher number of genera with a clearer separation or preference for sea ice and seawater (Table S4). The flavobacterial genera *Nonlabens*, *Psychroflexus*, *Maribacter*, and *Winogradskyella*, prevailed in the >3µm ICE-ref and ICE fractions where they constituted 58% and up to 18% of the *Flavobacteriales* respectively, whereas being absent in SW samples. *Psychroflexus* are common sea ice bacteria (Bowman, 2013; Boetius et al., 2015; Rapp et al., 2018), whereas *Nonlabens* also occur in brine and melt ponds (Fernández-Gómez et al., 2019). *Winogradskyella* and *Maribacter* are among the most prominent *Flavobacteria* associated with sea ice algae aggregates found in Arctic deep-sea sediments and sinking particulate organic matter from sea ice (Rapp et al., 2018; Amiraux et al., 2021). These findings highlight a relevant role of species of *Flavobacteria* in the sea-ice-pelagic and benthic coupling.

Polaribacter, Ulvibacter, Formosa and unassigned *Cryomorphaceae* taxa were well represented in ICE-ref and ICE samples (3 – 85% in the > 3 µm fraction and 1 – 23% in the 0.2 µm fraction) whereas being absent in SW (Table S4). *Polaribacter* can be found across different sea ice habitats in the central Arctic as well as the underlying seawater (Bowman, 2013; Boetius et al., 2015; Fernández-Gómez et al., 2019). Often associated to surface waters, the strong presence of these taxa also matches previous surveys of summer surface communities in the Artic (Rapp et al., 2018; Wietz et al., 2021). These taxa with the might have also likely benefited from nutrient input coming from the release of sea ice algae during ice melt owing their known ability to exploit diatom-derived metabolites (Buchan et al., 2014; Teeling et al., 2016).

Rhodobacterales represent a bacterial order known to be associated with surface Atlantic waters (Cardozo-Mino et al., 2021) and to prevail in the water column after the phytoplankton bloom in early autumn (Wietz et al., 2021). The abundance of *Rhodobacterales* may be due to their ability to degrade of complex compounds found after a phytoplankton bloom facilitating the seasonal transition (Wemheuer et al., 2015; Wietz et al., 2021). Of the *Rhodobacterales* only three genera *Octadecabacter, Yoonia-Loktanella* and unassigned *Rhodobacterales* were more abundant in ICE-ref and ICE samples than in SW samples (Table S4). *Octadecabacter* is a typical sea ice taxa (Deming and Eric Collins, 2017). *Yoonia-Loktanella* and *Sulfitobacter* (that dominated the *Rhodobacterales*) are able to demethylate dimethylsulfoniopropionate (DMSP) produced by many phytoplankton species including diatoms (Lyon et al., 2011; Kettles et al., 2014), as well as to prefer light conditions of the surface (Imhoff et al., 2018).

Rubritalea largely dominated verrucomicrobial ASVs in ICE-ref, constituting and 4 – 9% and 12 – 53% of the *Verrucomicrobiae* in the 0.2 µm and >3 µm fraction, respectively. *Verrucomicrobiae* abundance increases in summer in surface water of Fram Strait, especially in the warmer WSC (Wilson et al., 2017; Fadeev et al., 2018; Cardozo-Mino et al., 2021) and the Svalbard fjords where *Verrucomicrobiae* has been identified as a significant polysaccharide-degrading group (Cardman et al., 2014). Moreover, a recent study of *Verrucomicrobiae* genomes identified the ability to degrade sulphated fucans from brown macroalgae (Vidal-Melgosa et al., 2021) adding to the notion that the *Verrucomicrobiae* as

important degraders of complex compounds. *Verrucomicrobiae* is a significant bacterial constituent of sinking particles (Milici et al., 2017; Jain et al., 2019), suggesting them as relevant mediators in the ice- seawater connectivity during ice melt, with implications for carbon export.

Dissolved organic matter

We applied FT-ICR-MS to characterize DOM composition in ice and seawater before and after melt, aiming at identifying ice-specific molecules and whether they remain detectable after melt. The ICE-ref comprised 5301 molecular formulae across the all samples. There was a significantly higher number of molecular formulae containing sulfur and phosphorus in ICE-ref compared to SW-ref (Figure 4A) (Bonferroni-corrected results of pairwise Fisher test $p <$ 0.001), but no difference in nitrogen-containing compounds. The modified aromaticity index (AI_{mod}) was significantly lower in ICE-ref than SW-ref of (median seawater = 0.21, ice = 0.17; Mann-Whitney test, $p<0.01$). No statistically significant difference in masses (m/z) was observed. The degradation index (I_{DEG}) an index representing the degradation state of solid-phase extracted DOM samples was slightly higher for the ice (mean=0.72) compared to the seawater reference samples (0.67), both within the range in Atlantic surface waters (Flerus et al., 2012). Only 121 molecular formulae were exclusive to ICE-ref, neither detected in the SW-ref nor SW. 66% of ice-specific molecular formulae contained sulfur and showed very low AI_{mod} values, indicating highly aliphatic compounds (Norman et al., 2011). The placement of those compounds in a van Krevelen diagram (Figure 4C) indicates rather freshly produced DOM (D'Andrilli et al., 2015), supporting an autochthonous origin of those compounds. Searching ice-specific formulae in the metabolomicsworkbench.org, pubchem and chemspider databases tentatively identified some of the masses, including compounds of putative algal origin (Table 2). Over the melting process only approximately 10% of ICE-ref compounds remained detectable, indicating microbial transformation or being below the detection limit after dilution in seawater (Figure 5).

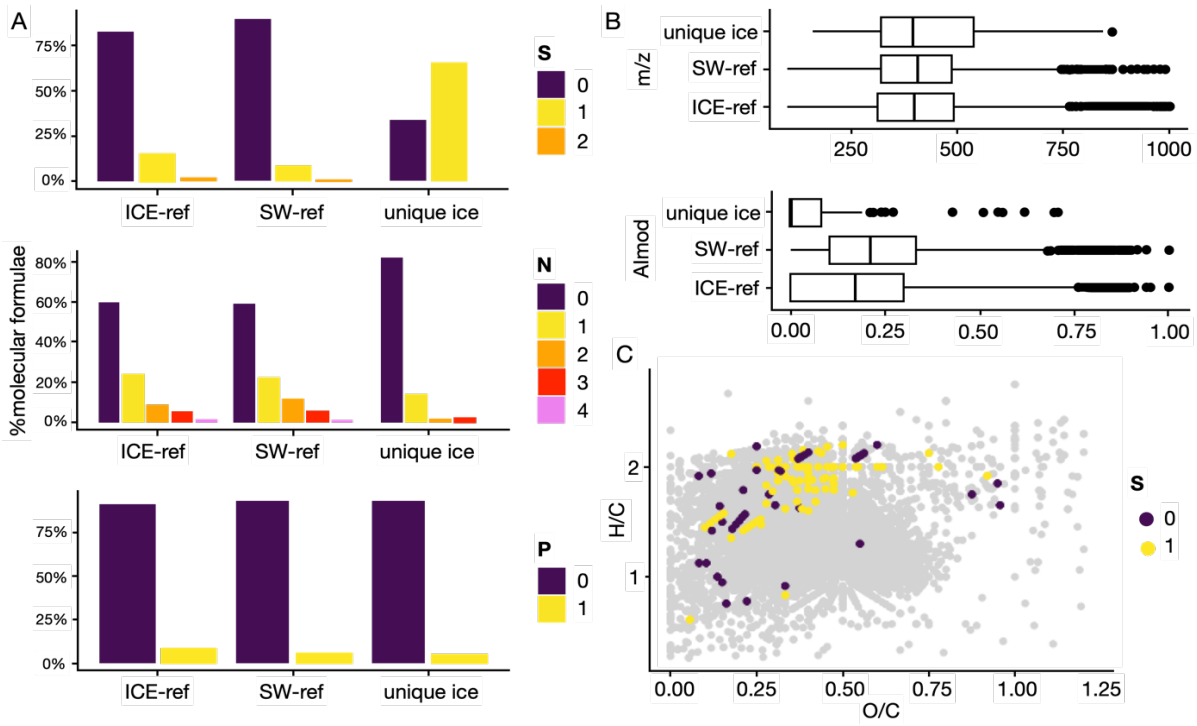

Figure 4. (A) Relative abundance of molecular formula containing different numbers of sulfur (S), nitrogen (orN) and phosphorus (P) atoms in ICE-ref, SW-ref and unique to ICE-ref / ICE. (B) Distribution of m/z (molecular mass) and the modified aromaticity index in the respective class of samples. (C) Van Krevelen plot of molecular formulae in ICE-ref where colored points indicate presence and absence of sulfur in the molecular formula and correspond to formulae uniquely and ubiquitously found in ice reference samples, but not seawater references or seawater controls.

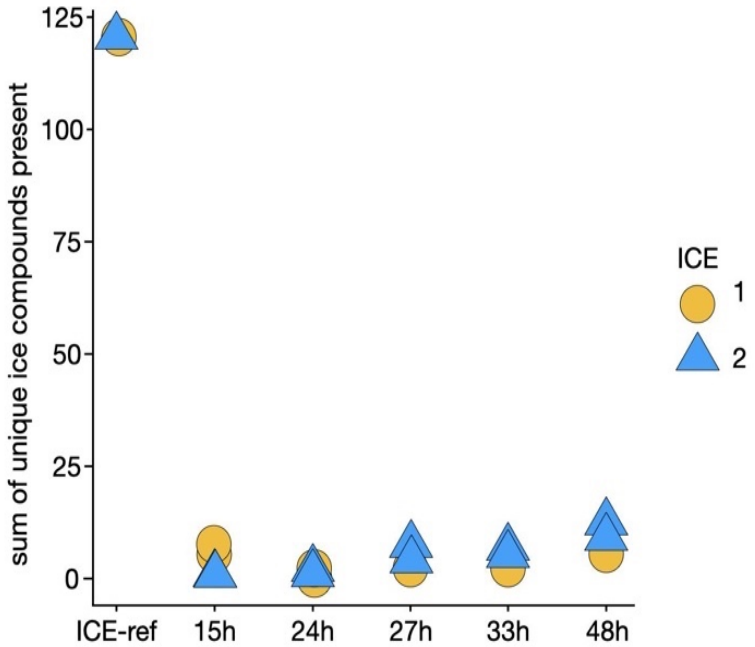

Figure 5. Molecular formula found only in sea ice samples. Numbers correspond to the two ice cores with two replicates each.

Table 2: Ice-specific masses with hits in metabolomicsworkbench, chemspider or pubchem databases.

formula	m/z	Database hit
C20H30O3	317.212256	11,12-epoxy-sarcophytoxide (diterpenoid; invertebrate)
C19H34O4	325.2384442	11-methoxy-12,13-epoxy-9-octadecenoic acid
C42H62O8	693.4374151	Bislatumlide A (diterpene; invertebrate)
C20H19O3N3	348.1353651	Different natural products (e.g. Cyclo-L-Trp-L-Tyr)
C22H22O3	333.1496326	Enhygrolide B
C39H56O7	635.3955713	Leonurusoleanolide (pentacyclic triterpenoid)
C23H38O7	425.2544759	Prostaglandin
C24H42O21	665.2145302	Tetrasaccharide (e.g. beta-galactotetraose or alpha-maltotetraose)

The prevalence of molecular formulae potentially constructing aliphatic compounds coincided with the enrichment of hydrocarbon-degrading bacteria in the ICE-ref samples. *Glaciecola* (*Alteromonadales*), *Oleispira*, *Oleiphilus* and unassigned ASVs to *Saccharospirillaceae* (*Oceanospirillales*) were more abundant in the larger fraction (> 3 µm) of ICE-ref and ICE (up to 56%) compared to SW (< 4%) (Table S4). *Glaciecola* and *Oleispira* are capable to degrade hydrocarbons and lipids in sea ice (Brakstad et al., 2008; Kube et al., 2013; Søreide et al., 2013; Peeb et al., 2022). Aliphatic hydrocarbons might have been released from decaying diatoms, proving an energy source (Han et al., 1968; Han and Calvin, 1969; Cono et al., 2022).

Table 1. Monosaccharide concentration (µM) obtained by HPAEC analysis and delta values in the ICE-ref, and ICE. Samples were taken after 15 h (T1).

Monosaccharide	ICE-ref	ICE at 15 h	Change at 15 h (Δ)
Glucosamine	0.15 ± 0.08	0.11 ± 0.03	0.04
Galactose	0.45 ± 0.34	0.29 ± 0.08	0.17
Glucose	3.10 ± 1.28	0.77 ± 0.73	2.33
Mannose	1.73 ± 0.59	1.32 ± 0.97	0.40
Xylose	2.00 ± 0.23	1.51 ± 0.84	0.50
Galacturonic acid	0.09 ± 0.05	0.05 ± 0.03	0.04
Mannuronic acid	0.01 ± 0.01	0.04 ± 0.06	-0.04

Monosaccharides

To support the analysis of compounds and metabolites in the sea ice, released after melt and possibly influencing microbial dynamics, we applied HPLC to quantify major marine monosaccharides in ice samples after acid hydrolysis. Comparison to SW failed due to analytical issues with these samples, i.e. we can only provide a tentative overview of carbohydrates in sea ice and their concentrations after melt. Overall, ICE-ref and ICE samples at 15 h contained on average 2.3 and 1.2 µM of glucose, mannose and xylose, respectively (Table 3), consistent with sea-ice carbohydrate concentrations in the Laptev Sea (Krembs and Engel, 2001), the Chukchi Sea and in Fram Strait (Meiners et al., 2003, 2008) including MYI in an ice melt experiment (Amon et al., 2001), FYI (Aslam et al., 2016), and the bottom sea ice (Riedel et al., 2006). We assume that carbohydrates mostly originated from primary producers (Riedel et al., 2006), but ice-affiliated *Gammaproteobacteria* and the flavobacterial including *Winogradskyella* and *Maribacter* also produce polymeric compounds and might contribute to the carbohydrate pool (Consolazione et al., 2018; Caruso et al., 2019; Wolter et al., 2021). Glucose concentrations decreased most after 15 h (2.33) compared to mannose and xylose (0.4 and 0.5, respectively), which might be linked to dilution but also due to bacterial degradation. Hence, ice-released carbohydrates presumably support bacterial metabolism at the sea ice-water interface (Thomas, 2017). The prevalence of *Flavobacteria* specialized in polysaccharide and algal monosaccharide degradation supports the notion how ice-derived substrates fuel the microbial loop after melt. These processes can be influenced by the alteration of EPS production in pennate diatoms in response to changes in the environment and nutrient limitation (Underwood et al., 2004; Mishra and Jha, 2009; Thomas et al., 2010). For instance, xylose and mannose production by *Fragilariopsis*, the most abundant diatom in our samples, changes under low nutrient conditions which in return changes the properties of EPS produced by the diatom in brine channels to adapt to changeling conditions (Aslam et al., 2012, 2018).

Conclusions

The present study addressed the connectivity between microbial communities in sea ice and in the underlying seawater. We corroborated that seawater and sea ice harbour distinct bacterial and eukaryotic communities, with further differentiation by size fraction. The prevalence of heterotrophic protists in the seawater coincide with sampling in late summer, characterized by with low nutrient and chlorophyll concentrations. Seawater and melt pond taxonomic groups such as *Actinobacteria* and the chlorophytes *Pyramimonadales* and *Micromonas* identified in the sea ice likely corresponded to refrozen water in the sea ice core. Our results support the notion that the sea ice shapes microbial diversity at the MIZ. Diatoms showed connectivity between seawater and ice. Bacterial signatures of this putative seeding included *Flavobacteria* taxa known for their association to algae aggregates increased in samples with strong dominance of diatoms. the presence of long-chain aliphatics sulfur-containing compounds in the original ice illustrates a specific chemical signature including known algal metabolites, indicating that ice melt provides a suite of molecules that sustains e.g. hydrocarbon degraders.

Overall, our study provides important insights into how melting ice at the end of its life cycle inoculates the underlying seawater, and influences microbial dynamics. The finding of specific patterns in the >3µm size fraction indicates that these processes also influence benthopelagic coupling through sinking ice-derived particles. These insights are valuable for the current and future Arctic Ocean, where accelerated melting will increasingly affect microbial diversity with consequences for ecosystem functioning and carbon cycling.

Conflict of Interest

The authors declare that the research was conducted in the absence of any commercial or financial relationships that could be construed as a potential conflict of interest.

Author contributions

MW and MC-M conceived the study and performed fieldwork. KM conducted amplicon sequencing and contributed to interpretation of the results. JM and TD evaluated FT-ICR-MS data. SVM and JHH performed monosaccharide HPLC. MC-M analyzed the data and wrote the manuscript with guidance from MW, JM, KM and AB. All authors critically revised the manuscript and gave their approval of the submitted version.

Acknowledgements

We thank the captain, crew and scientists of RV Polarstern PS121 expedition. We thank Daniel Scholz, Swantje Rogge, Sascha Lehmenhecker, Julia Grosse, HeliService Emden for the transportation to the sea ice and Bear safety during sampling. Erika Allhusen and Ilka Peeken for the ice corer. We thank Katrin Klaproth and Ina Uber for DOC and FT-ICR-MS analyses. We thank Alek Bolte for HPLC analysis of monosaccharides. We thank Chyrene Moncada for DNA extractions and Jakob Barz and Swantje Rogge for library preparation. This work was conducted in the framework of the HGF Infrastructure Program FRAM of the Alfred-Wegener-Institute Helmholtz Center for Polar and Marine Research. Additional funding was provided by the Max Planck Society and the Hector Fellow Academy.

References

AMAP (2017). Snow, water, ice and permafrost. Summary for policy-makers.

Amiraux, R., Rontani, J.-F., Armougom, F., Frouin, E., Babin, M., Artigue, L., et al. (2021). Bacterial diversity and lipid biomarkers in sea ice and sinking particulate organic material during the melt season in the Canadian Arctic. *Elem. Sci. Anthr.* 9.

Amon, R. M. W., Fitznar, H.-P., and Benner, R. (2001). Linkages among the bioreactivity, chemical composition, and diagenetic state of marine dissolved organic matter. *Limnol. Oceanogr.* 46, 287–297. doi:10.4319/lo.2001.46.2.0287.

Andersen, K. S., Kirkegaard, R. H., Karst, S. M., and Albertsen, M. (2018). ampvis2: an R package to analyse and visualise 16S rRNA amplicon data. *BioRxiv*, 299537.

Ardyna, M., Mundy, C. J., Mayot, N., Matthes, L. C., Oziel, L., Horvat, C., et al. (2020). Under-Ice Phytoplankton Blooms: Shedding Light on the "Invisible" Part of Arctic Primary Production. *Front. Mar. Sci.* 7. Available at: https://www.frontiersin.org/articles/10.3389/fmars.2020.608032.

Arrigo, K. R. (2014). Sea Ice Ecosystems. *Ann. Rev. Mar. Sci.* 6, 439–467. doi:10.1146/annurev-marine-010213-135103.

Arrigo, K. R., Perovich, D. K., Pickart, R. S., Brown, Z. W., Van Dijken, G. L., Lowry, K. E., et al. (2012). Massive phytoplankton blooms under arctic sea ice. *Science (80-.).* 336, 1408. doi:10.1126/science.1215065.

Aslam, S. N., Cresswell-Maynard, T., Thomas, D. N., and Underwood, G. J. C. (2012). Production and Characterization of the Intra- and Extracellular Carbohydrates and Polymeric Substances (EPS) of Three Sea-Ice Diatom Species, and Evidence for a Cryoprotective Role for EPS. *J. Phycol.* 48, 1494–1509. doi:10.1111/jpy.12004.

Aslam, S. N., Michel, C., Niemi, A., and Underwood, G. J. C. (2016). Patterns and drivers of carbohydrate budgets in ice algal assemblages from first year Arctic sea ice. *Limnol. Oceanogr.* 61, 919–937. doi:10.1002/lno.10260.

Aslam, S. N., Strauss, J., Thomas, D. N., Mock, T., and Underwood, G. J. C. (2018). Identifying metabolic pathways for production of extracellular polymeric substances by the diatom Fragilariopsis cylindrus inhabiting sea ice. *ISME J.* 12, 1237–1251. doi:10.1038/s41396-017-0039-z.

Azam, F., and Malfatti, F. (2007). Microbial structuring of marine ecosystems. *Nat. Rev. Microbiol.* 5, 782–791. doi:10.1038/nrmicro1747.

Bachy, C., Sudek, L., Choi, C. J., Eckmann, C. A., Nöthig, E.-M., Metfies, K., et al. (2022). Phytoplankton Surveys in the Arctic Fram Strait Demonstrate the Tiny Eukaryotic Alga Micromonas and Other Picoprasinophytes Contribute to Deep Sea Export. *Microorg.* 10. doi:10.3390/microorganisms10050961.

Balmonte, J. P., Teske, A., and Arnosti, C. (2018). Structure and function of high Arctic pelagic, particle-associated and benthic bacterial communities. *Environ. Microbiol.* 20, 2941–2954.

Balzano, S., Gourvil, P., Siano, R., Chanoine, M., Marie, D., Lessard, S., et al. (2012). Diversity of cultured photosynthetic flagellates in the northeast Pacific and Arctic Oceans in summer. *Biogeosciences* 9, 4553–4571. doi:10.5194/bg-9-4553-2012.

Belevich, T. A., Ilyash, L. V, Milyutina, I. A., Logacheva, M. D., and Troitsky, A. V (2020). Photosynthetic Picoeukaryotes Diversity in the Underlying Ice Waters of the White Sea, Russia. *Diversity* 12. doi:10.3390/d12030093.

Bienhold, C., Boetius, A., and Ramette, A. (2012). The energy–diversity relationship of complex bacterial communities in Arctic deep-sea sediments. *ISME J.* 6, 724–732. doi:10.1038/ismej.2011.140.

Bluhm, B. A., Hop, H., Vihtakari, M., Gradinger, R., Iken, K., Melnikov, I. A., et al. (2018). Sea ice meiofauna distribution on local to pan-Arctic scales. *Ecol. Evol.* 8, 2350–2364. doi:10.1002/ece3.3797.

Boetius, A., Albrecht, S., Bakker, K., Bienhold, C., Felden, J., Fernández-Méndez, M., et al. (2013). Export of algal biomass from the melting arctic sea ice. *Science (80-.).* 339, 1430–1432. doi:10.1126/science.1231346.

Boetius, A., Anesio, A. M., Deming, J. W., Mikucki, J. A., and Rapp, J. Z. (2015). Microbial ecology of the cryosphere: Sea ice and glacial habitats. *Nat. Rev. Microbiol.* 13, 677–690. doi:10.1038/nrmicro3522.

Bowman, J. P. (2013). "Sea-Ice Microbial Communities BT - The Prokaryotes: Prokaryotic Communities and Ecophysiology," in, eds. E. Rosenberg, E. F. DeLong, S. Lory, E. Stackebrandt, and F. Thompson (Berlin, Heidelberg: Springer Berlin Heidelberg), 139–161. doi:10.1007/978-3-642-30123-0_46.

Brakstad, O. G., Nonstad, I., Faksness, L.-G., and Brandvik, P. J. (2008). Responses of Microbial Communities in Arctic Sea Ice After Contamination by Crude Petroleum Oil.

Microb. Ecol. 55, 540–552. doi:10.1007/s00248-007-9299-x.

Buchan, A., LeCleir, G. R., Gulvik, C. A., and González, J. M. (2014). Master recyclers: features and functions of bacteria associated with phytoplankton blooms. *Nat. Rev. Microbiol.* 12, 686–698. doi:10.1038/nrmicro3326.

Callahan, B. J., McMurdie, P. J., Rosen, M. J., Han, A. W., Johnson, A. J. A., and Holmes, S. P. (2016). DADA2: High-resolution sample inference from Illumina amplicon data. *Nat. Methods* 13, 581–583. doi:10.1038/nmeth.3869.

Cardman, Z., Arnosti, C., Durbin, A., Ziervogel, K., Cox, C., Steen, A. D., et al. (2014). Verrucomicrobia are candidates for polysaccharide-degrading bacterioplankton in an Arctic fjord of Svalbard. *Appl. Environ. Microbiol.* 80, 3749–3756. doi:10.1128/AEM.00899-14.

Cardozo-Mino, M. G., Fadeev, E., Salman-Carvalho, V., and Boetius, A. (2021). Spatial Distribution of Arctic Bacterioplankton Abundance Is Linked to Distinct Water Masses and Summertime Phytoplankton Bloom Dynamics (Fram Strait, 79°N). *Front. Microbiol.* 12, 1067. doi:10.3389/fmicb.2021.658803.

Caruso, C., Rizzo, C., Mangano, S., Poli, A., Di Donato, P., Nicolaus, B., et al. (2019). Isolation, characterization and optimization of EPSs produced by a cold-adapted Marinobacter isolate from Antarctic seawater. *Antarct. Sci.* 31, 69–79. doi:10.1017/S0954102018000482.

Castellani, G., Veyssière, G., Karcher, M., Stroeve, J., Banas, S. N., Bouman, A. H., et al. (2022). Shine a light: Under-ice light and its ecological implications in a changing Arctic Ocean. *Ambio* 51, 307–317. doi:10.1007/s13280-021-01662-3.

Cono, V. L., Smedile, F., Crisafi, F., Marturano, L., Toshchakov, S. V, Spada, G. L., et al. (2022). Wintertime Simulations Induce Changes in the Structure, Diversity and Function of Antarctic Sea Ice-Associated Microbial Communities. *Microorg.* 10. doi:10.3390/microorganisms10030623.

Consolazione, C., Carmen, R., Santina, M., Annarita, P., Paola, D. D., Ilaria, F., et al. (2018). Production and Biotechnological Potential of Extracellular Polymeric Substances from Sponge-Associated Antarctic Bacteria. *Appl. Environ. Microbiol.* 84, e01624-17. doi:10.1128/AEM.01624-17.

D'Andrilli, J., Cooper, W. T., Foreman, C. M., and Marshall, A. G. (2015). An ultrahigh-resolution mass spectrometry index to estimate natural organic matter lability. *Rapid Commun. Mass Spectrom.* 29, 2385–2401. doi:https://doi.org/10.1002/rcm.7400.

Dąbrowska, A. M., Wiktor, J. M., Merchel, M., and Wiktor, J. M. (2020). Planktonic Protists of the Eastern Nordic Seas and the Fram Strait: Spatial Changes Related to Hydrography During Early Summer. *Front. Mar. Sci.* 7. doi:10.3389/fmars.2020.00557.

Dai, A., Luo, D., Song, M., and Liu, J. (2019). Arctic amplification is caused by sea-ice loss under increasing CO 2. *Nat. Commun.* 10, 121. doi:10.1038/s41467-018-07954-9.

del Campo, J., and Massana, R. (2011). Emerging Diversity within Chrysophytes, Choanoflagellates and Bicosoecids Based on Molecular Surveys. *Protist* 162, 435–448. doi:10.1016/j.protis.2010.10.003.

Deming, J. W., and Eric Collins, R. (2017). Sea ice as a habitat for Bacteria, Archaea and viruses. *Sea Ice*, 326–351. doi:10.1002/9781118778371.ch13.

Docquier, D., and Koenigk, T. (2021). Observation-based selection of climate models projects Arctic ice-free summers around 2035. *Commun. Earth Environ.* 2, 144. doi:10.1038/s43247-021-00214-7.

Eicken, H., Lensu, M., Leppäranta, M., Tucker III, W. B., Gow, A. J., and Salmela, O. (1995).

Thickness, structure, and properties of level summer multiyear ice in the Eurasian sector of the Arctic Ocean. *J. Geophys. Res. Ocean.* 100, 22697–22710. doi:10.1029/95JC02188.

Elwood, H. J., Olsen, G. J., and Sogin, M. L. (1985). The small-subunit ribosomal RNA gene sequences from the hypotrichous ciliates Oxytricha nova and Stylonychia pustulata. *Mol. Biol. Evol.* 2, 399–410. doi:10.1093/oxfordjournals.molbev.a040362.

Fadeev, E., Rogge, A., Ramondenc, S., Nöthig, E.-M., Wekerle, C., Bienhold, C., et al. (2021). Sea ice presence is linked to higher carbon export and vertical microbial connectivity in the Eurasian Arctic Ocean. *Commun. Biol.* 4, 1255. doi:10.1038/s42003-021-02776-w.

Fadeev, E., Salter, I., Schourup-Kristensen, V., Nöthig, E. M., Metfies, K., Engel, A., et al. (2018). Microbial communities in the east and west fram strait during sea ice melting season. *Front. Mar. Sci.* 5, 429. doi:10.3389/fmars.2018.00429.

Fernández-Gómez, B., Díez, B., Polz, M. F., Arroyo, J. I., Alfaro, F. D., Marchandon, G., et al. (2019). Bacterial community structure in a sympagic habitat expanding with global warming: brackish ice brine at 85–90 °N. *ISME J.* 13, 316–333. doi:10.1038/s41396-018-0268-9.

Fernández-Méndez, M., Turk-Kubo, K. A., Buttigieg, P. L., Rapp, J. Z., Krumpen, T., Zehr, J. P., et al. (2016). Diazotroph Diversity in the Sea Ice, Melt Ponds, and Surface Waters of the Eurasian Basin of the Central Arctic Ocean. *Front. Microbiol.* 7. doi:10.3389/fmicb.2016.01884.

Flerus, R., Lechtenfeld, O. J., Koch, B. P., McCallister, S. L., Schmitt-Kopplin, P., Benner, R., et al. (2012). A molecular perspective on the ageing of marine dissolved organic matter. *Biogeosciences* 9, 1935–1955. doi:10.5194/bg-9-1935-2012.

Giovannoni, S. J. (2017). SAR11 Bacteria: The Most Abundant Plankton in the Oceans. *Ann. Rev. Mar. Sci.* 9, 231–255. doi:10.1146/annurev-marine-010814-015934.

Grossart, H.-P., and Simon, M. (2007). Interactions of planktonic algae and bacteria: effects on algal growth and organic matter dynamics. *Aquat. Microb. Ecol.* 47, 163–176. doi:10.3354/ame047163.

Guillou, L., Bachar, D., Audic, S., Bass, D., Berney, C., Bittner, L., et al. (2013). The Protist Ribosomal Reference database (PR2): A catalog of unicellular eukaryote Small Sub-Unit rRNA sequences with curated taxonomy. *Nucleic Acids Res.* 41, D597–D604. doi:10.1093/nar/gks1160.

Han, J., and Calvin, M. (1969). Hydrocarbon distribution of algae and bacteria, and microbiological activity in sediments. *Proc. Natl. Acad. Sci.* 64, 436–443.

Han, J., McCarthy, E. D., Hoeven, W. Van, Calvin, M., and Bradley, W. H. (1968). Organic geochemical studies, II. A preliminary report on the distribution of aliphatic hydrocarbons in algae, in bacteria, and in a recent lake sediment. *Proc. Natl. Acad. Sci.* 59, 29–33.

Hardge, K., Peeken, I., Neuhaus, S., Krumpen, T., Stoeck, T., and Metfies, K. (2017a). Sea ice origin and sea ice retreat as possible drivers of variability in Arctic marine protist composition. *Mar. Ecol. Prog. Ser.* 571, 43–57.

Hardge, K., Peeken, I., Neuhaus, S., Lange, B. A., Stock, A., Stoeck, T., et al. (2017b). The importance of sea ice for exchange of habitat-specific protist communities in the Central Arctic Ocean. *J. Mar. Syst.* 165, 124–138. doi:10.1016/j.jmarsys.2016.10.004.

Hatam, I., Charchuk, R., Lange, B., Beckers, J., Haas, C., and Lanoil, B. (2014). Distinct bacterial assemblages reside at different depths in Arctic multiyear sea ice. *FEMS Microbiol. Ecol.* 90, 115–125. doi:10.1111/1574-6941.12377.

Hatam, I., Lange, B., Beckers, J., Haas, C., and Lanoil, B. (2016). Bacterial communities from Arctic seasonal sea ice are more compositionally variable than those from multi-year sea ice. *ISME J.* 10, 2543–2552. doi:10.1038/ismej.2016.4.

Herlemann, D. P. R., Labrenz, M., Jürgens, K., Bertilsson, S., Waniek, J. J., and Andersson, A. F. (2011). Transitions in bacterial communities along the 2000 km salinity gradient of the Baltic Sea. *ISME J.* 5, 1571–1579. doi:10.1038/ismej.2011.41.

Hop, H., Vihtakari, M., Bluhm, B. A., Assmy, P., Poulin, M., Gradinger, R., et al. (2020). Changes in Sea-Ice Protist Diversity With Declining Sea Ice in the Arctic Ocean From the 1980s to 2010s. *Front. Mar. Sci.* 7. doi:10.3389/fmars.2020.00243.

Hsieh, T. C., Ma, K. H., and Chao, A. (2016). iNEXT: an R package for rarefaction and extrapolation of species diversity (H ill numbers). *Methods Ecol. Evol.* 7, 1451–1456.

Imhoff, J. F., Rahn, T., Künzel, S., and Neulinger, S. C. (2018). Photosynthesis Is Widely Distributed among Proteobacteria as Demonstrated by the Phylogeny of PufLM Reaction Center Proteins. *Front. Microbiol.* 8. doi:10.3389/fmicb.2017.02679.

Jacob, M., Soltwedel, T., Boetius, A., and Ramette, A. (2013). Biogeography of Deep-Sea Benthic Bacteria at Regional Scale (LTER HAUSGARTEN, Fram Strait, Arctic). *PLoS One* 8, e72779. doi:10.1371/journal.pone.0072779.

Jain, A., Krishnan, K. P., Singh, A., Thomas, F. A., Begum, N., Tiwari, M., et al. (2019). Biochemical composition of particles shape particle-attached bacterial community structure in a high Arctic fjord. *Ecol. Indic.* 102, 581–592. doi:10.1016/j.ecolind.2019.03.015.

Junge, K., Imhoff, F., Staley, T., and Deming, W. (2002). Phylogenetic Diversity of Numerically Important Arctic Sea-Ice Bacteria Cultured at Subzero Temperature. *Microb. Ecol.* 43, 315–328. doi:10.1007/s00248-001-1026-4.

Kauko, H. M., Olsen, L. M., Duarte, P., Peeken, I., Granskog, M. A., Johnsen, G., et al. (2018). Algal Colonization of Young Arctic Sea Ice in Spring. *Front. Mar. Sci.* 5. Available at: https://www.frontiersin.org/article/10.3389/fmars.2018.00199.

Kettles, N. L., Kopriva, S., and Malin, G. (2014). Insights into the Regulation of DMSP Synthesis in the Diatom Thalassiosira pseudonana through APR Activity, Proteomics and Gene Expression Analyses on Cells Acclimating to Changes in Salinity, Light and Nitrogen. *PLoS One* 9, e94795. doi:10.1371/journal.pone.0094795.

Kilias, E. S., Peeken, I., and Metfies, K. (2014). Insight into protist diversity in Arctic sea ice and melt-pond aggregate obtained by pyrosequencing. *Polar Res.* 33, 23466. doi:10.3402/polar.v33.23466.

Kraemer, S., Ramachandran, A., Colatriano, D., Lovejoy, C., and Walsh, D. A. (2020). Diversity and biogeography of SAR11 bacteria from the Arctic Ocean. *ISME J.* 14, 79–90. doi:10.1038/s41396-019-0499-4.

Krembs, C., and Engel, A. (2001). Abundance and variability of microorganisms and transparent exopolymer particles across ice–water interface of melting first-year sea ice in the Laptev Sea (Artic). *Mar. Biol.* 138, 173–185. doi:10.1007/s002270000396.

Kube, M., Chernikova, T. N., Al-Ramahi, Y., Beloqui, A., Lopez-Cortez, N., Guazzaroni, M.-E., et al. (2013). Genome sequence and functional genomic analysis of the oil-degrading bacterium Oleispira antarctica. *Nat. Commun.* 4, 2156. doi:10.1038/ncomms3156.

Lalande, C., Bauerfeind, E., Nöthig, E. M., and Beszczynska-Möller, A. (2013). Impact of a warm anomaly on export fluxes of biogenic matter in the eastern Fram Strait. *Prog. Oceanogr.* 109, 70–77. doi:10.1016/j.pocean.2012.09.006.

Lalande, C., Nöthig, E., and Fortier, L. (2019). Algal export in the Arctic Ocean in times of

global warming. *Geophys. Res. Lett.* 46, 5959–5967. doi:10.1029/2019GL083167.

Laney, S. R., and Sosik, H. M. (2014). Phytoplankton assemblage structure in and around a massive under-ice bloom in the Chukchi Sea. *Deep Sea Res. Part II Top. Stud. Oceanogr.* 105, 30–41. doi:10.1016/j.dsr2.2014.03.012.

Lannuzel, D., Tedesco, L., van Leeuwe, M., Campbell, K., Flores, H., Delille, B., et al. (2020). The future of Arctic sea-ice biogeochemistry and ice-associated ecosystems. *Nat. Clim. Chang.* 10, 983–992. doi:10.1038/s41558-020-00940-4.

Laukert, G., Frank, M., Bauch, D., Hathorne, E. C., Rabe, B., von Appen, W.-J., et al. (2017). Ocean circulation and freshwater pathways in the Arctic Mediterranean based on a combined Nd isotope, REE and oxygen isotope section across Fram Strait. *Geochim. Cosmochim. Acta* 202, 285–309. doi:10.1016/j.gca.2016.12.028.

Lewis, K. M., Van Dijken, G. L., and Arrigo, K. R. (2020). Changes in phytoplankton concentration now drive increased Arctic Ocean primary production. *Science (80-.).* 369, 198–202. doi:10.1126/science.aay8380.

Lin, L., Lei, R., Hoppmann, M., Perovich, D. K., and He, H. (2022). Changes in the annual sea ice freeze-thaw cycle in the Arctic Ocean from 2001 to 2018. *Cryosph. Discuss.* 2022, 1–30. doi:10.5194/tc-2022-137.

Lizotte, M. P. (2003). "The Microbiology of Sea Ice," in *Sea Ice* Wiley Online Books., 184–210. doi:10.1002/9780470757161.ch6.

Lyon, B. R., Lee, P. A., Bennett, J. M., DiTullio, G. R., and Janech, M. G. (2011). Proteomic Analysis of a Sea-Ice Diatom: Salinity Acclimation Provides New Insight into the Dimethylsulfoniopropionate Production Pathway. *Plant Physiol.* 157, 1926–1941. doi:10.1104/pp.111.185025.

Martin, A., McMinn, A., Davy, S. K., Anderson, M. J., Miller, H. C., Hall, J. A., et al. (2012). Preliminary evidence for the microbial loop in Antarctic sea ice using microcosm simulations. *Antarct. Sci.* 24, 547–553. doi:10.1017/S0954102012000491.

Martin, M. (2011). Cutadapt removes adapter sequences from high-throughput sequencing reads. *EMBnet.journal* 17, 10. doi:10.14806/ej.17.1.200.

McMurdie, P. J., and Holmes, S. (2013). Phyloseq: An R Package for Reproducible Interactive Analysis and Graphics of Microbiome Census Data. *PLoS One* 8, e61217. doi:10.1371/journal.pone.0061217.

Meiners, K., Gradinger, R., Fehling, J., Civitarese, G., and Spindler, M. (2003). Vertical distribution of exopolymer particles in sea ice of the Fram Strait (Arctic) during autumn. *Mar. Ecol. Ser.* 248, 1–13. doi:10.3354/meps248001.

Meiners, K., Krembs, C., and Gradinger, R. (2008). Exopolymer particles: microbial hotspots of enhanced bacterial activity in Arctic fast ice (Chukchi Sea). *Aquat. Microb. Ecol.* 52, 195–207. doi:10.3354/ame01214.

Merder, J., Freund, J. A., Feudel, U., Hansen, C. T., Hawkes, J. A., Jacob, B., et al. (2020). ICBM-OCEAN: Processing Ultrahigh-Resolution Mass Spectrometry Data of Complex Molecular Mixtures. *Anal. Chem.* 92, 6832–6838. doi:10.1021/acs.analchem.9b05659.

Metfies, K., Bauerfeind, E., Wolf, C., Sprong, P., Frickenhaus, S., Kaleschke, L., et al. (2017). Protist communities in moored long-term sediment traps (Fram Strait, Arctic)-preservation with mercury chloride allows for PCR-based molecular genetic analyses. *Front. Mar. Sci.* 4, 301. doi:10.3389/fmars.2017.00301.

Metfies, K., Hoppmann, M., Tippenhauer, S., and Rohardt, G. (2021). Continuous thermosalinograph oceanography along RV POLARSTERN cruise track PS121. doi:10.1594/PANGAEA.930022.

Metfies, K., von Appen, W.-J., Kilias, E., Nicolaus, A., and Nöthig, E.-M. (2016). Biogeography and photosynthetic biomass of arctic marine pico-eukaroytes during summer of the record sea ice minimum 2012. *PLoS One* 11, e0148512.

Mikkelsen, D. M., Rysgaard, S., and Glud, N. R. (2008). Microalgal composition and primary production in Arctic sea ice: a seasonal study from Kobbefjord (Kangerluarsunnguaq), West Greenland. *Mar. Ecol. Prog. Ser.* 368, 65–74. doi:10.3354/meps07627.

Milici, M., Vital, M., Tomasch, J., Badewien, T. H., Giebel, H.-A., Plumeier, I., et al. (2017). Diversity and community composition of particle-associated and free-living bacteria in mesopelagic and bathypelagic Southern Ocean water masses: Evidence of dispersal limitation in the Bransfield Strait. *Limnol. Oceanogr.* 62, 1080–1095. doi:10.1002/lno.10487.

Mishra, A., and Jha, B. (2009). Isolation and characterization of extracellular polymeric substances from micro-algae Dunaliella salina under salt stress. *Bioresour. Technol.* 100, 3382–3386. doi:10.1016/j.biortech.2009.02.006.

Müller, S., Vähätalo, A. V, Stedmon, C. A., Granskog, M. A., Norman, L., Aslam, S. N., et al. (2013). Selective incorporation of dissolved organic matter (DOM) during sea ice formation. *Mar. Chem.* 155, 148–157. doi:10.1016/j.marchem.2013.06.008.

Mundy, C. J., Gosselin, M., Ehn, J. K., Belzile, C., Poulin, M., Alou, E., et al. (2011). Characteristics of two distinct high-light acclimated algal communities during advanced stages of sea ice melt. *Polar Biol.* 34, 1869–1886. doi:10.1007/s00300-011-0998-x.

Nicolaus, M., Katlein, C., Maslanik, J., and Hendricks, S. (2012). Changes in Arctic sea ice result in increasing light transmittance and absorption. *Geophys. Res. Lett.* 39. doi:https://doi.org/10.1029/2012GL053738.

Niemi, A., Meisterhans, G., and Michel, C. (2014). Response of under-ice prokaryotes to experimental sea-ice DOM enrichment. *Aquat. Microb. Ecol.* 73, 17–28.

Niemi, A., Michel, C., Hille, K., and Poulin, M. (2011). Protist assemblages in winter sea ice: setting the stage for the spring ice algal bloom. *Polar Biol.* 34, 1803–1817. doi:10.1007/s00300-011-1059-1.

Norman, L., Thomas, D. N., Stedmon, C. A., Granskog, M. A., Papadimitriou, S., Krapp, R. H., et al. (2011). The characteristics of dissolved organic matter (DOM) and chromophoric dissolved organic matter (CDOM) in Antarctic sea ice. *Deep Sea Res. Part II Top. Stud. Oceanogr.* 58, 1075–1091. doi:10.1016/j.dsr2.2010.10.030.

Nöthig, E. M., Bracher, A., Engel, A., Metfies, K., Niehoff, B., Peeken, I., et al. (2015). Summertime plankton ecology in fram strait-a compilation of long-and short-term observations. *Polar Res.* 34, 23349. doi:10.3402/polar.v34.23349.

Notz, D., and Community, S. (2020). Arctic sea ice in CMIP6. *Geophys. Res. Lett.* 47. doi:10.1029/2019GL086749.

Oksanen, J., Blanchet, F. G., Kindt, R., Legendre, P., Minchin, P. R., O'hara, R. B., et al. (2013). Community ecology package. *R Packag. version* 2.

Olli, K., Wexels Riser, C., Wassmann, P., Ratkova, T., Arashkevich, E., and Pasternak, A. (2002). Seasonal variation in vertical flux of biogenic matter in the marginal ice zone and the central Barents Sea. *J. Mar. Syst.* 38, 189–204. doi:10.1016/S0924-7963(02)00177-X.

Onda, D. F., Wolf, C., Metfies, K., Salter, I., and Noethig, E. (2020). Changes in exported key phytoplankton taxa related to a warm anomaly in the Fram Strait inferred from three complementary 18S rRNA gene meta-barcoding primer sets. *Authorea Prepr.*, 1–21.

Palmisano, A. C., and Garrison, D. L. (1993). Microorganisms in Antarctic sea ice. *Antarct.*

Microbiol. Wiley-Liss, New York 167.

Parada, A. E., Needham, D. M., and Fuhrman, J. A. (2016). Every base matters: assessing small subunit rRNA primers for marine microbiomes with mock communities, time series and global field samples. *Environ. Microbiol.* 18, 1403–1414.

Pedrós-Alió, C., Potvin, M., and Lovejoy, C. (2015). Diversity of planktonic microorganisms in the Arctic Ocean. *Prog. Oceanogr.* 139, 233–243. doi:10.1016/j.pocean.2015.07.009.

Peeb, A., Dang, N. P., Truu, M., Nõlvak, H., Petrich, C., and Truu, J. (2022). Assessment of Hydrocarbon Degradation Potential in Microbial Communities in Arctic Sea Ice. *Microorganisms* 10. doi:10.3390/microorganisms10020328.

Peng, G., and Meier, W. N. (2018). Temporal and regional variability of Arctic sea-ice coverage from satellite data. *Ann. Glaciol.* 59, 191–200. doi:10.1017/aog.2017.32.

Pernthaler, A., Pernthaler, J., and Amann, R. (2002). Fluorescence in situ hybridization and catalyzed reporter deposition for the identification of marine bacteria. *Appl. Environ. Microbiol.* 68, 3094–3101. doi:10.1128/AEM.68.6.3094-3101.2002.

Piontek, J., Meeske, C., Hassenrück, C., Engel, A., and Jürgens, K. (2022). Organic matter availability drives the spatial variation in the community composition and activity of Antarctic marine bacterioplankton. *Environ. Microbiol.* n/a. doi:10.1111/1462-2920.16087.

Polyakov, I., Pnyushkov, A., Alkire, M., Igor, A., Baumann, T., Carmack, E., et al. (2017). Greater role for Atlantic inflows on sea-ice loss in the Eurasian Basin of the Arctic Ocean. *Science (80-.).* 356, 285–291. doi:10.1126/science.aai8204.

Quast, C., Pruesse, E., Yilmaz, P., Gerken, J., Schweer, T., Yarza, P., et al. (2013). The SILVA ribosomal RNA gene database project: Improved data processing and web-based tools. *Nucleic Acids Res.* 41, D590–D596. doi:10.1093/nar/gks1219.

Ramondenc, S., Nöthig, E.-M., Hufnagel, L., Bauerfeind, E., Busch, K., Knüppel, N., et al. (2022). Effects of Atlantification and changing sea-ice dynamics on zooplankton community structure and carbon flux between 2000 and 2016 in the eastern Fram Strait. *Limnol. Oceanogr.* n/a. doi:10.1002/lno.12192.

Rapp, J. Z., Fernández-Méndez, M., Bienhold, C., and Boetius, A. (2018). Effects of ice-algal aggregate export on the connectivity of bacterial communities in the central Arctic Ocean. *Front. Microbiol.* 9, 1035. doi:10.3389/fmicb.2018.01035.

Richardson, A. J. (2008). In hot water: zooplankton and climate change. *ICES J. Mar. Sci.* 65, 279–295. doi:10.1093/icesjms/fsn028.

Riedel, A., Michel, C., and Gosselin, M. (2006). Seasonal study of sea-ice exopolymeric substances on the Mackenzie shelf: implications for transport of sea-ice bacteria and algae. *Aquat. Microb. Ecol.* 45, 195–206. doi:10.3354/ame045195.

Rossel, P. E., Bienhold, C., Boetius, A., and Dittmar, T. (2016). Dissolved organic matter in pore water of Arctic Ocean sediments: Environmental influence on molecular composition. *Org. Geochem.* 97, 41–52. doi:10.1016/j.orggeochem.2016.04.003.

Rossel, P. E., Bienhold, C., Hehemann, L., Dittmar, T., and Boetius, A. (2020). Molecular Composition of Dissolved Organic Matter in Sediment Porewater of the Arctic Deep-Sea Observatory HAUSGARTEN (Fram Strait). *Front. Mar. Sci.* 7. doi:10.3389/fmars.2020.00428.

Rudels, B., Fahrbach, E., Meincke, J., Budéus, G., and Eriksson, P. (2002). The East Greenland Current and its contribution to the Denmark Strait overflow. *ICES J. Mar. Sci.* 59, 1133–1154. doi:10.1006/jmsc.2002.1284.

Sherr, E. B., Sherr, B. F., Wheeler, P. A., and Thompson, K. (2003). Temporal and spatial

variation in stocks of autotrophic and heterotrophic microbes in the upper water column of the central Arctic Ocean. *Deep Sea Res. Part I Oceanogr. Res. Pap.* 50, 557–571. doi:10.1016/S0967-0637(03)00031-1.

Simon, M., Grossart, H. P., Schweitzer, B., and Ploug, H. (2002). Microbial ecology of organic aggregates in aquatic ecosystems. *Aquat. Microb. Ecol.* 28, 175–211. doi:10.3354/ame028175.

Soltwedel, T., Bauerfeind, E., Bergmann, M., Bracher, A., Budaeva, N., Busch, K., et al. (2016). Natural variability or anthropogenically-induced variation? Insights from 15 years of multidisciplinary observations at the arctic marine LTER site HAUSGARTEN. *Ecol. Indic.* 65, 89–102. doi:10.1016/j.ecolind.2015.10.001.

Søreide, J. E., Carroll, M. L., Hop, H., Ambrose, W. G., Hegseth, E. N., and Falk-Petersen, S. (2013). Sympagic-pelagic-benthic coupling in Arctic and Atlantic waters around Svalbard revealed by stable isotopic and fatty acid tracers. *Mar. Biol. Res.* 9, 831–850. doi:10.1080/17451000.2013.775457.

Stedmon, C. A., Thomas, D. N., Granskog, M., Kaartokallio, H., Papadimitriou, S., and Kuosa, H. (2007). Characteristics of Dissolved Organic Matter in Baltic Coastal Sea Ice: Allochthonous or Autochthonous Origins? *Environ. Sci. Technol.* 41, 7273–7279. doi:10.1021/es071210f.

Stroeve, J. C., Markus, T., Boisvert, L., Miller, J., and Barrett, A. (2014). Changes in Arctic melt season and implications for sea ice loss. *Geophys. Res. Lett.* 41, 1216–1225. doi:10.1002/2013GL058951.

Stroeve, J., and Notz, D. (2018). Changing state of Arctic sea ice across all seasons. *Environ. Res. Lett.* 13, 103001. doi:10.1088/1748-9326/aade56.

Teeling, H., Fuchs, B. M., Becher, D., Klockow, C., Gardebrecht, A., Bennke, C. M., et al. (2012). Substrate-controlled succession of marine bacterioplankton populations induced by a phytoplankton bloom. *Science (80-.).* 336, 608–611. doi:10.1126/science.1218344.

Teeling, H., Fuchs, B. M., Bennke, C. M., Krüger, K., Chafee, M., Kappelmann, L., et al. (2016). Recurring patterns in bacterioplankton dynamics during coastal spring algae blooms. *Elife* 5, e11888. doi:10.7554/eLife.11888.

Thaler, M., Lovejoy, C., and Wommack, E K. (2015). Biogeography of Heterotrophic Flagellate Populations Indicates the Presence of Generalist and Specialist Taxa in the Arctic Ocean. *Appl. Environ. Microbiol.* 81, 2137–2148. doi:10.1128/AEM.02737-14.

Thomas, D. N. (2017). *Sea ice*. John Wiley & Sons.

Thomas, D. N., Papadimitriou, S., and Michel, C. (2010). *Biogeochemistry of sea ice*. Wiley-Blackwell Oxford, UK.

Tisserand, L., Dadaglio, L., Intertaglia, L., Catala, P., Panagiotopoulos, C., Obernosterer, I., et al. (2020). Use of organic exudates from two polar diatoms by bacterial isolates from the Arctic Ocean. *Philos. Trans. A. Math. Phys. Eng. Sci.* 378, 20190356. doi:10.1098/rsta.2019.0356.

Underwood, G., Fietz, S., Papadimitriou, S., Thomas, D., and Dieckmann, S. (2010). Distribution and composition of dissolved extracellular polymeric substances (EPS) in Antarctic sea ice. *Mar. Ecol. Prog. Ser.* 404, 1–19. Available at: https://www.int-res.com/abstracts/meps/v404/p1-19/.

Underwood, G. J. C., Boulcott, M., Raines, C. A., and Waldron, K. (2004). Environmental effects on exopolymer production by marine benthic diatoms: dynamics, changes in composition, and pathways of production. *J. Phycol.* 40, 293–304. doi:10.1111/j.1529-8817.2004.03076.x.

Underwood, G. J. C., Michel, C., Meisterhans, G., Niemi, A., Belzile, C., Witt, M., et al. (2019). Organic matter from Arctic sea-ice loss alters bacterial community structure and function. *Nat. Clim. Chang.* 9, 170–176. doi:10.1038/s41558-018-0391-7.

Unfried, F., Becker, S., Robb, C. S., Hehemann, J.-H., Markert, S., Heiden, S. E., et al. (2018). Adaptive mechanisms that provide competitive advantages to marine bacteroidetes during microalgal blooms. *ISME J.* 12, 2894–2906. doi:10.1038/s41396-018-0243-5.

van Leeuwe, M. A., Fenton, M., Davey, E., Rintala, J.-M., Jones, E. M., Meredith, M. P., et al. (2022). On the phenology and seeding potential of sea-ice microalgal species. *Elem. Sci. Anthr.* 10, 29. doi:10.1525/elementa.2021.00029.

van Leeuwe, M. A., Tedesco, L., Arrigo, K. R., Assmy, P., Campbell, K., Meiners, K. M., et al. (2018). Microalgal community structure and primary production in Arctic and Antarctic sea ice: A synthesis. *Elem. Sci. Anthr.* 6, 4. doi:10.1525/elementa.267.

Vaulot, D., Eikrem, W., Viprey, M., and Moreau, H. (2008). The diversity of small eukaryotic phytoplankton (≤3 µm) in marine ecosystems. *FEMS Microbiol. Rev.* 32, 795–820. doi:10.1111/j.1574-6976.2008.00121.x.

Vidal-Melgosa, S., Sichert, A., Francis, T. Ben, Bartosik, D., Niggemann, J., Wichels, A., et al. (2021). Diatom fucan polysaccharide precipitates carbon during algal blooms. *Nat. Commun.* 12, 1150. doi:10.1038/s41467-021-21009-6.

von Appen, W.-J., Waite, A. M., Bergmann, M., Bienhold, C., Boebel, O., Bracher, A., et al. (2021). Sea-ice derived meltwater stratification slows the biological carbon pump: results from continuous observations. *Nat. Commun.* 12, 1–16.

Wang, M., and Overland, J. E. (2012). A sea ice free summer Arctic within 30 years: An update from CMIP5 models. *Geophys. Res. Lett.* 39. doi:https://doi.org/10.1029/2012GL052868.

Wemheuer, B., Wemheuer, F., Hollensteiner, J., Meyer, F.-D., Voget, S., and Daniel, R. (2015). The green impact: bacterioplankton response toward a phytoplankton spring bloom in the southern North Sea assessed by comparative metagenomic and metatranscriptomic approaches. *Front. Microbiol.* 6. doi:10.3389/fmicb.2015.00805.

Wickham, H. (2016). "Getting Started with ggplot2," in *ggplot2* (Springer), 11–31. doi:10.1007/978-3-319-24277-4_2.

Wickham, H., Averick, M., Bryan, J., Chang, W., McGowan, L., François, R., et al. (2019). Welcome to the Tidyverse. *J. Open Source Softw.* 4, 1686. doi:10.21105/joss.01686.

Wietz, M., Bienhold, C., Metfies, K., Torres-Valdés, S., von Appen, W.-J., Salter, I., et al. (2021). The polar night shift: seasonal dynamics and drivers of Arctic Ocean microbiomes revealed by autonomous sampling. *ISME Commun.* 1, 76. doi:10.1038/s43705-021-00074-4.

Wilson, B., Müller, O., Nordmann, E. L., Seuthe, L., Bratbak, G., and Øvreås, L. (2017). Changes in marine prokaryote composition with season and depth over an Arctic polar year. *Front. Mar. Sci.* 4, 95. doi:10.3389/fmars.2017.00095.

Wolter, L. A., Mitulla, M., Kalem, J., Daniel, R., Simon, M., and Wietz, M. (2021). CAZymes in Maribacter dokdonensis 62–1 From the Patagonian Shelf: Genomics and Physiology Compared to Related Flavobacteria and a Co-occurring Alteromonas Strain. *Front. Microbiol.* 12. doi:10.3389/fmicb.2021.628055.

Xing, P., Hahnke, R. L., Unfried, F., Markert, S., Huang, S., Barbeyron, T., et al. (2015). Niches of two polysaccharide-degrading Polaribacter isolates from the North Sea during a spring diatom bloom. *ISME J.* 9, 1410–1422. doi:10.1038/ismej.2014.225.

Xu, D., Kong, H., Yang, E.-J., Li, X., Jiao, N., Warren, A., et al. (2020). Contrasting Community

Composition of Active Microbial Eukaryotes in Melt Ponds and Sea Water of the Arctic Ocean Revealed by High Throughput Sequencing. *Front. Microbiol.* 11. doi:10.3389/fmicb.2020.01170.

Zhang, F., Cao, S., Gao, Y., and He, J. (2019). Distribution and environmental correlations of picoeukaryotes in an Arctic fjord (Kongsfjorden, Svalbard) during the summer. *Polar Res.* 38. doi:10.33265/polar.v38.3390.

Supplementary Material

Table S1. Summary of the number of eukaryotic sequences obtained for each sample and number of sequences after bioinformatic processing with DADA2 as well as calculated alpha diversity indices. SW: seawater control, ICE: ice melt and sea water set up.

DNA sample	No. of sequences after DADA2	Observed richness (No. of ASVs)	Chao 1 richness estimator	Shannon diversity index	Inverse Simpsons diversity index	Richness coverage (%)	Sample completeness (%)	Size fraction (µm)	Sampling time (h)
3 µm SW 15h	275132	695	759.21	3.91	13.71	91	99.97	3	17h
3 µm SW 48h	13874	80	1199.33	4.68	36.52	43	99.67	3	48h
3µm-ICE-ref	196318	695	754.92	4.35	34.51	92	99.96	3	NA
3 µm ICE 15h	156704	724	796.38	3.36	7.29	91	99.93	3	17h
3 µm ICE 33h	235942	903	977.94	4.16	20.35	92	99.95	3	33h
3 µm ICE 48h	606820	1148	174.09	2.05	6.43	96	99.99	3	48h
0.2 µm-SW-ref	77243	647	717.94	4.45	35.62	90	99.87	0.22	NA
0.2 µm SW 15h	505752	622	700.33	1.84	2.54	89	99.98	0.22	17h
0.2 µm SW 48h	345022	448	495.23	1.39	2.04	90	99.98	0.22	48h
0.2 µm-ICE-ref	200702	82	125.15	1.70	4.30	63	99.98	0.22	NA
0.2 µm ICE 15h	460287	840	899.25	2.93	5.31	93	99.98	0.22	17h
0.2 µm ICE 27h	151033	640	694.44	2.55	4.01	92	99.95	0.22	27h
0.2 µm ICE 33h	246208	709	772.98	2.60	3.86	92	99.96	0.22	33h
0.2 µm ICE 48h	370071	509	564.10	2.09	4.01	90	99.98	0.22	48h

Table S2. Summary of the number of bacterial sequences obtained for each sample and number of sequences after bioinformatic processing with DADA2 as well as calculated alpha diversity indices. SW: seawater control, ICE: ice melt and sea water set up.

DNA sample	No. of sequences after DADA2	Observed richness (No. of ASVs)	Chao 1 richness estimator	Shannon diversity index	Inverse Simpsons diversity index	Richness coverage (%)	Sample completeness (%)	Size fraction (µm)	Sampling time (h)
3 µm SW 15h	164005	803	874.96	4.23	25.91	92	99.94	3	15h
3 µm SW 48h	62706	250	1011.01	4.04	25.28	64	99.86	3	48h
3µm-ICE-ref	92385	378	469.53	3.40	17.73	80	99.89	3	NA
3 µm ICE 15h	177223	864	959.67	4.50	41.10	90	99.93	3	15h
3 µm ICE 33h	73807	635	778.93	4.07	24.88	81	99.79	3	33h
3 µm ICE 48h	344123	866	383.50	3.74	20.99	85	99.96	3	48h
0.2 µm-SW-ref	102792	731	789.26	4.82	47.00	92	99.92	0.22	NA
0.2 µm SW 15h	394871	847	945.88	4.43	40.00	89	99.97	0.22	15h
0.2 µm SW 48h	261377	786	860.62	4.22	30.57	91	99.96	0.22	48h
0.2 µm-ICE-ref	146642	242	408.88	3.44	18.18	58	99.94	0.22	NA
0.2 µm ICE 15h	332780	905	983.76	4.72	56.12	92	99.97	0.22	15h
0.2 µm ICE 27h	142147	790	872.97	4.71	56.61	90	99.92	0.22	27h
0.2 µm ICE 33h	264435	829	886.34	4.63	50.72	93	99.97	0.22	33h
0.2 µm ICE 48h	388050	810	918.67	4.08	19.95	88	99.97	0.22	48h

Table S3. Relative abundance of relative eukaryotic genera in main orders. SW: seawater control, ICE: ice melt and sea water set up.

	0.2 µm								3 µm					
	SW-ref	15h SW	48h SW	ICE-ref	15h ICE	27h ICE	33h ICE	48h ICE	15h SW	48h SW	ICE-ref	15h ICE	33h ICE	48h ICE
Bacillariophyta														
Fragilariopsis	62.7	46.2	44.3	25.0	56.3	71.1	58.3	52.1	44.3	41.4	0.3	26.8	31.1	38.9
Minutocellus	7.5	44.9	45.0	66.7	30.2	19.7	30.7	34.8	25.9	24.1	0.1	44.6	20.3	11.0
Attheya	0.1	0.1	0.1	0.0	0.1	0.4	0.5	0.3	0.4	13.8	3.5	5.4	20.6	16.8
Navicula	0.1	0.1	0.0	0.0	0.2	0.2	0.5	0.1	0.2	0.0	37.2	0.8	1.6	1.6
Chaetoceros	4.5	0.2	0.4	0.0	0.6	0.2	0.4	0.2	3.1	0.0	15.4	4.4	3.4	2.8
Eucampia	7.8	0.0	0.0	8.3	0.1	0.3	0.2	0.2	5.6	0.0	0.4	0.4	0.4	1.5
Naviculales	0.0	0.0	0.0	0.0	0.7	0.3	0.4	0.9	0.1	6.9	2.5	1.9	4.3	3.5
Actinocyclus	3.5	0.2	0.1	0.0	0.1	0.1	0.6	0.2	1.6	3.4	0.1	1.5	1.8	1.9
Cylindrotheca	0.0	0.0	0.0	0.0	0.3	0.2	0.3	0.4	0.1	0.0	9.5	0.2	0.6	2.0
Arcocellulus	0.3	1.6	2.3	0.0	1.3	0.7	1.2	1.6	0.9	0.0	0.0	2.2	0.9	0.4
Bacillaria	0.0	0.0	0.0	0.0	0.3	0.3	0.3	0.1	0.0	0.0	4.5	0.4	1.0	4.8
Thalassiosira	3.8	0.0	0.0	0.0	0.1	0.2	0.3	0.0	1.1	0.0	0.0	0.5	0.5	1.1
Dinophyceae														
Dinophyceae un	33.6	27.5	22.8	33.3	23.0	15.1	6.2	19.8	39.6	0.1	2.0	10.2	4.6	6.9
Woloszynskia	8.2	4.4	5.5	0.0	1.3	2.0	7.1	15.1	2.5	98.9	6.2	18.1	13.3	12.4
Gymnodiniales un	17.3	38.4	33.8	0.0	26.6	16.1	9.1	24.0	20.5	0.0	0.0	2.0	0.3	1.5
Apocalathium	0.1	3.1	11.3	0.0	7.4	20.9	36.2	11.1	0.1	0.4	19.4	12.5	19.8	20.0
Heterocapsa	2.6	2.2	3.5	22.2	3.7	8.6	11.1	1.7	5.3	0.1	16.0	6.2	12.1	9.7
Polarella	0.0	4.8	6.9	22.2	0.4	5.7	15.8	3.0	1.2	0.1	19.1	1.3	15.3	7.3
Gyrodinium	5.5	2.6	3.4	0.0	16.3	10.5	5.5	6.3	4.8	0.2	4.2	8.5	13.0	20.6
Prorocentrum	9.6	5.5	1.5	11.1	5.0	4.7	1.2	4.4	10.0	0.0	0.0	16.7	0.9	2.3
Gymnodinium	10.3	7.2	2.3	0.0	7.7	4.9	3.2	3.3	9.0	0.0	1.2	1.0	2.7	2.2
Suessiaceae un	0.0	0.1	8.1	11.1	0.1	0.9	0.3	0.5	0.3	0.0	14.3	3.9	6.0	3.1
Thoracosphaeraceae un	4.1	0.4	0.5	0.0	0.2	2.1	1.4	2.6	3.6	0.1	2.6	6.6	2.3	3.6
Gymnodiniaceae un	0.1	0.6	0.3	0.0	2.4	2.4	0.9	1.9	0.2	0.0	7.6	0.3	2.8	2.9
Pelagodinium	4.2	2.3	0.0	0.0	1.1	0.1	0.5	1.8	1.2	0.0	0.7	1.7	0.9	0.7

Tripos	2.8	0.1	0.0	0.0	0.3	0.0	0.0	2.0	0.0	0.0	0.1	4.3	0.7	1.7
Prymnesiophyceae														
Phaeocystis	54.5	59.2	61.7	20.0	70.0	79.8	67.8	57.5	38.2	66.7	4.2	34.4	43.1	65.9
Chrysochromulina	39.0	35.0	30.0	40.0	26.1	14.9	27.6	35.2	47.2	33.3	57.8	51.3	40.8	27.3
Isochrysidaceae un	0.0	0.0	0.0	0.0	0.0	0.0	0.0	0.0	0.0	0.0	23.7	0.1	4.9	0.5
Prymnesium	1.8	0.7	1.8	0.0	0.4	1.0	0.8	2.9	4.8	0.0	0.7	8.8	2.9	1.2
Prymnesiales un	1.6	2.9	3.6	0.0	1.6	1.4	1.6	1.6	1.6	0.0	3.5	0.9	2.1	0.9
Pseudohaptolina	0.0	0.0	0.0	0.0	0.0	0.1	0.0	0.5	0.0	0.0	9.2	0.4	1.8	0.3
Coccolithus	0.1	0.0	0.0	0.0	0.0	0.0	0.0	0.0	0.3	0.0	0.0	1.4	1.6	0.5
Chlorophyta														
Chloroparvula	52.1	92.8	94.9	99.8	85.1	88.8	89.0	92.1	85.3	70.0	1.1	87.1	71.1	73.1
Micromonas	34.6	6.4	4.5	0.2	12.7	9.7	8.9	7.0	7.1	29.9	1.1	6.1	4.4	6.1
Carteria	0.0	0.0	0.0	0.0	0.0	0.0	0.5	0.0	0.5	0.0	59.6	1.1	12.6	9.3
Mantoniella	1.5	0.4	0.2	0.0	0.7	0.5	0.5	0.3	4.3	0.0	8.0	2.9	4.9	5.3
Pyramimonadales un	0.2	0.0	0.0	0.0	0.0	0.0	0.1	0.0	0.3	0.0	15.5	0.4	2.6	1.9
Pyramimonas	0.1	0.0	0.0	0.0	0.0	0.0	0.1	0.0	0.1	0.0	11.2	0.2	2.1	1.7

Table S4. Relative abundance of relative bacterial genera in main orders. SW: seawater control, ICE: ice melt and sea water set up.

	0.2µm								3µm					
	SW-ref	15h SW	48h SW	ICE-ref	15h ICE	27h ICE	33h ICE	48h ICE	15h SW	48h SW	ICE-ref	15h ICE	33h ICE	48h ICE
Flavobacteriales														
Polaribacter	5.1	12.9	16.6	84.8	15.8	20.9	17.1	18.9	4.9	11.9	19.1	10.5	19.0	23.3
Ulvibacter	6.1	14.7	16.4	3.1	11.1	11.9	13.1	7.1	23.5	2.7	9.4	16.4	11.8	13.3
NS5 marine group	22.1	21.5	18.0	0.0	18.0	16.9	17.5	8.4	2.8	0.1	0.1	3.2	2.6	1.2
Nonlabens	0.0	0.1	0.1	4.3	2.6	4.9	3.2	2.4	0.2	0.1	41.1	7.1	18.1	15.4
Formosa	5.8	10.1	12.1	0.0	8.7	8.1	9.6	2.8	9.1	0.0	4.4	6.6	3.9	4.1
Cryomorphaceae un	20.1	8.6	6.2	0.0	10.3	7.1	7.7	2.8	2.6	0.1	0.4	1.7	1.5	1.8
NS9 marine group un	11.7	3.8	2.7	0.0	3.8	3.2	3.2	0.9	15.7	6.0	1.1	7.6	3.7	4.3
Pseudofulvibacter	1.3	1.4	1.1	0.2	2.3	1.7	2.4	0.9	15.1	11.4	0.0	15.1	5.0	6.1
NS4 marine group	5.0	4.8	4.0	3.5	5.0	3.8	4.4	3.1	1.0	0.0	0.0	1.0	0.6	0.3
Psychroflexus	0.0	0.0	0.0	0.0	0.3	0.7	0.3	0.1	0.1	0.0	1.8	4.6	11.4	11.7
Fluviicola	2.2	2.5	2.2	0.0	2.2	1.7	2.0	0.6	6.9	0.0	0.2	4.5	2.2	1.7
Maribacter	0.0	0.0	0.0	0.0	0.4	0.8	0.5	0.6	0.2	0.0	11.3	1.5	5.9	4.3
NS7 marine group un	7.1	2.8	2.2	0.0	3.2	1.9	2.3	0.7	1.2	0.0	0.0	0.7	0.5	0.7
NS2b marine group	2.4	3.7	3.7	0.0	2.8	2.7	2.8	0.8	1.8	0.0	0.0	1.4	0.6	0.4
Aurantivirga	1.3	1.8	2.7	0.0	1.4	2.0	1.8	2.0	2.6	0.0	0.1	2.4	1.1	0.9
Flavobacteriales un	3.2	2.1	1.9	0.0	2.4	1.4	1.9	0.5	0.2	0.0	0.0	0.1	0.1	0.2
Winogradskyella	0.0	0.0	0.0	0.0	0.1	0.1	0.1	0.1	0.1	0.0	3.8	0.8	2.2	1.9
Rhodobacterales														
Sulfitobacter	7.7	22.0	33.0	17.8	18.7	16.7	22.1	47.1	15.1	82.8	6.7	12.1	11.0	8.2
Planktomarina	44.7	42.7	37.0	0.0	33.8	31.8	31.2	10.6	28.6	2.2	0.1	18.5	8.2	2.3
Octadecabacter	0.5	2.9	3.9	7.8	13.2	17.0	16.8	14.8	8.1	0.2	57.3	24.8	35.9	43.8
Ascidiaceihabitans	33.6	26.4	21.2	0.0	23.7	22.6	18.3	5.2	35.6	0.2	0.0	24.4	9.4	4.0
Yoonia-Loktanella	0.4	1.3	1.8	71.5	4.8	6.0	6.6	11.6	3.3	2.0	27.6	14.0	29.5	35.0
Rhodobacteraceae un	1.2	1.0	0.8	2.7	2.0	2.6	2.2	1.1	2.3	0.0	6.0	3.7	4.7	4.6
Amylibacter	8.6	2.7	1.6	0.0	2.9	2.6	2.1	6.6	5.0	0.1	0.0	1.3	0.5	0.3

Roseobacter clade NAC11-7 lineage	2.0	0.6	0.5	0.0	0.5	0.4	0.4	3.0	1.0	2.2	0.1	0.3	0.2	0.1
Verrucomicrobiales														
Roseibacillus	51.4	62.4	60.0	0.9	54.1	51.1	45.5	47.6	71.4	98.7	0.7	63.1	30.9	39.1
Luteolibacter	48.4	37.5	39.7	0.1	41.6	42.9	47.9	43.5	28.5	0.5	2.9	25.2	16.5	13.7
Rubritalea	0.1	0.2	0.3	99.0	4.3	5.9	6.5	8.9	0.1	0.8	96.2	11.7	52.6	47.1
Alteromonadales														
Paraglaciecola	48.8	15.9	28.0	10.3	71.6	66.3	56.0	23.6	13.3	0.2	37.2	39.2	39.5	56.5
Colwellia	10.7	37.9	37.8	89.6	13.5	20.3	18.8	15.2	62.8	99.8	5.3	17.6	12.2	14.6
Glaciecola	0.5	1.5	0.0	0.2	6.0	5.7	9.4	1.1	4.1	0.0	56.4	38.7	45.2	26.6
Pseudoalteromonas	8.2	37.1	20.7	0.0	3.5	2.9	9.9	8.2	6.8	0.0	0.1	2.1	1.7	1.1
Alteromonas	26.6	6.8	3.7	0.0	4.8	4.2	5.1	15.2	3.6	0.0	0.0	2.1	0.6	0.3
Alteromonadaceae un	0.0	0.0	0.0	0.0	0.0	0.0	0.0	35.3	0.0	0.0	0.0	0.0	0.0	0.0
Colwelliaceae un	0.0	0.0	9.8	0.0	0.6	0.5	0.6	1.3	9.0	0.0	0.3	0.0	0.4	0.8
Marinobacter	5.2	0.0	0.0	0.0	0.1	0.0	0.3	0.1	0.2	0.0	0.1	0.0	0.1	0.0
Oceanospirillales														
Nitrincolaceae un	76.2	68.6	73.2	1.2	53.9	50.1	57.4	14.6	72.6	66.5	28.6	50.3	35.4	25.0
Kangiellaceae un	2.0	4.2	2.5	93.6	18.9	17.6	7.5	31.1	2.8	0.0	24.6	12.5	18.9	33.4
Pseudohongiella	18.5	24.5	21.6	0.1	22.6	28.2	29.5	5.3	21.6	0.1	8.6	21.8	21.6	10.3
Halomonas	0.5	0.5	0.4	3.6	0.5	0.6	1.1	47.7	0.4	33.4	1.1	2.5	3.0	0.4
Oleispira	0.0	0.0	0.1	1.5	2.3	2.0	1.9	0.7	0.2	0.0	30.9	9.4	17.4	25.4
Litoricola	1.4	2.2	2.2	0.0	1.4	1.0	2.1	0.2	2.0	0.0	0.0	1.6	1.8	0.3
Saccharospirillaceae un	0.0	0.0	0.0	0.0	0.4	0.5	0.3	0.3	0.0	0.0	4.6	1.4	0.6	4.8
Oleiphilus sp	0.0	0.0	0.0	0.0	0.0	0.0	0.0	0.0	0.0	0.0	1.7	0.0	0.0	0.1

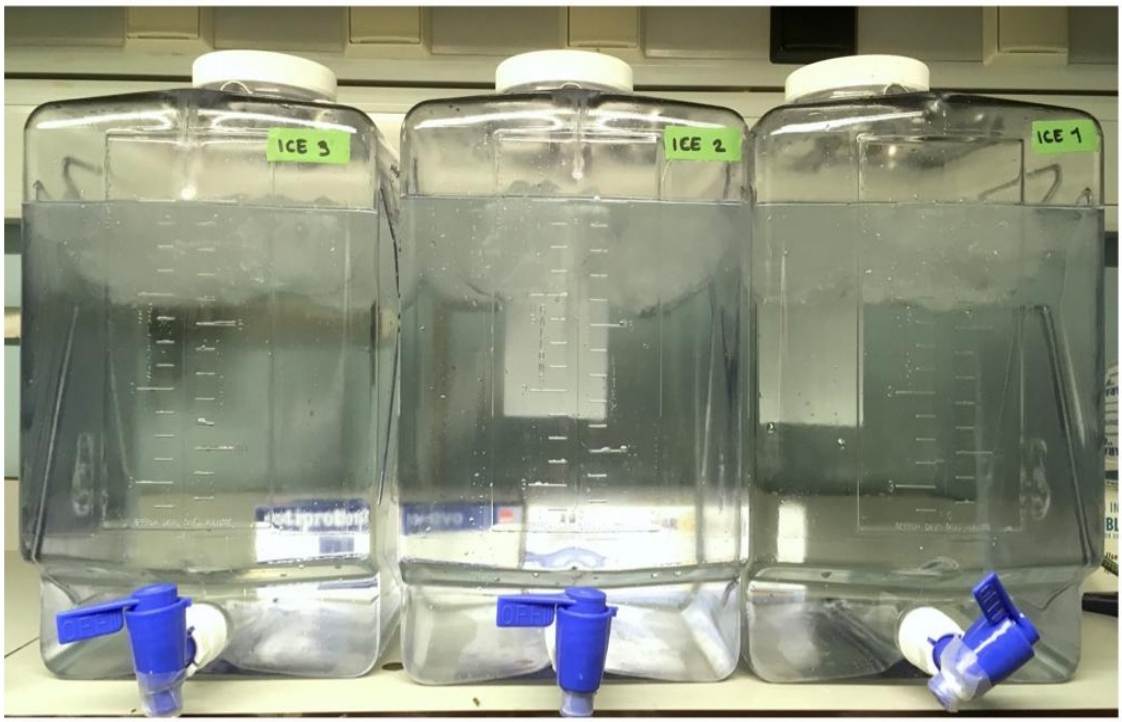

Figure S1. Experiment setup displaying the sea ice core pieces melting after 15h.

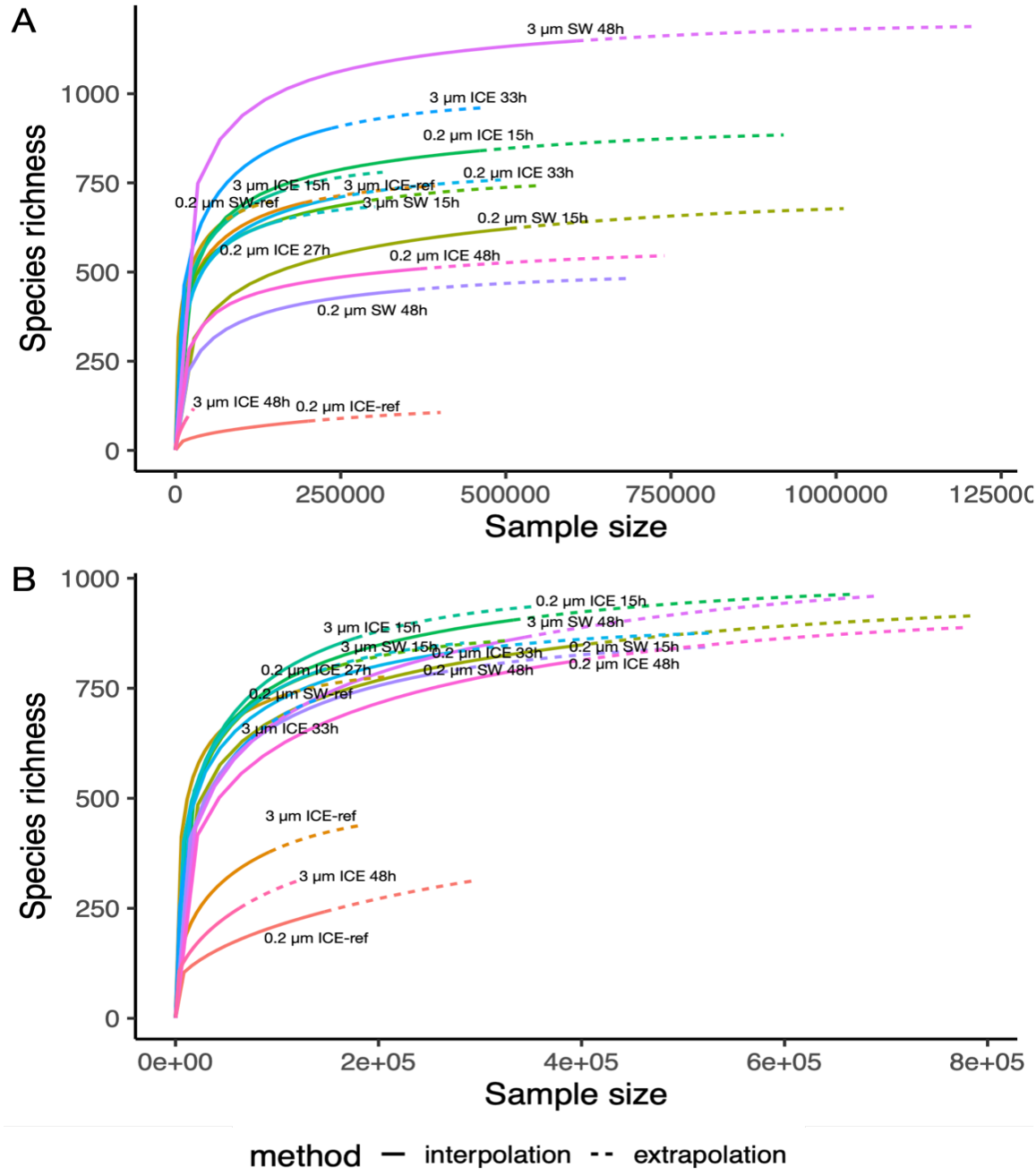

Figure S2. Rarefaction curves for (A); eukaryotic and (B); bacterial communities.

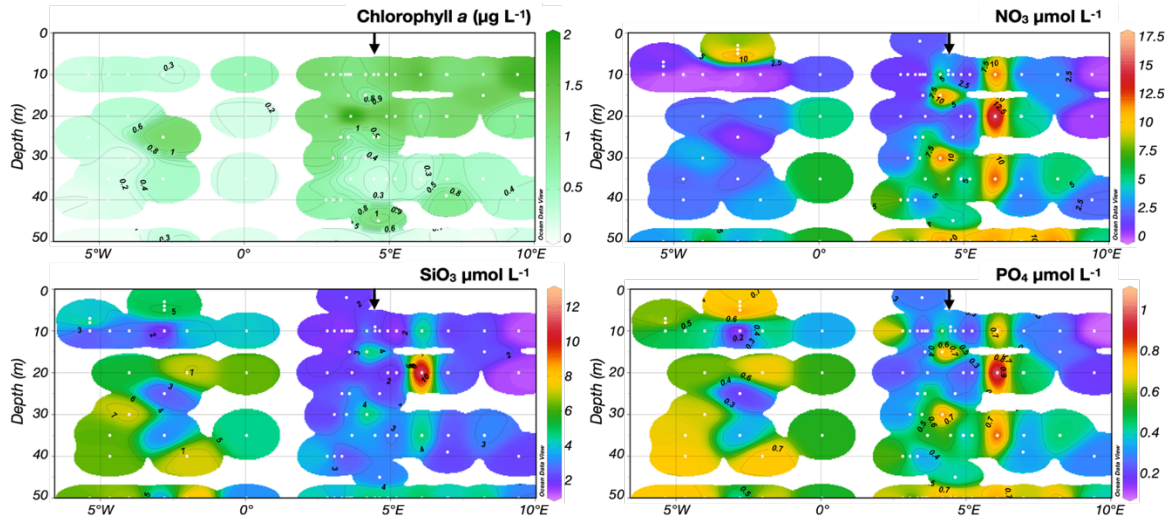

Figure S3. Nutrient profile at the ~ 79°N transect (79°N - 80°N) measured in-situ at the first 50 m during PS121 expedition to Fram Strait, white dots represent sampled nutrient data. The black arrow indicates the location of station N4 where we sampled surface seawater.

2. General Discussion

The AO is warming four times as fast as the global average (Rantanen et al., 2022), and model predictions suggest a seasonally ice-free Arctic in the next decades (Wang and Overland, 2012; Overland and Wang, 2013; Notz and Stroeve, 2018), as early as in 13 years (Docquier and Koenigk, 2021). The Fram Strait is the largest and deepest (~ 5500 m) entrance and exchange site between the Atlantic and the AO (Beszczynska-Moeller et al., 2011). The Fram Strait is also a highly influenced by oceanographic dynamics, where the two opposing hydrographic regimes, EGC and WSC partly converge. Records of pronounced increases of heat transported with the Atlantic water extended over the past decades in the region (Beszczynska-Möller et al., 2012), as well as increases in sea ice area export south of the Strait (Smedsrud et al., 2011; Behnam et al., 2019; Krumpen et al., 2019), that evidently have impacted the AO (Polyakov et al., 2011, 2013a, 2017). Hence, the Strait is a key area to track ecosystem changes in the AO. However, to fully understand the impacts of global climate change in the Arctic ecosystem, baselines need to be established, and patterns of change need to be studied across different temporal and spatial scales, in order to identify drivers of variation and indicators of change.

2.1 Towards a comprehensive picture of the Arctic microbiome in Fram Strait, the main gateway to the Arctic Ocean

To date, numerous studies on eukaryotic communities have addressed important ecological processes and ecological impacts of climate change on the primary producers at the basis of the food web with focus on the photic layer of the water column (Kilias et al., 2013, 2014, 2020; Nöthig et al., 2015; Metfies et al., 2016, 2017; Bachy et al., 2022; Ramondenc et al., 2022). Molecular surveys based on next-generation sequencing of the 16S and 18S rRNA genes provided the first overview of composition and community structure with a greater focus on pelagic bacteria and archaea in the water column of Fram Strait (Wilson et al., 2017; Fadeev et al., 2018; Müller et al., 2018; Fadeev et al., 2021a; Wietz et al., 2021). Moreover, other studies have focused on summer bacterial organic matter degradation across the

different regions of the Fram Strait (Piontek et al., 2014, 2015; von Jackowski et al., 2020). Only recently a new study made a comparative assessment of the functional gene diversity and metabolic capacities of bacteria in Fram Strait (Priest et al., 2022). Overall, these studies provided valuable information about the diversity, distribution and potential function of microbial communities across Fram Strait. This thesis also offers a new perspective, by combining observations of active bacteria and archaea together with eukaryotes and viruses, in order to provide baseline knowledge about the gene expression of these communities (Chapter I). The thesis expands on these observations, and provides new insights into actual cell abundances of key bacterial and archaeal groups (Chapter II). It includes long-term evaluations of microbial composition in sinking particles (Chapter III), and an experimental approach for observing microbial dynamics when sea ice melts in seawater (Chapter IV). Altogether, this thesis will allow for the identification of key microbial indicators (MI) and environmental drivers of change to help predict future changes in the AO ecosystem.

Molecular studies have focused on the evaluation of environmental factors in shaping microbial communities and on the seasonal transition of such communities in the western (EGC) and the eastern (WSC) part of the Strait. Prior to this thesis, cell abundances (standing stocks) of key bacteria and archaea in surface and deep sea (>2000 m) waters of Fram Strait remained unaddressed (Fram Strait sill depth is approximately 2600 m with a maximum depth of 5600 m at the Molloy Hole). Chapter II provided the first cell abundances of key taxonomic groups, from surface (0-30 m) down to deeper waters (2500 m). The observations of Chapter I and Chapter II, free of compositional-bias, are needed to fully understand the biogeochemical roles of these microbes in the water column.

2.2 Microbial gene expression was distinct between different water masses

The opposite flowing boundary currents (EGC and WSC) that carry different water masses residing in the upper ~300 m of the water column, are one of the specific features of the Fram Strait (Rudels et al., 2002; Beszczynska-Moeller et al., 2011; Beszczynska-Möller et al., 2012). Signs of an increase of AW intrusion into the AO through Fram Strait, "Atlantification" (Polyakov et al., 2017) were already present since the beginning of the early 20th century

(Tesi et al., 2022). The influence of distinct water masses, which affect the AO oceanographic characteristics (Polyakov et al., 2013a, 2020a, 2020b), the microbial community composition in the water column (Galand et al., 2010) and benthic communities (Hamdan et al., 2013), has been identified as a possible driver of diversity also in Fram Strait (Müller et al., 2018). Yet the role of water masses in driving the distribution and activities of microbial communities in Fram Strait remained largely unexplored.

The results of Chapter I, provided an overview of active bacteria, archaea, microbial eukaryotes and viruses in three different water masses. Based on differential expression analysis we identified that different water masses characterized by different oceanographical conditions were the main driver of expression. The water masses identified at the time of sampling were: PSWw, and AW in the east and PSW in the west. They harboured different active communities. Key metabolic activities at the surface were attributed to the late phytoplankton bloom dominated by diatoms (*Skeletonema*, *Fragilariopsis* and *Eucampia*) and chlorophytes (*Bathycoccus* and *Micromonas*), whereas chemolithotrophic activities associated with AOA (*Nitrosopumilales* and unclassified *Thaumarchaeota*) were present in the deeper AW. On the western part of the Strait, *Chaetoceros* and SAR202 were significantly more active than in other water masses.

The overall representation of archaea in Chapter I matched with cell abundances and depth profiles of archaea and *Thaumarchaeota* discussed in Chapter II. In both studies the ecosystem state was characterized by a late phytoplankton bloom indicated for example by low nutrient concentrations. In Chapter I, samples were taken later in the season (10th August – 13th September), and based on the composition of the bloom, the lower chlorophyll and nutrient concentrations the bloom in Chapter I might have been in a more advanced decaying state compared to the bloom in Chapter II. The abundance of *Nitrosopumilales* could increase at the surface during the winter months in the eastern Fram Strait likely due to vertical mixing (Wietz et al., 2021). A high-throughput sequencing study of the 16S rRNA gene combined with functional gene clone libraries of archaeal amoA (Müller et al., 2018), suggested that the different water masses play an important role in influencing the distribution of *Thaumarchaeota* in the water column rather than ammonium concentrations. The authors suggested that based on the distribution patterns of different *Thaumarchaeota*

ecotypes in the water column, water masses of Atlantic origin in the north-west of Svalbard (in the eastern Fram Strait) could exercise a dual role of limiting and facilitating dispersal of *Thaumarchaeota* OTUs. Frontal zones such as the ones in Fram Strait have shown to influence community composition, due to water mass mixing, as well as oceanographic dynamics such as the development of mesoscale eddies that influence the distribution of bacterioplankton in the Strait (Agogué et al., 2011; Djurhuus et al., 2017; Hernando-Morales et al., 2017; Fadeev et al., 2021b). Furthermore, in Chapter I we found that the reconstructed small-subunit rRNA (SSU rRNAs) of archaea (*Nitrosopumilales*) in the AW matched with the expression of transcripts coding for genes involved in ammonia oxidation i.e. AmoC and AmoA subunits of ammonia monooxygenase. Moreover, based on shared PFAMS between the water masses located in the eastern part of the Strait: PSWw and the underlying AW showed that ammonia oxidation was among the most expressed exclusive functions from AW independent of size fraction (Figure 1). Hence, *Thaumarchaeota* appear to be key players in the AW and this further highlights the relevance of chemolithotrophic processes in the deeper waters of the Strait. The role of *Thaumarchaeota* in ammonia oxidation is key in nutrient replenishment, especially of nitrate (Hatzenpichler, 2012), which could limit primary productivity at the surface with decreasing deep winter mixing due to the continued atmospheric warming and the loss of winter sea ice (Tuerena et al., 2021).

Overall, the main active heterotrophic bacteria responding to the surface phytoplankton bloom were *Bacteroidetes, Gammaproteobacteria*, *Rhodobacterales* and *Verrucomicrobiae* in the Chapters I to III and were observed to follow sea ice diatoms and substrate sourced from sea ice in the microcosm experiment described in Chapter IV. These results fit well with previously suggested MIs of phytoplankton bloom stages in Fram Strait described in the works of (Fadeev, 2018; Fadeev et al., 2018, 2021a; Wietz et al., 2021; Priest et al., 2022). *Flavobacteriales*, *Gammaproteobacteria* and *Alphaproteobacteria* are often referred to as key taxa in the degradation of organic matter (Buchan et al., 2014). The transcriptional dominance of *Alteromonadales* and *Flavobacteriales* (*Bacteroidetes*) during the bloom decay phase (Chapter I) was also observed in a decaying bloom from a mesocosm with in situ-like conditions of the Northwest Iberian upwelling system (Pontiller et al., 2022). This could be explained by distinct biogeographical patterns of different ecotypes of bacterioplankton groups (e.g., Wietz et al., 2010). The strong presence of these groups under different bloom

composition and experimental conditions, reflects the functional versatility and range of life strategies that characterize them (Buchan et al., 2014). In part this can be realized through niche partitioning or specialization in specific polysaccharides described for *Bacteroidetes* (Krüger et al., 2019; Avcı et al., 2020).

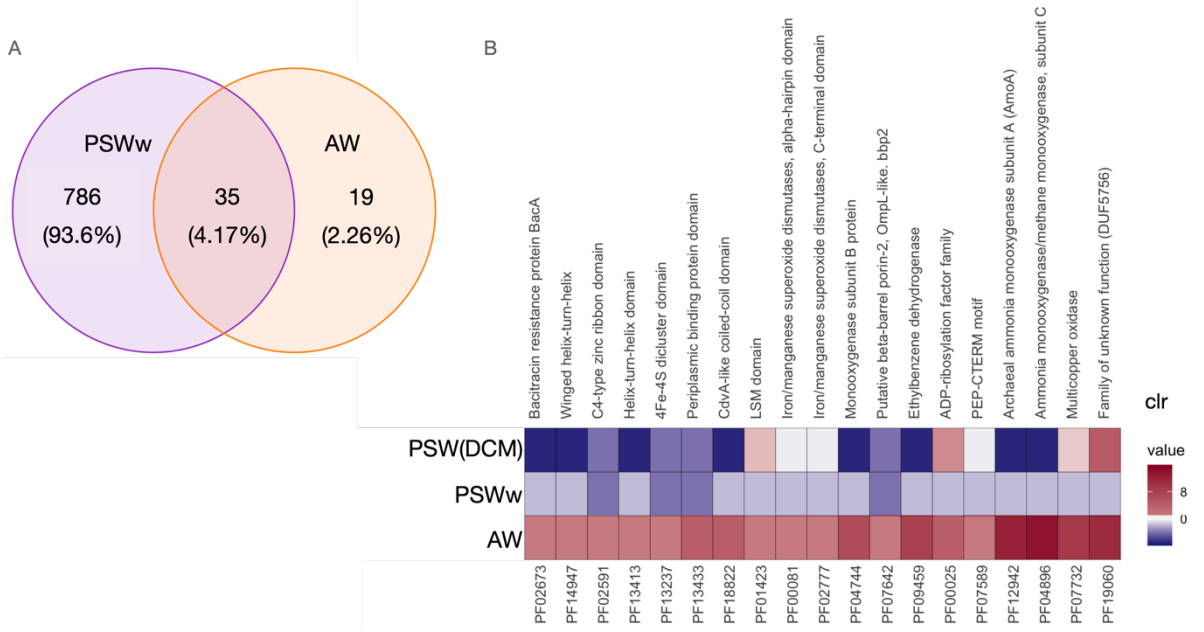

Figure 1. Differences in functional expression between water masses. A) Unique and shared protein families (PFAMs) between the water masses in the WSC independent from size fractionation. B) Comparison of unique PFAMs in the AW, PSW and their representation in different water masses. Abundances were calculated based on clr-transformed counts. AW: Atlantic water. PSWw: Warm Polar Surface water. PSW: Polar Surface water.

Less abundant groups in Chapter II (*Marinimicrobia* (SAR406), SAR324 and SAR202) were found to be significantly active in the water masses analysed in Chapter I; both *Marinimicrobia* (SAR406) and SAR324 in the PSWw and AW, whereas SAR202 was significantly more active in the epipelagic of PSW (100-200 m). These groups were not part of the microbial community of sinking particles nor found in abundance in the experiment presented in Chapter IV. Based on relative abundances it has been suggested that these groups could be indicators of winter and pre-bloom conditions (Fadeev et al., 2018; Wietz et al., 2021; Priest et al., 2022). These groups are also thought to be more abundant in meso- and bathypelagic waters in different oceanographic regions (Galand et al., 2010; Salazar et al., 2016; Wilson et al., 2017; Saw et al., 2020). The combined results of Chapter I and II further suggest that due to the significant activity of SAR342 and SAR406 and their known metabolic diversity, and their distribution across the Strait and with depth, they participate in nutrient regeneration,

for instance in nitrogen or sulfur cycling (Hawley et al., 2017; Malfertheiner et al., 2022). Additionally, in Chapter I the activity of SAR202 co-occurred with higher concentrations of refractory DOC in the PSW. SAR202 abundance was previously associated with Arctic winter conditions at the ice-covered EGC (Fadeev et al., 2018) and with deep-sea sediments of Fram Strait (Rapp, 2018). In Chapter I SAR202 was found at the lowermost bounds of the euphotic zone in PSW. Together, the strong chemolithotrophic activity by AOA in the AW and of SAR202 in the PSW could be an indication that chemolithotrophic activity re-emerges from the deeper waters with the disappearance of the phytoplankton bloom in autumn and the increase of less labile carbon after the heterotrophic degradation at the surface in summer (von Jackowski et al., 2020).

2.3 Sea ice dynamics and increasing water temperature affected bacterial and eukaryotic composition of sinking particles in Fram Strait with implications for carbon export

Sinking particles are the major conduit of carbon, energy and microorganisms to the deep sea, and play a key role in the global carbon cycle via the BCP, as the main form of transport of atmospheric carbon fixed in the upper ocean by primary production to the deep sea (De La Rocha and Passow, 2007; Turner, 2015). These aggregates serve as hotspots of microbial activity (Azam and Malfatti, 2007), with a higher concentration of cell density and enzymatic activity (Kellogg et al., 2011) compared to the free-living counterpart. Furthermore, sinking particles feed most of the organic matter to the dark ocean (Herndl and Reinthaler, 2013), and act as vectors of microbial dispersion from the surface to the deep ocean layers (Mestre et al., 2018; Fadeev et al., 2021a). Hence, evaluation of sinking particle dynamics is key to understanding pelagic-benthic–coupling in the global oceans.

Much of the current knowledge about microbial composition of sinking particles and variations over time is derived from studies from other oceanographic regions, including the microbial observatories in the western North Atlantic Ocean (Bermuda Atlantic Time-series Study "BATS" (e.g., Cruz et al., 2021)), in the subtropical North Pacific Ocean (Hawaii Ocean Time-series "HOT" (Karl and Lukas, 1996), station"ALOHA" in the North Pacific Subtropical Gyre (e.g., Karl and Church, 2014; Fontanez et al., 2015; Boeuf et al., 2019; Poff et al., 2021), in the California Current ecosystem (e.g., Fender et al., 2019) and the abyssal zone of the

California Current ecosystem "Station M" (e.g., Smith K.L and Druffel, 1998; Preston et al., 2020). Advances have been made to understand the molecular bacterial and eukaryal composition of particles, fecal pellets and aggregates (Table 1). Despite such efforts, prior to this thesis, long-term studies of microbial composition of sinking particles and studies at higher latitudes were not available.

Table 1. Overview of predominant phytoplankton, zooplankton and bacterial/archaeal taxonomic groups in sinking particles, aggregates and fecal pellets reported from selected molecular and microscopy studies in different oceanographic regions.

Oceanographic region and station	Sampling depth (m)	Sampling time	Particle collection method	Remarks	Phytoplankton assemblages	Zooplankton assemblages	Bacterial /archaea assemblages	References
North Pacific Subtropical Gyre station ALOHA	4000 m	March to November 2014 (9-months)	Sediment traps	Samples obtained during 2014 when particle flux was near the low end of historical values	Metagenomes: *Rhizaria* (*Foraminifera*) *Cnidaria* *Syndiniales* Metatranscriptomes: *Mollusca* *Cercozoa* *Oligohymenophorea*	*Crustacea* mainly pteropods,	Metagenomes and Metatranscriptomes : *Alteromonadales* *Campylobacterales* *Oceanospirillales*	(Boeuf et al., 2019)
North Pacific Subtropical Gyre station ALOHA	150 m to 500 m	Deployed on July 14, 2012	Free-drifting sediment trap array, particle interceptor traps (PITs)	Taxonomic composition and metagenomic study using PITs containing a preservative (poisoned traps) compared to preservative-free (live traps)	Live and poisoned traps: *Dinoflagellata, Protalveolata, Retaria, Metazoa, and unclassified Stramenopiles*	*Metazoa* (mostly copepods)	Live and poisoned traps: *Alteromonadales, Vibrio* *Prochlorococcus* *Oceanospirillales, Flavobacteriales*	(Fontanez et al., 2015)
North Pacific Subtropical Gyre station ALOHA	4000 m	March 2014 to November 2016	Sediment traps	Metagenomic time-series study at abysall depths	*Rhizaria*, *Opisthokonta,* and *Alveolata*. *Radiolaria*, copepods, and F*ungi* increased during the elevated carbon flux event	Pteropods	*Campylobacterales* *Gammaproteobacteria* *Alteromonadales.* During elevated carbon flux event *Alphaproteobacteria* , *Bacteroidetes* increased	(Poff et al., 2021)
Subtropical North Atlantic (Sargasso Sea) BATS	Upper 300 m	Collected in autumn (12 to 14 Sept.) of 2017 and during spring (12 to 15 March) of 2018	Surface-tethered Particle Interceptor Traps (PITs) (Gel trap)	Seasonal study	Both seasons: *Dinoflagelates* and *Syndiniales* Spring 2018*:* Diatoms, ciliates, *Cercozoa*, and chlorophytes of the order *Mamiellales*	Autumn 2017: Cyclopoid and calanoid copepods (Fall). Spring 2018: *Pleuromamma* spp., *Euphausiids*	Autumn 2017: *Bacteroidia, Gammaproteobacteria, Bacilli, Actinobacteria* *Alphaproteobacteria* Spring: *Bacteroidia* *Gammaproteobacterial*	(Ivory et al., 2019; Blanco-Bercial, 2020; Cruz et al., 2021)

North East Pacific Ocean (California Current ecosystem), Station M	3900 m and 3950 m	November 2016–July 2017	Sediment traps	9-months study with a high flux event in summer at abyssal depths	Radiolaria, *Dinoflagellata*, *Metazoa*, and *Discoba*. Diatoms dominated during the high flux event (*Thalassiosira)*	*Crustacea*: amphipods and copepods	*Bacteroidia* and Gammaproteobacteria (*Alteromonadales, Nitrosococcales Cellvibrionales*). SAR116, *Roseobacter* NAC11-7 during the high flux event	(Preston et al., 2020)
Cape Blanc (Mauritania)	100 and 400 m	Collected samples from 3 days in April 2011	Marine snow collected from drifting sediment trap	Study comparing free-living bacterial (from CTD) and marine snow bacteria using CARD-FISH	n.d	n.d	*Bacteroidetes Gammaproteobacteria Alteromonas Roseobacter*	(Thiele et al., 2015)
Fram Strait LTER HAUSGARTEN (central station)	~ 300 m	First two weeks of September from 2000 to 2011	Sediment traps (pilot study of mercury chloride fixed samples)	Ten-year study that included 18S T-RFLP and microscopy counts of phytoplankton and 454-pyrosequencing of 2009 and 2010 samples	*Mamiellophyceae*, Chrysochromulina spp., *Ichtyosporea*, *Metazoa*, *Fungi*, *Syndiniales* and *Rhizaria*	n.d	n.d	(Metfies et al., 2017)
Fram Strait LTER HAUSGARTEN (central station)	180–280 m, 800–1320 m, 2320–2550 m	2000-2016	Sediment traps	Time-series study of zooplankton composition based on swimmers and sinkers	n.d	*copepoda, foraminifera, ostracoda, amphipoda, pteropoda, and chaetognatha*	n.d	(Ramondenc et al., 2022)
Fram Strait LTER HAUSGARTEN (central station)	80–280 m	2000-2012	Sediment traps	Time-series study of sinking particle microbial composition and the relationship with environmental variables	*Bacillariophyta, Prymnesiophyceae*, *Mamiellophyceae*, *Dinophyceae*, *Syndiniales*, *Chaunacanthida*	Copepods: *Calanus spp., Metridia spp.,*	*Cellvibrionales, Alteromonadales, Flavobacteriales, Entomoplasmatales*	Chapter III, This thesis

n.d.: not determined

A growing body of evidence points to the composition of surface phytoplankton as a key factor influencing particle composition, and thus the quantity and quality of organic matter that feeds the deep-sea realm (Simon et al., 2002; Buesseler and Boyd, 2009; Guidi et al., 2009; Herndl and Reinthaler, 2013; Bach et al., 2016, 2019). In addition, other processes such as grazing and repackaging into fecal pellets, heterotrophic microbial activity and interaction between aggregates and suspended ballast minerals adds to the numerous transformations of these particles as they descend through the water column (Iversen and Ploug, 2010; Fontanez et al., 2015; Turner, 2015; Steinberg and Landry, 2017). A time series study in Fram Strait surface waters, which included quantitative microscopic analysis of phytoplankton and protozooplankton (1998 and 2011) and remote-sensing data, revealed that changes in summertime phytoplankton composition were partially attributed to a passing WWA event from 2005 to 2007. The WWA resulted from an increased warming of the AW carried by the WSC entering the AO (Nöthig et al., 2015). This phenomenon was reflected in lower fecal pellet production and low organic matter in sediments during this time (Lalande et al., 2013; Jacob, 2014). This thesis expands these observations to the molecular composition of sinking particles at ~300 m between 2000 and 2012. The samples included in Chapter III were those samples with highest POC fluxes in each year and thus a good representation of organic matter export in the region. The results presented in Chapter III revealed that sinking particle communities spanned a variety of trophic levels and life strategies, including zooplankton (mainly copepods), autotrophs: diatoms of *Bacillariophyta* (*Chaetoceros* and *Thalassiosira*), *Prymnesiophyceae* (flagellates of *Phaeocystis* and *Chrysochromulina*), and *Chlorophyta*, mainly *Mamiellophyceae*, heterotrophic protists and parasitic protists (*Dinophyceae* and *Syndiniales*) and a few radiolarians represented by the order *Chaunacanthida.* These observations were generally in accordance with previous eukaryotic surveys (Nöthig et al., 2015). Our results further suggest that the shift in dominant species started earlier with the onset of a WWA with coccolithophores present until 2006, and that the summer flagellate *Phaeocystis* was already significantly abundant from summer 2004. Despite a few mismatches due to different methods applied, Chapter III underlines the applicability and benefit of molecular studies to address long-term ecosystem changes and to identify drivers of change in these communities in Fram Strait.

Bacteria that dominated the sinking particles were composed of copiotrophic taxa and typical bloom-responders, mainly taxa of the classes *Gammaproteobacteria* (*Cellvibrionales* and *Alteromonadales*), *Bacteroidia* (*Flavobacteriales*), and *Verrucomicrobiae*. The order *Bacilli* (*Entomoplasmatales*) associated to zooplankton comprised a significant proportion of the ASVs. Taxa of the *Gammaproteobacteria* (*Alteromonadales*) and *Bacteroidia* are among the most commonly found groups in sinking particles (Table 1). Despite the diverse geographical sources of most sinking particle studies, the reported dominant groups that colonize the particles in the twilight zone of the global ocean might be driven to an extent by similar factors, likely related to the metabolic potential of organic matter degradation (DeLong et al., 2006; Buchan et al., 2014; Kong et al., 2021).

Diatoms are a dominant component of the microbiome in polar oceans and part of the sympagic and pelagic ecosystems (Armbrust, 2009; Miettinen, 2018; van Leeuwe et al., 2018; Gilbertson et al., 2022). Results in Chapter III confirmed that the fast growing and chain-forming *Chaetoceros* export carbon via sinking particles in the Fram Strait. *Chaetoceros* dominated sinking particles and were a major component of the eukaryotic community in samples that matched a larger presence of sea ice and the higher proportion of meltwater regime in the sediment trap catchment area (Chapter III). *Chaetoceros* increases in abundance were linked to sea ice and meltwater (Chapter I, Chapter III and Chapter IV). *Chaetoceros* can be found in sea ice, surface seawater and in melted water underlying the sea ice (Chapter IV). The diatom abundance in the summer might be related to stratified waters from meltwater regimes (von Appen et al., 2021). During the WWA overall diatom abundances decreased significantly, which substantially altered the overall composition of the sinking particles and reduced the POC exported to the deep sea. These changes in composition in the sinking particles were mainly attributed to warmer conditions and changes in sea ice dynamics. Experimental work proved the susceptibility of *Chaetoceros* to temperature changes (Li et al., 2017) and thus predicted this group to be vulnerable to global warming (Chaffron et al., 2022). Only recently, two studies showed how sea ice is a key factor that greatly influences carbon export efficiency and transport of functionally important microbial groups via diatom-dominated aggregates to the deep sea of Fram Strait (Fadeev et al., 2020; von Appen et al., 2021). Moreover, metagenomic screening of *Chaetoceros* species from a global expedition study (TARA Oceans; (Sunagawa et al., 2015)) further

highlights the relevance of *Chaetoceros* for the AO, with lower dispersal in the Pacific and Southern Oceans (Nef et al., 2022). Hence, *Chaetoceros* might be a MI to investigate fundamental changes in the microbiome of the Arctic ecosystem with consequences for carbon export.

During the WWA, we observed the presence of other diatoms, mainly *Thalassiosira* and a single sample with a high abundance of *Melosira* during the WWA. *Melosira* massive algal biomass falls are considered sporadic and rare in the Arctic ecosystem, but significant to carbon export (Boetius et al., 2013; Wiedmann et al., 2020). The presence of *Melosira* in one sample may result from a transient ice floe in the area, despite the general absence of sea ice during this time. Based on WGCNA and network analysis described in Chapter III, *Thalasiossira* presence was associated with early spring conditions and higher proportions of the mixed layer regime. Furthermore, some species of *Thalasiossira* have shown resistance to higher temperatures under experimental conditions (Wolf, 2019), however this might have not been the only explanation for the shift in diatom composition. The WWA brought a myriad of factors that may have contributed to the shift of phytoplankton species. For instance, the composition of the extracellular polysaccharide EPS of diatoms could change as a result of low nutrient concentrations (Chapter IV). Such changes in EPS could alter the aggregation properties of diatoms (Aslam et al., 2012, 2018) affecting sinking velocities (Seebah et al., 2014). Moreover, as the bacterial composition of the particles also shifted, it is possible that bacterial production of EPS by the new set of bacteria, such as *Marinobacter* (*Alteromonadales*), contributed to increased aggregations of diatoms, affecting the sinking velocity (Gärdes et al., 2010). Thus, the POC might have been overall low due to the absence of the main carbon sinker (*Chaetoceros*) but not significantly lower compared to other non-WWA samples, a pattern also described by (Vernet et al., 2017; Nöthig et al., 2020). To conclusively understand the coupled impacts of variables associated with global climate change, the implementation of contemporary samples of sea ice, seawater, particles and sediments is recommended for a complete picture of changes in sympagic-pelagic-benthic coupling. It will further allow, with the results of this thesis, to expand our knowledge of the Arctic microbiome and to identify the responses and possible resilience mechanisms of different key MI species from surface to the deep sea.

As "Atlantification" of the AO becomes more established (Polyakov et al., 2017, 2020a), and the AW temperatures continue to rise (Tsubouchi et al., 2021), time series studies face new challenges to identify MI at the MIZ. The passing WWA of 2005 to 2007 provided a unique opportunity to study the bacterial responses and the interactions with eukaryotes based on co-occurrence network analyses (Chapter III). As with the eukaryotic communities, changes in bacterial communities appeared to be group-specific. Taxa that increased in abundance during the WWA included *Alcanivorax* (*Oceanospirillales*), *Psychromonas*, *Marinobacter* (both *Alteromonadales*) and *Sulfitobacter* (*Rhodobacterales*). A significantly higher activity of *Alteromonadales*, *Oceanospirillales* and *Rhodobacterales* was observed in the PSWw alongside the decaying phytoplankton bloom (Chapter I). The samples included in Chapter I were obtained during September of 2019, the warmest month and the seasonal sea ice minimum of 2019. A year characterized by a sharp decrease in sea ice compared to previous ones (Melsheimer and Spreen, 2019; Yadav et al., 2020). Main functions expressed were associated with substrate uptake via ABC transporters. *Alteromonadales* and *Rhodobacterales* are key POC degraders, due to the large gene repertoire for the degradation of proteins and polysaccharides and the high expression of transporter proteins involved in the uptake of L-amino-acids, carbohydrates and of high-molecular-weight organic matter (McCarren et al., 2010; Kong et al., 2021). The results of Chapter I underline the relevance of *Alteromonadales*, *Oceanospirillales* and *Rhodobacterales* in the transformation of organic matter. Combined, the results of Chapter III and Chapter I suggest that the sinking particles of the WWA experienced a higher retention time at the surface and thus a more active heterotrophic microbial loop. Furthermore, these observations confirm previous hypotheses that low sea ice conditions impact microbial composition and export of aggregates to the deep sea (Fadeev et al., 2021a), and extend these observations to a coupled effect of sea ice and warmer conditions indicative of "Atlantification".

3. Perspectives and methodological considerations for long-term studies

3.1 Observations on seasonal dynamics

Polar regions are characterized by strong seasonality in light, temperature and sea ice cover that drive the development of phytoplankton blooms. It is expected that the ice-free summer will become longer (Notz and Stroeve, 2018), and with extended advection of phytoplankton from the Atlantic into the AO (Vernet et al., 2019) it may further extend the productive season. Hence, the timing of phytoplankton growth in Fram Strait and the AO will be altered e.g. the bloom might start earlier. Therefore, in order to understand seasonal succession and potential shifts in timing, a higher temporal resolution of samples than those included in Chapter III is needed.

In Chapter III we described differences between spring and summer microbial community composition in sinking particles, implying seasonal succession. In contrast with other time series studies (Table 1 e.g., Boeuf et al., 2019; Preston et al., 2020; Poff et al., 2021) our samples represent one to two time points (period defined for the complete opening time of the cups) per year usually first one in spring and a second one in summer. In this study, we did not observe a shift in the timing of the high POC flux events. In spring, high POC flux events in post-WWA samples occurred between April and May. Since there are no samples available prior to 2000 and only one spring sample pre-WWA in March, we cannot deduce that the timing of the peak of POC has significantly shifted. Although, the phytoplankton bloom is light-limited, trends towards earlier spring blooms have been observed in the AO (Kahru et al., 2011). Thus, future studies on sinking particles should include a higher resolution of samples covering the transition from winter to autumn e.g. from March to October in order to determine if the start of the bloom has shifted. This new incorporation of samples will allow for a better delineation of the development of the seasons necessary to understand implications for the ecosystem.

Additionally, results of Chapter III indicated that meltwater regimes coupled with sea ice dynamics are important for bloom composition. Recent studies at the MIZ have shown how meltwater drives algae spring blooms (Lester et al., 2021), and how different oceanographic regimes could have different consequences for carbon export (von Appen et al., 2021). During the melt period the strong stratification constrained at the euphotic zone helps the

phytoplankton grow at the sea ice edge that later peaks within distance from the sea ice edge (Lester et al., 2021). In Chapter III, spring samples were characterized with a higher proportion of mixed layer regime combined with the meltwater and lower POC flux than summer samples (although not significantly different). Summer samples were dominated by the meltwater regime. Moreover, the proximity of the sea ice to the mooring site in pre-WWA and post-WWA samples resulted in a meltwater regime, whereas the WWA was marked by higher proportions of a mixed layer regime with weaker stratification and lower POC flux, when the sea ice was further away. These observations match a recent study in the area in which the presence of sea ice was linked to higher carbon export efficiency through diatom-dominated aggregates that sink faster, also entailing a stronger vertical microbial connectivity (Fadeev et al., 2021a). Other studies have reported that sea-ice derived meltwater stratification can slow the biological carbon pump, resulting in a delayed export of organic matter to depth, in comparison to a mixed layer regime (von Appen et al., 2021). The results of this thesis suggest that the monitoring of early bloom development is necessary to understand the impact of meltwater regimes on particle flux. Monitoring of sea ice edge bloom initiation should start early in the year rather than from constrained time points and could benefit from a higher number of samples. Moreover, to identify the "origin" of the meltwater regime in the water column (presence of sea ice and ice melt compared to strong stratification after sea ice is gone) it is recommended to further compare the results from the particle-tracking model (Chapter III) with the satellite-derived assessments in (von Appen et al., 2021). To study how blooms are initiated at the ice edge and how they evolve over time, seasonal studies at the sea ice edge (EGC) and in the core AW (WSC) should be carried out making use of remote samplers as part of the long-term monitoring in the framework of the Ocean Observing System FRAM at the LTER HAUSGARTEN.

3.2 Monitoring microbial dynamics

The fixative that was used in the sampling cups of the sediment traps (Chapter III) was $HgCl_2$ 0.14%, proved successful for DNA isolation and amplification (Metfies et al., 2017; Wietz et al., 2022). However, in total 5% of the samples in Chapter III showed signs of decomposition and were removed from the data set. Decomposed samples were described as rotten, of black colour, sulfidic smell, and with strong zooplankton decomposition. Decomposed

samples corresponded to summer 2002, spring 2003, summer 2004, spring 2007 and spring 2007. An alternative to circumvent this issue would be to reduce the days the cups are programmed to be open to collect samples. The average days the cups were open was 14 (range: 7 – 31 days). For instance, to reduce from 14 days to 5 to 7 days during the productive season when a higher flux of organic matter is expected.

The results in Chapter I and Chapter II, highlighted the significance of the information that can be gained by the implementation of metatranscriptomic analyses and high-throughput microscopy to identify key players and functions in the active microbiome of the AO. The introduction of omics methodologies in Chapter IV deepened our understanding of how the microbiome (eukaryotes, bacteria, archaea and viruses) actively responded to a late phytoplankton bloom during the warmest month of the year when the sea ice reached the minimum extent in the region. Future studies should make use of omics approaches (e.g., metagenomics, metatranscriptomics and metaproteomics) in addition to next-generation sequencing to understand how the microbiome changes and adapts to significant environmental alterations (sea ice and temperature changes) in different geographical locations (eastern and western Fram Strait) or habitats (particles, seawater and sea ice) over long (e.g., Chapter III) of short (e.g., Chapter IV) periods of time. The introduction of such methods will allow to address in more detail future ecological questions such as: What were those key functions expressed by the MI in the sinking particles? e.g. (increase of ABC transporter for the uptake of amino acids and carbohydrates (e.g., Sowell et al., 2009; Jiao and Zheng, 2011), what changed in the CAZymes and PULs gene expression to allow for a more active loop during the WWA (e.g., Xing et al., 2015)). Are there any signs of functional plasticity or niche differentiation within taxonomic groups e.g. the *Flavobacteria* that responded to sea ice diatoms (Chapter IV) and in the sinking particles during the WWA (Chapter III)? This thesis provides first insight into the links between specific MIs and the ecological role they played. It introduced for the first time the presence of viruses of MIs (e.g. *Alteromonadales* and *Bacteroidetes*), providing that the microbiome of the AO is far more complex than previously thought. Moreover, this thesis shows the importance of long-term studies to understand future impacts and proved that the WWA affected bacterial communities and possibly the interaction with eukaryotes seen via co-occurrence network analyses. It addressed the role of sea ice and the different bacteria that could affected from

accelerated ice melting. Envisioning that the Fram Strait will continue to rapidly change, e.g. with higher AW inflow and accelerated ice melt, this thesis suggests a reduction in carbon export, a faster, more efficient recycling of organic matter at the surface and provided insights into the taxa that could benefit in the future microbiome of the Fram Strait from surface to the deep sea.

References

Aagaard, K., and Carmack, E. C. (1989). The role of sea ice and other fresh water in the Arctic circulation. *J. Geophys. Res. Ocean.* 94, 14485–14498. doi:10.1029/JC094iC10p14485.

Aagaard, K., Swift, J. H., and Carmack, E. C. (1985). Thermohaline circulation in the Arctic Mediterranean seas. *J. Geophys. Res. Ocean.* 90, 4833–4846. doi:10.1029/JC090iC03p04833.

Agogué, H., Lamy, D., Neal, P. R., Sogin, M. L., and Herndl, G. J. (2011). Water mass-specificity of bacterial communities in the North Atlantic revealed by massively parallel sequencing. *Mol. Ecol.* 20, 258–274. doi:10.1111/j.1365-294X.2010.04932.x.

Alldredge, A. L., and Silver, M. W. (1988). Characteristics, dynamics and significance of marine snow. *Prog. Oceanogr.* 20, 41–82. doi:10.1016/0079-6611(88)90053-5.

Alonso-Sáez, L., Sánchez, O., Gasol, J. M., Balagué, V., and Pedrós-Alio, C. (2008). Winter-to-summer changes in the composition and single-cell activity of near-surface Arctic prokaryotes. *Environ. Microbiol.* 10, 2444–2454. doi:10.1111/j.1462-2920.2008.01674.x.

Ardyna, M., and Arrigo, K. R. (2020). Phytoplankton dynamics in a changing Arctic Ocean. *Nat. Clim. Chang.* 10, 892–903. doi:10.1038/s41558-020-0905-y.

Armbrust, E. V. (2009). The life of diatoms in the world's oceans. *Nature* 459, 185–192. doi:10.1038/nature08057.

Arrigo, K. R. (2003). Primary Production in Sea Ice. *Sea Ice*, 143–183. doi:10.1002/9780470757161.ch5.

Arrigo, K. R. (2014). Sea Ice Ecosystems. *Ann. Rev. Mar. Sci.* 6, 439–467. doi:10.1146/annurev-marine-010213-135103.

Arrigo, K. R. (2017). Sea ice as a habitat for primary producers. *Sea Ice*, 352–369. doi:10.1002/9781118778371.ch14.

Arrigo, K. R., Perovich, D. K., Pickart, R. S., Brown, Z. W., Van Dijken, G. L., Lowry, K. E., et al. (2012). Massive phytoplankton blooms under arctic sea ice. *Science (80-.).* 336, 1408. doi:10.1126/science.1215065.

Arrigo, K. R., and van Dijken, G. L. (2015). Continued increases in Arctic Ocean primary production. *Prog. Oceanogr.* 136, 60–70. doi:10.1016/j.pocean.2015.05.002.

Aslam, S. N., Cresswell-Maynard, T., Thomas, D. N., and Underwood, G. J. C. (2012). Production and Characterization of the Intra- and Extracellular Carbohydrates and Polymeric Substances (EPS) of Three Sea-Ice Diatom Species, and Evidence for a Cryoprotective Role for EPS. *J. Phycol.* 48, 1494–1509. doi:10.1111/jpy.12004.

Aslam, S. N., Strauss, J., Thomas, D. N., Mock, T., and Underwood, G. J. C. (2018). Identifying metabolic pathways for production of extracellular polymeric substances by the diatom Fragilariopsis cylindrus inhabiting sea ice. *ISME J.* 12, 1237–1251. doi:10.1038/s41396-017-0039-z.

Avcı, B., Krüger, K., Fuchs, B. M., Teeling, H., and Amann, R. I. (2020). Polysaccharide niche partitioning of distinct Polaribacter clades during North Sea spring algal blooms. *ISME J.* 14, 1369–1383.

Azam, F., Fenchel, T., Field, J. G., Gray, J. S., Meyer-Reil, L. A., and Thingstad, F. (1983). The Ecological Role of Water-Column Microbes in the Sea. *Mar. Ecol. Prog. Ser.* 10, 257–263.

Azam, F., and Malfatti, F. (2007). Microbial structuring of marine ecosystems. *Nat. Rev. Microbiol.* 5, 782–791. doi:10.1038/nrmicro1747.

Bach, L. T., Boxhammer, T., Larsen, A., Hildebrandt, N., Schulz, K. G., and Riebesell, U. (2016). Influence of plankton community structure on the sinking velocity of marine aggregates. *Global Biogeochem. Cycles* 30, 1145–1165.

Bach, L. T., Stange, P., Taucher, J., Achterberg, E. P., Algueró-Muñiz, M., Horn, H., et al. (2019). The Influence of Plankton Community Structure on Sinking Velocity and Remineralization Rate of Marine Aggregates. *Global Biogeochem. Cycles* 33, 971–994. doi:10.1029/2019GB006256.

Bachy, C., Sudek, L., Choi, C. J., Eckmann, C. A., Nöthig, E.-M., Metfies, K., et al. (2022). Phytoplankton Surveys in the Arctic Fram Strait Demonstrate the Tiny Eukaryotic Alga Micromonas and Other Picoprasinophytes Contribute to Deep Sea Export. *Microorg.*10. doi:10.3390/microorganisms10050961.

Basedow, S. L., Sundfjord, A., von Appen, W. J., Halvorsen, E., Kwasniewski, S., and Reigstad, M. (2018). Seasonal variation in transport of Zooplankton Into the Arctic basin through the Atlantic Gateway, Fram Strait. *Front. Mar. Sci.* 5, 194. doi:10.3389/fmars.2018.00194.

Bauerfeind, E., Nöthig, E. M., Beszczynska, A., Fahl, K., Kaleschke, L., Kreker, K., et al. (2009). Particle sedimentation patterns in the eastern Fram Strait during 2000-2005: Results from the Arctic long-term observatory HAUSGARTEN. *Deep. Res. Part I Oceanogr. Res. Pap.* 56, 1471–1487. doi:10.1016/j.dsr.2009.04.011.

Behnam, Krumpen, T., Smedsrud, L. H., and Gerdes, R. (2019). Fram Strait sea ice export affected by thinning: comparing high-resolution simulations and observations. *Clim. Dyn.* 53, 3257–3270. doi:10.1007/s00382-019-04699-z.

Bélanger, S., Babin, M., and Tremblay, J.-É. (2013). Increasing cloudiness in Arctic damps the increase in phytoplankton primary production due to sea ice receding. *Biogeosciences* 10, 4087–4101. doi:10.5194/bg-10-4087-2013.

Beszczynska-Moeller, A., Woodgate, R. A., Lee, C., Melling, H., and Karcher, M. (2011). A synthesis of exchanges through the main oceanic gateways to the Arctic Ocean. *Oceanography* 24, 82–99.

Beszczynska-Möller, A., Fahrbach, E., Schauer, U., and Hansen, E. (2012). Variability in Atlantic water temperature and transport at the entrance to the Arctic Ocean, 19972010. *ICES J. Mar. Sci.* 69, 852–863. doi:10.1093/icesjms/fss056.

Blanco-Bercial, L. (2020). Metabarcoding Analyses and Seasonality of the Zooplankton Community at BATS. *Front. Mar. Sci.* 7. doi:10.3389/fmars.2020.00173.

Bluhm, B. A., Hop, H., Vihtakari, M., Gradinger, R., Iken, K., Melnikov, I. A., et al. (2018). Sea ice meiofauna distribution on local to pan-Arctic scales. *Ecol. Evol.* 8, 2350–2364. doi:10.1002/ece3.3797.

Bluhm, B. A., Kosobokova, K. N., and Carmack, E. C. (2015). A tale of two basins: An integrated physical and biological perspective of the deep Arctic Ocean. *Prog. Oceanogr.* 139, 89–121. doi:https://doi.org/10.1016/j.pocean.2015.07.011.

Boé, J., Hall, A., and Qu, X. (2009). September sea-ice cover in the Arctic Ocean projected to vanish by 2100. *Nat. Geosci.* 2, 341–343. doi:10.1038/ngeo467.

Boetius, A., Albrecht, S., Bakker, K., Bienhold, C., Felden, J., Fernández-Méndez, M., et al. (2013). Export of algal biomass from the melting arctic sea ice. *Science (80-.).* 339, 1430–1432. doi:10.1126/science.1231346.

Boetius, A., Anesio, A. M., Deming, J. W., Mikucki, J. A., and Rapp, J. Z. (2015). Microbial ecology of the cryosphere: Sea ice and glacial habitats. *Nat. Rev. Microbiol.* 13, 677–690. doi:10.1038/nrmicro3522.

Boeuf, D., Edwards, B. R., Eppley, J. M., Hu, S. K., Poff, K. E., Romano, A. E., et al. (2019). Biological composition and microbial dynamics of sinking particulate organic matter at abyssal depths in the oligotrophic open ocean. *Proc. Natl. Acad. Sci. U. S. A.* 116, 11824–11832. doi:10.1073/pnas.1903080116.

Bowman, J. P. (2013). "Sea-Ice Microbial Communities BT - The Prokaryotes: Prokaryotic Communities and Ecophysiology," in, eds. E. Rosenberg, E. F. DeLong, S. Lory, E. Stackebrandt, and F. Thompson (Berlin, Heidelberg: Springer Berlin Heidelberg), 139–161. doi:10.1007/978-3-642-30123-0_46.

Bowman, J. S., Rasmussen, S., Blom, N., Deming, J. W., Rysgaard, S., and Sicheritz-Ponten, T. (2012). Microbial community structure of Arctic multiyear sea ice and surface seawater by 454 sequencing of the 16S RNA gene. *ISME J.* 6, 11–20. doi:10.1038/ismej.2011.76.

Boyd, P. W., and Trull, T. W. (2007). Understanding the export of biogenic particles in oceanic waters: Is there consensus? *Prog. Oceanogr.* 72, 276–312. doi:10.1016/j.pocean.2006.10.007.

Bratbak, G., Thingstad, F., and Heldal, M. (1994). Viruses and the microbial loop. *Microb. Ecol.* 28, 209–221. doi:10.1007/BF00166811.

Buchan, A., LeCleir, G. R., Gulvik, C. A., and González, J. M. (2014). Master recyclers: features and functions of bacteria associated with phytoplankton blooms. *Nat. Rev. Microbiol.* 12, 686–698. doi:10.1038/nrmicro3326.

Buesseler, K. O., and Boyd, P. W. (2009). Shedding light on processes that control particle export and flux attenuation in the twilight zone of the open ocean. *Limnol. Oceanogr.* 54, 1210–1232. doi:10.4319/lo.2009.54.4.1210.

Campbell, K., Matero, I., Bellas, C., Turpin-Jelfs, T., Anhaus, P., Graeve, M., et al. (2022). Monitoring a changing Arctic: Recent advancements in the study of sea ice microbial communities. *Ambio* 51, 318–332. doi:10.1007/s13280-021-01658-z.

Carmack, E. C. (2007). The alpha/beta ocean distinction: A perspective on freshwater fluxes, convection, nutrients and productivity in high-latitude seas. *Deep Sea Res. Part II Top. Stud. Oceanogr.* 54, 2578–2598. doi:10.1016/j.dsr2.2007.08.018.

Carmack, E., Polyakov, I., Padman, L., Fer, I., Hunke, E., Hutchings, J., et al. (2015). Toward quantifying the increasing role of oceanic heat in sea ice loss in the new Arctic. *Bull. Am. Meteorol. Soc.* 96, 2079–2105. doi:10.1175/BAMS-D-13-00177.1.

Carmack, E., and Wassmann, P. (2006). Food webs and physical–biological coupling on pan-Arctic shelves: Unifying concepts and comprehensive perspectives. *Prog. Oceanogr.* 71, 446–477. doi:https://doi.org/10.1016/j.pocean.2006.10.004.

Caron, D. A., Gast, R. J., and Garneau, M.-È. (2017). Sea ice as a habitat for micrograzers. *Sea Ice*, 370–393. doi:10.1002/9781118778371.ch15.

Chaffron, S., Delage, E., Budinich, M., Vintache, D., Henry, N., Nef, C., et al. (2022). Environmental vulnerability of the global ocean epipelagic plankton community interactome. *Sci. Adv.* 7, eabg1921. doi:10.1126/sciadv.abg1921.

Cho, B. C., and Azam, F. (1988). Major role of bacteria in biogeochemical fluxes in the ocean's interior. *Nature* 332, 441–443. doi:10.1038/332441a0.

Christman, G., Cottrell, M., Popp, B., Gier, E., and Kirchman, D. (2011). Abundance, Diversity, and Activity of Ammonia-Oxidizing Prokaryotes in the Coastal Arctic Ocean in Summer and Winter. *Appl. Environ. Microbiol.* 77, 2026–2034. doi:10.1128/AEM.01907-10.

Church, M. J., DeLong, E. F., Ducklow, H. W., Karner, M. B., Preston, C. M., and Karl, D. M. (2003). Abundance and distribution of planktonic Archaea and Bacteria in the waters west of the Antarctic Peninsula. *Limnol. Oceanogr.* 48, 1893–1902.

doi:10.4319/lo.2003.48.5.1893.
Collins, R. E., and Deming, J. W. (2011). Abundant dissolved genetic material in Arctic sea ice Part II: Viral dynamics during autumn freeze-up. *Polar Biol.* 34, 1831–1841. doi:10.1007/s00300-011-1008-z.
Comiso, J. C., Parkinson, C. L., Gersten, R., and Stock, L. (2008). Accelerated decline in the Arctic sea ice cover. *Geophys. Res. Lett.* 35. doi:10.1029/2007GL031972.
Cruz, B. N., Brozak, S., and Neuer, S. (2021). Microscopy and DNA-based characterization of sinking particles at the Bermuda Atlantic Time-series Study station point to zooplankton mediation of particle flux. *Limnol. Oceanogr.* 66, 3697–3713. doi:10.1002/lno.11910.
Darnis, G., and Fortier, L. (2014). Temperature, food and the seasonal vertical migration of key arctic copepods in the thermally stratified Amundsen Gulf (Beaufort Sea, Arctic Ocean). *J. Plankton Res.* 36, 1092–1108. doi:10.1093/plankt/fbu035.
De La Rocha, C. L., and Passow, U. (2007). Factors influencing the sinking of POC and the efficiency of the biological carbon pump. *Deep. Res. Part II Top. Stud. Oceanogr.* 54, 639–658. doi:10.1016/j.dsr2.2007.01.004.
Decho, A. W., and Gutierrez, T. (2017). Microbial Extracellular Polymeric Substances (EPSs) in Ocean Systems. *Front. Microbiol.* 8. doi:10.3389/fmicb.2017.00922.
DeLong, E. F., Preston, C. M., Mincer, T., Rich, V., Hallam, S. J., Frigaard, N.-U., et al. (2006). Community Genomics among Stratified Microbial Assemblages in the Ocean's Interior. *Science (80-.).* 311, 496–503.
Deming, J. W., and Eric Collins, R. (2017). Sea ice as a habitat for Bacteria, Archaea and viruses. *Sea Ice*, 326–351. doi:10.1002/9781118778371.ch13.
DeVries, T., Le Quéré, C., Andrews, O., Berthet, S., Hauck, J., Ilyina, T., et al. (2019). Decadal trends in the ocean carbon sink. *Proc. Natl. Acad. Sci.* 116, 11646–11651. doi:10.1073/pnas.1900371116.
DeVries, T., and Weber, T. (2017). The export and fate of organic matter in the ocean: New constraints from combining satellite and oceanographic tracer observations. *Global Biogeochem. Cycles* 31, 535–555. doi:10.1002/2016GB005551.
Dittmar, T., and Kattner, G. (2003). The biogeochemistry of the river and shelf ecosystem of the Arctic Ocean: a review. *Mar. Chem.* 83, 103–120. doi:10.1016/S0304-4203(03)00105-1.
Djurhuus, A., Boersch-Supan, P. H., Mikalsen, S.-O., and Rogers, A. D. (2017). Microbe biogeography tracks water masses in a dynamic oceanic frontal system. *R. Soc. open Sci.* 4, 170033. doi:10.1098/rsos.170033.
Docquier, D., and Koenigk, T. (2021). Observation-based selection of climate models projects Arctic ice-free summers around 2035. *Commun. Earth Environ.* 2, 144. doi:10.1038/s43247-021-00214-7.
Ducklow, H. W., Steinberg, D. K., and Buesseler, K. O. (2001). Upper ocean carbon export and the biological pump. *Oceanography* 14, 50–58. doi:10.5670/oceanog.2001.06.
Eicken, H., Lensu, M., Leppäranta, M., Tucker III, W. B., Gow, A. J., and Salmela, O. (1995). Thickness, structure, and properties of level summer multiyear ice in the Eurasian sector of the Arctic Ocean. *J. Geophys. Res. Ocean.* 100, 22697–22710. doi:10.1029/95JC02188.
Ekwurzel, B., Schlosser, P., Mortlock, R. A., Fairbanks, R. G., and Swift, J. H. (2001). River runoff, sea ice meltwater, and Pacific water distribution and mean residence times in the Arctic Ocean. *J. Geophys. Res. Ocean.* 106, 9075–9092. doi:10.1029/1999JC000024.
Ewert, M., and Deming, J. W. (2013). Sea Ice Microorganisms: Environmental Constraints and

Extracellular Responses. *Biology (Basel).* 2, 603–628. doi:10.3390/biology2020603.
Fadeev, E. (2018). Ecological observations of pelagic bacterial and archaeal communities in the Atlantic-Arctic boundary zone.
Fadeev, E., Rogge, A., Ramondenc, S., Nöthig, E.-M., Wekerle, C., Bienhold, C., et al. (2020). Sea-ice retreat may decrease carbon export and vertical microbial connectivity in the Eurasian Arctic basins. *Nat. Res.* doi:10.21203/rs.3.rs-101878/v1.
Fadeev, E., Rogge, A., Ramondenc, S., Nöthig, E.-M., Wekerle, C., Bienhold, C., et al. (2021a). Sea ice presence is linked to higher carbon export and vertical microbial connectivity in the Eurasian Arctic Ocean. *Commun. Biol.* 4, 1255. doi:10.1038/s42003-021-02776-w.
Fadeev, E., Salter, I., Schourup-Kristensen, V., Nöthig, E. M., Metfies, K., Engel, A., et al. (2018). Microbial communities in the east and west fram strait during sea ice melting season. *Front. Mar. Sci.* 5, 429. doi:10.3389/fmars.2018.00429.
Fadeev, E., Wietz, M., von Appen, W.-J., Iversen, M. H., Nöthig, E.-M., Engel, A., et al. (2021b). Submesoscale physicochemical dynamics directly shape bacterioplankton community structure in space and time. *Limnol. Oceanogr.* 66, 2901–2913. doi:10.1002/lno.11799.
Fender, C. K., Kelly, T. B., Guidi, L., Ohman, M. D., Smith, M. C., and Stukel, M. R. (2019). Investigating Particle Size-Flux Relationships and the Biological Pump Across a Range of Plankton Ecosystem States From Coastal to Oligotrophic. *Front. Mar. Sci.* 6. doi:10.3389/fmars.2019.00603.
Fernández-Méndez, M., Katlein, C., Rabe, B., Nicolaus, M., Peeken, I., Bakker, K., et al. (2015). Photosynthetic production in the central Arctic Ocean during the record sea-ice minimum in 2012. *Biogeosciences* 12, 3525–3549. doi:10.5194/bg-12-3525-2015.
Fernández-Méndez, M., Olsen, L. M., Kauko, H. M., Meyer, A., Rösel, A., Merkouriadi, I., et al. (2018). Algal Hot Spots in a Changing Arctic Ocean: Sea-Ice Ridges and the Snow-Ice Interface. *Front. Mar. Sci.* 5. doi:10.3389/fmars.2018.00075.
Fontanez, K. M., Eppley, J. M., Samo, T. J., Karl, D. M., and DeLong, E. F. (2015). Microbial community structure and function on sinking particles in the North Pacific Subtropical Gyre. *Front. Microbiol.* 6, 469. doi:10.3389/fmicb.2015.00469.
Frey, K. E., Comiso, J. C., Cooper, L. W., Grebmeier, J. M., and Stock, L. V (2021). Arctic Ocean Primary Productivity: The Response of Marine Algae to Climate Warming and Sea Ice Decline. doi:https://doi.org/10.25923/kxhb-dw16.
Galand, P. E., Potvin, M., Casamayor, E. O., and Lovejoy, C. (2010). Hydrography shapes bacterial biogeography of the deep Arctic Ocean. *ISME J.* 4, 564–576. doi:10.1038/ismej.2009.134.
Gao, Y., Sun, J., Li, F., He, S., Sandven, S., Yan, Q., et al. (2015). Arctic sea ice and Eurasian climate: a review. *Adv. Atmos. Sci.* 32, 92–114. doi:10.1007/s00376-014-0009-6.
Gärdes, A., Kaeppel, E., Shehzad, A., Seebah, S., Teeling, H., Yarza, P., et al. (2010). Complete genome sequence of Marinobacter adhaerens type strain (HP15), a diatom-interacting marine microorganism. *Stand. Genomic Sci.* 3, 97–107. doi:10.4056/sigs.922139.
Gilbertson, R., Langan, E., and Mock, T. (2022). Diatoms and Their Microbiomes in Complex and Changing Polar Oceans. *Front. Microbiol.* 13. doi:10.3389/fmicb.2022.786764.
Gosselin, M., Levasseur, M., Wheeler, P. A., Horner, R. A., and Booth, B. C. (1997). New measurements of phytoplankton and ice algal production in the Arctic Ocean. *Deep Sea Res. Part II Top. Stud. Oceanogr.* 44, 1623–1644. doi:10.1016/S0967-0645(97)00054-4.

Gradinger, R. (2009). Sea-ice algae: Major contributors to primary production and algal biomass in the Chukchi and Beaufort Seas during May/June 2002. *Deep Sea Res. Part II Top. Stud. Oceanogr.* 56, 1201–1212. doi:10.1016/j.dsr2.2008.10.016.

Gradinger, R., and Ikävalko, J. (1998). Organism incorporation into newly forming Arctic sea ice in the Greenland Sea. *J. Plankton Res.* 20, 871–886. doi:10.1093/plankt/20.5.871.

Gradinger, R. R. (2001). Adaptation of Arctic and Antarctic ice metazoa to their habitat1 1Presented at the 94th Annual Meeting of the Deutsche Zoologische Gesellschaft in Osnabrück, June 4–8, 2001. *Zoology* 104, 339–345. doi:10.1078/0944-2006-00039.

Gruber, N., Clement, D., Carter, B. R., Feely, R. A., van Heuven, S., Hoppema, M., et al. (2019). The oceanic sink for anthropogenic CO2 from 1994 to 2007. *Science (80-.).* 363, 1193–1199. doi:10.1126/science.aau5153.

Guidi, L., Legendre, L., Reygondeau, G., Uitz, J., Stemmann, L., and Henson, S. A. (2015). A new look at ocean carbon remineralization for estimating deepwater sequestration. *Global Biogeochem. Cycles* 29, 1044–1059. doi:10.1002/2014GB005063.

Guidi, L., Stemmann, L., Jackson, G. A., Ibanez, F., Claustre, H., Legendre, L., et al. (2009). Effects of phytoplankton community on production, size and export of large aggregates: A world-ocean analysis. *Limnol. Oceanogr.* 54, 1951–1963. doi:10.4319/lo.2009.54.6.1951.

Hamdan, L. J., Coffin, R. B., Sikaroodi, M., Greinert, J., Treude, T., and Gillevet, P. M. (2013). Ocean currents shape the microbiome of Arctic marine sediments. *ISME J.* 7, 685–696. doi:10.1038/ismej.2012.143.

Hancke, K., Lund-Hansen, L. C., Lamare, M. L., Højlund Pedersen, S., King, M. D., Andersen, P., et al. (2018). Extreme Low Light Requirement for Algae Growth Underneath Sea Ice: A Case Study From Station Nord, NE Greenland. *J. Geophys. Res. Ocean.* 123, 985–1000. doi:10.1002/2017JC013263.

Hardge, K., Peeken, I., Neuhaus, S., Krumpen, T., Stoeck, T., and Metfies, K. (2017). Sea ice origin and sea ice retreat as possible drivers of variability in Arctic marine protist composition. *Mar. Ecol. Prog. Ser.* 571, 43–57.

Harding, K., Turk-Kubo, K. A., Sipler, R. E., Mills, M. M., Bronk, D. A., and Zehr, J. P. (2018). Symbiotic unicellular cyanobacteria fix nitrogen in the Arctic Ocean. *Proc. Natl. Acad. Sci.* 115, 13371–13375. doi:10.1073/pnas.1813658115.

Hatam, I., Charchuk, R., Lange, B., Beckers, J., Haas, C., and Lanoil, B. (2014). Distinct bacterial assemblages reside at different depths in Arctic multiyear sea ice. *FEMS Microbiol. Ecol.* 90, 115–125. doi:10.1111/1574-6941.12377.

Hatzenpichler, R. (2012). Diversity, Physiology, and Niche Differentiation of Ammonia-Oxidizing Archaea. *Appl. Environ. Microbiol.* 78, 7501–7510. doi:10.1128/AEM.01960-12.

Hawley, A. K., Nobu, M. K., Wright, J. J., Durno, W. E., Morgan-Lang, C., Sage, B., et al. (2017). Diverse Marinimicrobia bacteria may mediate coupled biogeochemical cycles along eco-thermodynamic gradients. *Nat. Commun.* 8, 1507. doi:10.1038/s41467-017-01376-9.

Henson, S. A., Sanders, R., and Madsen, E. (2012). Global patterns in efficiency of particulate organic carbon export and transfer to the deep ocean. *Global Biogeochem. Cycles* 26. doi:10.1029/2011GB004099.

Henson, S. A., Sanders, R., Madsen, E., Morris, P. J., Le Moigne, F., and Quartly, G. D. (2011). A reduced estimate of the strength of the ocean's biological carbon pump. *Geophys. Res. Lett.* 38. doi:10.1029/2011GL046735.

Hernando-Morales, V., Ameneiro, J., and Teira, E. (2017). Water mass mixing shapes bacterial biogeography in a highly hydrodynamic region of the Southern Ocean. *Environ. Microbiol.* 19, 1017–1029. doi:10.1111/1462-2920.13538.

Herndl, G. J., and Reinthaler, T. (2013). Microbial control of the dark end of the biological pump. *Nat. Geosci.* 6, 718–724. doi:10.1038/ngeo1921.

Herndl, G. J., Reinthaler, T., Teira, E., Van Aken, H., Veth, C., Pernthaler, A., et al. (2005). Contribution of Archaea to total prokaryotic production in the deep atlantic ocean. *Appl. Environ. Microbiol.* 71, 2303–2309. doi:10.1128/AEM.71.5.2303-2309.2005.

Hill, V., and Cota, G. (2005). Spatial patterns of primary production on the shelf, slope and basin of the Western Arctic in 2002. *Deep Sea Res. Part II Top. Stud. Oceanogr.* 52, 3344–3354. doi:10.1016/j.dsr2.2005.10.001.

Hop, H., Vihtakari, M., Bluhm, B. A., Assmy, P., Poulin, M., Gradinger, R., et al. (2020). Changes in Sea-Ice Protist Diversity With Declining Sea Ice in the Arctic Ocean From the 1980s to 2010s. *Front. Mar. Sci.* 7. doi:10.3389/fmars.2020.00243.

Hop, H., Wold, A., Meyer, A., Bailey, A., Hatlebakk, M., Kwasniewski, S., et al. (2021). Winter-Spring Development of the Zooplankton Community Below Sea Ice in the Arctic Ocean. *Front. Mar. Sci.* 8. doi:10.3389/fmars.2021.609480.

Hopwood, M. J., Carroll, D., Dunse, T., Hodson, A., Holding, J. M., Iriarte, J. L., et al. (2020). Review article: How does glacier discharge affect marine biogeochemistry and primary production in the Arctic? *Cryosph.* 14, 1347–1383. doi:10.5194/tc-14-1347-2020.

Inall, M. E., Murray, T., Cottier, F. R., Scharrer, K., Boyd, T. J., Heywood, K. J., et al. (2014). Oceanic heat delivery via Kangerdlugssuaq Fjord to the south-east Greenland ice sheet. *J. Geophys. Res. Ocean.* 119, 631–645. doi:10.1002/2013JC009295.

Iversen, M. H., and Ploug, H. (2010). Ballast minerals and the sinking carbon flux in the ocean: Carbon-specific respiration rates and sinking velocity of marine snow aggregates. *Biogeosciences* 7, 2613–2624. doi:10.5194/bg-7-2613-2010.

Ivory, J. A., Steinberg, D. K., and Latour, R. J. (2019). Diel, seasonal, and interannual patterns in mesozooplankton abundance in the Sargasso Sea. *ICES J. Mar. Sci.* 76, 217–231. doi:10.1093/icesjms/fsy117.

Jacob, M. (2014). Influence of Global Change on microbial communities in Arctic sediments.

Jahn, A., Kay, J. E., Holland, M. M., and Hall, D. M. (2016). How predictable is the timing of a summer ice-free Arctic? *Geophys. Res. Lett.* 43, 9113–9120. doi:https://doi.org/10.1002/2016GL070067.

Jakobsson, M. (2002). Hypsometry and volume of the Arctic Ocean and its constituent seas. *Geochemistry, Geophys. Geosystems* 3, 1–18. doi:https://doi.org/10.1029/2001GC000302.

Jakobsson, M., Grantz, A., Kristoffersen, Y., and Macnab, R. (2003). Physiographic provinces of the Arctic Ocean seafloor. *GSA Bull.* 115, 1443–1455. doi:10.1130/B25216.1.

Jakobsson, M., Mayer, L., Coakley, B., Dowdeswell, J. A., Forbes, S., Fridman, B., et al. (2012). The international bathymetric chart of the Arctic Ocean (IBCAO) version 3.0. *Geophys. Res. Lett.* 39. doi:10.1029/2012GL052219.

Jiao, N., Herndl, G. J., Hansell, D. A., Benner, R., Kattner, G., Wilhelm, S. W., et al. (2010). Microbial production of recalcitrant dissolved organic matter: long-term carbon storage in the global ocean. *Nat. Rev. Microbiol.* 8, 593–599. doi:10.1038/nrmicro2386.

Jiao, N., and Zheng, Q. (2011). The Microbial Carbon Pump: from Genes to Ecosystems. *Appl. Environ. Microbiol.* 77, 7439–7444. doi:10.1128/AEM.05640-11.

Johannessen, O., Muench, R., and Overland, J. (1994). *The Polar Oceans and Their Role in*

Shaping the Global Environment. doi:10.1029/GM085.

Jones, E. P. (2001). Circulation in the arctic ocean. *Polar Res.* 20, 139–146. doi:10.1111/j.1751-8369.2001.tb00049.x.

Junge, K., Imhoff, F., Staley, T., and Deming, W. (2002). Phylogenetic Diversity of Numerically Important Arctic Sea-Ice Bacteria Cultured at Subzero Temperature. *Microb. Ecol.* 43, 315–328. doi:10.1007/s00248-001-1026-4.

Junge, K., Krembs, C., Deming, J., Stierle, A., and Eicken, H. (2001). A microscopic approach to investigate bacteria under in situ conditions in sea-ice samples. *Ann. Glaciol.* 33, 304–310. doi:10.3189/172756401781818275.

Kahru, M., Brotas, V., Manzano-Sarabia, M., and Mitchell, B. G. (2011). Are phytoplankton blooms occurring earlier in the Arctic? *Glob. Chang. Biol.* 17, 1733–1739. doi:10.1111/j.1365-2486.2010.02312.x.

Karl, D. M., and Church, M. J. (2014). Microbial oceanography and the Hawaii Ocean Time-series programme. *Nat. Rev. Microbiol.* 12, 699–713. doi:10.1038/nrmicro3333.

Karl, D. M., and Lukas, R. (1996). The Hawaii Ocean Time-series (HOT) program: Background, rationale and field implementation. *Deep Sea Res. Part II Top. Stud. Oceanogr.* 43, 129–156. doi:10.1016/0967-0645(96)00005-7.

Karner, M. B., Delong, E. F., and Karl, D. M. (2001). Archaeal dominance in the mesopelagic zone of the Pacific Ocean. *Nature* 409, 507–510. doi:10.1038/35054051.

Kauko, H. M., Olsen, L. M., Duarte, P., Peeken, I., Granskog, M. A., Johnsen, G., et al. (2018). Algal Colonization of Young Arctic Sea Ice in Spring. *Front. Mar. Sci.* 5. Available at: https://www.frontiersin.org/article/10.3389/fmars.2018.00199.

Kawakami, H., and Honda, M. C. (2007). Time-series observation of POC fluxes estimated from 234Th in the northwestern North Pacific. *Deep Sea Res. Part I Oceanogr. Res. Pap.* 54, 1070–1090. doi:10.1016/j.dsr.2007.04.005.

Kellogg, C. T. E., Carpenter, S. D., Renfro, A. A., Sallon, A., Michel, C., Cochran, J. K., et al. (2011). Evidence for microbial attenuation of particle flux in the Amundsen Gulf and Beaufort Sea: elevated hydrolytic enzyme activity on sinking aggregates. *Polar Biol.* 34, 2007–2023. doi:10.1007/s00300-011-1015-0.

Kilias, E. S., Junges, L., Šupraha, L., Leonard, G., Metfies, K., and Richards, T. A. (2020). Chytrid fungi distribution and co-occurrence with diatoms correlate with sea ice melt in the Arctic Ocean. *Commun. Biol.* 3, 183. doi:10.1038/s42003-020-0891-7.

Kilias, E. S., Nöthig, E., Wolf, C., and Metfies, K. (2014). Picoeukaryote plankton composition off West Spitsbergen at the entrance to the Arctic Ocean. *J. Eukaryot. Microbiol.* 61, 569–579.

Kilias, E., Wolf, C., Nöthig, E.-M., Peeken, I., and Metfies, K. (2013). Protist distribution in the Western Fram Strait in summer 2010 based on 454-pyrosequencing of 18S rDNA. *J. Phycol.* 49, 996–1010. doi:10.1111/jpy.12109.

Kirchman, D. L., Elifantz, H., Dittel, A. I., Malmstrom, R. R., and Cottrell, M. T. (2007). Standing stocks and activity of Archaea and Bacteria in the western Arctic Ocean. *Limnol. Oceanogr.* 52, 495–507. doi:10.4319/lo.2007.52.2.0495.

Klenke, M., and Schenke, H. W. (2002). A new bathymetric model for the central Fram Strait. *Mar. Geophys. Res.* 23, 367–378. doi:10.1023/A:1025764206736.

Kong, L.-F., He, Y.-B., Xie, Z.-X., Luo, X., Zhang, H., Yi, S.-H., et al. (2021). Illuminating Key Microbial Players and Metabolic Processes Involved in the Remineralization of Particulate Organic Carbon in the Ocean's Twilight Zone by Metaproteomics. *Appl. Environ. Microbiol.* 87, e00986-21. doi:10.1128/AEM.00986-21.

Korhonen, M., Rudels, B., Marnela, M., Wisotzki, A., and Zhao, J. (2013). Time and space variability of freshwater content, heat content and seasonal ice melt in the Arctic Ocean from 1991 to 2011. *Ocean Sci.* 9, 1015–1055. doi:10.5194/os-9-1015-2013.

Krüger, K., Chafee, M., Francis, T. Ben, Del Rio, T. G., Becher, D., Schweder, T., et al. (2019). In marine Bacteroidetes the bulk of glycan degradation during algae blooms is mediated by few clades using a restricted set of genes. *ISME J.* 13, 2800–2816. doi:10.1038/s41396-019-0476-y.

Krumpen, T., Belter, H. J., Boetius, A., Damm, E., Haas, C., Hendricks, S., et al. (2019). Arctic warming interrupts the Transpolar Drift and affects long-range transport of sea ice and ice-rafted matter. *Sci. Rep.* 9, 1–9.

Lalande, C., Bauerfeind, E., Nöthig, E. M., and Beszczynska-Möller, A. (2013). Impact of a warm anomaly on export fluxes of biogenic matter in the eastern Fram Strait. *Prog. Oceanogr.* 109, 70–77. doi:10.1016/j.pocean.2012.09.006.

Lalande, C., Nöthig, E., and Fortier, L. (2019). Algal export in the Arctic Ocean in times of global warming. *Geophys. Res. Lett.* 46, 5959–5967. doi:10.1029/2019GL083167.

Legendre, L., Rivkin, R. B., Weinbauer, M. G., Guidi, L., and Uitz, J. (2015). The microbial carbon pump concept: Potential biogeochemical significance in the globally changing ocean. *Prog. Oceanogr.* 134, 432–450. doi:10.1016/j.pocean.2015.01.008.

Lester, C. W., Wagner, T. J. W., McNamara, D. E., and Cape, M. R. (2021). The Influence of Meltwater on Phytoplankton Blooms Near the Sea-Ice Edge. *Geophys. Res. Lett.* 48, e2020GL091758. doi:10.1029/2020GL091758.

Leu, E., Mundy, C. J., Assmy, P., Campbell, K., Gabrielsen, T. M., Gosselin, M., et al. (2015). Arctic spring awakening – Steering principles behind the phenology of vernal ice algal blooms. *Prog. Oceanogr.* 139, 151–170. doi:10.1016/j.pocean.2015.07.012.

Leu, E., Søreide, J. E., Hessen, D. O., Falk-Petersen, S., and Berge, J. (2011). Consequences of changing sea-ice cover for primary and secondary producers in the European Arctic shelf seas: Timing, quantity, and quality. *Prog. Oceanogr.* 90, 18–32. doi:10.1016/j.pocean.2011.02.004.

Lewis, K. M., Van Dijken, G. L., and Arrigo, K. R. (2020). Changes in phytoplankton concentration now drive increased Arctic Ocean primary production. *Science (80-.).* 369, 198–202. doi:10.1126/science.aay8380.

Li, X., Roevros, N., Dehairs, F., and Chou, L. (2017). Biological responses of the marine diatom Chaetoceros socialis to changing environmental conditions: A laboratory experiment. *PLoS One* 12, e0188615. doi:10.1371/journal.pone.0188615.

Liu, Q., Zhao, Q., McMinn, A., Yang, E. J., and Jiang, Y. (2021). Planktonic microbial eukaryotes in polar surface waters: recent advances in high-throughput sequencing. *Mar. Life Sci. Technol.* 3, 94–102. doi:10.1007/s42995-020-00062-y.

Lizotte, M. P. (2003). "The Microbiology of Sea Ice," in *Sea Ice* Wiley Online Books., 184–210. doi:10.1002/9780470757161.ch6.

Lovejoy, C., Massana, R., and Pedrós-Alió, C. (2006). Diversity and Distribution of Marine Microbial Eukaryotes in the Arctic Ocean and Adjacent Seas. *Appl. Environ. Microbiol.* 72, 3085–3095. doi:10.1128/AEM.72.5.3085-3095.2006.

Lovejoy, C., and Potvin, M. (2011). Microbial eukaryotic distribution in a dynamic Beaufort Sea and the Arctic Ocean. *J. Plankton Res.* 33, 431–444.

Malfertheiner, L., Martínez-Pérez, C., Zhao, Z., Herndl, G. J., and Baltar, F. (2022). Phylogeny and Metabolic Potential of the Candidate Phylum SAR324. *Biology (Basel).* 11. doi:10.3390/biology11040599.

Martin, J., JÉ, T., Gagnon, J., Tremblay, G., Lapoussière, A., Jose, C., et al. (2010). Prevalence, structure and properties of subsurface chlorophyll maxima in Canadian Arctic waters. *Mar. Ecol. Prog. Ser.* 412, 69–84. doi:10.3354/meps08666.

McCarren, J., Becker, J. W., Repeta, D. J., Shi, Y., Young, C. R., Malmstrom, R. R., et al. (2010). Microbial community transcriptomes reveal microbes and metabolic pathways associated with dissolved organic matter turnover in the sea. *Proc. Natl. Acad. Sci.* 107, 16420–16427. doi:10.1073/pnas.1010732107.

McClelland, J. W., Déry, S. J., Peterson, B. J., Holmes, R. M., and Wood, E. F. (2006). A pan-arctic evaluation of changes in river discharge during the latter half of the 20th century. *Geophys. Res. Lett.* 33. doi:10.1029/2006GL025753.

McLaughlin, F. A., and Carmack, E. C. (2010). Deepening of the nutricline and chlorophyll maximum in the Canada Basin interior, 2003–2009. *Geophys. Res. Lett.* 37. doi:10.1029/2010GL045459.

Melsheimer, C., and Spreen, G. (2019). AMSR2 ASI sea ice concentration data, Arctic, version 5.4 (NetCDF) (July 2012 - December 2019). doi:10.1594/PANGAEA.898399.

Meltofte, H., Barry, T., Berteaux, D., Bültmann, H., Christiansen, J. S., Cook, J. A., et al. (2013). *Arctic Biodiversity Assesment. Synthesis.* Conservation of Arctic Flora and Fauna (CAFF).

Mestre, M., Ruiz-González, C., Logares, R., Duarte, C. M., Gasol, J. M., and Sala, M. M. (2018). Sinking particles promote vertical connectivity in the ocean microbiome. *Proc. Natl. Acad. Sci. U. S. A.* 115, E6799–E6807. doi:10.1073/pnas.1802470115.

Metfies, K., Bauerfeind, E., Wolf, C., Sprong, P., Frickenhaus, S., Kaleschke, L., et al. (2017). Protist communities in moored long-term sediment traps (Fram Strait, Arctic)-preservation with mercury chloride allows for PCR-based molecular genetic analyses. *Front. Mar. Sci.* 4, 301. doi:10.3389/fmars.2017.00301.

Metfies, K., von Appen, W.-J., Kilias, E., Nicolaus, A., and Nöthig, E.-M. (2016). Biogeography and photosynthetic biomass of arctic marine pico-eukaroytes during summer of the record sea ice minimum 2012. *PLoS One* 11, e0148512.

Miettinen, A. (2018). Diatoms in Arctic regions: Potential tools to decipher environmental changes. *Polar Sci.* 18, 220–226. doi:10.1016/j.polar.2018.04.001.

Müller, O., Wilson, B., Paulsen, M. L., Ruminska, A., Armo, H. R., Bratbak, G., et al. (2018). Spatiotemporal dynamics of ammonia-oxidizing Thaumarchaeota in Distinct Arctic water masses. *Front. Microbiol.* 9, 24. doi:10.3389/fmicb.2018.00024.

Nef, C., Madoui, M.-A., Pelletier, É., and Bowler, C. (2022). Whole-genome scanning reveals selection mechanisms in epipelagic Chaetoceros diatom populations. *bioRxiv*, 2022.05.19.492674. doi:10.1101/2022.05.19.492674.

Nöthig, E. M., Bracher, A., Engel, A., Metfies, K., Niehoff, B., Peeken, I., et al. (2015). Summertime plankton ecology in fram strait-a compilation of long-and short-term observations. *Polar Res.* 34, 23349. doi:10.3402/polar.v34.23349.

Nöthig, E. M., Ramondenc, S., Haas, A., Hehemann, L., Walter, A., Bracher, A., et al. (2020). Summertime Chlorophyll a and Particulate Organic Carbon Standing Stocks in Surface Waters of the Fram Strait and the Arctic Ocean (1991–2015). *Front. Mar. Sci.* 7. doi:10.3389/fmars.2020.00350.

Notz, D., and Stroeve, J. (2018). The Trajectory Towards a Seasonally Ice-Free Arctic Ocean. *Curr. Clim. Chang. Reports* 4, 407–416. doi:10.1007/s40641-018-0113-2.

Nummelin, A., Ilicak, M., Li, C., and Smedsrud, L. H. (2016). Consequences of future increased Arctic runoff on Arctic Ocean stratification, circulation, and sea ice cover. *J. Geophys.*

Res. Ocean. 121, 617–637. doi:10.1002/2015JC011156.

Olsen, L. M., Laney, S. R., Duarte, P., Kauko, H. M., Fernández-Méndez, M., Mundy, C. J., et al. (2017). The seeding of ice algal blooms in Arctic pack ice: The multiyear ice seed repository hypothesis. *J. Geophys. Res. Biogeosciences* 122, 1529–1548. doi:10.1002/2016JG003668.

Overland, J. E., and Wang, M. (2013). When will the summer Arctic be nearly sea ice free? *Geophys. Res. Lett.* 40, 2097–2101. doi:https://doi.org/10.1002/grl.50316.

Perovich, D. K. (2011). The changing Arctic sea ice cover. *Oceanography* 24, 162–173.

Perovich, D. K., and Polashenski, C. (2012). Albedo evolution of seasonal Arctic sea ice. *Geophys. Res. Lett.* 39. doi:10.1029/2012GL051432.

Pester, M., Schleper, C., and Wagner, M. (2011). The Thaumarchaeota: an emerging view of their phylogeny and ecophysiology. *Curr. Opin. Microbiol.* 14, 300–306. doi:10.1016/j.mib.2011.04.007.

Petrich, C., and Eicken, H. (2017). Overview of sea ice growth and properties. *Sea Ice*, 1–41. doi:10.1002/9781118778371.ch1.

Piontek, J., Sperling, M., Nöthig, E. M., and Engel, A. (2014). Regulation of bacterioplankton activity in Fram Strait (Arctic Ocean) during early summer: The role of organic matter supply and temperature. *J. Mar. Syst.* 132, 83–94. doi:10.1016/j.jmarsys.2014.01.003.

Piontek, J., Sperling, M., Nöthig, E. M., and Engel, A. (2015). Multiple environmental changes induce interactive effects on bacterial degradation activity in the arctic ocean. *Limnol. Oceanogr.* 60, 1392–1410. doi:10.1002/lno.10112.

Piwosz, K., Wiktor, J. M., Niemi, A., Tatarek, A., and Michel, C. (2013). Mesoscale distribution and functional diversity of picoeukaryotes in the first-year sea ice of the Canadian Arctic. *ISME J.* 7, 1461–1471. doi:10.1038/ismej.2013.39.

Poff, K. E., Leu, A. O., Eppley, J. M., Karl, D. M., and DeLong, E. F. (2021). Microbial dynamics of elevated carbon flux in the open ocean's abyss. *Proc. Natl. Acad. Sci. U. S. A.* 118. doi:10.1073/pnas.2018269118.

Polyak, L., Alley, R. B., Andrews, J. T., Brigham-Grette, J., Cronin, T. M., Darby, D. A., et al. (2010). History of sea ice in the Arctic. *Quat. Sci. Rev.* 29, 1757–1778. doi:https://doi.org/10.1016/j.quascirev.2010.02.010.

Polyakov, I. V., Pnyushkov, A. V., Alkire, M. B., Ashik, I. M., Baumann, T. M., Carmack, E. C., et al. (2017). Greater role for Atlantic inflows on sea-ice loss in the Eurasian Basin of the Arctic Ocean. *Science (80-.).* 356, 285–291. doi:10.1126/science.aai8204.

Polyakov, I. V, Alexeev, V. A., Ashik, I. M., Bacon, S., Beszczynska-Möller, A., Carmack, E. C., et al. (2011). Fate of Early 2000s Arctic Warm Water Pulse. *Bull. Am. Meteorol. Soc.* 92, 561–566. doi:10.1175/2010BAMS2921.1.

Polyakov, I. V, Alkire, M. B., Bluhm, B. A., Brown, K. A., Carmack, E. C., Chierici, M., et al. (2020a). Borealization of the Arctic Ocean in Response to Anomalous Advection From Sub-Arctic Seas. *Front. Mar. Sci.* 7. doi:10.3389/fmars.2020.00491.

Polyakov, I. V, Bhatt, U. S., Walsh, J. E., Abrahamsen, E. P., Pnyushkov, A. V, and Wassmann, P. F. (2013a). Recent oceanic changes in the Arctic in the context of long-term observations. *Ecol. Appl.* 23, 1745–1764. doi:10.1890/11-0902.1.

Polyakov, I. V, Pnyushkov, A. V, Rember, R., Padman, L., Carmack, E. C., and Jackson, J. M. (2013b). Winter convection transports Atlantic water heat to the surface layer in the eastern Arctic Ocean. *J. Phys. Oceanogr.* 43, 2142–2155. doi:10.1175/JPO-D-12-0169.1.

Polyakov, I. V, Rippeth, T. P., Fer, I., Alkire, M. B., Baumann, T. M., Carmack, E. C., et al.

(2020b). Weakening of Cold Halocline Layer Exposes Sea Ice to Oceanic Heat in the Eastern Arctic Ocean. *J. Clim.* 33, 8107–8123. doi:10.1175/JCLI-D-19-0976.1.

Pontiller, B., Martínez-García, S., Joglar, V., Amnebrink, D., Pérez-Martínez, C., González, J. M., et al. (2022). Rapid bacterioplankton transcription cascades regulate organic matter utilization during phytoplankton bloom progression in a coastal upwelling system. *ISME J.* 16, 2360–2372. doi:10.1038/s41396-022-01273-0.

Popova, E. E., Yool, A., Coward, A. C., Aksenov, Y. K., Alderson, S. G., de Cuevas, B. A., et al. (2010). Control of primary production in the Arctic by nutrients and light: insights from a high resolution ocean general circulation model. *Biogeosciences* 7, 3569–3591. doi:10.5194/bg-7-3569-2010.

Popova, E. E., Yool, A., Coward, A. C., Dupont, F., Deal, C., Elliott, S., et al. (2012). What controls primary production in the Arctic Ocean? Results from an intercomparison of five general circulation models with biogeochemistry. *J. Geophys. Res. Ocean.* 117. doi:10.1029/2011JC007112.

Poulin, M., Daugbjerg, N., Gradinger, R., Ilyash, L., Ratkova, T., and von Quillfeldt, C. (2011). The pan-Arctic biodiversity of marine pelagic and sea-ice unicellular eukaryotes: a first-attempt assessment. *Mar. Biodivers.* 41, 13–28. doi:10.1007/s12526-010-0058-8.

Preston, C. M., Durkin, C. A., and Yamahara, K. M. (2020). DNA metabarcoding reveals organisms contributing to particulate matter flux to abyssal depths in the North East Pacific ocean. *Deep. Res. Part II Top. Stud. Oceanogr.* 173, 104708. doi:10.1016/j.dsr2.2019.104708.

Priest, T., Appen, W.-J. von, Oldenburg, E., Popa, O., Torres-Valdés, S., Bienhold, C., et al. (2022). Variations in Atlantic water influx and sea-ice cover drive taxonomic and functional shifts in Arctic marine bacterial communities. *bioRxiv*, 2022.08.12.503524. doi:10.1101/2022.08.12.503524.

Ramondenc, S., Nöthig, E.-M., Hufnagel, L., Bauerfeind, E., Busch, K., Knüppel, N., et al. (2022). Effects of Atlantification and changing sea-ice dynamics on zooplankton community structure and carbon flux between 2000 and 2016 in the eastern Fram Strait. *Limnol. Oceanogr.* n/a. doi:10.1002/lno.12192.

Rantanen, M., Karpechko, A. Y., Lipponen, A., Nordling, K., Hyvärinen, O., Ruosteenoja, K., et al. (2022). The Arctic has warmed nearly four times faster than the globe since 1979. *Commun. Earth Environ.* 3, 168. doi:10.1038/s43247-022-00498-3.

Rapp, J. Z. (2018). Diversity and function of microbial communities in the Arctic Ocean.

Rapp, J. Z., Fernández-Méndez, M., Bienhold, C., and Boetius, A. (2018). Effects of ice-algal aggregate export on the connectivity of bacterial communities in the central Arctic Ocean. *Front. Microbiol.* 9, 1035. doi:10.3389/fmicb.2018.01035.

Riedel, A., Michel, C., Gosselin, M., and LeBlanc, B. (2008). Winter–spring dynamics in sea-ice carbon cycling in the coastal Arctic Ocean. *J. Mar. Syst.* 74, 918–932. doi:10.1016/j.jmarsys.2008.01.003.

Różańska, M., Poulin, M., and Gosselin, M. (2008). Protist entrapment in newly formed sea ice in the Coastal Arctic Ocean. *J. Mar. Syst.* 74, 887–901. doi:10.1016/j.jmarsys.2007.11.009.

Rudels, B. (2015). Arctic Ocean circulation, processes and water masses: A description of observations and ideas with focus on the period prior to the International Polar Year 2007–2009. *Prog. Oceanogr.* 132, 22–67. doi:10.1016/j.pocean.2013.11.006.

Rudels, B., Anderson, L. G., and Jones, E. P. (1996). Formation and evolution of the surface mixed layer and halocline of the Arctic Ocean. *J. Geophys. Res. Ocean.* 101, 8807–8821.

doi:https://doi.org/10.1029/96JC00143.
Rudels, B., and Carmack, E. (2022). Arctic Ocean Water Mass Structure and Circulation. *Oceanography* 35. doi:10.5670/oceanog.2022.116.
Rudels, B., Fahrbach, E., Meincke, J., Budéus, G., and Eriksson, P. (2002). The East Greenland Current and its contribution to the Denmark Strait overflow. *ICES J. Mar. Sci.* 59, 1133–1154. doi:10.1006/jmsc.2002.1284.
Rudels, B., Schauer, U., Björk, G., Korhonen, M., Pisarev, S., Rabe, B., et al. (2012). Observations of water masses and circulation in the Eurasian Basin of the Arctic Ocean from the 1990s to the late 2000s. *Ocean Sci. Discuss.* 9, 2695–2747. doi:10.5194/osd-9-2695-2012.
Salazar, G., Cornejo-Castillo, F. M., Benítez-Barrios, V., Fraile-Nuez, E., Álvarez-Salgado, X. A., Duarte, C. M., et al. (2016). Global diversity and biogeography of deep-sea pelagic prokaryotes. *ISME J.* 10, 596–608. doi:10.1038/ismej.2015.137.
Saw, J., Nunoura, T., Hirai, M., Takaki, Y., Parsons, R., Michelsen, M., et al. (2020). Pangenomics Analysis Reveals Diversification of Enzyme Families and Niche Specialization in Globally Abundant SAR202 Bacteria. *MBio* 11, e02975-19. doi:10.1128/mBio.02975-19.
Sazhin, A. F., Romanova, N. D., Kopylov, A. I., and Zabotkina, E. A. (2019). Bacteria and Viruses in Arctic Sea Ice. *Oceanology* 59, 339–346. doi:10.1134/S0001437019030196.
Schröter, F., Havermans, C., Kraft, A., Knüppel, N., Beszczynska-Möller, A., Bauerfeind, E., et al. (2019). Pelagic amphipods in the eastern fram strait with continuing presence of Themisto compressa based on sediment trap time series. *Front. Mar. Sci.* 6, 311. doi:10.3389/fmars.2019.00311.
Screen, J. A., and Deser, C. (2019). Pacific Ocean Variability Influences the Time of Emergence of a Seasonally Ice-Free Arctic Ocean. *Geophys. Res. Lett.* 46, 2222–2231. doi:https://doi.org/10.1029/2018GL081393.
Seebah, S., Fairfield, C., Ullrich, M. S., and Passow, U. (2014). Aggregation and Sedimentation of Thalassiosira weissflogii (diatom) in a Warmer and More Acidified Future Ocean. *PLoS One* 9, e112379. Available at: 10.1371/journal.pone.0112379.
Serreze, M. C., Barrett, A. P., Stroeve, J. C., Kindig, D. N., and Holland, M. M. (2009). The emergence of surface-based Arctic amplification. *Cryosph.* 3, 11–19. doi:10.5194/tc-3-11-2009.
Serreze, M. C., and Barry, R. G. (2011). Processes and impacts of Arctic amplification: A research synthesis. *Glob. Planet. Change* 77, 85–96. doi:10.1016/j.gloplacha.2011.03.004.
Siegel, D. A., Buesseler, K. O., Behrenfeld, M. J., Benitez-Nelson, C. R., Boss, E., Brzezinski, M. A., et al. (2016). Prediction of the Export and Fate of Global Ocean Net Primary Production: The EXPORTS Science Plan. *Front. Mar. Sci.* 3. doi:10.3389/fmars.2016.00022.
Simon, M., Grossart, H. P., Schweitzer, B., and Ploug, H. (2002). Microbial ecology of organic aggregates in aquatic ecosystems. *Aquat. Microb. Ecol.* 28, 175–211. doi:10.3354/ame028175.
Smedsrud, L. H., Halvorsen, M. H., Stroeve, J. C., Zhang, R., and Kloster, K. (2017). Fram Strait sea ice export variability and September Arctic sea ice extent over the last 80 years. *Cryosph.* 11, 65–79. doi:10.5194/tc-11-65-2017.
Smedsrud, L. H., Sirevaag, A., Kloster, K., Sorteberg, A., and Sandven, S. (2011). Recent wind driven high sea ice area export in the Fram Strait contributes to Arctic sea ice decline.

Cryosph. 5, 821–829. doi:10.5194/tc-5-821-2011.

Smith, K. L., Ruhl, H. A., Huffard, C. L., Messié, M., and Kahru, M. (2018). Episodic organic carbon fluxes from surface ocean to abyssal depths during long-term monitoring in NE Pacific. *Proc. Natl. Acad. Sci.* 115, 12235–12240. doi:10.1073/pnas.1814559115.

Smith K.L, J., and Druffel, E. R. M. (1998). Long time-series monitoring of an abyssal site in the NE Pacific: an introduction. *Deep Sea Res. Part II Top. Stud. Oceanogr.* 45, 573–586. doi:10.1016/S0967-0645(97)00094-5.

Soltwedel, T., Bauerfeind, E., Bergmann, M., Bracher, A., Budaeva, N., Busch, K., et al. (2016). Natural variability or anthropogenically-induced variation? Insights from 15 years of multidisciplinary observations at the arctic marine LTER site HAUSGARTEN. *Ecol. Indic.* 65, 89–102. doi:10.1016/j.ecolind.2015.10.001.

Soltwedel, T., Bauerfeind, E., Bergmann, M., Budaeva, N., Hoste, E., Jaeckisch, N., et al. (2005). Hausgarten: Multidisciplinary investigations at a Deep-Sea, long-term observatory in the Arctic Ocean. *Oceanography* 18, 46–61. doi:10.5670/oceanog.2005.24.

Sowell, S. M., Wilhelm, L. J., Norbeck, A. D., Lipton, M. S., Nicora, C. D., Barofsky, D. F., et al. (2009). Transport functions dominate the SAR11 metaproteome at low-nutrient extremes in the Sargasso Sea. *ISME J.* 3, 93–105. doi:10.1038/ismej.2008.83.

Steinberg, D. K., and Landry, M. R. (2017). Zooplankton and the Ocean Carbon Cycle. *Ann. Rev. Mar. Sci.* 9, 413–444. doi:10.1146/annurev-marine-010814-015924.

Stöven, T., Tanhua, T., Hoppema, M., and von Appen, W.-J. (2016). Transient tracer distributions in the Fram Strait in 2012 and inferred anthropogenic carbon content and transport. *Ocean Sci.* 12, 319–333. doi:10.5194/os-12-319-2016.

Stroeve, J., and Notz, D. (2018). Changing state of Arctic sea ice across all seasons. *Environ. Res. Lett.* 13, 103001. doi:10.1088/1748-9326/aade56.

Sunagawa, S., Coelho, L. P., Chaffron, S., Kultima, J. R., Labadie, K., Salazar, G., et al. (2015). Structure and function of the global ocean microbiome. *Science (80-.).* 348, 1261359. doi:10.1126/science.1261359.

Takahashi, T., Sutherland, S. C., Sweeney, C., Poisson, A., Metzl, N., Tilbrook, B., et al. (2002). Global sea–air CO2 flux based on climatological surface ocean pCO2, and seasonal biological and temperature effects. *Deep Sea Res. Part II Top. Stud. Oceanogr.* 49, 1601–1622. doi:10.1016/S0967-0645(02)00003-6.

Terhaar, J., Lauerwald, R., Regnier, P., Gruber, N., and Bopp, L. (2021). Around one third of current Arctic Ocean primary production sustained by rivers and coastal erosion. *Nat. Commun.* 12, 169. doi:10.1038/s41467-020-20470-z.

Tesi, T., Muschitiello, F., Mollenhauer, G., Miserocchi, S., Langone, L., Ceccarelli, C., et al. (2022). Rapid Atlantification along the Fram Strait at the beginning of the 20th century. *Sci. Adv.* 7, eabj2946. doi:10.1126/sciadv.abj2946.

Thiele, S., Fuchs, B. M., Amann, R., and Iversen, M. H. (2015). Colonization in the photic zone and subsequent changes during sinking determine bacterial community composition in marine snow. *Appl. Environ. Microbiol.* 81, 1463–1471. doi:10.1128/AEM.02570-14.

Thomas, D. N. (2017). *Sea ice*. John Wiley & Sons.

Thomas, D. N., Papadimitriou, S., and Michel, C. (2009). Biogeochemistry of Sea Ice. *Sea Ice*, 425–467. doi:10.1002/9781444317145.ch12.

Torres-Valdés, S., Tsubouchi, T., Bacon, S., Naveira-Garabato, A. C., Sanders, R., McLaughlin, F. A., et al. (2013). Export of nutrients from the Arctic Ocean. *J. Geophys. Res. Ocean.* 118, 1625–1644. doi:https://doi.org/10.1002/jgrc.20063.

Tremblay, J.-É., Bélanger, S., Barber, D. G., Asplin, M., Martin, J., Darnis, G., et al. (2011). Climate forcing multiplies biological productivity in the coastal Arctic Ocean. *Geophys. Res. Lett.* 38. doi:10.1029/2011GL048825.

Tsubouchi, T., Våge, K., Hansen, B., Larsen, K. M. H., Østerhus, S., Johnson, C., et al. (2021). Increased ocean heat transport into the Nordic Seas and Arctic Ocean over the period 1993–2016. *Nat. Clim. Chang.* 11, 21–26. doi:10.1038/s41558-020-00941-3.

Tuerena, R. E., Hopkins, J., Buchanan, P. J., Ganeshram, R. S., Norman, L., von Appen, W.-J., et al. (2021). An Arctic Strait of Two Halves: The Changing Dynamics of Nutrient Uptake and Limitation Across the Fram Strait. *Global Biogeochem. Cycles* 35, e2021GB006961. doi:10.1029/2021GB006961.

Turner, J. T. (2015). Zooplankton fecal pellets, marine snow, phytodetritus and the ocean's biological pump. *Prog. Oceanogr.* 130, 205–248. doi:10.1016/j.pocean.2014.08.005.

van Leeuwe, M. A., Tedesco, L., Arrigo, K. R., Assmy, P., Campbell, K., Meiners, K. M., et al. (2018). Microalgal community structure and primary production in Arctic and Antarctic sea ice: A synthesis. *Elem. Sci. Anthr.* 6, 4. doi:10.1525/elementa.267.

Vernet, M., Ellingsen, I. H., Seuthe, L., Slagstad, D., Cape, M. R., and Matrai, P. A. (2019). Influence of Phytoplankton Advection on the Productivity Along the Atlantic Water Inflow to the Arctic Ocean. *Front. Mar. Sci.* 6. doi:10.3389/fmars.2019.00583.

Vernet, M., Richardson, T. L., Metfies, K., Eva-Maria Nöthig, and Peeken, I. (2017). Models of plankton community changes during a warm water anomaly in Arctic waters show altered trophic pathways with minimal changes in carbon export. *Front. Mar. Sci.* 4, 160. doi:10.3389/fmars.2017.00160.

Volk, T., and Hoffert, M. I. (1985). Ocean Carbon Pumps: Analysis of Relative Strengths and Efficiencies in Ocean-Driven Atmospheric CO2 Changes. *Carbon Cycle Atmos. CO2 Nat. Var. Archean to Present*, 99–110. doi:10.1029/GM032p0099.

von Appen, W.-J., Waite, A. M., Bergmann, M., Bienhold, C., Boebel, O., Bracher, A., et al. (2021). Sea-ice derived meltwater stratification slows the biological carbon pump: results from continuous observations. *Nat. Commun.* 12, 1–16.

von Jackowski, A., Grosse, J., Nöthig, E.-M., and Engel, A. (2020). Dynamics of organic matter and bacterial activity in the Fram Strait during summer and autumn. *Philos. Trans. R. Soc. A Math. Phys. Eng. Sci.* 378, 20190366. doi:10.1098/rsta.2019.0366.

Walsh, J. J., McRoy, C. P., Coachman, L. K., Goering, J. J., Nihoul, J. J., Whitledge, T. E., et al. (1989). Carbon and nitrogen cycling within the Bering/Chukchi Seas: Source regions for organic matter effecting AOU demands of the Arctic Ocean. *Prog. Oceanogr.* 22, 277–359. doi:10.1016/0079-6611(89)90006-2.

Wang, M., and Overland, J. E. (2012). A sea ice free summer Arctic within 30 years: An update from CMIP5 models. *Geophys. Res. Lett.* 39. doi:https://doi.org/10.1029/2012GL052868.

Wassmann, P. (2015). Overarching perspectives of contemporary and future ecosystems in the Arctic Ocean. *Prog. Oceanogr.* 139, 1–12. doi:10.1016/j.pocean.2015.08.004.

Wassmann, P., Bauerfeind, E., Fortier, M., Fukuchi, M., Hargrave, B., Moran, B., et al. (2004). "Particulate Organic Carbon Flux to the Arctic Ocean Sea Floor BT - The Organic Carbon Cycle in the Arctic Ocean," in, eds. R. Stein and R. W. MacDonald (Berlin, Heidelberg: Springer Berlin Heidelberg), 101–138. doi:10.1007/978-3-642-18912-8_5.

Wassmann, P., Duarte, C. M., Agustí, S., and Sejr, M. K. (2011). Footprints of climate change in the Arctic marine ecosystem. *Glob. Chang. Biol.* 17, 1235–1249. doi:https://doi.org/10.1111/j.1365-2486.2010.02311.x.

Wassmann, P., and Reigstad, M. (2011). Future Arctic Ocean seasonal ice zones and implications for pelagic-benthic coupling. *Oceanography* 24, 220–231. doi:10.5670/oceanog.2011.74.

Weissenberger, J., and Grossmann, S. (1998). Experimental formation of sea ice: importance of water circulation and wave action for incorporation of phytoplankton and bacteria. *Polar Biol.* 20, 178–188. doi:10.1007/s003000050294.

Weydmann, A., Carstensen, J., Goszczko, I., Dmoch, K., Olszewska, A., and Kwasniewski, S. (2014). Shift towards the dominance of boreal species in the Arctic: Inter-annual and spatial zooplankton variability in the West Spitsbergen Current. *Mar. Ecol. Prog. Ser.* 501, 41–52. doi:10.3354/meps10694.

Wiedmann, I., Ershova, E., Bluhm, B. A., Nöthig, E.-M., Gradinger, R. R., Kosobokova, K., et al. (2020). What Feeds the Benthos in the Arctic Basins? Assembling a Carbon Budget for the Deep Arctic Ocean. *Front. Mar. Sci.* 7. doi:10.3389/fmars.2020.00224.

Wietz, M., Bienhold, C., Metfies, K., Torres-Valdés, S., von Appen, W.-J., Salter, I., et al. (2021). The polar night shift: seasonal dynamics and drivers of Arctic Ocean microbiomes revealed by autonomous sampling. *ISME Commun.* 1, 76. doi:10.1038/s43705-021-00074-4.

Wietz, M., Gram, L., Jørgensen, B., and Schramm, A. (2010). Latitudinal patterns in the abundance of major marine bacterioplankton groups. *Aquat. Microb. Ecol.* 61, 179–189. doi:10.3354/ame01443.

Wietz, M., Metfies, K., Bienhold, C., Wolf, C., Janssen, F., Salter, I., et al. (2022). Impact of preservation method and storage period on ribosomal metabarcoding of marine microbes: Implications for remote automated samplings. *Front. Microbiol.* 13. doi:10.3389/fmicb.2022.999925.

Wilson, B., Müller, O., Nordmann, E. L., Seuthe, L., Bratbak, G., and Øvreås, L. (2017). Changes in marine prokaryote composition with season and depth over an Arctic polar year. *Front. Mar. Sci.* 4, 95. doi:10.3389/fmars.2017.00095.

Wolf, K. (2019). Adaptive potential of the Arctic diatom Thalassiosira hyalina to climate change: intraspecific diversity, plasticity and population dynamics.

Woodgate, R. A., and Aagaard, K. (2005). Revising the Bering Strait freshwater flux into the Arctic Ocean. *Geophys. Res. Lett.* 32. doi:10.1029/2004GL021747.

Xing, P., Hahnke, R. L., Unfried, F., Markert, S., Huang, S., Barbeyron, T., et al. (2015). Niches of two polysaccharide-degrading Polaribacter isolates from the North Sea during a spring diatom bloom. *ISME J.* 9, 1410–1422. doi:10.1038/ismej.2014.225.

Yadav, J., Kumar, A., and Mohan, R. (2020). Dramatic decline of Arctic sea ice linked to global warming. *Nat. Hazards* 103, 2617–2621. doi:10.1007/s11069-020-04064-y.

Zhang, J., Spitz, Y. H., Steele, M., Ashjian, C., Campbell, R., Berline, L., et al. (2010). Modeling the impact of declining sea ice on the Arctic marine planktonic ecosystem. *J. Geophys. Res. Ocean.* 115. doi:10.1029/2009JC005387.

Zhang, X., Walsh, J. E., Zhang, J., Bhatt, U. S., and Ikeda, M. (2004). Climatology and Interannual Variability of Arctic Cyclone Activity: 1948–2002. *J. Clim.* 17, 2300–2317. doi:10.1175/1520-0442(2004)017<2300:CAIVOA>2.0.CO;2.

Zhong, Z.-P., Rapp, J. Z., Wainaina, J. M., Solonenko, N. E., Maughan, H., Carpenter, S. D., et al. (2020). Viral ecogenomics of arctic cryopeg brine and sea ice. *Msystems* 5, e00246-20. doi:10.1128/mSystems.00246-20.

Acknowledgements

I would like to thank Prof. Antje Boetius and the Hector Fellow Academy for accepting me as a PhD student for allowing me to pursue my career in scientific research at the HGP MPG Joint Research Group for Deep-Sea Ecology and Technology at the Max Planck Institute for Marine Microbiology. A special thanks to Dr. Christina Bienhold for the support, and guidance with my projects, and for encouraging me to always be better. A special thank you to all listed co-authors for their dedicated support in the development the chapters included in this thesis. I would like to specially thank Dr. Verena Carvalho and Dr. Eduard Fadeev for their continuous support since I started my scientific career at the MPI. Thank you to all HGP MPG Joint Research Group past and present members for all the support and life experiences.

Thank you Prof. Thostern Brinkhoff for reviewing this thesis.

A special thanks, dankeschön and gracias to my family Fernando, Dora, Manu and friends for your love unconditional support and words of encouragement! Thank you Rashi, Sina for your support during the writing phase and all YR and staff members of the HFA for all the support, scientific discussion and life experiences. Thank you, Nils, for all the support and unconditional love. Gracias Missy, Cesario, Lunette, Bonnie for your fluffy encouragement.